UNCLASSIFIED

ORNL-1753(Del.)

Subject Category: REACTORS—POWER

I

HOMOGENEOUS REACTOR PROJECT QUARTERLY PROGRESS REPORT FOR PERIOD ENDING APRIL 30, 1954

UNITED STATES ATOMIC ENERGY COMMISSION
Technical Information Extension, Oak Ridge, Tennessee

AEC RESEARCH AND DEVELOPMENT REPORT

Photostat Price $ 27.30
Microfilm Price $ 8.10

Available from the
Office of Technical Services
Department of Commerce
Washington 25, D. C.

UNCLASSIFIED

613 001

DECLASSIFIED

~~CONFIDENTIAL~~

II

This report has been reviewed under the Declas ication Guide of 1955.

LEGAL NOTICE

This report was prepared as an account of Government ed work. Neither the United States, nor the Commission, nor any person acting o of the Commission:

A. Makes any warranty or representation, express ed, with respect to the accuracy, completeness, or usefulness of the information ed in this report, or that the use of any information, apparatus, method, or proce osed in this report may not infringe privately owned rights; or

B. Assumes any liabilities with respect to t , or for damages resulting from the use of any information, apparatus, method, or isclosed in this report.

As used in the above, "person acting f of the Commission" includes any employee or contractor of the Commission extent that such employee or contractor prepares, handles or distributes, or prov ess to, any information pursuant to his employment or contract with the Commis

This report s been reproduced directly from the best available copy

Printed n USA, Charge $1.10. Available from the Technical rmation Extension, P. O. Box 1001, Oak Ridge, Tennessee lease direct to the same address inquiries covering th rocurement of classified AEC reports.

DO NOT X-RAY

~~CONFIDENTIAL~~

AEC, Oak Ridge, Tenn.

DECLASSIFIED

ORNL-1753(Rev.)

Contract No. W-7405-eng-26

HOMOGENEOUS REACTOR PROJECT

QUARTERLY PROGRESS REPORT

For Period Ending April 30, 1954

Project Director – J. A. Swartout
Engineering – J. A. Lane
Chemistry – C. H. Secoy
Corrosion – E. G. Bohlmann
Chemical Technology – F. R. Bruce
Metallurgy – E. C. Miller

Compiled by H. F. McDuffie

DATE ISSUED

September 17, 1954

OAK RIDGE NATIONAL LABORATORY
Operated by
CARBIDE AND CARBON CHEMICALS COMPANY
A Division of Union Carbide and Carbon Corporation
Post Office Box P
Oak Ridge, Tennessee

SUMMARY

PART I

HOMOGENEOUS REACTOR EXPERIMENT

Further analysis of the data on the performance of copper as an internal catalyst indicated that the major inconsistencies between the reactor data and in-pile bomb data can be resolved by the assumption of a hot region within the core. Analysis based on a central region that is 15°C hotter than the average core temperature provides a qualitative explanation for the difference between theoretical (uniform temperature throughout) and actual data.

Operation of the HRE was discontinued early in the quarter, after three runs for the purpose of collecting Xe^{135} for neutron cross-section measurements. From the final run, 1000 curies of Xe^{135} was delivered to the Physics Group.

Decontamination and dismantling of the reactor, in preparation for the HRT, were begun immediately. Radiation levels of several thousand roentgens per hour were reduced to 20-50 r/hr in 30 days by decontamination and decay. Disassembly of the reactor is about 75% complete. As of May 10, 1954, all of the reactor and reflector components have been removed and only miscellaneous small parts and shielding remain. The distribution of fission-product activities found in the decontaminating solutions as compared with those found in the fuel suggests that essentially all the fission products which are strong gamma emitters were adsorbed on the walls of the equipment or settled out as precipitates in the system.

PART II

HOMOGENEOUS REACTOR TEST

Reactor Analysis

Statics Calculations. Criticality calculations have been completed for three blankets as follows: (1) D_2O, (2) ThO_2 slurry, and (3) unenriched UO_2SO_4 solutions. Thermal and fast fluxes and adjoint functions for the D_2O and UO_2SO_4 blankets are reported along with the temperature coefficient of reactivity.

Kinetics Studies. The response of the HRT to increases in reactivity is expected to be similar to the HRE. No instabilities are evident for the calculated conditions. The arrangement of the pressurizer has been studied from the standpoint of the core-pressure rise which results from a sudden reactivity increase. For the worst case, which results from starting the circulating pump with the core at low power and 280°C, and 100°C fuel in the heat exchanger, k_{eff} would be increased at the rate of 1.4% per second and the core-pressure rise would be less than 200 psi. A pressure increase of more than 250 psi might cause damage to the ¼-in. thick zirconium core tank.

Operational Planning

HRT Start-up Procedure. For the HRT start-up procedure, it is proposed to fill the high-pressure circulating system with D_2O condensate and then to add concentrated fuel solution until criticality is reached. Fuel and D_2O inventories and pump rates have been specified so that the rate of reactor temperature increase will be limited to 1.2°C per minute after criticality is obtained. The equilibrium temperature after this type of start-up will be approximately 245°C.

Shutdown will be accomplished by removing fuel from the core circulating loop, thereby causing a reduction in concentration and temperature. By this method, the reactor temperature can be reduced from 280 to 100°C in 2 hr.

HRT Design

General Considerations. Revised HRT flow sheet and design-data sheets are presented. Although the initial reactor operation will be with a D_2O blanket, the changes made during the past quarter will permit the HRT to demonstrate the production of plutonium with a low Pu^{240} content in a UO_2SO_4-D_2O blanket.

Reactor Steam System. The reactor heat-removal system is being designed to absorb as much as 13.5 Mw of heat – twice the normal heat generation in the core and blanket. No increase in electrical generation capacity is planned, over the 312 kva available from the existing HRE equipment. A summary of the study which led to the decision to use the HRE turbine generator with a steam killer is presented.

Valves. The design of ⅛, ½, and 1-in. 2500-psi bellows-sealed valves has been completed and the drawings have been issued.

Core Tank and Pressure Vessel. A contract has been negotiated with the Newport News Shipbuilding

& Dry Dock Co. for the design, development, and fabrication of a 32-in.-dia, ¼-in.-thick zirconium core tank and a 60-in.-ID 4-in.-thick stainless-steel-clad pressure vessel. The concept of these vessels is discussed.

Main Heat Exchangers. Drawings and specifications for the fuel solution and blanket heat exchangers have been completed and released for competitive bids.

Pressurizers. A preliminary design has been made for the pressurizers which maintain the fuel and blanket circulating systems at 2000 psi. It has been tentatively decided to use steam pressurization, the heat source being provided by electric heaters outside the vessel. Gas pressurization is also being considered. Problems related to the pressurizer design include (1) the provision of sufficient vapor or gas volume to limit the pressure increase resulting from rapid reactivity increases, (2) protection against phase separation and corrosion at high operating temperatures, and (3) provision for pressure equalization between core and blanket systems during the dumping operation.

Recombiner-Condenser Unit. The catalytic recombiner and recombined-vapor condenser have been designed in a single vessel. This unit is intended to handle approximately 15 cfm of the stoichiometric mixture of deuterium and oxygen which is not recombined by the dissolved copper catalyst in the core during start-up or low-temperature operation. The condenser also serves to condense the D_2O vapor which flashes from the core and blanket solutions during dumps from high temperatures. A surface of 159 sq ft would be required to condense the fuel-solution vapors in a 2.4-min dump time.

Outer-Dump-Tank Condenser. A design for the outer-dump-tank condenser, which must remove the heat released from the decay of fission products in the fuel solution, has been based on a heat release of approximately 170 kw and a required condensing surface of 27.6 sq ft. This preliminary design is presented.

Fuel-Dump-Tank Design. A study of possible fuel-dump-tank arrangements has resulted in a decision to use 14-in.-dia horizontal tanks 30 ft long and coated externally with cadmium. This arrangement permits a maximum linear concentration of 0.5 kg of U^{235} per foot. At this concentration with any mixture of light and heavy water the tank should never become critical when totally immersed in light water.

HRT Evaporator Design. Two designs have been proposed for the HRT low-pressure evaporators. One is a jacketed pipe similar to the HRE evaporator, and the other is a shell-and-tube calandria type. A choice between the two has not been made.

HRT Shield Design. The K-25 General Engineering Department is assisting in the design of the HRT shield. The shield is to be in the form of a 25-ft-deep steel tank with removable concrete plugs on top. The structure is being designed to withstand the pressure rise that results from spillage of the high-temperature reactor solutions. The design further assumes that the tank will be filled with water for the protection of personnel during maintenance operation. The pit will be located within the confines of the existing HRE building.

Equipment and Shield Layouts. Two figures are presented to show a study arrangement of equipment and piping in the shielding pit.

Control of Xenon Poisoning by Stripping with Gas. Evidence is presented which indicates that the xenon poison level in the HRT can be maintained below 1% by continuous stripping with only 2% of the decomposition gases which would be produced if no Cu^{++} catalyst were present for recombination. As a result of this study, it is planned to add a sufficient amount of copper to recombine only 98% of the decomposition gases so that the remaining 2% can be used for xenon stripping.

Engineering Development

HRT Core. A full-scale steel flow model of the HRT core is being built in order to investigate and minimize the amount of flow separation near the sphere wall in the lower hemisphere. Testing and evaluation of the model should be completed by June 1.

HRT Blanket. A small-scale flow model, which consists of an 8-in. hollow steel sphere centrally located inside an 18-in. plastic sphere, has been built and some qualitative flow studies with cold water have been carried out. Blanket flow tests are planned in the full-scale HRT model being built by Newport News Shipbuilding & Drydock Co.

Alternate Core. A 4-ft flow model of the alternate core configuration, which incorporates concentric inlet and outlet pipes, has been installed. The unit will be used to examine the parameters involved in projecting the 18-in.-model data to larger scale reactors. Preliminary tests indicate satisfactory operation.

Gas Separators. A low-pressure and low-temperature plastic model of the proposed HRT gas separator has been built and tested. Gas removal was nearly complete, with water entrainment of 0.3 to 0.5 gpm. The flow angle at the recovery vanes was measured and found to require vanes with a 45-deg intake angle as opposed to the 45-deg discharge angle of the rotation vanes.

Small Reactor Components – HRT Fuel and Blanket Pump Development (230-500 gpm Pumps). Two 400A pumps will be received from Westinghouse Electric Corporation in July or August and three 300A pumps are on order. Fabrication of the motors has been started, but a delivery date cannot be established until final specifications have been approved. Allis-Chalmers will submit a proposal on a 500-gpm, top maintenance pump and test loop. Orders for HRT pumps will be placed as soon as final designs and specifications have been completed.

Pulsafeeder Pump Development. Check-valve improvements have resulted in higher speed, higher capacity, and quieter operation. This will permit the use of HRE-size diaphragms in HRT pumps. A proposal from Lapp Insulator Co., Inc., on these pumps is expected in the near future. This company has done some development on larger heads which may be needed for future reactors.

Controls and Instrumentation

Control Panel. Scale mock-ups of the graphic and nongraphic panels have been made. A choice will be made between these two approaches on the basis of operating convenience. Pneumatic miniature instruments which can be unplugged during operation are recommended for both panels.

Control-Valve Program. Orders for 2000-psi, 300°C stainless steel bellows have been placed with Breeze Corporations, Inc., and the Badger Manufacturing Company.

Contracts have been awarded to four manufacturers for an HRT ½-in. valve for use at 2000 psi and 300°C. Bids from nine companies ranged from $1442 to $5000 for a single test valve. Valve requirements for the entire soup system have been detailed.

Nuclear Instrumentation. Nuclear instrumentation in the HRT will be limited to two fission chambers with counting-rate circuits and one compensated chamber with a Log N circuit. A multichannel radiation monitoring unit will also be included.

Waterproofing of Instrumentation. Since all reactor components will be submerged during maintenance and repair operations, it will be necessary to waterproof instrument leads. A large assortment of waterproof wiring, connectors, and switches has been assembled and will be tested after submergence under 25 ft of water.

PART III

GENERAL HOMOGENEOUS REACTOR STUDIES

Engineering Development

Gas Separators. Additional runs on the experimental 5000-gpm gas separator were made with the use of a spherical Pitot tube. Further effort will be devoted to modifying the gas take-off in order to decrease local turbulences and to minimize the amount of entrainment.

High-Pressure Catalytic Recombiner and Entrainment Separator. Construction of the components for the high-pressure recombiner loop is about 80% complete, and final assembly will be finished during the next quarter. The experimental program for the loop has been drawn up. A high-pressure entrainment-separator loop is planned in order to evaluate wire-mesh demisters and entrainment problems.

Intermediate and Large Reactor Components. *Main Fuel-and-Gas Condenser Heat Exchangers.* – Although contract negotiation has not been completed with the Foster Wheeler Corp., design and fabrication of the major heat exchangers required for a 50-Mw system are proceeding. The contractor has begun development work on two problems: tube-joint-weld development and investigation of tube-testing methods.

Heat-Exchanger Development. – The tube-screening test outlined in the last progress report is being continued. A test installation is being constructed which will permit estimation of the magnitude of the inside scale coefficient of heat transfer of various tubes.

Status of the 4000-gpm Loop. – A rather large leak in the metal bellows of the balance system was detected with a Consolidated helium leak detector. While steps are being taken to repair this leak, leak detection is progressing on the remainder of the loop.

Small Gas Circulator Development. – Both Allis-Chalmers and Westinghouse are preparing proposals for a 20-cfm gas circulator and completely instrumented test loop for testing of the gas circulators at design conditions.

ORNL 5-gpm Pump. An operating endurance test of the ORNL 5-gpm pump has been under way for some time in order to determine the life expectancy of its various parts. One pump has run for a total of 1800 hr while circulating water at 250°C. Because it was desirable to increase the heat output of the pump, a variable-frequency source was built and the pump was operated at 110 v at frequencies from 60 to 100 cycles.

Corrosion

With the revival of interest in a concentrated uranyl sulfate solution blanket and in HRT core concentrations ranging from 0.04 to 0.021 *m*, the dynamic-corrosion studies are being extended to cover the temperature range of 100 to 320°C at concentrations ranging from 0 to 1.34 *m*.

The titanium loop has been run 400 hr at 275°C with 1.34 *m* uranyl sulfate solution with no appreciable effect on the solution, the specimens, or the loop components.

Preliminary studies on the effect of the presence of iodide and chloride in the solution indicate that there is no effect on the portions of the system (type 347 stainless steel) exposed to the solution phase but that there is severe pitting in the vapor phase if oxidation to the halogens occurs. Titanium and Zircaloy-2 were not attacked appreciably in either phase.

Further studies on the oxide films obtained in type 347 stainless steel systems have not uniformly confirmed the presence of water of hydration in the nonprotective films formed at temperatures lower than 250°C. Chemical analyses have shown compositions in the following ranges: uranium, 1 to 4%; iron, 43 to 60%; chromium, 1 to 9%; Ni less than 0.2%; no consistent patterns have been observed so far.

The mock-up of the HB-4 in-pile loop has been completed, and one test has been run in it. Several difficulties were encountered, but the over-all performance was satisfactory. In this and several other loop package-test runs, correlation of corrosion calculated on the basis of oxygen utilization and the amount of nickel in solution was good. Also, further tests on the in-pile-loop coupon holder show good agreement with the results obtained under similar conditions for the standard coupon holder in the 100A loop. The performance of the Cu^{++} as hydrogen-oxygen recombiner was also encouraging, although some indications of a decreased efficiency with time will require further testing in subsequent runs.

Two somewhat more serious problems have arisen with the Graphitar No. 14 bearings used in the pump. Small amounts of bearing wear in a small system such as the in-pile loop result in rapid depletion of the relatively low total amount of oxygen in the system because of the oxidation of the resulting carbon particles to CO_2 in the high-temperature portions of the loop. Such oxygen depletion could result in uranium precipitation, with consequent danger to the validity and continuity of the experiment. Erratic, excessive bearing wear has been encountered in test runs and must be eliminated prior to in-pile operation. Also, the Graphitar No. 14 contains small percentages of chloride, which, because of the low relative volume of the system, could result in troublesome chloride concentrations in the solution under test. Metal-bearing replacements for the Graphitar are being investigated.

Installation of the equipment at the LITR and in the loop dismantling facility is approximately 95% complete.

Static-corrosion studies which were undertaken during the past quarter included (1) vapor-phase corrosion attack on type 347 stainless steel exposed to above 0.17 *m* uranyl sulfate solutions at 250°C; (2) the corrosion of Zircaloy-2 at 250°C in 0.02 *m* uranyl sulfate solutions containing various fluoride concentrations; (3) the corrosion of type 347 stainless steel, Zircaloy-2, and titanium, Ti-75A, in 5 *m* uranyl sulfate solution at 300°C; (4) the results of Huey tests with types 304L and 347 stainless steel; and (5) the corrosion of crystal-bar zirconium and Zircaloy-2 in water and steam at elevated temperatures.

Metallurgy

Stress-relief annealing at 1000°F was found to effect an improvement in dynamic-corrosion resistance of austenitic-stainless-steel welds in 0.17 *m* uranyl sulfate solutions, relative to the as-welded or to the higher-temperature post-heat-treatment conditions, although no consistent correlation with microstructure was observed. As-deposited Composition H welds (nominal 18% Cr, 13% Ni, 5% Mn, columbium stabilized), which contain no ferrite, were found to be more corrosion resistant than types 347 and 308L stainless steel welds, containing 3 to 11% ferrite, in dynamic-corrosion tests of both pin- and flat-plate-type

specimens. Metallographic studies showed that the portions of weld deposits which support stable oxide films contain an abundance of randomly dispersed carbide particles.

Failures of bent sections of type 347 stainless-steel-welded pipes in dynamic-corrosion Loop C were shown to have been due to stress-corrosion cracking. These failures emphasize the necessity for stress-relief annealing after fabrication and careful inspection, including suitable laboratory corrosion tests, of HRP materials when they are received. Similar transgranular cracking was responsible for failure of type 347 stainless steel capillary tubing in in-pile mock-up Loop BB, while an intergranular type attack led to the failure of a type 316 stainless steel Parker fitting cap from dynamic-corrosion Loop H.

Investigation of failure of an HRE mock-up let-down valve showed shrinkage voids and selective attack on complex-carbide particles of the Stellite 6 overlay, and severe intergranular attack in the type 347 stainless steel base alloy.

Exposure of Zircaloy-2 and commercial titanium to low-velocity 0.02 *m* uranyl sulfate for 682 hr at 320°C, and of commercial titanium only to low-velocity 0.02 *m* uranyl sulfate for 529 hr at 300°C, had no noticeable effect on the impact behavior of these materials. Preliminary work was performed on the notched-specimen, slow-bend testing program in which various grades of commercial titanium will be used.

Instrumentation and Controls

Instrumentation for the in-pile corrosion-loop program is practically complete. The effects of instrument failure and misoperation have been reviewed in connection with the safety of the proposed experiments in the LITR.

Instrument engineering for all phases of the general homogeneous reactor studies has continued, with emphasis on the slurry-circulation loops, the high-pressure-recombiner loop, entrainment-separation test system, 400-gpm pump test loops, and completion of a variable-frequency motor-generator facility.

Boiling Homogeneous Reactor Studies

In order to provide information on the most satisfactory core arrangement for a boiling homogeneous reactor, experimental and theoretical work has been directed toward the two important phases of the problem: (1) the transport of the vapor generated within the core to the surface of the core and (2) removal of this vapor from the associated entraining liquid. With respect to vapor transport, either natural or forced circulation is superior to natural vapor rise.

Reactor Analysis

Calculations for 19 different possible two-region convertor reactors were carried out in connection with a program designed to determine the combination of nuclear characteristics which would lead to the lowest unit cost for power and high-quality plutonium. The primary conclusion is that the unit cost may be decreased most effectively by finding ways to increase productivity for a given capital outlay. Changes aimed at improvement of the breeding gain or reduction of operating costs by use of cheaper, more depleted blanket feeds are of minor importance so long as the total reactor operating power is not appreciably affected. The desirability of obtaining better experimental values for the Np^{239} cross section and for the solubilities of neptunium and plutonium is emphasized.

Aqueous Solution and Radiation Chemistry

Studies of the effect of reactor irradiation on the corrosion of type 347 stainless steel by uranyl sulfate solution have again suggested the existence of a radiation effect. Out-of-pile tests on highly polished surfaces yield reproducible results, in which the initial corrosion rate is about 20 mpy. After this short initial period the rate drops quickly and levels off at less than 0.1 mpy. In the in-pile tests, although the initial corrosion rate is essentially the same as in the out-of-pile tests, the curve does not level off so fast, and after about three days it actually shows a greater corrosion rate. At the end of five days of irradiation, when the experiments were terminated, the rate was about 6 or 7 mpy. Work is being continued to ascertain the factors responsible for the observed effect.

Studies of the yield of nitrogen gas from reactor-irradiated thorium nitrate solutions give a value of the order of 10^{-3} molecule per 100 ev, which is less, by a factor of at least 100, than the previously reported values for uranyl nitrate solutions. However, the conditions differ in that the energy input from fission is almost absent in the thorium nitrate irradiations.

Work on the development of methods for the determination of composition, volume, and density of the three phases in the UO_3-SO_3-H_2O system above 300°C is being continued. Several proposed techniques have been proved to be impractical without prolonged development and have been discarded.

Precise measurement of the acidity of uranyl sulfate solutions at 25°C as a function of the SO_4^{--} concentration and the UO_3 to SO_3 ratio has proved to be very useful in determining the solubility of UO_3 in uranyl sulfate solutions in the temperature range from 150 to 300°C.

Revised data for the liquid-liquid equilibrium and for hydrolytic precipitation from stoichiometric UO_2F_2 solutions are presented. The solid phase formed by hydrolytic precipitation in the low-concentration range has been identified as a solid solution between $UO_2(OH)_2$ and either $UO_2(OH)F \cdot \frac{1}{2}H_2O$ or $UO_2F_2 \cdot H_2O$.

Thorium Oxide Blanket Development

The results of runs completed during the quarter ending April 30, 1954, in which thorium oxide slurries were circulated at 250°C, confirmed earlier observations; the components most severely attacked were the pump and flow restrictor. The substitution of corrosion-resistant materials, such as platinum, gold, titanium, zirconium, and Zircaloy-2, for the 347 stainless steel orifices (flow restrictors) resulted in the minimization or elimination of the attack in these components. The use of titanium for the wear rings, impeller hubs, and impeller effectively reduced the attack in these areas.

Stainless steel in straight pipes and elbows has shown little, if any, attack by thorium oxide slurries at velocities below 20 fps.

It is concluded from the present data that attack consists in the removal of the protective oxide layer in the high-velocity areas, by chemical attack or abrasion, followed by a rapid chemical dissolution with continuous removal of the corrosion products by the slurry.

The least abrasive (in laboratory tests) thorium oxide slurry which has yet been prepared at a thorium concentration of 800 to 1000 g/liter was made from thorium hydroxide. This hydroxide was precipitated from thorium formate solution with ammonium hydroxide and dehydrated at 500°C; the resulting oxide was autoclaved in water at 250°C.

The addition of 10 mole % Al_2O_3 to ThO_2 partially inhibited the crystallization of the thoria. The Al_2O_3 was added by coprecipitation of the hydroxides and subsequent calcination of the mixtures at 545°C. The addition of 20 to 30 mole % Al_2O_3 and 10 to 40 mole % ZrO_2 or Bi_2O_3 in similar experiments did not inhibit the crystallization process.

Studies of the properties of thorium formate showed that it exists as the monohydrate at 100°C, becomes anhydrous at 125 to 175°C, and decomposes to the oxide at 225 to 250°C. The thorium concentration of a saturated aqueous solution of the formate was 57.62 g/liter at room temperature and 24 g/liter at 97°C.

Titanium metal exhibited approximately the same abrasive resistance as type 304 stainless steel when tested with slurries of SiC and high-burned ThO_2 in laboratory jet-impingement abrasion tests. The greater resistance to erosion of titanium as compared with stainless steel in the slurry-pumping studies may result from the formation of a stronger oxide film in water at 250°C or its more rapid replacement when abraded.

Chemical Processing

During the past quarter, chemical processing has been directed toward developing methods for removing plutonium from the blanket of a two-region aqueous homogeneous plutonium producer and for controlling the neutron poisons in the fuel solution of the thorium breeder. This work has consisted in studying the chemistry of neptunium in the plutonium-producer blanket solution, setting up facilities to develop and test suitable solid-liquid separation devices, determining the solubility of rare-earth fission products in the fuel solution of the thermal breeder, and initiating a study of the chemistry, in the reactor fuel solution, of those fission products which would contribute significantly to the radiation hazard of a fuel leak from a homogeneous reactor.

The present knowledge of plutonium behavior in uranyl sulfate solutions under reactor conditions indicates that plutonium containing only 0.5% Pu^{240} can be produced by removing insoluble PuO_2 as it forms. Preliminary results indicate that the solubility of neptunium under reactor conditions is greater than the Np^{239} concentration expected in the reactor at equilibrium. If the neutron-capture cross section of Np^{239} is of the same order of

magnitude as that of Pu^{239}, it will be necessary to devise some means of removing the neptunium as well as the plutonium.

Solubility data for individual rare-earth sulfates and mixtures of these salts in 0.02 *m* UO_2SO_4–0.005 *m* H_2SO_4 solution indicate that at 275°C the fuel solution of the two-region homogeneous reactor will contain less than 0.10 mg/ml of total rare-earth sulfates. Based on these data, neutron poisoning due to rare-earth fission products in the reactor fuel solution can be held below 2% by removing the precipitated rare-earth sulfates. At present, this scheme of processing appears more attractive than the CaF_2 process if a suitable solid-liquid separation device can be developed. The Vitro Corp. has estimated that the CaF_2 process with complete fluoride removal by evaporation will cost at least 0.5 mill per kilowatt-hour of electricity produced.

A review of solid-liquid separation devices has shown liquid-solid cyclones to be the most promising separation device. A facility to test liquid-solid cyclones at temperatures up to 100°C has been completed, and a test loop is being designed for testing these devices under reactor temperature and pressure.

Preliminary design calculations have been made for plutonium and heavy-water recovery processing of both the HRT and K-49 reactors.

Reports previously issued in this series are as follows:

ORNL-527	Date issued, December 28, 1949
ORNL-630	Period Ending February 28, 1950
ORNL-730	Feasibility Report – Date Issued, July 6, 1950
ORNL-826	Period Ending August 31, 1950
ORNL-925	Period Ending November 30, 1950
ORNL-990	Period Ending February 28, 1951
ORNL-1057	Period Ending May 15, 1951
ORNL-1121	Period Ending August 15, 1951
ORNL-1221	Period Ending November 15, 1951
ORNL-1280	Period Ending March 15, 1952
ORNL-1318	Period Ending July 1, 1952
ORNL-1424	Period Ending October 1, 1952
ORNL-1478	Period Ending January 1, 1953
ORNL-1554	Period Ending March 31, 1953
ORNL-1605	Period Ending July 31, 1953
ORNL-1658	Period Ending October 31, 1953
ORNL-1678	Period Ending January 31, 1954

~~CONFIDENTIAL~~

CONTENTS

ORNL-1753 (DEL)

~~CONFIDENTIAL~~

PART III. GENERAL HOMOGENEOUS REACTOR STUDIES

Part I

HOMOGENEOUS REACTOR EXPERIMENT

S. E. Beall, Project Engineer
J. J. Hairston, J. D. Jones
J. W. Hill, S. I. Kaplan
A. L. Johnson, R. Smith, Jr.
G. H. Johnstone, S. Visner

INTERNAL GAS-RECOMBINATION EXPERIMENTS[1]

The HRE experiments on internal recombination of radiolytic gas by Cu^{++} ion were completed at the close of the previous quarter. The final concentration of copper sulfate was approximately 0.06 M, or 150% of the estimated concentration required for complete recombination in a static system at 250°C, 1000 psi total pressure, and a uniform power density of 20 kw/liter. The feasibility of internal recombination of decomposition gases in a homogeneous reactor was conclusively demonstrated in the course of 350 hr of operating time at 0.06 M Cu^{++} concentration. The highest power level for which all the gas was internally recombined was 1350 kw. The information obtained at lower Cu^{++} concentrations was presented in the preceding progress report,[2] wherein it was noted that the copper behaved qualitatively as expected, to a first approximation, but that the model of a static reactor system was inadequate to explain entirely the effect of reactor temperature and pressure. For example, at a total pressure of 1000 psig, the recombination rate, which is controlled by the temperature and partial pressure of hydrogen, reached a maximum at a core-outlet temperature of 245°C instead of at the expected 260°C. Based on the nuclear behavior of the reactor, the temperature at the core outlet has been accepted to be the same as the average core temperature. It was pointed out that the presence in the core of a region at a temperature approximately 20°C higher than the core outlet, as has been suggested by mixing experiments in the core model and by the analysis of the "walk-away" phenomenon, would tend to resolve the discrepancies.

Data on the behavior of the HRE with 150% copper (i.e., 50% in excess of the theoretical amount for complete recombination), though somewhat limited by the deterioration of the seats in the dump valve and the gas bleed valve for the pressurizer, are presented in Table 1. Values corresponding to a core-outlet temperature of 235°C are plotted in Fig. 1. Straight-line extrapolations parallel to the "no-copper" line yield intercepts which represent the reactor power where gas first appears. These intercepts were used in an analysis[3] made on the basis of divided flow through the core, assuming that part of the solution goes through a hotter region which generates 15% of the power and part through the main

[1] In the planning and analysis of these experiments, the HRE Group was assisted by P. N. Haubenreich, H. F. McDuffie, and C. H. Secoy.

[2] S. E. Beall *et al.*, *HRP Quar. Prog. Rep. Jan. 31, 1954*, ORNL-1678, p 4-7.

[3] P. N. Haubenreich, unpublished report.

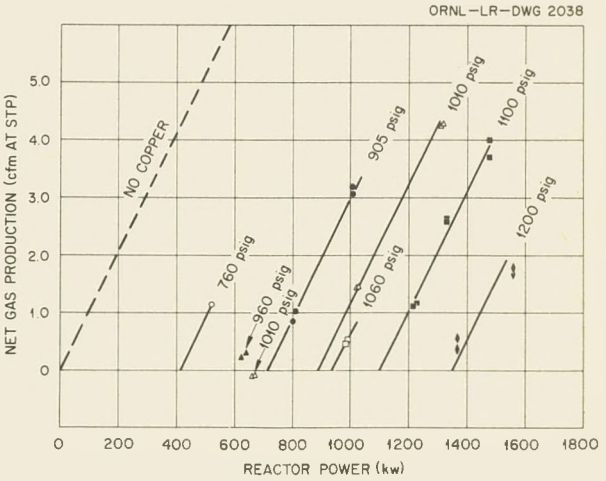

Fig. 1. Gas Production in HRE with 0.06 M Cu^{++} (150%) at a Core-Outlet Temperature of 235°C.

TABLE 1. INTERNAL GAS RECOMBINATION IN HRE WITH 0.06 M Cu^{++} (150%)*

Reactor Power (kw)	Total Reactor Pressure (psig)	Reactor Outlet Temperature (°C)	Gas Externally Recombined (cfm at STP)	Reactor Power Equivalent to Gas Internally Recombined (kw)	Cu^{++} Molarity
987	945	239	3.54	643	0.060
977	945	238	3.51	635	0.060
977	945	238	3.59	628	0.060
531	955	224	0.39	493	0.056
534	955	224	0.37	498	0.056
654	955	222	0.47	609	0.056
654	955	222	0.39	616	0.056
641	960	236	0.29	612	0.060
625	955	236	0.22	603	0.060
660	960	240	0.29	631	0.060
647	960	240	0.29	618	0.060
874	880	230	3.34	549	0.057
893	890	231	3.14	587	0.057
527	765	236	1.15	415	0.060
906	1020	228	0.74	834	0.057
884	1020	227	0.64	822	0.057
1310	1010	236	4.25	899	0.060
1320	1010	237	4.28	904	0.060
660	1010	236	−0.12	672	0.060
674	1005	236	−0.10	684	0.060
1026	1020	236	1.43	887	0.060
1030	1030	237	1.45	889	0.060
996	1060	234	0.52	946	0.060
993	1050	234	0.44	950	0.060
1003	1010	244	1.82	826	0.062
1003	1000	244	1.84	824	0.062
987	1005	245	1.50	841	0.062
947	1005	244	1.40	838	0.062
977	1025	245	1.20	860	0.062
1120	1020	244	2.21	905	0.062
1120	1000	244	2.60	866	0.062
1370	1180	235	0.54	1317	0.060
1370	1200	235	0.37	1354	0.060
784	1010	259	1.23	664	0.068
790	1000	260	1.74	620	0.068
940	1010	259	2.14	732	0.068
940	1010	259	2.26	770	0.068
1050	1105	259	1.30	923	0.068
1050	1105	259	1.25	928	0.068
1010	1030	245	1.45	869	0.062
1010	1030	246	1.52	861	0.062
1230	1110	236	1.15	1118	0.062
1220	1110	236	1.13	1110	0.060
1330	1120	236	2.60	1076	0.060
1330	1110	235	2.65	1078	0.060
1560	1210	236	1.77	1388	0.060
1560	1210	237	1.72	1393	0.060
1220	1210	260	0.64	1158	0.068
1220	1215	259	0.66	1153	0.068
1480	1200	257	1.43	1341	0.067
1470	1200	257	1.35	1358	0.067
1500	1210	258	1.72	1333	0.067
1490	1210	259	1.33	1361	0.068
1240	1120	259	2.16	1030	0.068
1230	1120	258	2.04	1030	0.067
806	905	235	0.86	722	0.060
812	905	235	1.03	712	0.060
1010	900	234	3.19	699	0.060
1010	900	234	3.07	711	0.060
1480	1100	234	4.00	1090	0.060
1460	1100	233	3.64	1101	0.060

*With no copper in the reactor, stoichiometric gas is produced at the rate of 10.5 cfm per 1000 kw at STP.

body of the core which generates 85% of the power. The temperature of the main body is within a few degrees of that of the core outlet, while the temperature of the hot central region increases with power level, being approximately 30°C above the outlet temperature at 1000 kw. The gas-recombination rates, as equivalent reactor power (reactor power at which gas first appears), calculated for both the one- and the two-temperature-region models, are shown in Fig. 2, in which they are plotted against the total reactor pressure. The experimental points are plotted for comparison. The curve calculated for a two-temperature-region core is in somewhat better agreement with the data than the curve based on a single-region-core model. Although no question about the adequacy of copper as an internal catalyst remained, a more thorough investigation of the minor inconsistencies between the static bomb tests and the HRE dynamic tests would have been desirable. Unfortunately, such an investigation was not possible because only a fairly limited range of power, temperature, and pressure could be obtained with the HRE at this time.

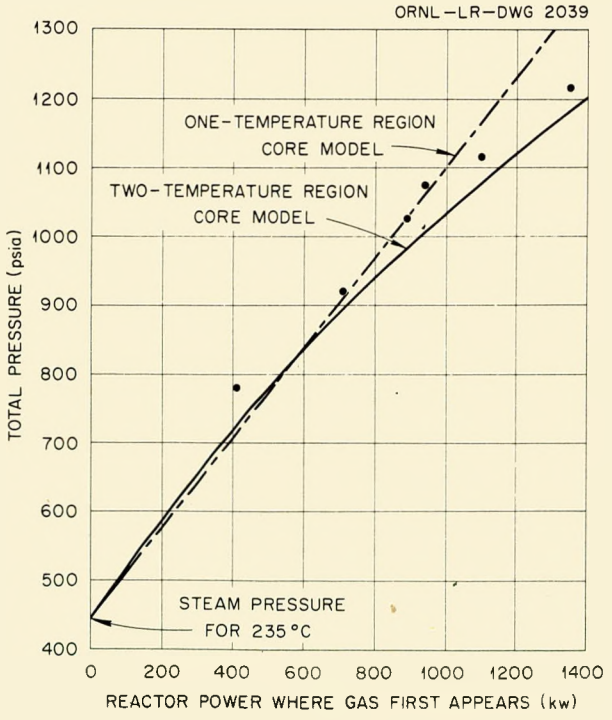

Fig. 2. Gas Recombination as a Function of Reactor Pressure with 0.06 M Cu^{++} at a Core-Outlet Temperature of 235°C.

FINAL EXPERIMENT – Xe^{135} GAS COLLECTION

After completion of the scheduled experiments on internal gas recombination, the reactor was operated on three separate occasions to permit the collection of a sufficient quantity of Xe^{135} gas for neutron-absorption cross-section studies.

The gas-collection equipment, which consisted primarily of a liquid-nitrogen-cooled charcoal bed, was attached to the reactor off-gas line downstream from the cold traps. Several thousand curies of the xenons and kryptons was collected and permitted to decay on the charcoal until only the isotope of interest, Xe^{135}, remained. In the final run, a total of about 1000 curies of the pure isotope was produced for the Physics Division. The collection of the gas was made by Chemistry Division personnel under the supervision of G. W. Parker.

HRE DECONTAMINATION AND DISMANTLING

Following completion of the runs for Xe^{135}, the fuel solution was concentrated and stored in the underground storage tanks. Decontamination was begun with cell-activity levels at several thousand roentgens per hour. After all equipment had been rinsed with hot water, 8 M HNO_3 was added to the system; after rinsing again, a 10% caustic solution which contained 1.5% tartaric acid and 1.5% hydrogen peroxide was added. These solutions were chosen for a mild action on the base metal so that its condition, with respect to previous corrosion by the fuel solution, would not be altered. Several successive cycles of the decontaminating solution and decay during the 30-day shutdown period reduced the levels of radioactivity to 20 to 50 r/hr.

While the fuel system was being decontaminated, the heavy water was removed from the reflector system, and it was found that about 165 lb, equivalent to about 5% per year, had been lost during 24 months of operation. The radioactivity in the reflector system was negligible, and the components were removed from the cell during the third week after shutdown. Removal of the main fuel heat exchanger and circulating pump was accomplished during the fifth week; the fuel cell or low-pressure system was dismantled during the sixth and seventh weeks. The reactor core assembly was removed next and, as expected, was more radioactive (about 300 r at a distance of 1 ft) than any other part.

The entire disassembly has proceeded much more rapidly than had been expected and should be completed by June 1. Most of the work was accomplished with a remote hacksaw and cutting torch. Personnel exposures have been kept to reasonable levels. Valuable assistance is being given by small groups of enlisted Navy personnel from KAPL.

DISTRIBUTION OF FISSION PRODUCTS IN THE HRE[4]

At the time of final shutdown, the HRE had operated for a total of 580 Mwhr. Based on the amount of fission products produced per liter of fuel solution, this operation time would correspond to about 10 days of full-power operation of either of the proposed K-23 or K-49 reactors. After shutdown, the HRE fuel was drained from the system, and the system was washed repeatedly with water until only traces of uranium were present in the wash solution. The system was then decontaminated by two treatments each of 35% nitric acid; 5% nitric acid; a solution of 10% sodium hydroxide, 2.5% sodium tartrate, and 1.5% hydrogen peroxide; and by numerous water washes.

The fuel solution, the solids contained in the fuel, and the decontamination solutions were analyzed for major long-lived fission products. The distribution of fission-product activities observed in these solutions was calculated as the ratio of the sum of the radioactivity observed in the solids suspended in the fuel solution and that removed during decontamination of the HRE to the radioactivity found in the fuel solution itself (Table 2). It should be pointed out that, while these data give a good indication of the distribution of activity between solid and liquid phases, they do not necessarily describe the distribution of fission products during actual operation of the reactor; the separation of phases was made at room temperature several days after the reactor was shut down. However, in most cases the ratios are so large that the fission products probably were either strongly adsorbed on the scale inside the reactor system or had very low solubility in the fuel solution and settled in the equipment while draining.

Of all the elements checked, only cesium was found to be completely in solution. Other than cerium and lanthanum, 80% of the rare-earth activities was also solution. (Based on laboratory data, the rare earths had not exceeded their solubility limit under reactor conditions.) Half the cerium was in solution, and no La^{140} was detected in the fuel solution. This apparent separation of rare earths is probably due to the barium parent of La^{140} being precipitated as it was formed. There is no apparent reason for the precipitation of cerium.

More than 90% of the activity due to the zirconium, niobium, barium, ruthenium, and iodine either was found in the solid suspended in the fuel or was deposited on the surfaces of the reactor system. This fact, plus the fact that 40 times as much of the gross gamma activity was removed during the decontamination of the reactor as was contained in the fuel solution, indicates that essentially all the fission products that are strong gamma emitters were adsorbed on the equipment or precipitated in the system.

TABLE 2. DISTRIBUTION OF FISSION PRODUCTS IN HRE

(Data obtained at room temperature after reactor shutdown)

Element	Ratio of Activity Out of Solution to Activity in HRE Soup*
Gross β	1.4
Gross γ	40
Zr	90
Nb	40
Cs	0.1
Ba	30
Sr	1
Ru	30
Ce	1
Other rare earths:	
β emitting (excludes only Ce)	0.2
γ emitting (> 95% was La^{140})	30
	20

*The activity out of solution was taken as the sum of the activity in the solids suspended in the fuel solution and the activity removed in decontaminating the HRE. These values are based on incomplete analytical data and should be considered as preliminary order-of-magnitude estimates.

[4]Contribution of D. E. Ferguson, D. O. Campbell, and D. C. Overholt of the Chemical Technology Division.

Part II
HOMOGENEOUS REACTOR TEST
REACTOR ANALYSIS

M. C. Edlund, Section Chief
H. C. Claiborne
J. P. DiLorenzo
T. B. Fowler
P. R. Kasten
L. C. Noderer
M. Tobias
V. K. Paré
P. M. Wood

STATICS CALCULATIONS FOR THE HRT

Method

Criticality calculations for the HRT based on the harmonics method[1] have been completed for three reflector systems: D_2O, ThO_2 slurry, and unenriched UO_2SO_4 solutions. Since the previous quarter, convergence of the extended harmonics method has been tested[1] for the ThO_2 slurry and UO_2SO_4 reflectors. The integral properties, absorptions in the core and the reflector, and neutron leakages, are given for the HRT to within 5% by the use of only two harmonics.

Data

Since the critical concentration of the HRT is strongly temperature dependent, the effect of chemical binding on the diffusion coefficient of thermal neutrons in D_2O was calculated[2] as a function of D_2O temperature. The scattering cross section for a deuteron in heavy water has a constant value of 3.35 barns above 0.5 ev and apparently gradually increases to about 7 barns as the neutron energy is reduced to 0.005 ev. This increase is explained if the Born approximation is used and if it is assumed that the cross section is proportional to the square of the reduced mass of the neutron-deuteron system, since at lower energies chemical binding increases the apparent mass of the deuteron.

If A is the apparent deuteron mass and σ_d is the deuteron scattering cross section, then, since the mass of the free deuteron is 2,

$$(1)\quad \sigma_d(A) = \left(\frac{2+1}{2}\right)^2\left(\frac{A}{A+1}\right)^2 \sigma_d(2) = \frac{9}{4}\left(\frac{A}{A+1}\right)^2 \sigma_d(2) .$$

The average cosine of the scattering angle in the laboratory system $\overline{\mu_d}$ is given by

$$(2)\quad \overline{\mu_d} = \frac{2}{3A}$$

For a given velocity, σ_d and σ_o (where the subscript o refers to oxygen) are obtained from AECU-2040. Equations 1 and 2 are solved for $\overline{\mu_d}$, and the diffusion coefficient D as a function of velocity is given by

$$(3)\quad D(v) = \frac{1}{3N}\,\frac{1}{2(1-\overline{\mu_d})\sigma_d + (1-\overline{\mu_o})\sigma_o} ,$$

where N is the number of D_2O molecules per cubic centimeter.

As a function of temperature, D is obtained from the following by numerical integration:

$$(4)\quad D(T) = \frac{\int_0^\infty D(v)\, v\, M_T(v)\, dv}{\int_0^\infty v\, M_T(v)\, dv} ,$$

where $M_T(v)$ is the Maxwellian velocity distribution corresponding to temperature T. Results for $N = 1.103$ g/cc are shown below:

Temperature (°C)	D (cm)
20	0.839
50	0.852
100	0.872
150	0.891
200	0.910
250	0.926
280	0.936
300	0.942
320	0.951

The value of D at 20°C (0.839) agrees with other experimental work, 0.83 ± 0.03 (Dexter *et al.*)[3] and 0.84 ± 0.01 (Woods *et al.*),[4] in which thermal-

[1] M. C. Edlund and L. C. Noderer, *An Harmonics Method Applied to D_2O Moderated Reactors*, ORNL CF-54-3-120 (March 18, 1954).

[2] L. C. Noderer, *Temperature Dependence of the Neutron Diffusion Coefficient in Heavy Water*, ORNL CF-54-4-142 (April 20, 1954).

[3] A. H. Dexter, B. Hamermesh, E. W. Hones, P. A. Morris, and G. R. Ringo, *Quarterly Report for September, October and November, 1951*, ANL-4746, p 14.

[4] D. C. Woods, S. W. Kash, and E. Martin, *Reactor Physics Quarterly Progress Report*, NAA-SR-230 (March 16, 1953), p 8.

neutron relaxation lengths in D_2O were measured with various additions of B_2O_3. A summary of the other data used in the calculations is given by P. M. Wood.[5]

CRITICAL CONCENTRATIONS

The critical concentrations for the three blanket systems are given in Figs. 3 and 4. The conversion ratios and the blanket-to-core power ratios for the low-enrichment UO_2SO_4 solution blankets are given in Table 3.

NEUTRON FLUXES AND ADJOINT FUNCTIONS

The fast and slow fluxes and adjoint functions at the expected operational mean temperature of 280°C were calculated[6] by the standard two-group method in which the age was adjusted so that the predicted critical concentration would be the same as that for the harmonics method with a Gaussian-Yukawa kernel. The results for a D_2O reflector and a low-enrichment uranyl sulfate blanket are given in Figs. 5 and 6. The thermal-neutron fluxes and fast and slow leakages for a core power of 5 Mw are given in Table 4.

CORE-CONCENTRATION AND TEMPERATURE COEFFICIENTS OF REACTIVITY

The core-concentration coefficient of reactivity dk_{eff}/dc, Fig. 7, was obtained by differentiating the critical equation. The uniform-temperature coefficient of reactivity $(dk_{eff}/dT)_U$ is then readily obtained from the slope of the critical concentration–temperature curve and the concentration coefficient of reactivity. When the temperature coefficient is obtained this way, it is assumed that

[5] P. M. Wood, *Constants for HRT Nuclear Calculations*, ORNL CF-54-3-160 (March 30, 1954).

[6] P. M. Wood, *Flux Distribution in HRT with 300 g/liter Natural Uranium Blanket*, ORNL CF-54-3-142 (March 22, 1954).

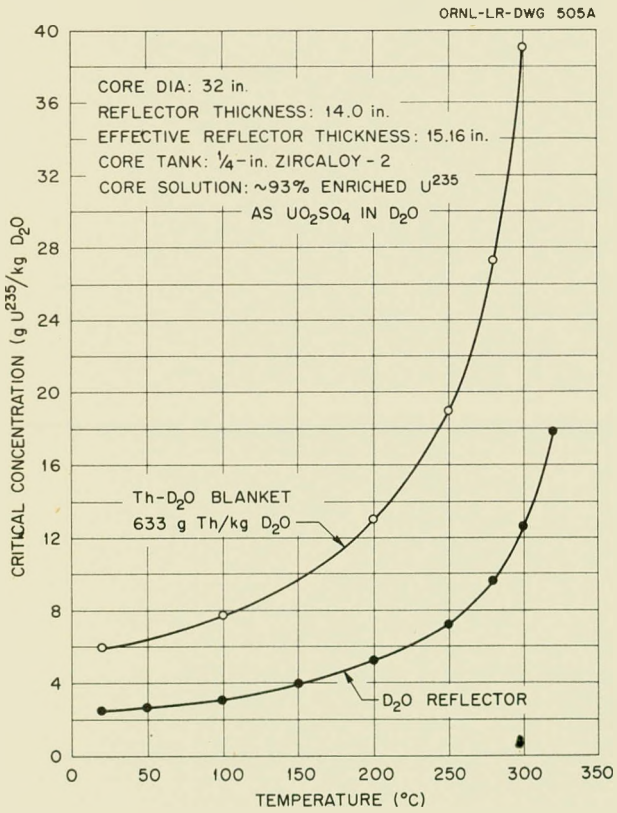

Fig. 3. Critical Concentration of U^{235} in Core of HRT with Th-D_2O Blanket.

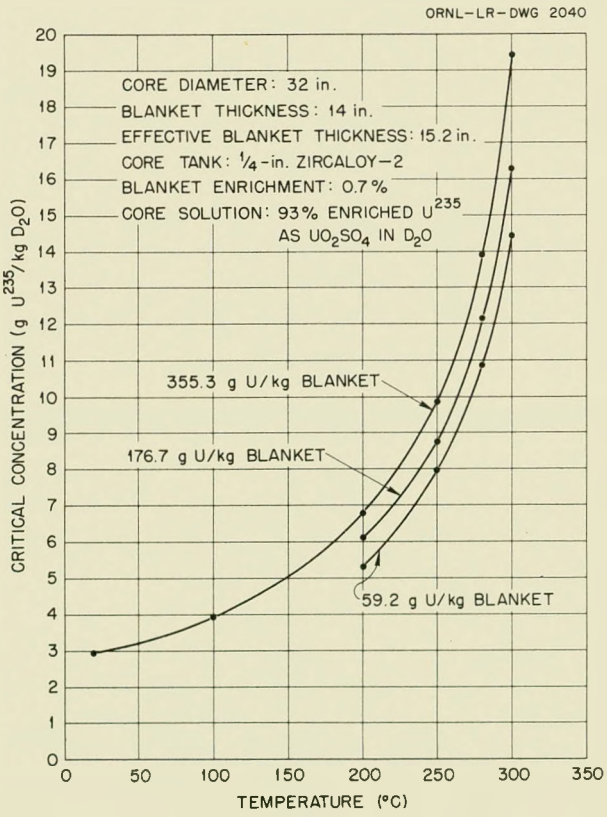

Fig. 4. Critical Concentration of U^{235} in Core of HRT with UO_2SO_4-D_2O Blanket.

TABLE 3. CONVERSION RATIOS AND BLANKET-TO-CORE RATIOS FOR LOW-ENRICHMENT UO_2SO_4 SOLUTION BLANKETS

Reactor Temperature	Blanket Enrichment (wt % of U^{235})	Blanket Concentration (g of U per kg of D_2O)	Critical Core Concentration (g of U^{235} per kg of D_2O)	Conversion Ratio			Pu per day (g) at 5 Mw Core Power
				C_R [a]	C_c [b]	$\frac{P_b}{P_c}$ [c]	
200	0.7	355.3	6.75	0.498	0.776	0.571	5.2
250	0.7	355.3	9.81	0.486	0.702	0.453	4.7
280	0.7	355.3	13.9	0.436	0.589	0.354	3.9
300	0.7	355.3	19.4	0.417	0.543	0.303	3.6
280	0.4	355.3	15.2	0.463	0.556	0.202	3.7
280	0.25	355.3	15.8	0.476	0.535	0.125	3.6
200	0.7	176.7	6.08	0.364	0.500	0.378	3.35
250	0.7	176.7	8.71	0.337	0.435	0.295	2.92
280	0.7	176.7	12.1	0.316	0.390	0.237	2.61
300	0.7	176.7	16.3	0.298	0.355	0.193	2.38
280	0.4	176.7	12.8	0.326	0.369	0.130	2.47
280	0.25	176.7	13.8	0.336	0.364	0.084	2.44
200	0.7	59.2	5.29	0.201	0.234	0.165	1.56
250	0.7	59.2	7.94	0.182	0.204	0.109	1.37
280	0.7	59.2	10.8	0.171	0.187	0.096	1.26
300	0.7	59.2	14.4	0.167	0.180	0.083	1.20
280	0.4	59.2	11.1	0.173	0.183	0.053	1.22
280	0.25	59.2	11.2	0.174	0.180	0.033	1.21

[a] $C_R = \frac{\text{Atoms } Pu^{239} \text{ formed}}{\text{Atom } U^{235} \text{ destroyed in reactor}}$.

[b] $C_c = \frac{\text{Atoms } Pu^{239} \text{ formed}}{\text{Atom } U^{235} \text{ destroyed in core}}$.

[c] $\frac{P_b}{P_c} = \frac{\text{Blanket power}}{\text{Core power.}}$

TABLE 4. THERMAL-NEUTRON FLUXES AND FAST AND SLOW LEAKAGES FOR A CORE POWER OF 5 Mw

	D_2O	355 g of Natural U per kg of D_2O	633 g of Th per kg of D_2O
Average thermal flux in core (neutrons/sq cm·sec)	8.2×10^{13}	6.1×10^{13}	2.9×10^{13}
Maximum thermal flux in core (neutrons/sq cm·sec)	1.1×10^{14}	8.8×10^{13}	4.6×10^{13}
Average thermal flux in blanket (neutrons/sq cm·sec)		2.0×10^{13}	9.1×10^{12}
Fast-neutron leakage out of reflector (neutrons/sec)	5.1×10^{16}	1.1×10^{17}	5.8×10^{16}
Slow-neutron leakage out of reflector (neutrons/sec)	1.6×10^{17}	8.5×10^{16}	3.6×10^{16}

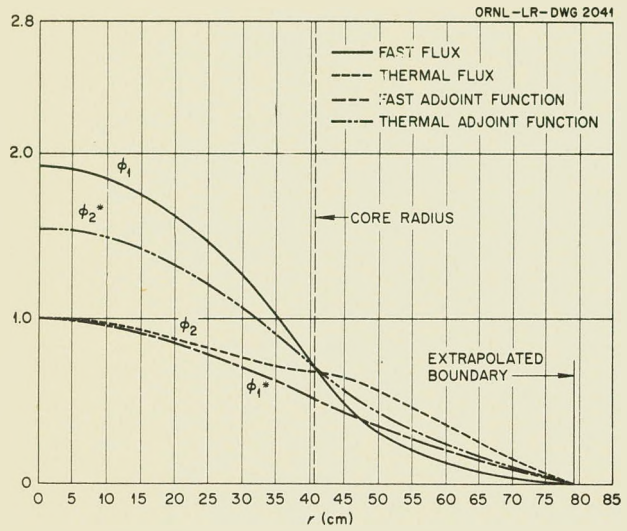

Fig. 5. Flux and Adjoint Functions in HRT at 280°C with D_2O Reflector.

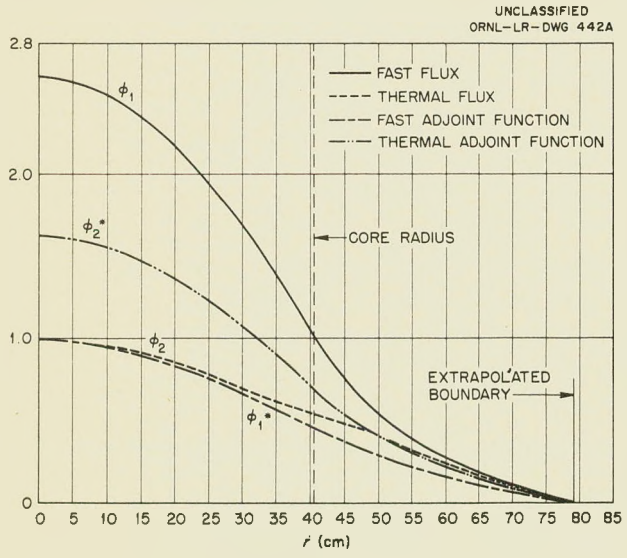

Fig. 6. Flux and Adjoint Functions in HRT at 280°C with 300 g of Natural Uranium per Liter of Blanket.

there is a uniform temperature throughout the reactor. Values of $(dk_{eff}/dT)_U$ for the reactor with D_2O reflector, 355 g of natural uranium per kilogram of D_2O and 633 g of thorium per kilogram of D_2O blanket, are plotted in Fig. 8 and listed in Table 5. The temperature coefficients with respect

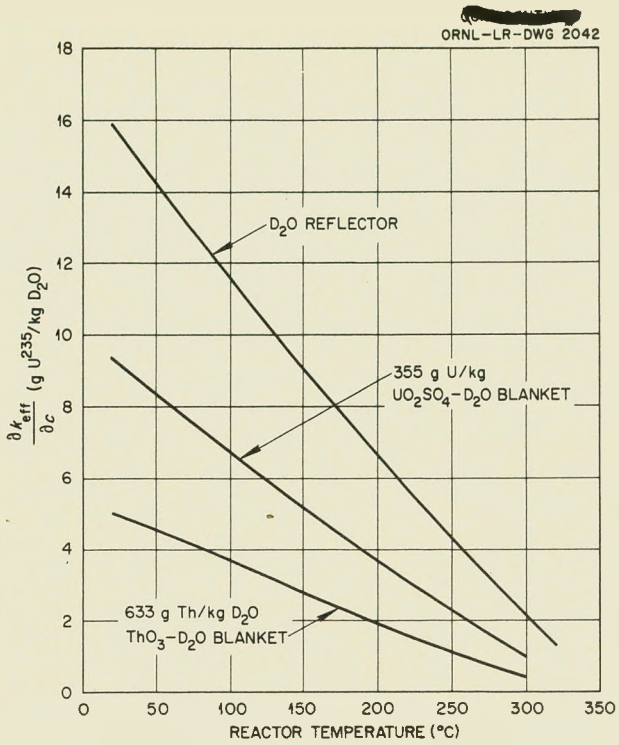

Fig. 7. Core-Concentration Coefficient of Reactivity in HRT.

to core temperature are considered in "Kinetic Studies of the HRT," which follows.

MEAN LIFETIME OF PROMPT NEUTRONS

The mean lifetime of prompt neutrons can be estimated by adding a $1/v$ neutron absorber, Σ_a, uniformly to the entire reactor and calculating $(\partial k_{eff}/\partial \Sigma_a)_{k_{eff}=1}$. The lifetime is then given by

$$\tau = -\frac{1}{v}\left(\frac{\partial k_{eff}}{\partial \Sigma_a}\right)_{k_{eff}=1},$$

where v is the average thermal-neutron velocity.

KINETIC STUDIES OF THE HRT

The response of the HRT to increases of reactivity should be similar to that observed for the HRE. The reactor model considered by Welton *et al.*[7] and Sangren[8] seems to be a reasonable one for estimating

[7] T. A. Welton *et al.*, *HRP Quar. Prog. Rep. Aug. 15, 1951*, ORNL-1121, p 87.

[8] W. C. Sangren, *Kinetic Calculations for Homogeneous Reactors*, ORNL-1205 (April 15, 1952).

TABLE 5. UNIFORM-TEMPERATURE COEFFICIENTS OF REACTIVITY FOR THE REACTOR WITH D_2O REFLECTOR AND THORIUM BLANKET

Reactor Temperature (°C)	D_2O Reflector (sec^{-1})	355 g of Natural U per kg of D_2O (sec^{-1})	633 g of Th per kg of D_2O (sec^{-1})
20	1.24×10^{-3}		
100	1.18×10^{-3}		
200	7.8×10^{-4}		
280	5.6×10^{-4}	3.4×10^{-4}	1.8×10^{-4}
300	5.0×10^{-4}		1.5×10^{-4}

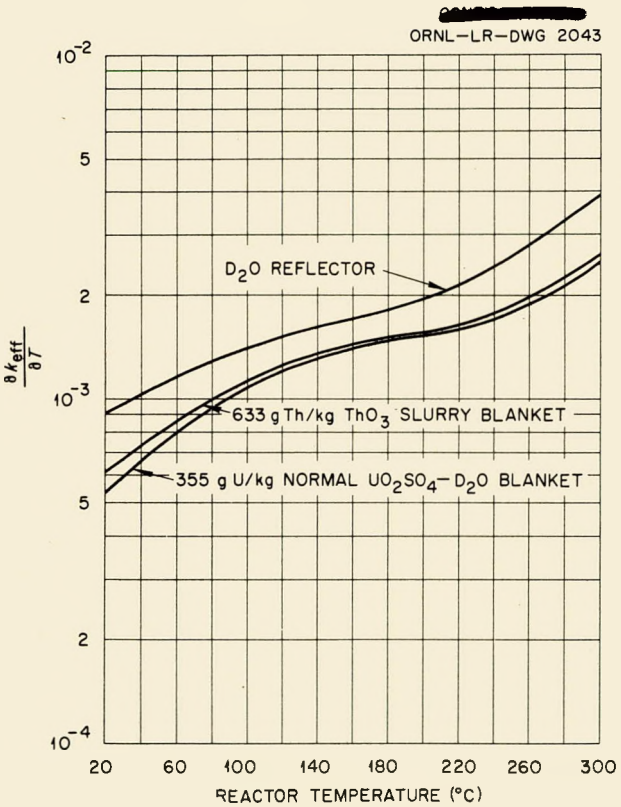

Fig. 8. Temperature Coefficient of Reactivity for HRT.

power and pressure surges for the HRT. A comparison of the prompt-neutron generation time τ, the core temperature coefficient $\partial k_{eff}/\partial T_c$, the mechanical frequency ω_H, the effective fraction of delayed neutrons β, and the nuclear frequency ω_n at operating power for the HRE and HRT is given in Table 6.

The limiting variable for the safety of the HRT during a power surge appears to be the pressure difference between the core and blanket. When the core pressure exceeds the pressure in the blanket by about 250 psi, the rather thin zirconium core tank is estimated to yield. This problem is being studied, and some preliminary results are given below.

The HRT, with any of the three blanket systems, appears to be stable against oscillations caused by coupling of the pressurizer system and the delayed neutrons which were first discussed by G. Trammell. Stability conditions have been calculated and are given in another part of this report.

Analysis of the operational behavior of the reactor system as a whole is now in progress.

CORE-PRESSURE RISE ASSOCIATED WITH INCREASES OF REACTIVITY

To obtain information about the safety of the HRT, the core-pressure rise has been calculated[9] as a function of reactivity added instantaneously to the HRT. Preliminary results obtained for the present HRT pressurizer arrangement (Fig. 9) indicate that the pressure rise in the core is less than 200 psi for reactivity steps up to 1.5%. The length of the pressurizer pipe (L) is 10 ft.

Calculations were made with a modification of the short formulas discussed by Welton *et al.*[7] The nonlinear equations of motion are being coded for integration by the ORACLE.

The curves in Fig. 9 corresponding to v_s = 2380 fps (v_s is the velocity of sound in the core solution) are for the case of no gas present in the core, and

[9] P. R. Kasten and V. K. Pare', *Safety of HRT*, ORNL CF-54-3-164 (March 25, 1954).

TABLE 6. COMPARISON OF NUCLEAR CHARACTERISTICS OF HRE AND HRT

	HRE Reflector, D_2O	HRT Reflectors		
		D_2O	355 g of U per kg of D_2O	633 g of Th per kg of D_2O
τ (sec)	0.837×10^{-4}	5.6×10^{-4}	3.4×10^{-4}	1.8×10^{-4}
$\frac{\partial k_{eff}}{\partial T_c}$ ($^\circ C^{-1}$)	1.6×10^{-3}	1.8×10^{-3}	1.8×10^{-3}	2.0×10^{-3}
ω_H^2 (sec^{-2})	2.5×10^4	2.5×10^3	2.5×10^3	2.5×10^3
ω_n^2 (sec^{-2})	48	25	63	126
β	5×10^{-3}	5×10^{-3}	5×10^{-3}	5×10^{-3}

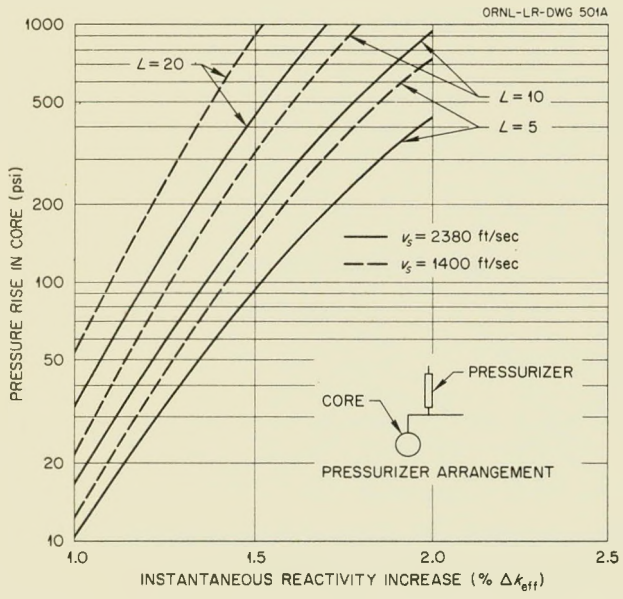

Fig. 9. Pressure Rise in HRT Core Vessel as a Function of Instantaneous Reactivity Increase, Length of Pressurizer Pipe (L), and Compressibility of Core Fluid (v_s).

those corresponding to v_s of 1400 fps represent the core with the lowest possible compressibility for the core medium. The results show the importance of pipe length and compressibility on the core-pressure rise, which decreases with decreasing L and increasing v_s.

In the HRT the most rapid increase of reactivity probably results from starting the fuel-circulating pump with the core at low power and design temperature (280°C) and cold fuel (100°C) in the heat exchanger. A rough estimate of the resulting rate of increase of k_{eff} without taking into account the statistical weight of the core entrance region and the flow of the cooler fluid gives 3.4%/sec. A two-group perturbation calculation[10] gives a considerably lower maximum rate of 1.4%/sec. The residual power of the reactor following a month of shutdown after a month of operation at 5 Mw will be about 2 kw, about 1 w of which is neutron power. A linear increase of reactivity in the HRT is related to an equivalent step change as a function of initial reactor power in Fig. 10, which shows that for an initial neutron power level of 1 w a rate of increase of reactivity of 1.4%/sec is equivalent to adding about 1.4% reactivity instantaneously. At 1 w, no gas would be present within the reactor core, and so the maximum core-pressure rise is estimated to be about 110 psi for a 10-ft pressurizer pipe length.

LINEARIZED STABILITY CRITERIA FOR CORE-PRESSURIZER SYSTEM OF HRT

The stability against oscillations caused by coupling of the core-pressurizer system, as determined from the linearized equations of mo-

[10] V. K. Pare', *Reactivity Effects of Non-Uniform Density Changes in HRT*, ORNL CF-54-4-182 (April 26, 1954).

tion,[11,12] has been investigated, and the results have been given in graphical form. Stability from small power oscillations is assured as long as operating conditions lie to the right or above the appropriate curve in Figs. 11–13.

[11]G. Trammell, *HRP Quar. Prog. Rep. Aug. 15, 1951*, ORNL-1121, p 88.

[12]P. R. Kasten, *Linearized Stability Criteria for HRT Type Reactors*, ORNL CF-54-4-183 (April 21, 1954).

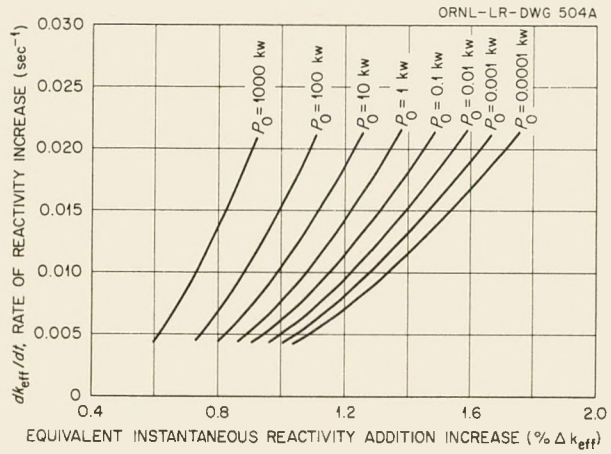

Fig. 10. Equivalent Instantaneous Reactivity Addition as a Function of the Rate of Reactivity Increase in the HRT, with Initial Reactor Power Level as a Parameter.

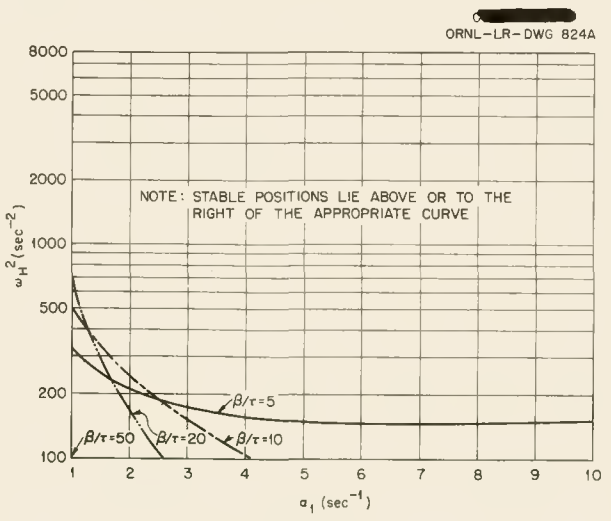

Fig. 11. Linearized Stability Criteria for HRT Type Reactors with $\omega_n^2 = 50$ sec^{-2}.

For the HRT the stability criteria are satisfied for all operating conditions presently proposed. However, as the power density is increased, the operating point shifts toward the region of instability. Above a power density of about 200 kw/liter, UO_2SO_4 blanket (values for ThO_2 and D_2O blankets are 100 and 400 kw/liter, respectively), linearized instability may occur. Operation in the so-called "unstable region" may be allowable, however, since nonlinear terms neglected in the analysis

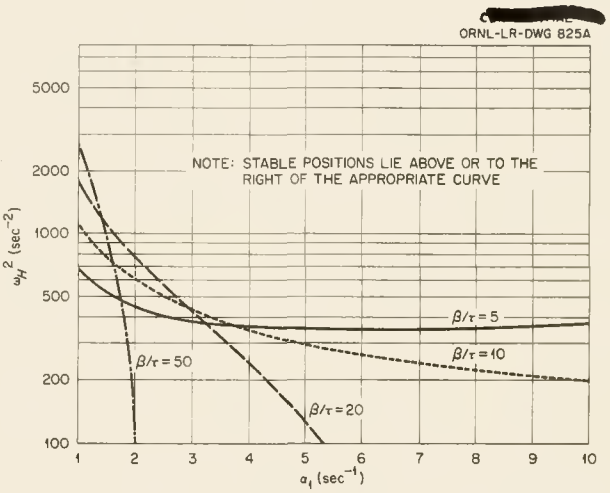

Fig. 12. Linearized Stability Criteria for HRT Type Reactors with $\omega_n^2 = 100$ sec^{-2}.

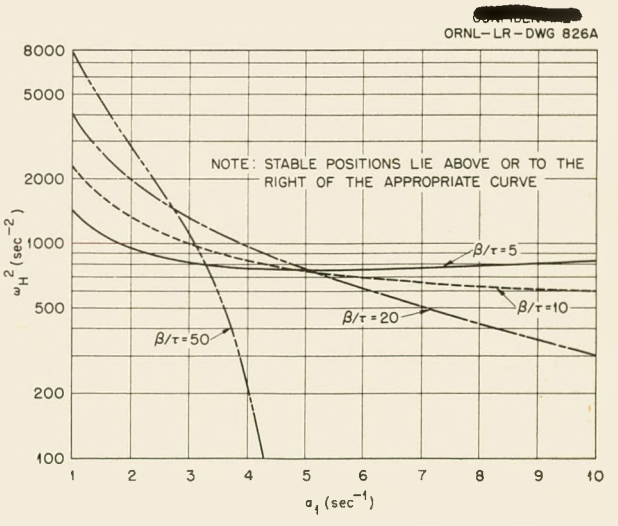

Fig. 13. Linearized Stability Criteria for HRT Type Reactors with $\omega_n^2 = 200$ sec^{-2}.

here may limit any power and pressure oscillations which result.

The condition which must be satisfied to ensure stability is

$$\alpha_1 \frac{\beta}{\tau}\left[\omega_b^2 + \frac{\beta}{\tau}\alpha_1 + \left(\frac{\beta}{\tau}\right)^2\right] > \left(\alpha_1 + \frac{\beta}{\tau}\right)^2 \omega_n^2 > 0 ,$$

where

α_1 = normalized friction coefficient, sec^{-1},
β/τ = (effective fraction of fission neutrons which are delayed)/(average lifetime of prompt neutrons), sec^{-1},
ω_b^2 = square of frequency of uncoupled hydraulic system, sec^{-2},
ω_n^2 = square of frequency of uncoupled nuclear system, sec^{-2}.

The operating point is that point which corresponds to actual values for ω_b^2 and α_1. If this point is above the curve or to the right of it for the appropriate value of β/τ on the figure having the appropriate ω_n^2, the reactor system is stable against small oscillations of pressure and power. The HRT values of ω_b^2, ω_n^2, α_1, and β/τ for P_0 = 5000 kw and v_s = 2000 fps as a function of the different blanket materials are listed in Table 7.

The operating points given in Table 7 all lie within the stable region.

TABLE 7. VALUES FOR ω_b^2, ω_n^2, α_1, AND β/τ FOR REASONABLE HRT OPERATING CONDITIONS AS A FUNCTION OF BLANKET MATERIAL

		Blanket Material		
		D_2O	UO_2SO_4	ThO_2
ω_b^2 (sec^{-2})	L^*= 10	2500	2500	2500
	L = 5	5000	5000	5000
ω_n^2 (sec^{-2})		25	63	126
α_1 (sec^{-1})	L = 10	6.8	6.8	6.8
	L = 5	2	2	2
β/τ (sec^{-1})		10	25	50

*L = length in feet between core and surface of pressurizer.

REACTIVITY EFFECTS OF NONUNIFORM DENSITY CHANGES

The temperature and density variables in the equations of motion (Eqs. 6–9, Ref. 8) which have been used to study the dynamics of homogeneous reactors are space averages over the multiplying region. These variables are entirely adequate for the study of the initial response of the reactor to rather large reactivity increases, as a result of which the peak of a power surge is reached in a time interval which is small compared with the transit time of the fuel through the core. Under these conditions the change in temperature has nearly the same spatial distribution as does the power. As a first-order approximation, the effect of nonuniform temperature, and hence density change, is merely an alteration of the density coefficient of reactivity in the space-independent equations of motion.

The above effect as compared with the effect on the core-temperature coefficient of a reflected reactor is, of course, greatest for a bare reactor. The temperature coefficient of reactivity for a cube where the temperature change is taken proportional to the power distribution is $(4/3)^3$ times as large as the coefficient calculated by using the average temperature. In the case of the HRT, this factor is less than 1.10 for all three blankets.

Results of calculations[10] for the HRT at 280°C with various blankets are given in Table 8.

Two-group importance functions for density changes have been computed for calculating these coefficients and reactivity changes due to changes in inlet fuel temperatures. The results for shutdown and restarting of the fuel-circulating pump were given above. The expression obtained from two-group perturbation theory for the change in k_{eff} caused by a change in density is

$$\Delta k_{eff} = \frac{\iiint_V \left(\frac{\Delta\rho}{\rho_0} F + \frac{\Delta\rho}{\Delta\rho + \rho_0} G - \frac{\Delta T}{2T_0} H\right) dV}{\iiint_V \frac{K}{P} \Sigma_s \phi_s \phi_f^* \, dV} ,$$

where

$$H = \Sigma_s \phi_s \left(\frac{K}{P}\phi_f^* - \phi_s^*\right) ,$$

$$F = H + \Sigma_f \phi_f (P\phi_s^* - \phi_f^*) ,$$

$$G = D_s \bar{\nabla}\phi_s \times \bar{\nabla}\phi_s^* + D_f \bar{\nabla}\phi_f \times \bar{\nabla}\phi_f^* ,$$

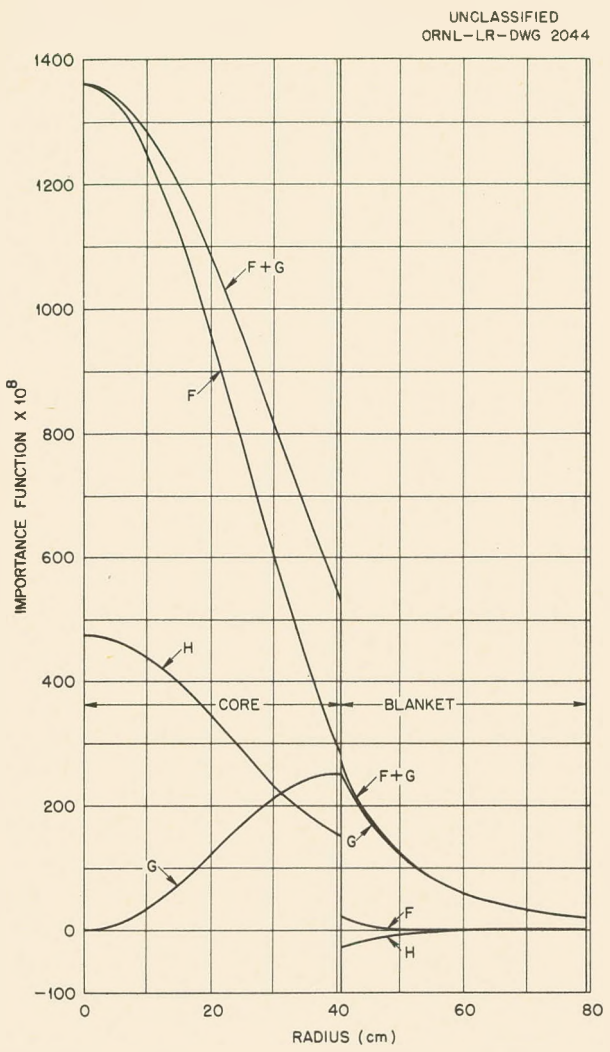

Fig. 14. Importance Functions for Density Changes in HRT at 280°C with Blanket Containing 355 g of Normal Uranium per Kilogram of D_2O.

ϕ = flux,
Σ = absorption cross section,
D = diffusion constant,
K = infinite multiplication constant,
P = resonance escape probability,
ρ_0 = critical density,
$\Delta\rho$ = change in density,
T_0 = critical absolute temperature,
ΔT = change in temperature,
V = reactor volume,
f = fast,
s = slow (thermal),
$*$ = adjoint.

The importance functions F, G, and H are plotted in Fig. 14 for the case of 355 g of normal uranium per kilogram of D_2O in the blanket. For this reactor,

$$\iiint_V \frac{K}{P} \Sigma_s \phi_s \phi_f^* \, dV$$

has the value 3.422. F and G determine the change of k_{eff} with density at constant temperature, and H determines the change of k_{eff} with temperature at constant density, assuming $1/v$ dependence of all thermal absorption cross sections.

TABLE 8. VALUES OF $\partial k_{eff}/\partial T$ FOR VARIOUS BLANKETS

D_2O ($^\circ C^{-1} \times 10^3$)	355 g of Normal U per kg of D_2O ($^\circ C^{-1} \times 10^3$)	633 g of Th per kg of D_2O ($^\circ C^{-1} \times 10^3$)	Definition of T
−1.85	−1.85	−2.00	Average core temperature, rapid heating
−1.81	−1.71	−1.91	Core temperature, uniform heating
−1.07	−0.76	−0.32	Blanket temperature, uniform heating
−2.88	−2.47	−2.23	Uniform heating, over-all temperature

OPERATIONAL PLANNING

S. E. Beall, Section Chief
S. Visner

HRT START-UP PROCEDURE

Owing to the large change in critical concentration – a factor of approximately 5 from room temperature to operating temperature – it is not feasible to dilute the fuel in the dump tank more than is required to lower the critical temperature for the core about 30°C. For start-up, then, the fuel solution is boiled, and the D_2O condensate which is removed is pumped into the core. After the D_2O is circulated and heated by external means to 200°C, the highly concentrated fuel solution is injected continuously into the core. After criticality is attained at 200°C, the reactor power will increase, owing to the continued increase in fuel concentration, go through a maximum which should not be dangerous, and level off at a value sufficient to raise the core temperature in step with the concentration. The time variation of the critical temperature for several initial dilutions is shown in Fig. 15 for operation with pure D_2O in the blanket as indicated by the following data:

Dilution (kg of D_2O)	Pulsafeeder Rate, 6.3 kg/min		Pulsafeeder Rate, 3.2 kg/min	
	τ (min)	$\partial\theta/\partial t$ at 200°C (°C/min)	τ (min)	$\partial\theta/\partial t$ at 200°C (°C/min)
0	7.1	22	14.2	11
100	17.7	5.7	35.4	2.8
150	21.7	3.2	43.4	1.6
200	25.1	2.2	50.2	1.1

Similarly, the time variation of the critical temperature is shown in Fig. 16 for 632.7 g of thorium per kilogram of D_2O (500 g of thorium per liter at 280°C) in the blanket as indicated by the following data:

Dilution (kg of D_2O)	Pulsafeeder Rate, 6.3 kg/min		Pulsafeeder Rate, 3.2 kg/min	
	τ (min)	$\partial\theta/\partial t$ at 200°C (°C/min)	τ (min)	$\partial\theta/\partial t$ at 200°C (°C/min)
150	21.7	3.2	43.4	1.6
200	25.1	2.3	50.2	1.2

The parameter, τ, is the mixing time for the system and depends on the pulsafeeder pumping rate and the solution inventories in the high-pressure and low-pressure systems. With the 200-kg initial dilution and the pulsafeeder pumping rate of 3.2 kg/min, which is one-half normal speed, the system would heat up initially at 1.2°C/min and the rate would steadily decrease as the temperature rises. This is considered to be satisfactory from considerations of thermal stress in the equipment.

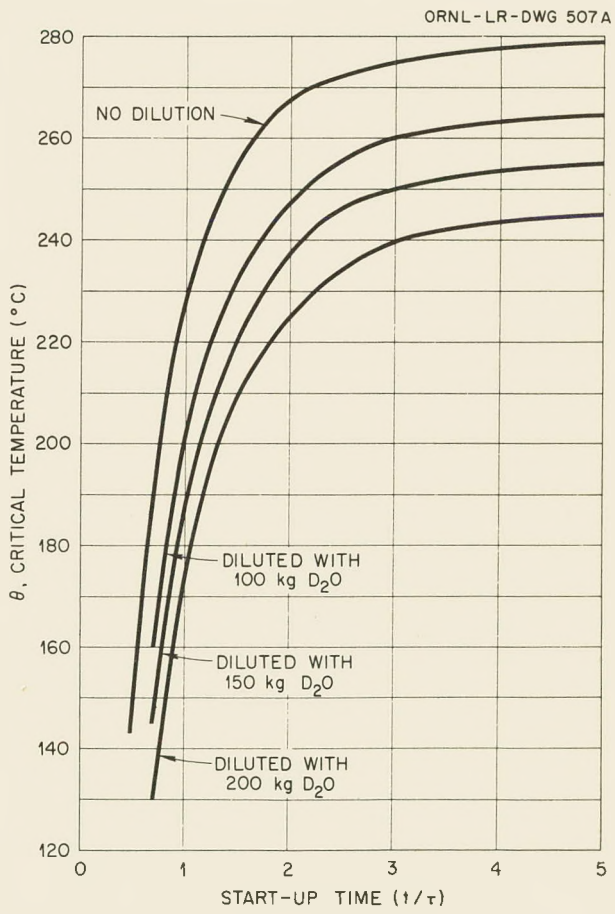

Fig. 15. Time Variation of Critical Temperature for Several Initial Dilutions for Start-up of HRT with Pure D_2O in Blanket. Working solution at 280°C, 480 kg; U^{235} inventory, 4.8 kg.

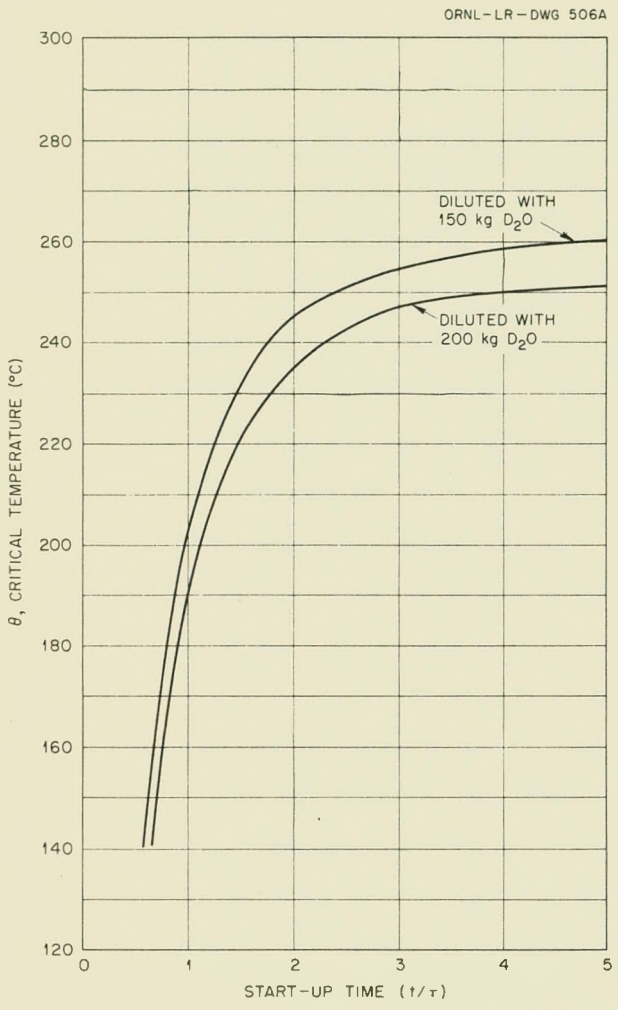

Fig. 16. Time Variation of Critical Temperature for Two Initial Dilutions for Start-up of HRT with 632.7 g of ThO_2 per Kilogram of D_2O in Blanket. Working solution at 280°C, 480 kg; U^{235} inventory, 13.1 kg.

RATES OF REACTIVITY INCREASE

Based on the assumption that the pulsafeeder was pumping full speed during the approach to criticality and continued to inject fuel into the core at the maximum speed of 6.3 kg/min after the reactor became critical, the rates of increase of reactivity have been calculated for the reactor becoming critical at 200°C and also at 20°C. To achieve the latter case in reality, it must be assumed that through misoperation the condensate in the core has not been heated prior to the fuel injection. Various D_2O inventories have been assumed. Although the calculations have been performed with constants appropriate for operation with a D_2O blanket, the results shown in Table 9 should be applicable to any type of blanket, provided the U^{235} inventory is consistent with the requirement that, at 280°C, there is 100 kg of working solution in the dump tanks.

In all cases shown, representing reasonable inventories, the rates of reactivity increase are no greater than those now considered available by rapid cooling of the core. In fact, attainment of a reactivity rate as high as 1%/sec would require a dump-tank inventory of less than 12 kg of solution.

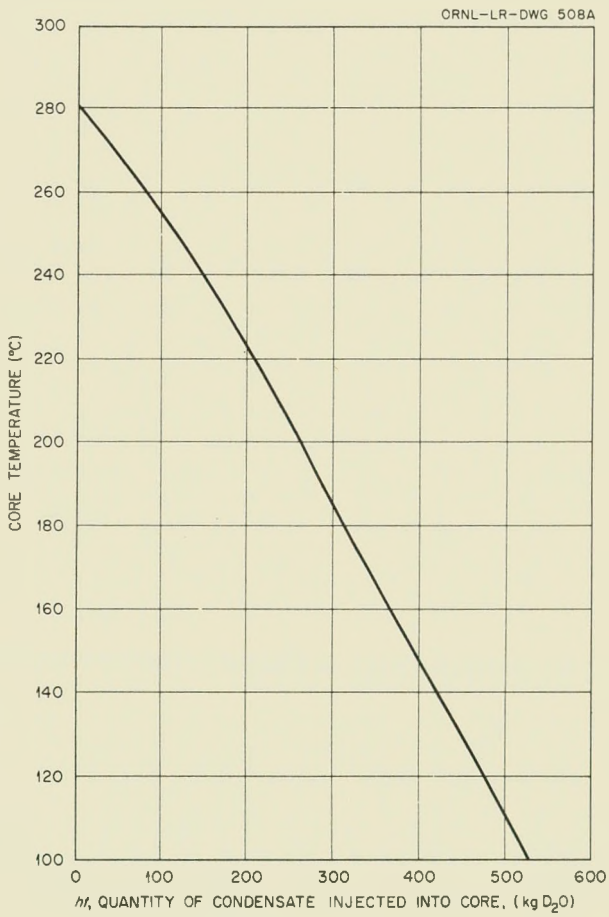

Fig. 17. Decrease in Core Temperature at Shutdown of HRT by Dilution with D_2O. Blanket, D_2O; high-pressure volume, 450 liters; concentration at 280°C, 9.7 g of U^{235} per kilogram of D_2O; h, 6.3 kg/min (pulsafeeder fast), 3.2 kg/min (pulsafeeder slow), 4 kg/min (evaporator rate).

TABLE 9. RATE OF REACTIVITY INCREASE FROM INJECTING FUEL (U^{235} INVENTORY, 4.8 kg; PULSAFEEDER FLOW RATE, 6.3 kg/min)

Core Temperature (°C)	D_2O Inventory (kg)		Rate of Change in Core Concentration (%/sec)	$\partial k_{eff}/\partial t$ (%/sec)
	Total	Low Pressure System		
200	680	248	0.047	0.016
	630	198	0.060	0.021
	580	148	0.080	0.027
	480	48	0.246	0.084
	436	4	2.92	1.00
20	680	180	0.169	0.065
	630	130	0.235	0.091
	580	80	0.381	0.147
	530	30	1.02	0.394
	512	12	2.59	1.00

There should be no problem in designing the low-pressure system so that an inventory greater than 12 kg would be required to feed the pulsafeeder with solution. The hazard associated with starting up the reactor by pumping the fuel solution directly into the core without first filling it with condensate may be more serious than is currently believed and will be considered at another time.

SHUTDOWN OF THE REACTOR

For an orderly shutdown, the solution in the core would be diluted by injecting condensate and allowing the excess solution to be let down to the dump tanks. The critical temperature, and therefore the reactor temperature, could be decreased to the vicinity of 100°C; then the solution would be dumped. The decrease in core temperature is shown in Fig. 17 as a function of the quantity of D_2O injected. At first, with condensate available in the storage tank, the rate of injection is limited by the pulsafeeder flow rate, up to 6.3 kg/min, and thereafter is limited by the rate of evaporation of the D_2O from the fuel dump tanks, 4 kg/min. For example, with 200 kg of D_2O from the storage tank, the temperature could be decreased from 280 to 222°C in 32 min, after which time it could be lowered to 100°C in an additional 88 min; thus the decrease from 280 to 100°C could be accomplished in a total of 120 min. Of course, the initial rate of decrease could easily be adjusted to one-half the quoted value for a total shutdown time of 2.5 hr. This calculation neglects any problem associated with cooling the reflector.

DESIGN

R. B. Briggs, Section Chief

R. E. Aven
R. H. Chapman
R. D. Cheverton
W. L. DeRieux
W. R. Gall
J. W. Hill
T. H. Mauney
J. R. McWherter
C. L. Segaser
W. Terry
T. H. Thomas
R. Van Winkle

F. C. Zapp

GENERAL CONSIDERATIONS

Some design data, a flow diagram, and some equipment designs for a small, two-region Homogeneous Reactor Test (HRT) were presented in the last report.[1] Since then a more firm basis for the design has been established, and more complete designs are now available for much of the equipment. It has been decided that the HRT will also be used in the development of chemical processes for the separation of fissionable materials from the blanket. The design presented here is for a 6-Mw reactor with a core containing a dilute UO_2SO_4-D_2O solution, highly enriched in U^{235}, and surrounded by a blanket of a solution containing 300 g of depleted uranium per liter of UO_2SO_4-D_2O. It is expected that the production of plutonium with a low Pu^{240} content will be developed in this system. With some modifications, the reactor can serve as a pilot plant for a thorium breeder in which a thorium oxide slurry is the blanket.

HRT FLOWSHEET AND DESIGN DATA

The latest conception of the HRT flowsheet is shown in Fig. 18. It is similar in many respects to the flowsheet shown in the previous report (Ref. 1, Fig. 13), but it differs in the following ways:

1. A blanket system containing a UO_2SO_4-D_2O solution is used in place of the D_2O reflector system.
2. The blanket is 13.75 in. thick and the blanket vessel has an inside diameter of 60 in.
3. The core and the blanket powers are 5 and 1 Mw, respectively.
4. The core and the blanket feed solutions both pass through their respective let-down coolers before entering the main high-pressure loops.
5. The condensate is to be introduced in the back of both the core solution and the blanket solution circulating pumps; it will also be introduced in the core and blanket pressurizers. Two 10-gph pulsafeeder pumps are utilized to furnish condensate for the circulating pumps and pressurizers.
6. The oxygen supplies are shown for the individual systems.
7. Both the solution-feed filter and the degassers have been removed.
8. The catalytic recombiner and the gas condenser are shown as one unit in both the core and the blanket low-pressure systems.
9. A steam drum is provided in the blanket steam system.
10. Steam from the blanket system is shown as going directly to the auxiliary condenser.
11. Safety relief valves have been incorporated in the condensate lines leading to both main heat exchangers.
12. Provision for freezing liquid in the process line is included throughout both systems in order to assure complete shutoff when desired.

The process-design basis for the core and the blanket systems is presented in Table 10. Conditions in the blanket constitute the only major change from previously reported data.

STEAM SYSTEM

The steam generated by the HRT will be condensed and the condensate will be returned to the cycle. A small amount of electric power (about 312 kw) can be generated through the use of the existing HRE turbine-generator set. A study[2] was made, however, of the economy of developing more fully the electric-power-generating potential of the steam. Several different arrangements were considered, such as use of secondhand equipment, modification of the HRE turbine, and purchase of a new 1500-kw turbogenerator. Costs of the steam

[1] R. B. Briggs *et al.*, *HRP Quar. Prog. Rep. Jan. 31, 1954*, ORNL-1678, p 21.

[2] R. C. Robertson, *Steam System for HRT, a Study* (to be issued).

DWG. E-18166A

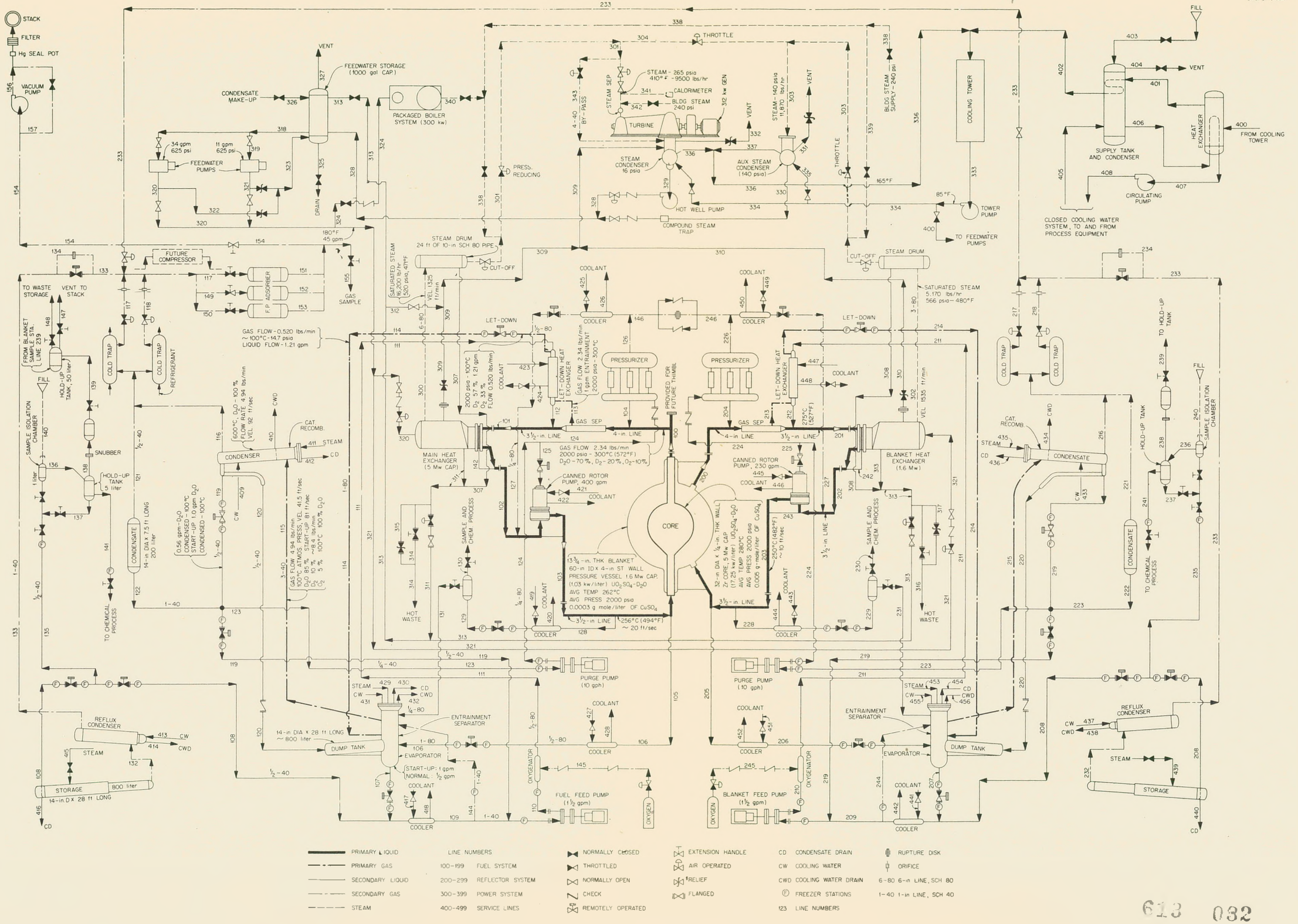

PRIMARY LIQUID
PRIMARY GAS
SECONDARY LIQUID
SECONDARY GAS
STEAM

LINE NUMBERS
100-199 FUEL SYSTEM
200-299 REFLECTOR SYSTEM
300-399 POWER SYSTEM
400-499 SERVICE LINES

NORMALLY CLOSED
THROTTLED
NORMALLY OPEN
CHECK
REMOTELY OPERATED

EXTENSION HANDLE
AIR OPERATED
RELIEF
FLANGED

CD CONDENSATE DRAIN
CW COOLING WATER
CWD COOLING WATER DRAIN
(F) FREEZER STATIONS
123 LINE NUMBERS

RUPTURE DISK
ORIFICE
6-80 6-in LINE, SCH 80
1-40 1-in LINE, SCH 40

613 032

Fig. 18. Flowsheet of HRT.

DECLASSIFIED

TABLE 10. HRT DESIGN DATA

	Core	Blanket
Power, kw	5000	1000
Pressure, psia	2000	2000
Vessel ID, in.	32	60
Vessel thickness, in.	1/4	4
Blanket thickness, in.		13 3/4
Vessel material	Zirconium	Stainless-steel-clad carbon steel
Volume, liters	290	1555
Specific power, kw/liter	17.3	0.64
Solution circulating rate, gpm	400 at 256°C	230 at 250°C
Maximum solution velocity, ft/sec	20 at 250°C	10 at 266°C
Inlet temperature, °C	256 (494°F)	250 (482°F)
Outlet temperature, °C	300 (572°F)	266 (511°F)
Solution	UO_2SO_4-D_2O + $CuSO_4$	UO_2SO_4-D_2O + $CuSO_4$
Uranium concentration, g/kg D_2O	16.3	360
Uranium enrichment, % U^{235}	93	0.4
Heat capacity at 2000 psi, Btu/lb/°F		
inlet (av from 494 to 572°F)	1.24	0.77
outlet		0.82
Average thermal conductivity, Btu/hr/sq ft/°F/ft	0.35	0.35
Viscosity at 2000 psia, lb/ft/hr		
inlet	0.29	0.59
outlet	0.24	0.63
Density at 2000 psi, lb/cu ft		
inlet	55.90	79.5
outlet	50.60	81.7
G for D_2O decomposition, molecules D_2/100 ev	1.67	0.87
Rate of formation of D_2, lb-mole/sec	0.00179	0.00032
Rate of formation of O_2, lb-mole/sec	0.00089	0.00016
Vapor pressure of D_2O over solution, psia	~1240	~750
Compressibility factor of D_2O vapor	0.702	0.78
Heat of recombination of D_2 and O_2, Btu/min	11,300 (199 kw)	2020 (35.4 kw)
Heat of vaporization of D_2O (outlet),		
Btu/lb	550	640
Btu/lb-mole	11,000	12,800
Gas dissolved in solution at outlet,		
g-mole D_2/liter	0.10	0.14
g-mole O_2/liter	0.05	0.07
Volume of gas generated (D_2 and O_2), cfs		
at 2000 psia	0.0148	0.00156
at STP	0.963	0.108
$CuSO_4$ concentration required for 100% recombination in solution, g-mole/liter	0.005	0.0003
Grams of Pu per day (at 5-Mw core power)		3.7

systems were compared on the basis of a 6.6-Mw reactor design power level, which is only slightly higher than the present design level. An equivalent full-load operating life of 8000 hr for the HRT was arbitrarily assumed in making the study, and the results are summarized in Table 11.

Plan A was selected for use in the HRT. This plan involves passing a part of the steam through the existing turbogenerator to develop the maximum capability of the generator and condenser and then dumping the remainder of the steam into steam killers. It may be noted that Plans D and E, both involving the use of low-cost secondhand equipment, indicate some economic encouragement, but it is doubtful that any arrangement would show a significant profit, primarily because of the expected short operating life. Besides the low initial cost, other considerations, such as available floor space in Building 7500 and the desirability of a system which requires a minimum of attention and control, led to the selection of a simple steam-dumping arrangement. Measurement of steam flow can be readily translated into the electric generation that would have been possible.

The HRT reactor power level will be regulated by the steam-flow control valve. The steam-condensing surface will be made adequate to absorb up to about 13.5 Mw of heat, approximately twice the normal power. It will probably take the form of commercially available instantaneous-type water heaters, or perhaps air-cooled condensers, which condense the steam at about 140 psia and discharge the condensate through a trap to a 1000-gal feedwater storage tank. The feedwater pumping system will consist of a new pump supplemented by the existing HRE feedwater pump.

Since the condensers require more cooling water than can readily be supplied from the ORNL water mains, it is proposed that a forced-draft cooling tower of about 1000-gpm capacity be installed adjacent to Building 7500.

No special problems are involved in the design of the steam system and circulating-water supply. Preparation of drawings and specifications is now under way so that installation can be started early in the program and construction personnel can be utilized more efficiently. A detailed design of the steam system is being prepared by the K-25 General Engineering Department.

TABLE 11. COMPARISON OF COSTS OF VARIOUS PLANS FOR HRT STEAM SYSTEM DESIGNED FOR 6.6-Mw REACTOR POWER LEVEL

	Plan[a]					
	A	B	C	D	E	F
Generating capacity, kw	312	725	825	825	1,150	1,450
Net power generated,[b] kw	240	647	747	747	1,037	1,337
Power worth of 8000 hr equivalent full-load operation at 5 mills/kwhr	$ 9,600	$25,880	$29,880	$29,880	$41,480	$ 53,480
Initial investment[c]	25,000	61,000	68,000	34,000	49,000	150,000
Initial investment in excess of that required for Plan A		36,000	43,000	9,000	24,000	125,000
Earnings from 8000 hr equivalent[d] full-load operation in excess of that derived from Plan A		16,280	20,280	20,280	31,880	43,880

[a]A – Steam-dumping condenser and HRE turbogenerator and condenser.
B – HRE turbine, new 1000-kva generator, HRE condenser and steam-dumping condenser.
C – HRE turbine, new 1000-kva generator, and new condenser.
D – HRE turbine, used 1000-kva generator, and used condenser.
E – Used 1500-kw turbogenerator and used condenser.
F – New 1500-kw turbogenerator and new condenser.

[b]Allowance has been made for auxiliary power required for steam and water circulating systems only.

[c]Does not include cost of addition to Building 7500, engineering, overhead, or additional electrical switch-gear that will be required.

[d]Does not include labor cost, interest on investment, depreciation, or possible resale value of equipment.

VALVES

Special valves for the HRT are being designed through the joint efforts of the Design and Instrument Sections. Work on the design and specifications for the prototype valves is nearing completion.

Sampling Valve

The design of a high-pressure stainless steel sampling valve reported previously[1] has been completed and is covered by drawing D-18142. A stainless steel bellows with a safe working-pressure rating of 3000 psi is the sealing member. The $\frac{1}{8}$-in. valve is hand-operated, with provision for later adaptation to air operation.

One valve has been fabricated by the ORNL Research Shop. A preliminary leak test that was run by the Instrument Department showed the leak rate to be 28 cc of water in 24 hr with a 1000-psi pressure difference across the seat. The valve is now being reworked to reduce leakage to the acceptable limit of 1 cc of water per 24 hr with a 1000-psi pressure difference.

High-Pressure Control Valves

Detailed designs have been completed and are tentatively approved for manufacture of the 0.5- and 1-in. high-pressure stainless steel valves described in the previous report.[1] A welded stainless steel bellows rated at 2500 psi is used for sealing. A secondary packing gland seal is employed for safety in event the bellows ruptures. Provision has been made for pressurizing the bellows to control the differential pressure across it. This feature also provides for sampling at the gland for leak detection. All parts on the valves are interchangeable except the bodies and the sealing plugs.

The valves are completely detailed on the following drawings: D-18149 – 0.5-in. Valve Assembly; D-18153 – 1-in. Valve Assembly; D-18154 – Details; D-18155 – Bellows Assembly and Details; D-18156 – 0.5-in. Body and Seat Details; D-18157 – 1-in. Body and Plug Details.

Valve Operator

Design is in progress on an air-pressure valve operator in which a stainless steel bellows is used instead of the neoprene diaphragm employed on commercially available operators. This operator will be used to control the 0.5-in. valve mentioned above. It is essentially a redesign of the aluminum bellows operator used on the HRE. The greater bellows area with its resulting larger seating force on the valve should provide tight shutoff.

HRT CORE TANK AND PRESSURE VESSEL

A conceptual design of the proposed core tank and pressure vessel has been completed, and a contract has been negotiated with the Newport News Shipbuilding and Dry Dock Company for the design, development, and fabrication of this equipment. The work to be performed by the contractor is based on the design by ORNL as shown in Fig. 19.

For the core tank, the diameter of 32 in. and the wall thickness of 0.25 in. were based upon nuclear considerations and materials characteristics. A core of smaller diameter would require a concentration greater than 20 g of U^{235} per liter; this would be undesirable for corrosion reasons if the core were to be surrounded by a strongly absorbing blanket. A core of larger diameter would prevent the reactor from being operated at high specific power with low total power. A core tank of lesser wall thickness would not have the desired strength, and a wall as thick as 0.5 in. would absorb more neutrons than the thinner wall and would be much more difficult to fabricate out of zirconium.

The inside diameter of the pressure vessel has been set at 60 in. This size is commercially available in stainless-steel-clad carbon steel and it results in a blanket thickness which is very near the acceptable minimum prescribed by neutron leakage calculations. A 4-in. wall thickness was chosen on the basis of strength requirements and availability of stainless-steel-clad plate. The stainless steel cladding on the inside of the vessel will be 5 to 10% of the carbon steel thickness. Estimation of the stresses in the pressure vessel and core tank, provision for adequate strength, and provision for differences in thermal expansion between the core tank and pressure vessel are the major design problems.

The heat productions in the vessel wall for the D_2O reflector and for a UO_2SO_4 blanket solution are shown in Fig. 20. Since the heat production is higher for the D_2O reflector, the pressure-vessel thickness should be determined for use with it. A stress analysis to determine the optimum pressure-vessel thickness for combined thermal and pressure stresses has been performed for this case, and the results are shown in Fig. 21 for several conditions. A 4-in.-thick wall appears to be adequate for operation at the design power of 5 Mw in the core and at

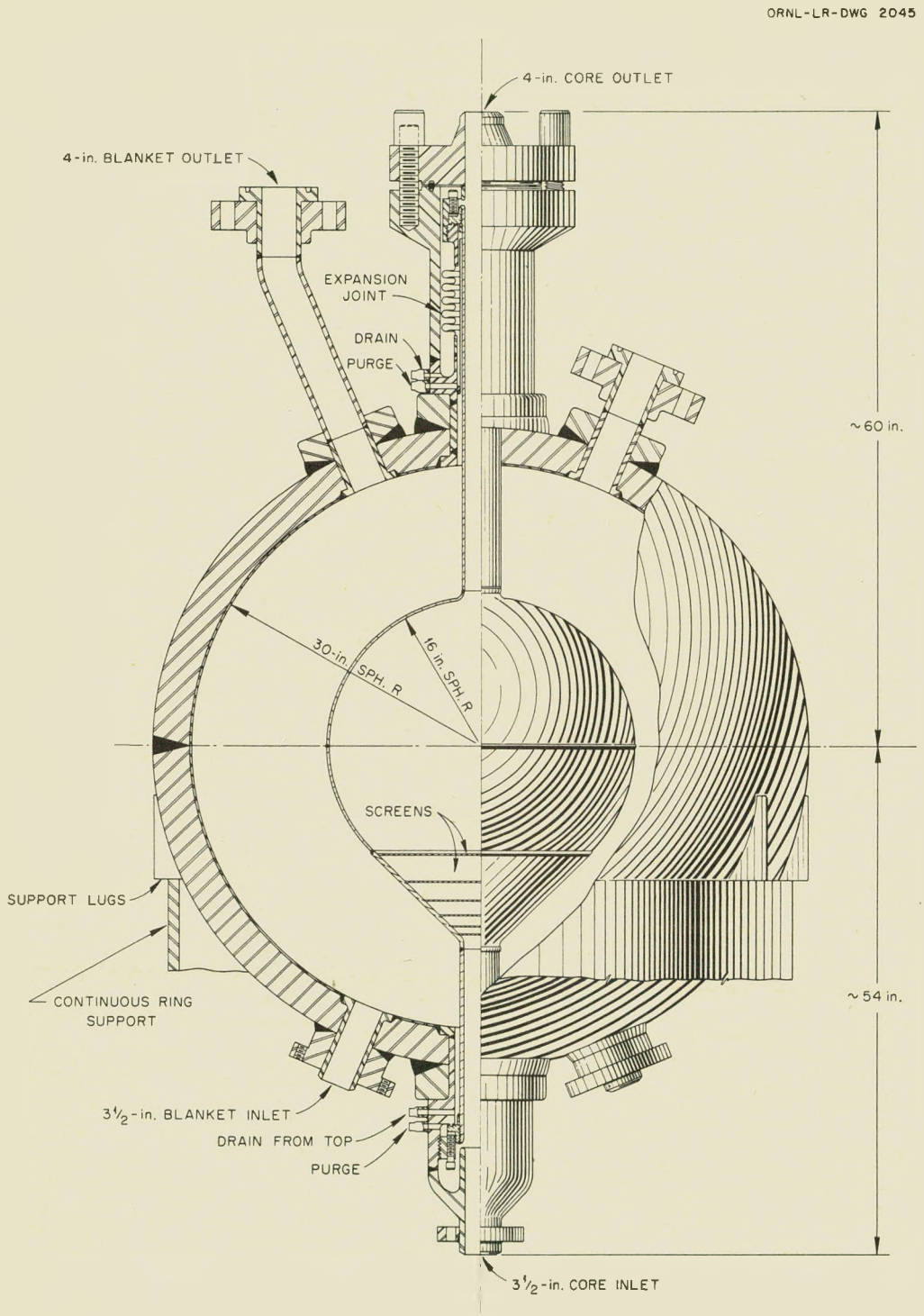

Fig. 19. HRT Reactor Vessel Assembly.

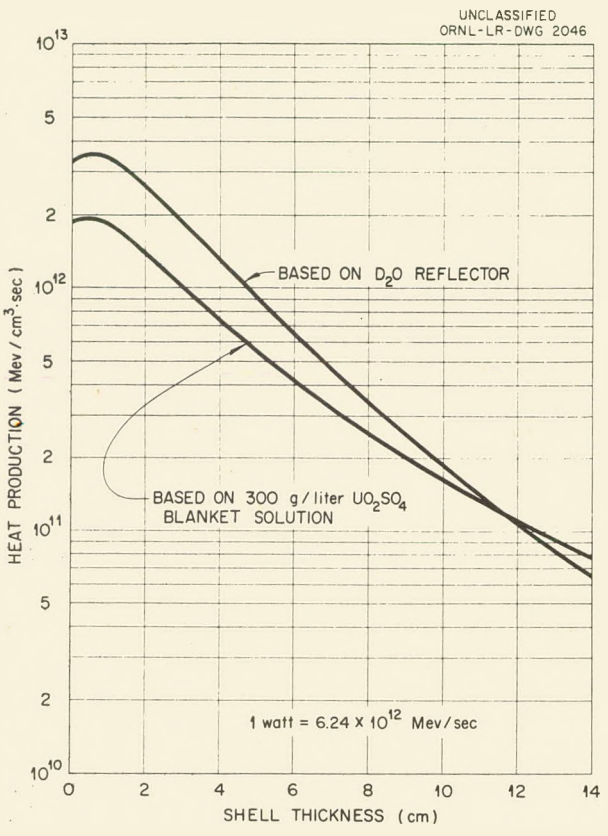

Fig. 20. Heat Production in HRT Pressure-Vessel Wall.

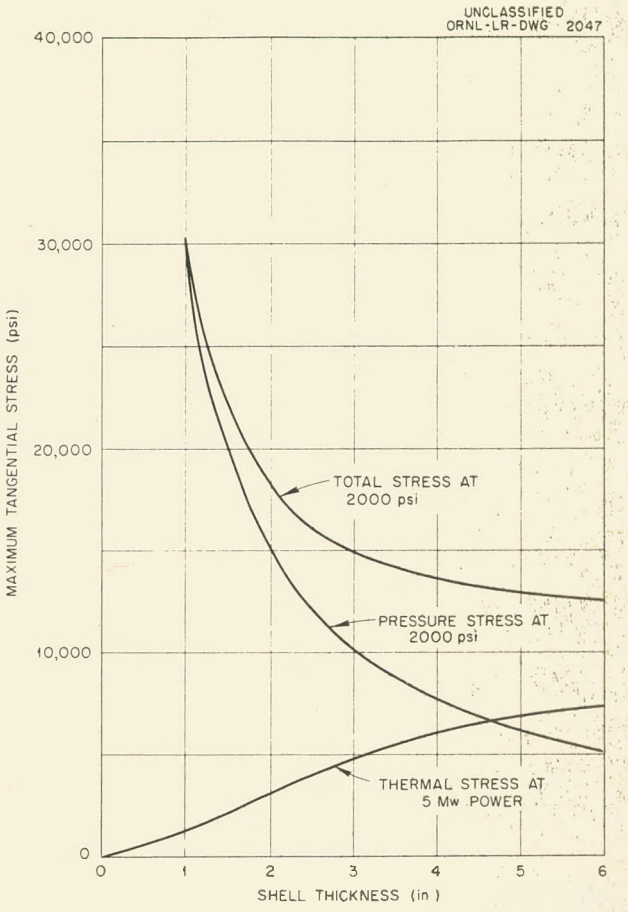

Fig. 21. Analysis of Thermal and Pressure Stresses in HRT Pressure-Vessel Wall.

pressures of 2000 to 2500 psi. Detailed analysis of the effect of the piping connections on the stresses will be made by personnel of the Newport News Shipbuilding and Dry Dock Company as the design progresses.

Since it is desired to use a minimum amount of material in the construction of the core tank, it is necessary to make a very thorough theoretical and experimental stress analysis. It has been estimated that the core tank will withstand an internal pressure of 225 psi before the stress exceeds 18,000 psi, sometimes assumed as the yield strength of Zircaloy-2, and an external pressure of 170 psi before elastic buckling occurs if both the spherical and conical portions are 0.25 in. thick. Greater strength is obtained by increasing the thickness of the conical portion. It must be realized that these estimates are not accurate. Apparently, zirconium plates have strongly directional properties which are not well known. Internal pressure and axial loading create high stresses at points of discontinuity such as the intersection of the inlet and outlet pipes with the conical and spherical portions of the tank. External pressure and axial loading may also cause high discontinuity stresses. Of greater concern under such loading is the stability of the shell.

Theoretical solutions to the above problems are being derived. One approximate solution for the stresses in the spherical portion of the shell has been based on the assumption that there is a sharp intersection between the outlet pipe and the shell and that the outlet pipe is infinitely rigid. Some experimental work is being done to determine the accuracy of this theory. Another theoretical solution, which takes into consideration the flexibility of the outlet pipe, is in progress.

In order to reduce the discontinuity stresses, the shell will probably be increased in thickness in the

area of the intersections. A theoretical solution is being derived to determine the necessary reinforcement. In this solution it is assumed that the outlet pipe is infinitely rigid and that there is a sharp intersection between the outlet pipe and sphere.

Complexity of the theoretical solution introduced by assuming a knuckle radius at transition points prohibits a derivation of the necessary reinforcement at this time. However, experimental results obtained from a very poorly machined model provide indications of the effects of the knuckle radius. Further tests will be conducted if better models can be obtained.

Since a spherical shell is more stable than a conical shell when subjected to external pressure, it is felt that the thickness of the cone should be increased over that of the sphere so that the two shells will be approximately equally stable. By using theoretical equations for the sphere and by assuming that the cone is a cylinder with a diameter equal to the maximum diameter of the cone, it is found that the wall thickness of the cone should be about 150% of that of the sphere.

The present reactor design employs a bellows expansion joint to absorb the differential thermal expansion between the core tank and the pressure vessel. There is difficulty involved in the design of the bellows under the conditions specified for the reactor. Procurement has been initiated on two identical bellows for use in testing the aluminum models. One of these bellows may be available for fatigue and corrosion testing in a loop.

The contract with the Newport News Shipbuilding and Dry Dock Company provides for the design of the reactor pressure vessel and core tank, for development of techniques for welding and forming zirconium, and for the design, fabrication, and testing of a pressure-vessel mock-up and four aluminum models of the core tank. Tests on the mock-up are to be completed in June. Design of the reactor vessel and core tank and development of fabrication methods are to be completed by August so that the reactor vessel can be delivered by January 1, 1955.

HEAT EXCHANGERS

Drawings and specifications for the main heat exchanger described in the previous report[1] have been completed and released for bids. Although the exchanger was designed for use in the core loop, it may be desirable to use the same unit in the blanket system. Calculations have been made to estimate the performance of the exchangers in the blanket system based upon the conditions reported in Table 10. If it is assumed that 230 gpm of blanket solution enters the exchanger at 266°C and leaves at 250°C, steam will be generated on the shell side at 560 psia and 478°F (248°C). This compares with 520 psia, 471°F steam produced in the exchanger in the core system. The pressure drop through the blanket exchanger is estimated to be 8.7 psi. A heat exchanger designed to produce 520-psia steam would require 40% less surface.

PRESSURIZER

It has been tentatively decided to use steam pressurization with the core and blanket pressurizers interconnected and with pressure-relief valves in the connecting pipe to allow vapor to flow from one pressurizer to the other when a pressure difference of 10 to 20 psi exists between the core and blanket systems.

An important function of the pressurizer is to provide a volume into which liquid from the core can be expelled in the event of a rapid temperature rise and density decrease resulting from a sudden increase in reactivity. Ideally, there should be no increase in pressure in the pressurizer, but this would require an impractical volume. The volume will be specified to limit the pressure change in the pressurizer to 100 psi during the most severe reactivity increase that can be conceived to occur in the HRT.

Maximum changes in reactivity have not been established; however, it is expected that the amount of liquid discharged into the pressurizer will be 0.5 to 2.5% of the core volume in approximately 0.1 sec. The relationship between the volume of liquid discharged into the pressurizer and the pressurizer volumes for gas and steam pressurization, if the pressure increase in the pressurizer is limited to 100 psi, is given in Table 12. Adiabatic compression of the vapor was assumed, and the condensation of steam by transfer of heat to the liquid discharged into the pressurizer was also considered.

In order to achieve a pressure of 2000 psia by steam pressurization, the solutions must be heated to approximately 335°C in the pressurizers. This temperature is above the point at which phase separation would occur in the blanket solution. If the pressurizer is made of titanium, the phase

TABLE 12. VAPOR VOLUME IN CORE PRESSURIZER NECESSARY TO LIMIT PRESSURE INCREASE TO 100 psi DURING POWER SURGE

Per Cent of Core Volume Discharged to Pressurizer	Liquid Volume (liters)	Vapor Volume Required in Pressurizer	
		Steam (liters)	Gas* (liters)
0.5	1.45	30** – 40***	50
1.0	2.90	50 – 70	100
1.5	4.50	80 – 110	150
2.5	7.25	120 – 180	250

*Gas assumed to be helium.

**Adiabatic compression of mixture of steam and liquid discharged into pressurizer assumed.

***Compression of dry steam assumed.

separation can be tolerated. If it is made of stainless steel, condensate must be supplied to the pressurizer to reduce the uranium concentration and thus prevent the formation of the highly corrosive heavy phase.

Studies are being made to determine procedures that will allow both blanket and core solutions to be dumped in 5 min or less without the core vessel being ruptured and without the solution being transferred between core and blanket by entrainment through the pressure-equalizing line connecting the two pressurizers. Under some operating conditions the core solution can be at 300°C and the blanket solution at 250°C. It appears that the core solution may have to be completely dumped before dumping of the blanket solution can begin. The relationship between the fraction of solution remaining in the core or blanket system during a dump and the pressures is presented in Fig. 22.

Preliminary comparisons between gas pressurization and steam have been made. The use of gas is advantageous because it would be unnecessary to heat the solutions to 335°C in order to achieve the desired 2000-psia operating pressure, and the pressure changes during a dump would be slower. Two of the more important disadvantages are:

1. There is danger of collecting an explosive mixture of D_2 and O_2 in the pressurizer. In the case of steam pressurization, the approach to an explosive mixture would be detected by measuring and relating the temperature and pressure in the vapor space; detection of explosive mixtures in a gas pressurizer appears to be much more difficult.

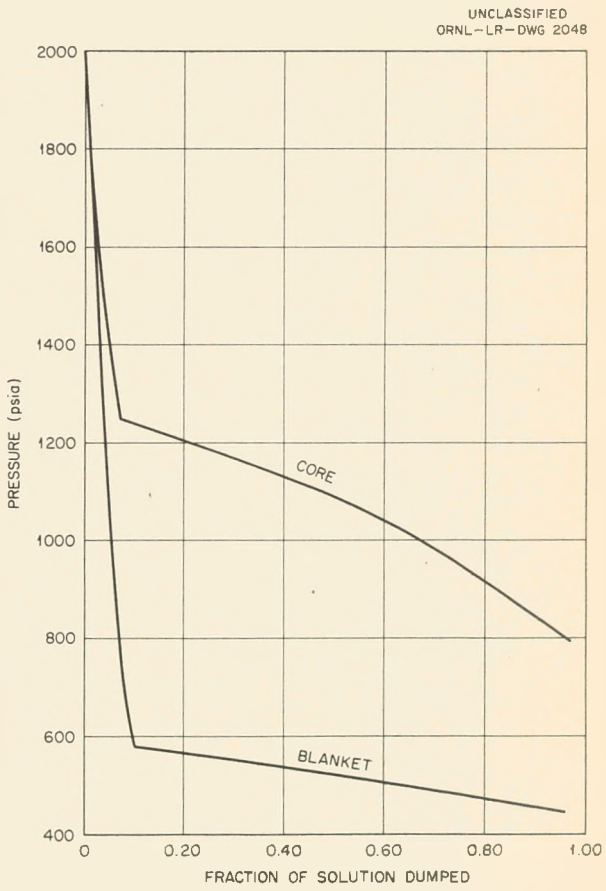

Fig. 22. Relationship Between HRT System Pressures During Dumping and Fraction of Solution Dumped.

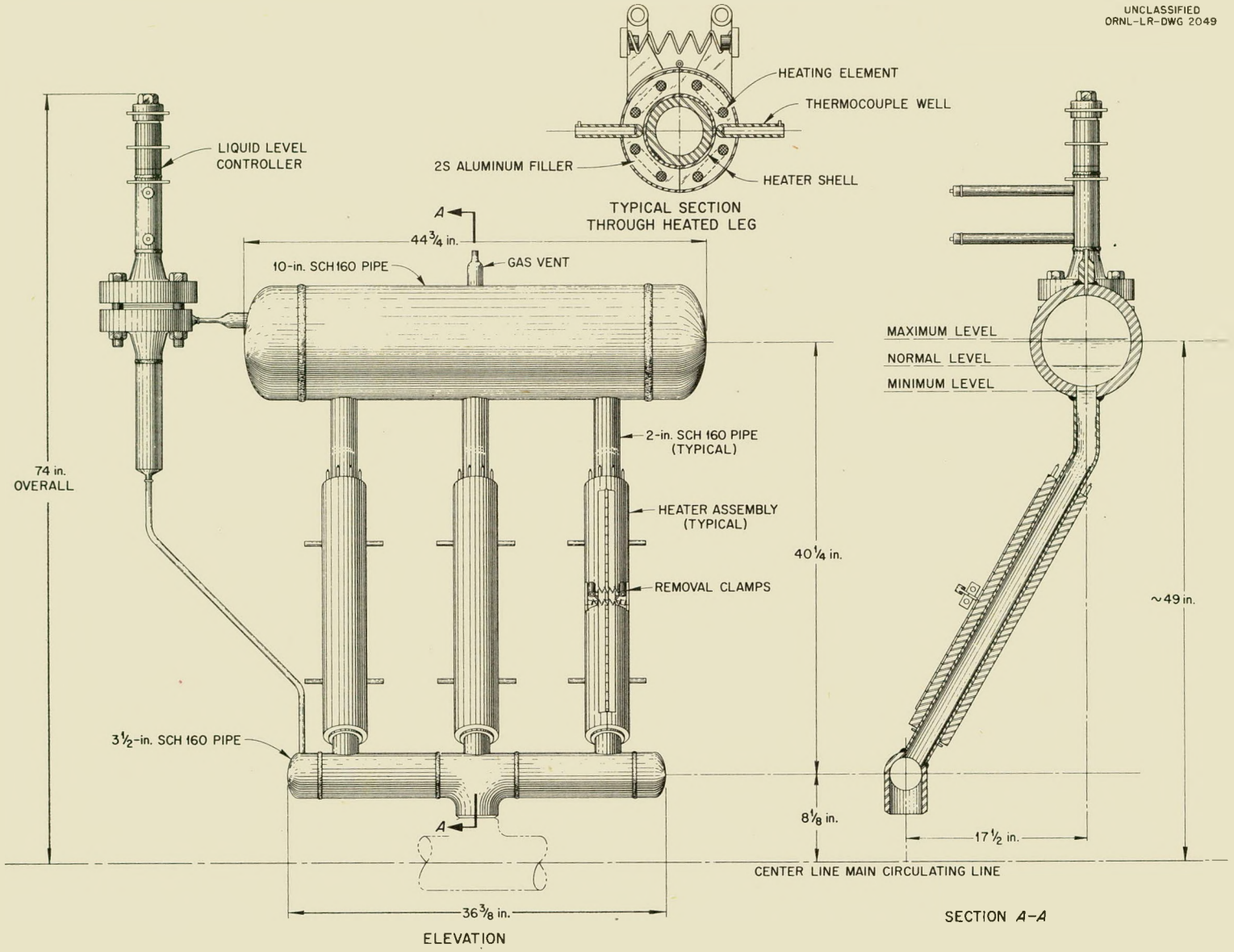

Fig. 23. HRT Fuel Pressurizer Assembly.

2. There would be large quantities of highly radioactive noncondensable gases to be handled in the low-pressure system and in the fission-product absorbers during a dump. Difficulty was experienced in disposing of the helium from reflector pressurization in the HRE.

The most recent pressurizer design is shown in Fig. 23. Electrically heated, clamshell assemblies are being considered for the heat source, although the design is easily convertible to liquid-metal or steam-jacket heating. Performance specifications are listed in Table 13. It is possible that the vapor volume will be increased.

TABLE 13. FUEL PRESSURIZER SPECIFICATIONS

Operating temperature, °C	335 (635°F)
Operating pressure, psia	2000
Material	Type 347 stainless steel
Nominal heat capacity, kw	21
Steady-state heat losses, kw	2
Time to pressurize fuel from 300°C saturated, hr	1
Fuel holdup at 50% "full" on level indicator, liters	18
Vapor volume, liters	30

A liquid-level controller similar to that used in the HRE and shown in Fig. 24 has been designed so that the sensing-element armature and float assembly is flanged to the pressurizer float chamber, thereby permitting removal and replacement. The range of the instrument is 5 in. to conform to the pressurizer design.

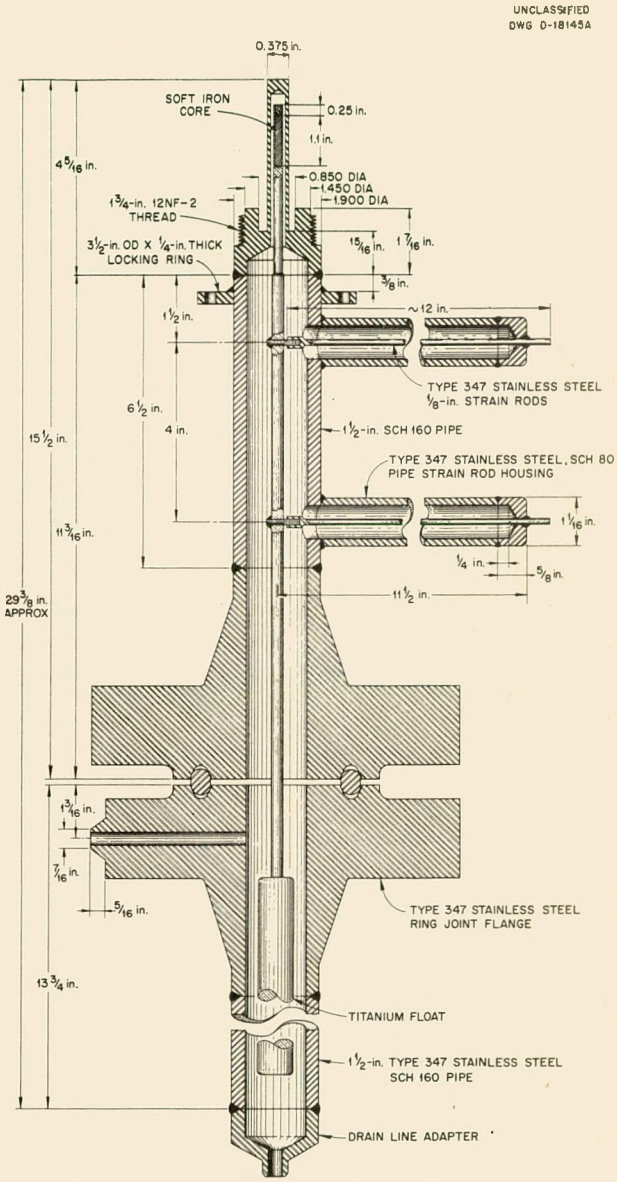

Fig. 24. Pressurizer Liquid-Level Controller.

RECOMBINER-CONDENSER UNIT

Under normal operating conditions in the HRT a quantity of decomposition gases ($D_2 + \frac{1}{2}O_2$) will be let down from 2000 psia to atmospheric pressure, recombined in a catalytic recombiner, and condensed in an off-gas condenser. The unit being considered at the present time combines the recombining and condensing operations as shown in Fig. 25. The cooling load on the condenser in the core off-gas system is 452,000 Btu/hr. A similar cooling load is assumed for the blanket off-gas system. A condenser cooling surface of about 20 sq ft is required.

It is desired, however, to use these condensers to remove heat from the high-pressure solutions when they are dumped. This is done by condensing the D_2O vapor which flashes out of the solution as the pressure is lowered to atmospheric. The condenser in the core system must remove 296,000 Btu from the fuel solution, and the blanket condenser must remove 1,090,000 Btu from the blanket solution. Consequently, the surface area required is much larger than the 20 sq ft needed for normal operation. The condensers considered have a cooling surface of 159 sq ft and are identical for both the core and the blanket gas systems. With these condensers the times required to cool and to condense

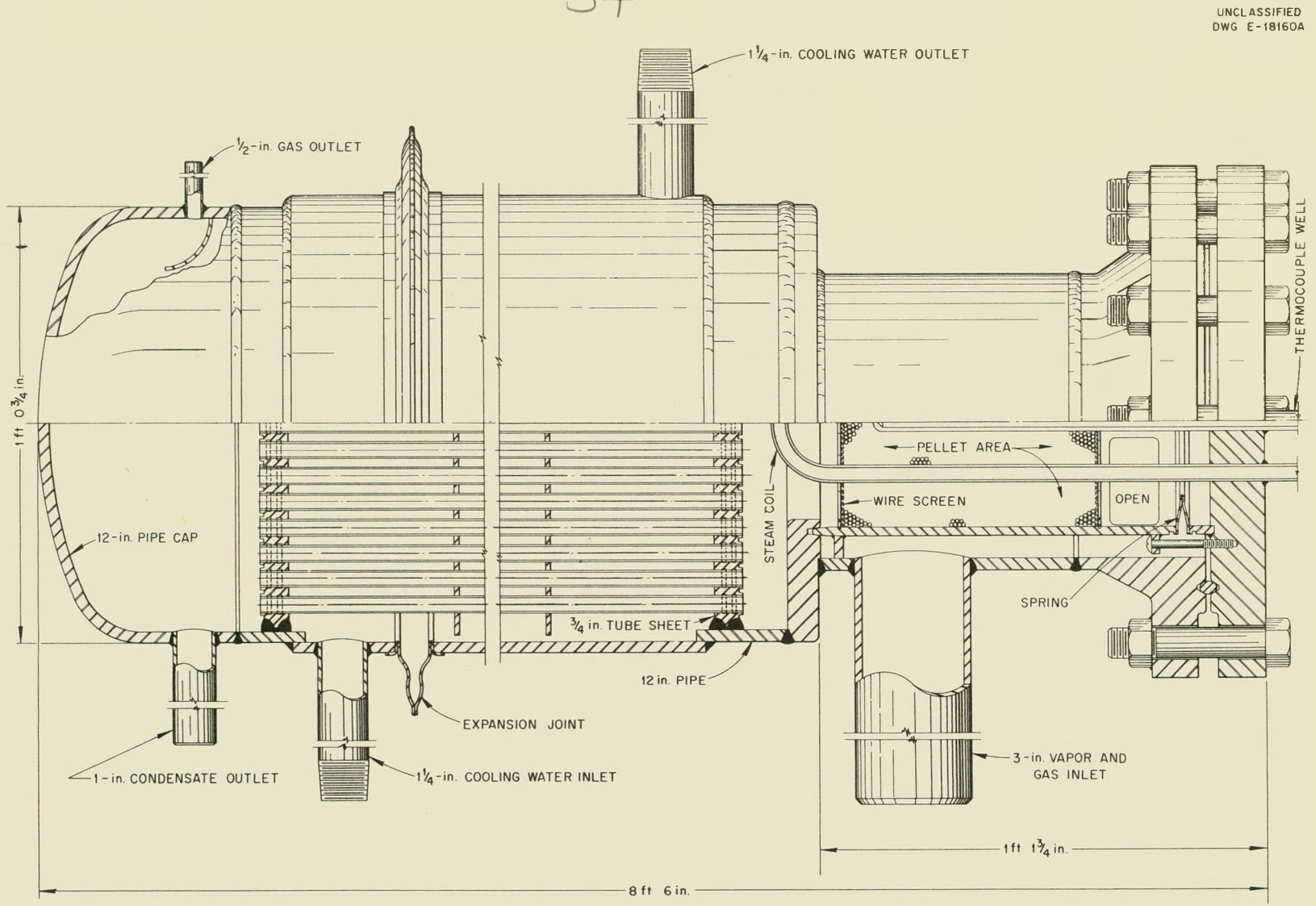

Fig. 25. HRT Recombiner-Condenser Assembly.

the fuel and blanket solutions to 212°F at 1 atm are 2.4 and 9.4 min, respectively.

The recombiner bed is 8 in. long and is housed in a 6-in. schedule-40 pipe. It is packed with $\frac{1}{8} \times \frac{1}{8}$ in. cylindrical pellets of platinized alumina. The bed has a gas capacity of 0.26 lb-mole/min; 10% of the gases is deuterium.

OUTER-DUMP-TANK CONDENSER CALCULATIONS FOR THE HRT

Calculations have been made for a condenser to dissipate the heat released from radioactive decay of the fission fragments in the fuel solution of the HRT after a dump to the outer fuel storage tanks. The required condensing surface area is 27.6 sq ft, which can be obtained with 55 ft of 1.5-in., schedule-10, type 347 stainless steel pipe. This size of pipe was selected as a compromise between the requirement of a thin metal wall for good heat transfer and a diameter and wall thickness consistent with the strength necessary to prevent collapse against a possible dump-tank pressure of 650 psi. The condenser calculations were based on a maximum heat release of 170 kw, determined from infinite operation of the reactor at 10 Mw and 15 min. after shutdown, as shown in Table 14.

TABLE 14. HEATING EFFECT AFTER SHUTDOWN FOLLOWING INFINITE OPERATION OF REACTOR

Time After Shutdown	Fission Product Power Level (kw)	
	After 5-Mw Initial Power	After 10-Mw Initial Power
15 min	85	170
30 min	70	140
1 hr	60	120
1 day	30	60
5 days	25	50
10 days	22.5	45
100 days	8.5	17

A suggested condenser design is shown in Fig. 26. Four units, each 14 ft long, are used to obtain the required surface.

FUEL-DUMP-TANK DESIGN

The capacity and dimensions of the fuel dump tank and condensate storage tank were investigated in regard to inventory, criticality, and start-up requirements.[3] In order to provide for operation with the blanket of ThO_2 slurry at 500 g of thorium per liter at 280°C, the required inventory for the fuel system is as follows: U^{235}, 15 kg; D_2O condensate, 200 kg; total D_2O, 680 kg. This inventory also allows for the holdup of 100 kg in the dump tank as working solution while the reactor is operating at design power and temperature. The solution can be stored in a horizontal tank that is coated on the outside with cadmium and is 14 in. in diameter and 30 ft long, which yields a linear concentration of 0.5 kg of U^{235} per foot. At this concentration and for any quantity of solvent and for any mixture of light and heavy water, the tank should never become critical when totally immersed in light water.

HRT EVAPORATOR DESIGN

An estimate has been made of the surface area required to evaporate 1 gal of fuel solution per minute at atmospheric pressure in order to control the solution concentration and to dilute below the explosive limit the gases of dissociation entering the recombiner. The general specifications for this evaporator are given in Table 15.

Two general designs of possible evaporator arrangements were considered. The first design studied was an arrangement similar to that used in the HRE; the alternate was a standard shell-and-tube calandria type of evaporator. The HRE type of evaporator is adequately described in the *HRE Design Manual*.[4] Figure 27 shows the calandria type of high-performance low-holdup evaporator considered as an alternate.

No decision has been made as to which type will be used in the HRT.

HRT SHIELD DESIGN

The cooperation of the K-25 General Engineering Department has been obtained to assist in the detailed design of the HRT shield. The proposed arrangement of shielding upon which the design will be based is shown in Fig. 28.

Design of the shield will take into consideration the following requirements:

1. The shield is to be a pit located inside Building 7500 (previously the site of the HRE), with the top of the pit at the present floor level.

[3] S. Visner, *Fuel Dump Tanks for HRT*, ORNL CF-54-4-30 (April 2, 1954).

[4] C. L. Segaser and F. C. Zapp, *HRE Design Manual*, ORNL CF-52-6-160 (Nov. 18, 1952).

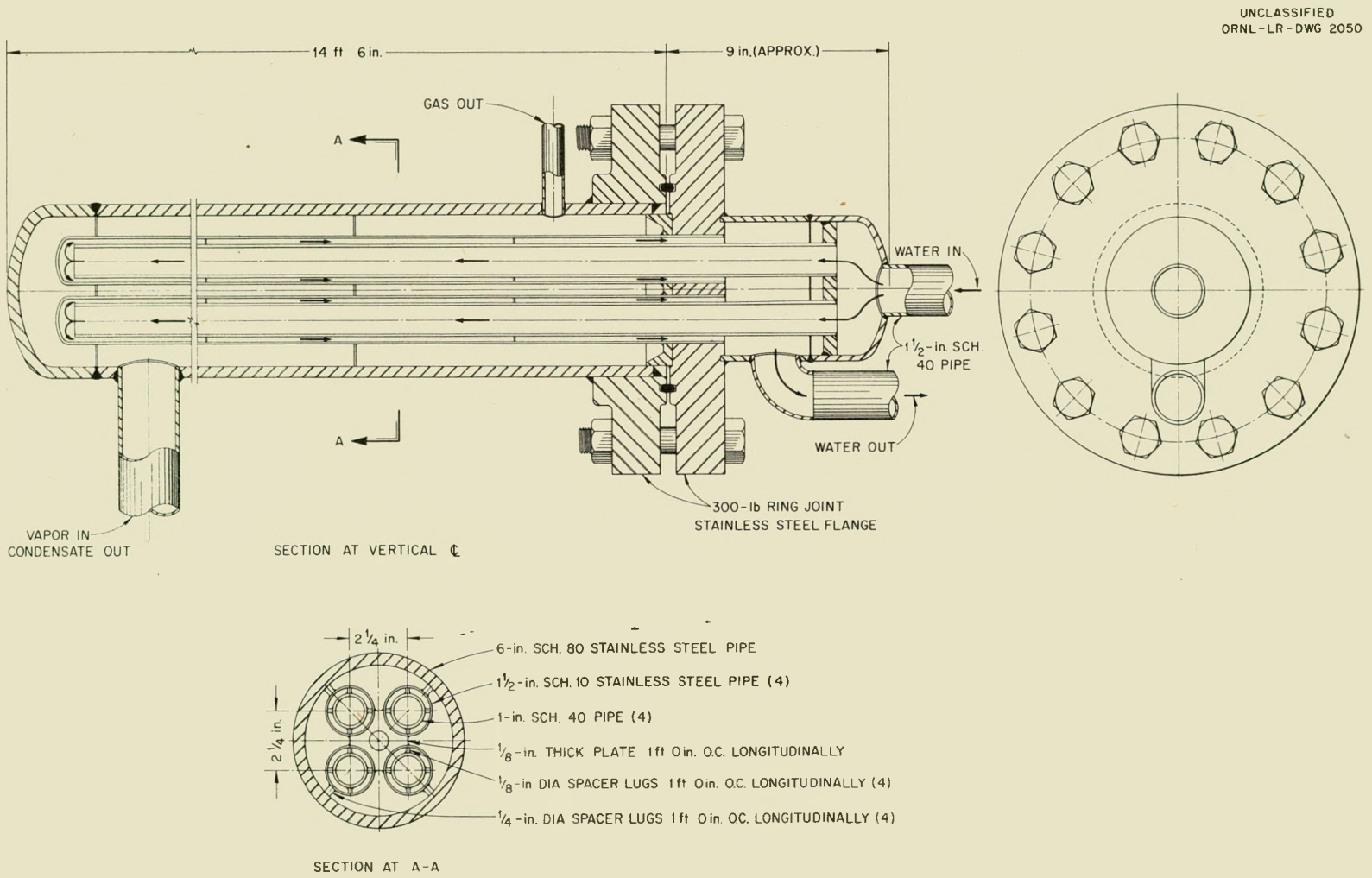

Fig. 26. Outer-Dump-Tank Condenser.

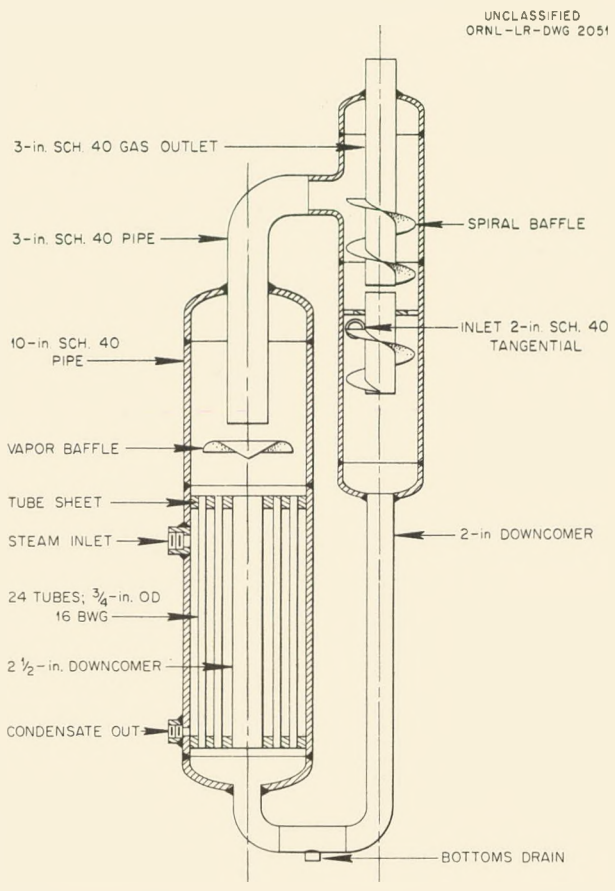

Fig. 27. HRT Fuel-Solution Evaporator.

2. The sides and top of the pit will be designed to give complete biological protection to personnel in the building when the reactor is operating at a power level of 10 Mw.

3. In the event of a major break in the high-pressure circulating system, the shield must contain the fuel solution and fission products; therefore the shield will be lined with a corrosion-resistant material and will be designed to withstand the pressure rise that would occur if the reactor contents were discharged into the pit.

4. The structure will be designed so that it can be filled with water for personnel protection during maintenance operations. The pit will be divided into two sections of approximately equal volume, which can be flooded separately.

5. The top of the shield will be divided into sections, and the entire cover will be removable. The plugs will be designed so that the small sections can be removed with a minimum of disturbance to the remainder of the cover. They will be stepped to prevent radiation streaming, and they will be of a mass that can be handled by means of the building crane. The edges of the plugs will be protected in order to prevent damage during handling.

6. The shield will be penetrated by service and instrument piping and conduits. The penetrations are to be designed to prevent excessive leakage of gas, water, and radiation.

7. It will be possible to subdivide the pit into sections by means of easily removable shielding partitions.

EQUIPMENT AND SHIELD LAYOUTS

The HRT plan and elevation layouts, Figs. 29 and 30, show the progress made in arranging equipment and piping relative to the shielding. The core and blanket solution systems have been arranged to place the core system steam generator near the turbine and thus to shorten the main steam line. Equipment and pipe flanges have been positioned so as to simplify remote removal.

The design of equipment is not yet sufficiently firm for final layouts to be established; therefore they are still being developed. In the elevation layout the arrangement will result in a considerable reduction in the over-all height of the equipment over that originally conceived; thus the necessary depth of excavation will be reduced.

PHYSICAL PROPERTIES OF HIGH-CONCENTRATION SOLUTIONS OF UO_2SO_4-D_2O

Physical properties of uranyl sulphate–heavy water solutions for use in design calculations for the HRT have been derived from a memorandum by R. Van Winkle[5] and from experimental data determined at Mound Laboratory.[6]

Figures 31, 32, and 33 show the density and viscosity of solutions at a concentration of 300 g of UO_2SO_4 per liter.

CONTROL OF XENON POISONING BY STRIPPING WITH GAS

In the normal operation of homogeneous reactors with aqueous uranyl sulfate fuels, Xe^{135} is generated and distributed throughout the system. Destruction of Xe^{135} is by burnup and by radioactive decay. Considerable amounts of decomposition

[5] R. Van Winkle, *Some Physical Properties of UO_2SO_4–D_2O Solutions*, ORNL CF-52-1-124 (Jan. 18, 1952).

[6] R. E. Aven, *Physical Properties of Solutions in the HRT*, ORNL CF-54-1-161 (Jan. 25, 1954).

gases (H_2 or D_2 and O_2) are also given off, and relatively large quantities of Xe^{135} are stripped out of the fuel solution by these gases. Therefore, if the decomposition gases are removed from the system by a gas separator, this becomes one of the better means of minimizing the Xe^{135} poison. Some xenon is removed when part of the fuel solution is removed for chemical processing, but this quantity

TABLE 15. GENERAL SPECIFICATIONS FOR HRT EVAPORATOR

Evaporation rate, gpm	1
Pressure in evaporator	Atmospheric
Temperature in evaporator, °F	212
Flow, gpm	
Gas	1.054
Liquid	2.42
Heat balance	
Evaporation rate, lb/hr	480
Heat transfer, Btu/hr	5.52×10^5
Heat transfer surface based on 62-psig saturated steam	
Tubes	$\frac{3}{4}$-in. OD, 16 BWG, type 347 stainless steel
Steam side coefficient, Btu/hr/sq ft/°F	1500
Boiling coefficient, $\Delta t_B{}^2$	230
Over-all coefficient, Btu/hr/sq ft/°F	658
Steam pressure, psig	62
Steam temperature, °F	310
Mean temperature difference, °F	98
Calculated area, sq ft	8.56

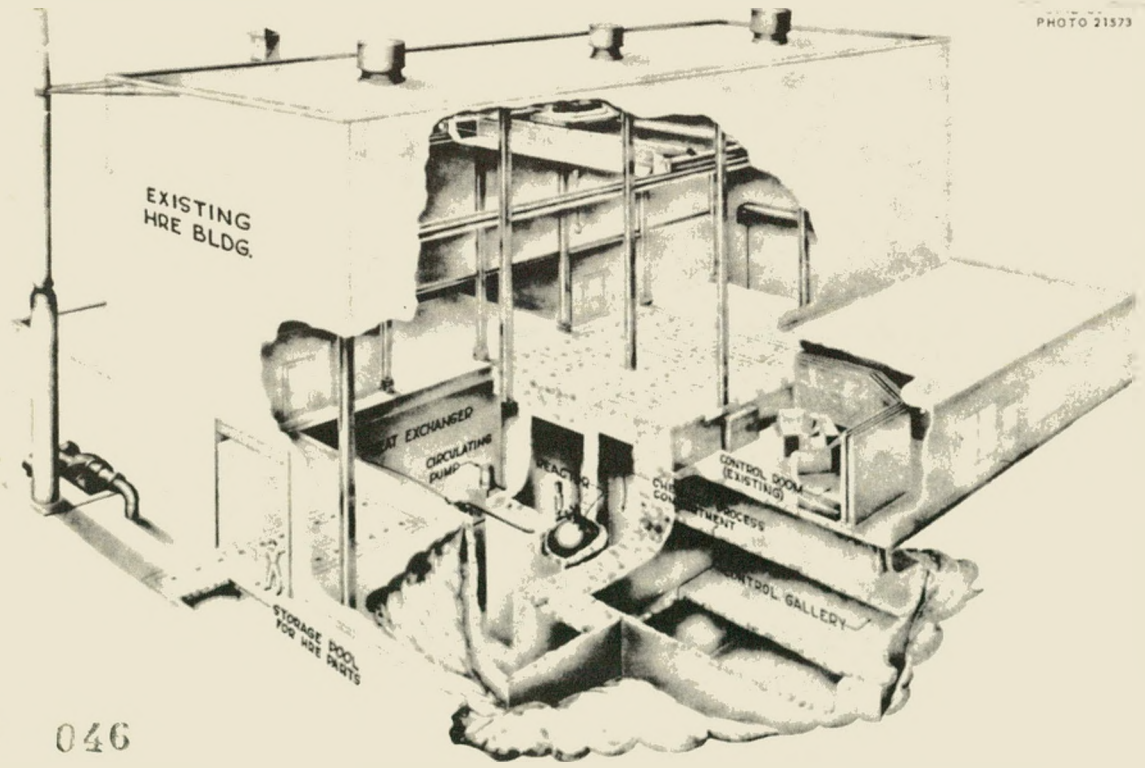

613 046

Fig. 28. HRT Installation.

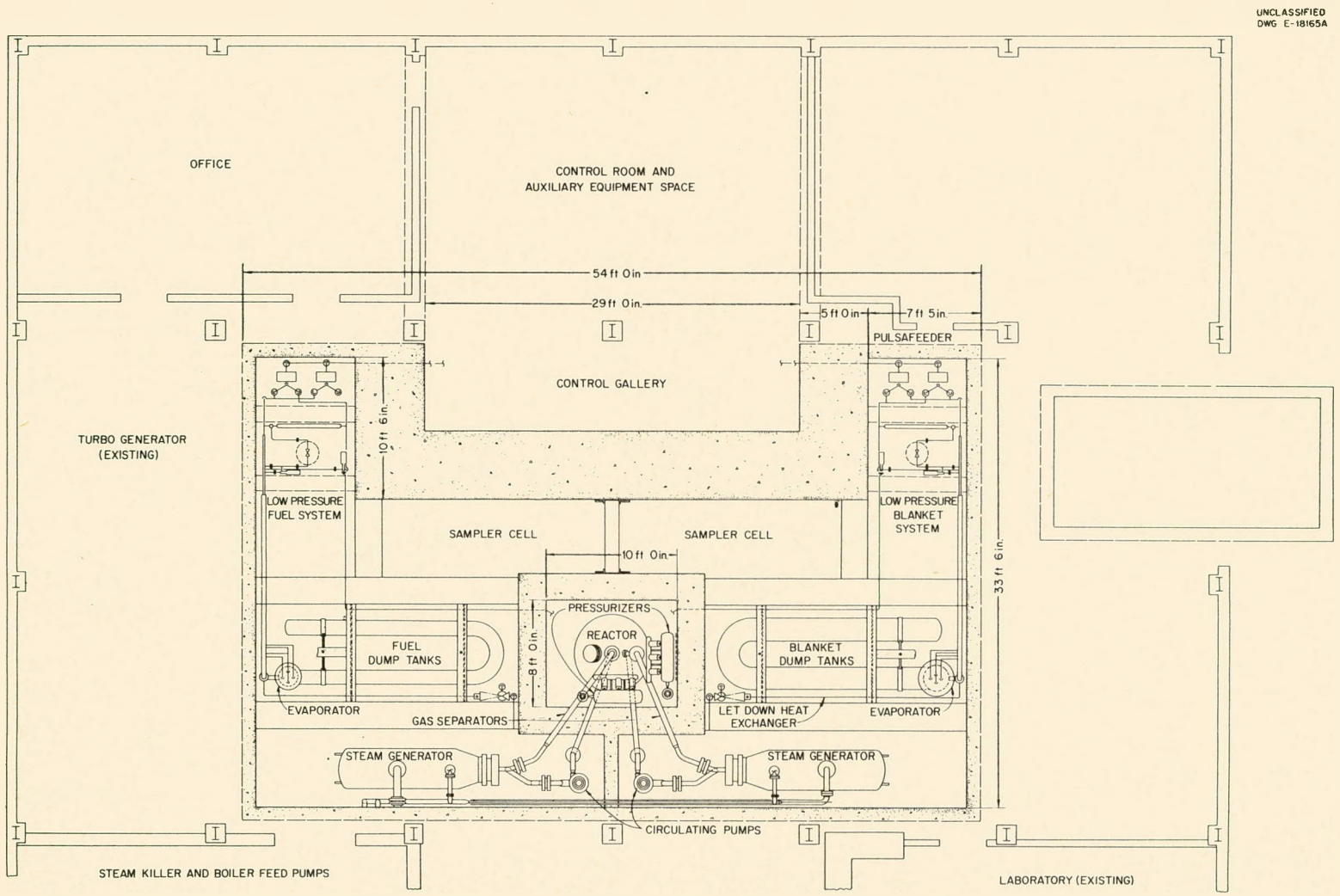

Fig. 29. HRT Preliminary Equipment Layout.

is negligible. Therefore, if the decomposition gases are not present, burnup and radioactive decay are the major means by which Xe^{135} is removed, and, unfortunately, the equilibrium poison level is rather high when burnup and decay are the only means of removal. This situation is the cause of some concern, since it now appears probable that a copper catalyst will be used in the fuel solution to recombine the hydrogen and oxygen as soon as they are formed. It may be desirable to allow some decomposition gases to form for the express purpose of removing part of the xenon gas.

By making a gas balance between the rate of xenon production and the total rate at which it is removed from the system, the following equation may be derived:[7]

$$Q = \left[\frac{y\alpha P\sigma_a}{\beta\Sigma_a(25)} - V_L(\Phi\sigma_a + \lambda) \right] \frac{1}{H},$$

[7] R. E. Aven, *Control of Xenon Poisoning by Stripping with Gas*, ORNL CF-54-2-200 (Feb. 19, 1954).

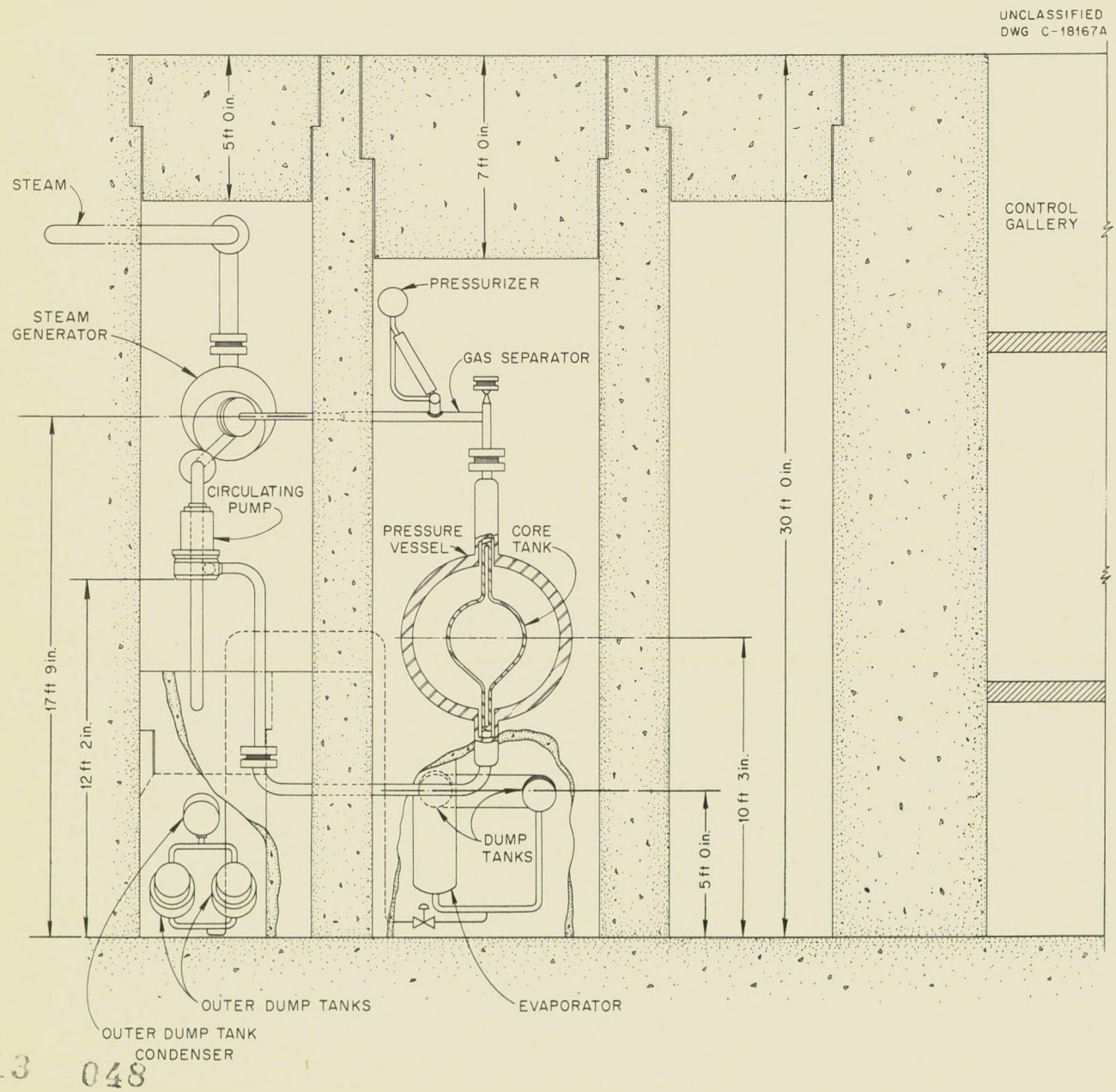

613 048

Fig. 30. HRT Equipment Layout Elevation.

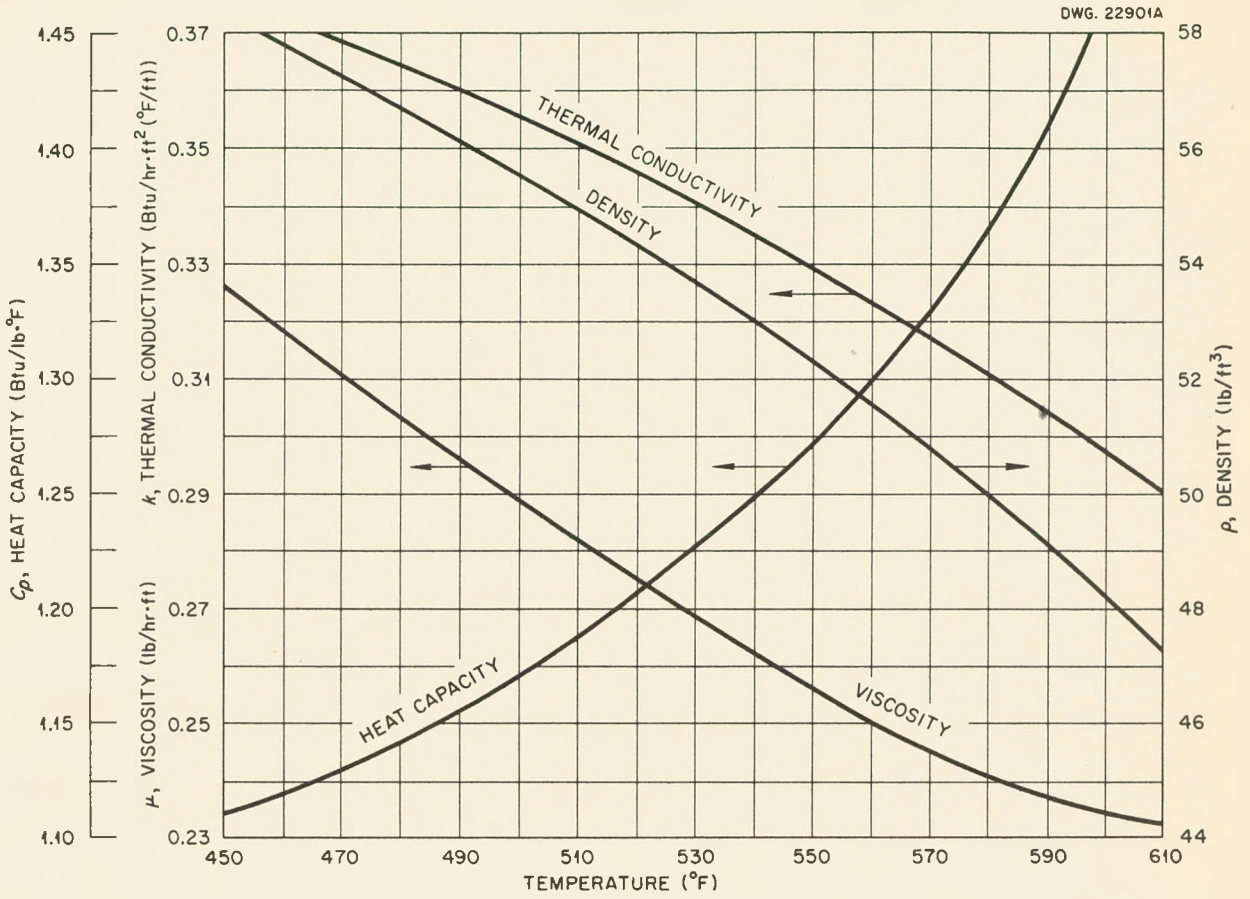

Fig. 31. Physical Properties of HRT Fuel Solution at 2000 psia Pressure and a Concentration of 10 g of Uranium per Kilogram of D_2O.

where

Q = rate of gas-bubble formation, cc/sec,

y = yield of Xe^{135} (or precursor) = 0.059 atoms/fission,

α = 3.38×10^{16} fissions/Mw-sec,

P = reactor power, Mw,

σ_a = absorption cross section of Xe^{135}, sq cm per atom,

$\beta = \dfrac{\Sigma_a(Xe^{135})}{\Sigma_a(25)}$ = equilibrium poison level,

V_L = volume of main loop, cc,

Φ = average thermal flux in main loop, $\dfrac{n}{\text{sq cm-sec}}$,

H = ratio of xenon in gas to xenon in liquid at equilibrium,

λ = decay constant for Xe^{135}, sec^{-1}.

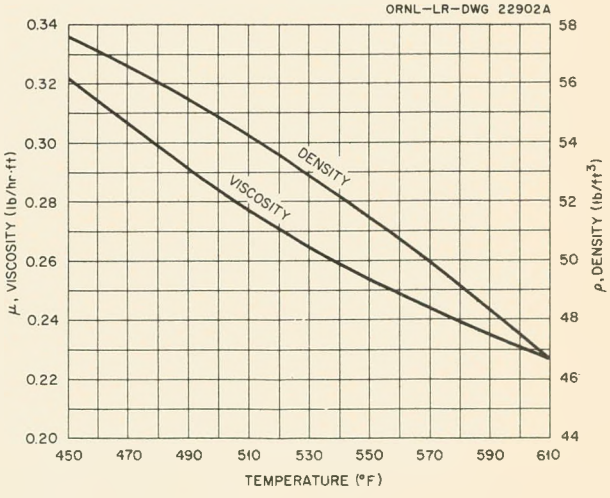

Fig. 32. Physical Properties of D_2O at 2000 psia.

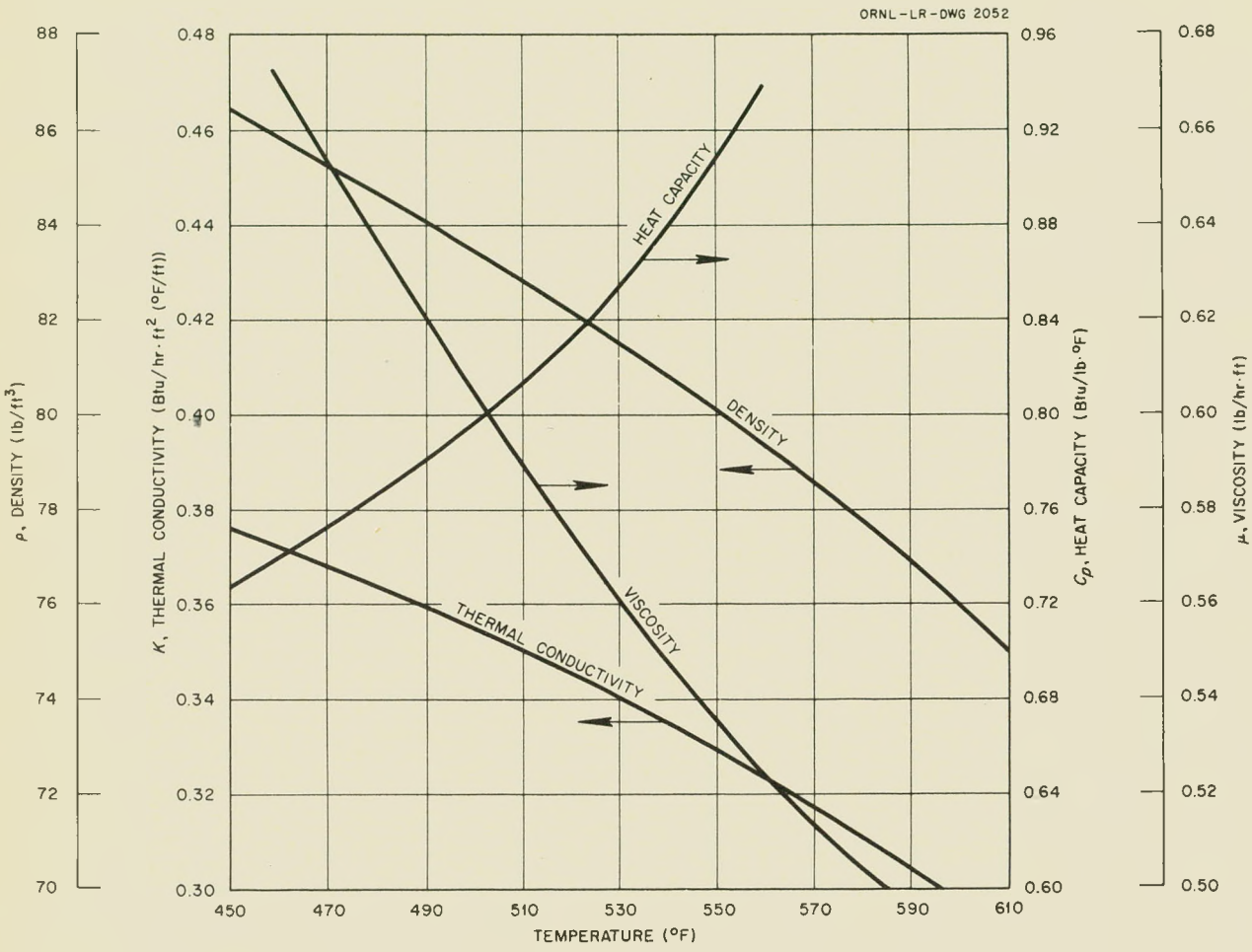

Fig. 33. Physical Properties of HRT Blanket Solution at 2000 psia Pressure. Concentration, 300 g of uranium per liter.

If no gas is available to strip out the xenon, the equilibrium poison level is then approximately 0.04. The rate of gas needed to maintain a desired poison level, β, can be computed from the above equation. Figures 34 and 35 give the actual volume of gas required vs the xenon poison level maintained in the main circulation loop of the HRT and in a larger 6-ft reactor, respectively. Figures 36 and 37 are plots of the fraction of the total gas production needed vs the total pressure on the system, at various poison levels, for the HRT and for the 6-ft reactor, respectively. The curves are drawn for systems operating at 300°C.

The xenon poison level in the HRT can be maintained below 1% by removing gas at a rate of 0.04 cfm. This is only 2% of the gas that would be produced when operating at 2000 psi without a Cu^{++} catalyst. In order to maintain the same level in a large reactor operating with a much lower concentration of U^{235} in the core, the removal of 25 cfm, or 20% of the gas produced without a Cu^{++} catalyst, would be required.

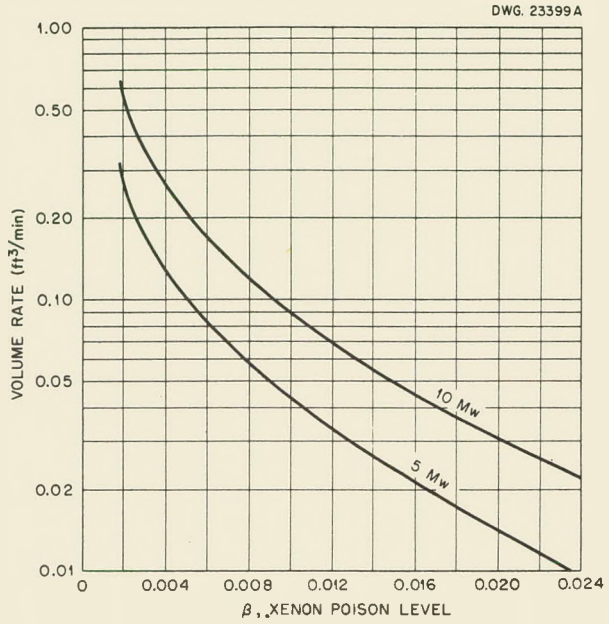

Fig. 34. Volume Rate of Gas Formation Required to Maintain Xenon Poison Level in HRT.

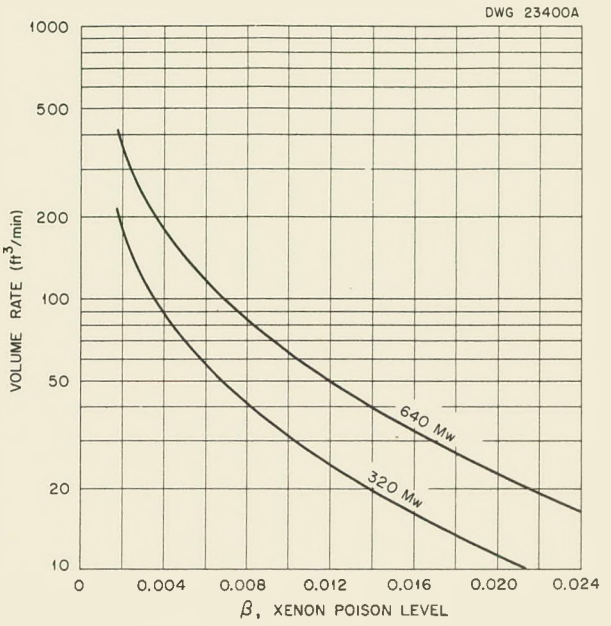

Fig. 35. Volume of Gas Formation Required to Maintain Xenon Poison Level in 6-ft Reactor.

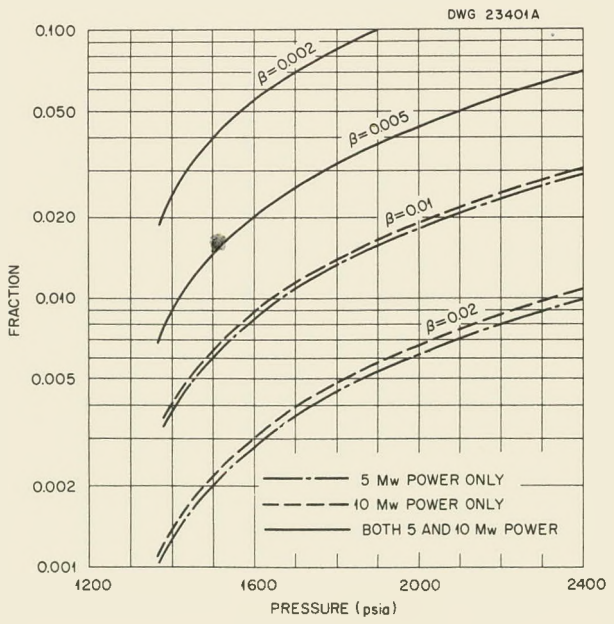

Fig. 36. Relationship Between Fraction of the Total Production of Gas Required to Maintain Xenon Poison Level in HRT and Pressure.

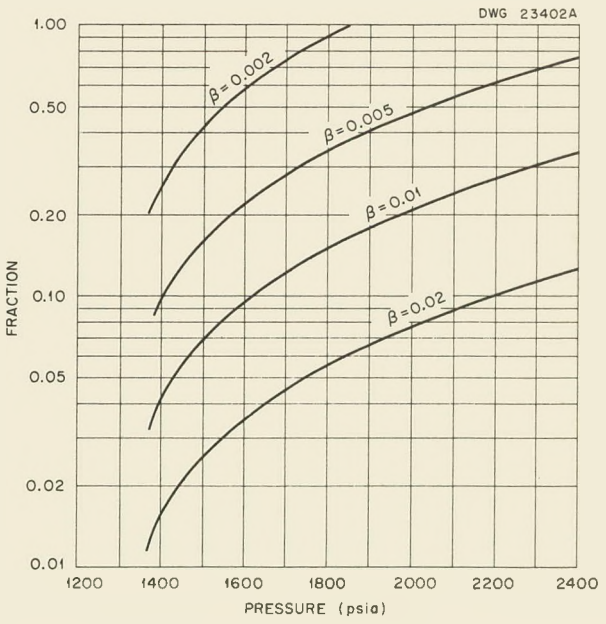

Fig. 37. Relationship Between the Fraction of the Total Production of Gas Required to Maintain Xenon Poison Level in 6-ft Reactor and Pressure.

HRT ENGINEERING DEVELOPMENT

C. B. Graham, Section Chief

J. M. Baker
J. S. Culver
D. M. Eissenberg
L. F. Goode
R. Goodman
J. A. Hafford
P. H. Harley
R. J. Kedl
L. B. Lesem
R. Meza
L. W. Roane
W. L. Ross
I. Spiewak
R. E. Wascher
C. D. Zerby

HRT CORE

The straight-through HRT reactor core contains six screens in the inlet diffuser in order to achieve the spreading of flow necessary to fill the sphere.[1] Since this design allows very little safety factor in the diffuser, a certain amount of flow separation is expected near the sphere wall in the lower hemisphere. Because this disturbance will occur in a low-flux region, it is probably acceptable for HRT use.

A full-scale steel flow model of the core is being built for test purposes. A vaned elbow will be tried in the bend preceding the core, in order to minimize the amount of separation. The testing and evaluation of the model should be completed by June 1.

HRT BLANKET

A small-scale flow model of the HRT blanket has been built, and some qualitative flow studies with cold water have been carried out. The model (Fig. 38) consists of an 8-in. hollow steel sphere centrally located inside an 18-in. plastic sphere. There are two inlets at the bottom of the blanket and an outlet at the top.

Isothermal flow tests, using both inlets, revealed a slow rise of water from bottom to top and some lateral turbulent mixing. The effect of nuclear heat generation was simulated by condensing steam inside the steel ball, thus supplying heat to the part of the blanket immediately surrounding the core. A natural circulation pattern was set up which almost completely masked that of the forced circulation. The hotter fluid near the core wall rose rapidly, and there was a downward current at the outside. Turbulent mixing was much greater than in the isothermal case. A temperature survey in the equatorial plane revealed that the fluid in the blanket (with the exception of the laminar film at the core-tank wall) was essentially at outlet temperature. At present, this system is being modified to allow the circulation of the thoria slurry.

Blanket flow tests are planned in the full-scale HRT model being built by Newport News Shipbuilding and Dry Dock Company.

ALTERNATE CORE

A 4-ft flow model of the alternate core configuration, which incorporates concentric inlet and outlet pipes,[2,3] has been installed. This unit will be used to examine the parameters involved in applying the data from the 18-in. model to larger scale returns. Preliminary tests indicate thorough mixing and a pressure drop of 1.5 velocity heads, as predicted.

HRT GAS SEPARATOR

A low-pressure and low-temperature plastic model of the proposed HRT gas separator has been built and tested, and the results are quite encouraging. Gas removal was nearly complete, with a water entrainment of 0.3 to 0.5 gpm. With a discharge angle of 45 deg in the rotation vanes, the required flow angle of the recovery vanes was measured and found to be 45 deg.

HRT MOCK-UP

It is planned that the critical components of the HRT (Fig. 39) will be mocked up prior to the actual assembly. Since the designs of the core and the blanket systems are very similar, the same loop can

[1] L. B. Lesem and I. Spiewak, *Straight Through HRT Core*, confidential memorandum to W. R. Gall, Feb. 25, 1954.

[2] L. B. Lesem and I. Spiewak, *Alternate Core Proposal for the HRT*, ORNL CF-54-1-80 (Jan. 19, 1954).

[3] R. Goodman, J. A. Hafford, L. B. Lesem, and I. Spiewak, *HRP Quar. Prog. Rep. Jan. 31, 1954*, ORNL-1678, p 33.

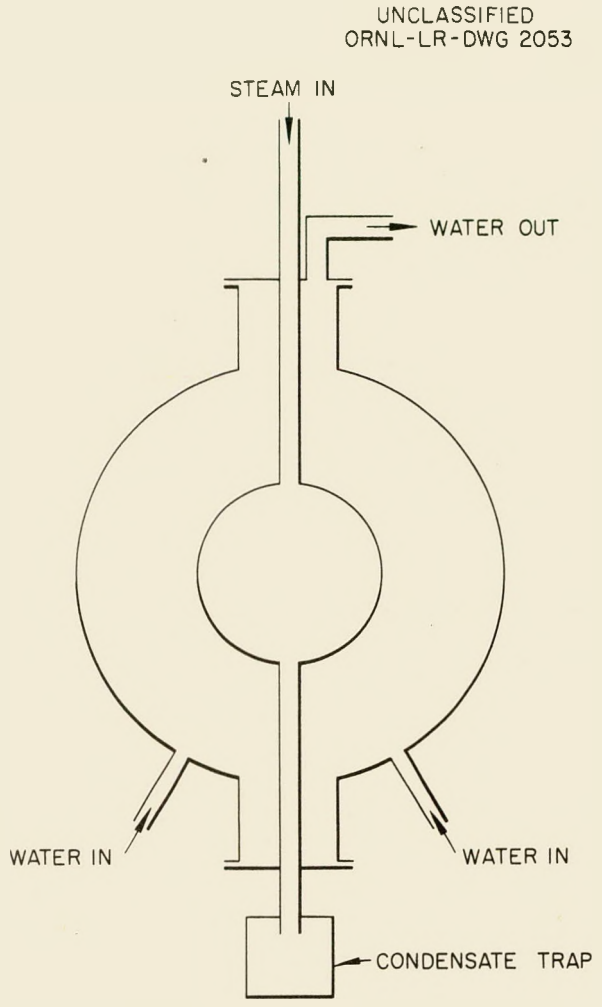

Fig. 38. HRT Blanket Model.

be used to test both systems. The engineering operation of the circulating pump, gas separator, pressurizer, letdown system, and pulsafeeder will be checked during mock-up operations. The mock-up will also be used to obtain corrosion data on concentrated soup in a stainless steel system.

HRT HEAT EXCHANGERS

Proposals have been requested for the design, fabrication, and testing of HRT fuel and blanket heat exchangers.

[4] W. L. Ross, *HRP Quar. Prog. Rep. Jan. 31, 1954*, ORNL-1678, p 38.

HRT FUEL AND BLANKET PUMP DEVELOPMENT (230 TO 500 gpm PUMPS)

The design of the Westinghouse Model 400A pump, presently on order,[4] has been changed so that it will serve as the HRT fuel-pump prototype. The pump casing, originally designed for operation at 1000 psi, has been redesigned to contain a pressure of 2000 psi. Also, thicknesses of the suction and inlet pipes have been changed so that they are acceptable for use in the HRT.

These pumps, which are all-stainless-steel construction, are to be delivered in July or August. Titanium reinforcing will be added and tested as soon as the titanium is available for the construction of the necessary parts.

The Allis-Chalmers Mfg. Co. is completing preliminary designs for an alternate canned-rotor fuel-circulating pump for the HRT. The pump will be rated at 500 gpm and 100 ft of head at 300°C and 2000 psi. The rotor and bearing chamber will be cooled to below 212°F. Special features of this pump will include pressurized fluid-piston bearings and "top maintenance."

Both Westinghouse and Allis-Chalmers are submitting proposals for the construction of loops with instrumentation for the development and testing of the pumps. Specifications call for long-term operation with fuel solution at HRT conditions.

Westinghouse is presently redesigning the Model 150C pump to deliver 300 gpm with a head of 65 ft, or, when the impeller is modified, to deliver 230 gpm with a head of approximately 50 ft. The motor of this pump (Model 300A) will be the same as the motor of the original model. The new design will include changes necessary to fulfill certain HRT specifications and to make the pump suitable for HRT blanket operation.

The Model 150C pumps on order[4] will be completed as Model 300A pumps and will serve as the HRT blanket pump prototypes. Delivery of these pumps is anticipated in late summer of this year. Developmental testing will be carried on in loops similar to the ones used for the fuel pumps.

Orders for HRT fuel and blanket pumps will be placed as soon as final designs and specifications have been completed.

PULSAFEEDER-PUMP DEVELOPMENT

Work on the pulsafeeder pumps has recently been directed toward developing a satisfactory pump for the core and blanket systems of the HRT. Present

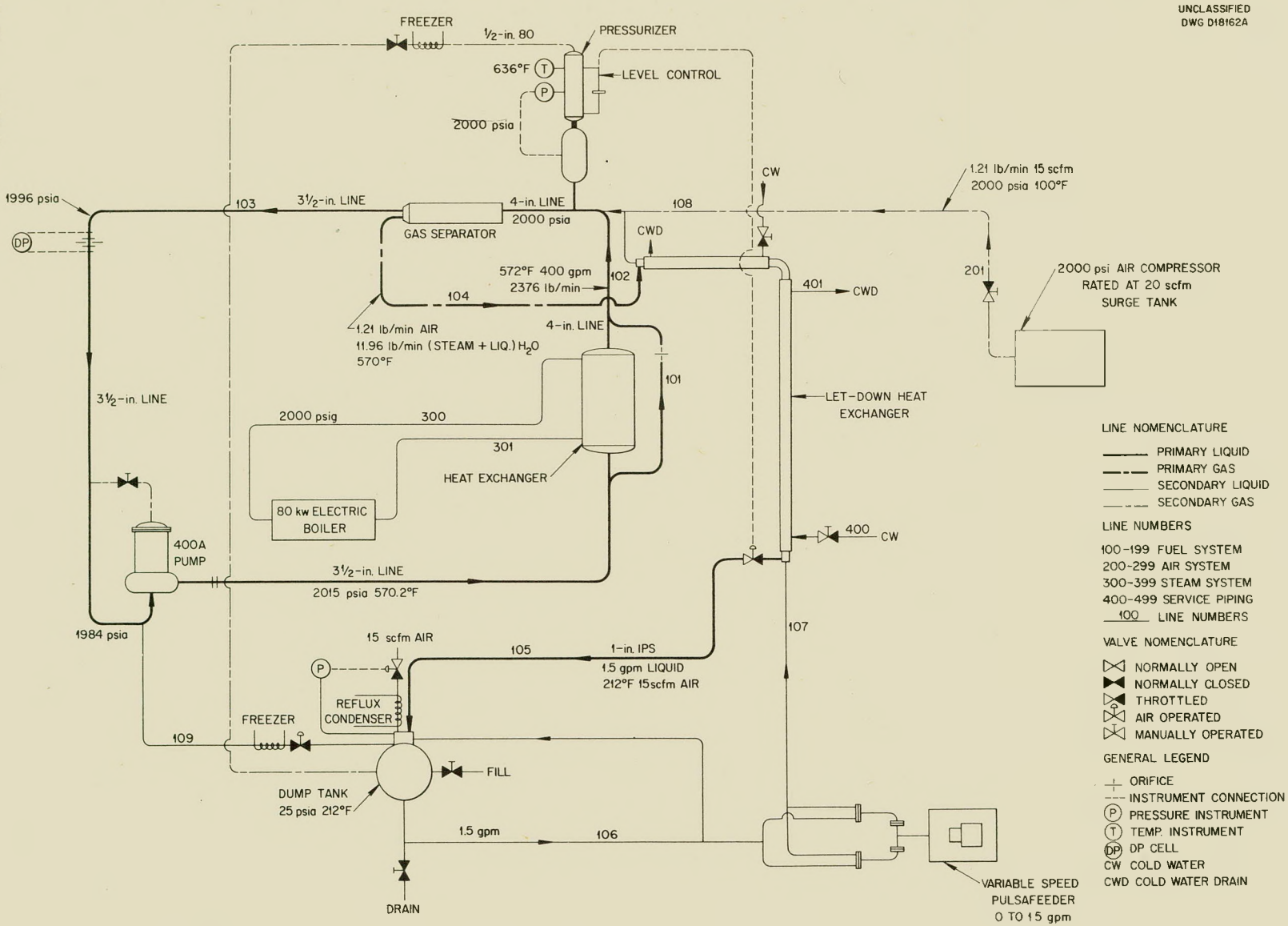

Fig. 39. Mock-up of Critical HRT Components.

reactor flow sheets show core and blanket feed pumps which deliver 1.5 gpm at 2000 psi.

The manufacturer of these pumps has done some work on the development of units larger than those used on the HRE in anticipation of requests for a larger pump of a specific design. The proposed design calls for a somewhat larger head than the one used in the HRE pumps and a heavier diaphragm which will operate in a very shallow, dished cavity. A heavier diaphragm will not puncture so readily and a short stroke will result in lower stresses; thus the life of the diaphragm should be improved.

Concurrent with this effort, work was initiated to improve check-valve operation and to reduce the chatter which had been so annoying and caused so much damage to the HRE. A typical valve assembly is shown in Fig. 40. An early model pump head, in which the valve assemblies could be readily modified, was used to make two types of ball-guiding cages (Figs. 41*a* and 41*b*). In addition to modifying the geometry of the cage, a variable stop was installed so the ball could rise to any desired distance off the seat. Initial tests indicated that the primary source of the chatter was in the discharge check valves. A reduction of $\frac{3}{16}$ in. (from the standard $\frac{5}{16}$ in. to $\frac{1}{8}$ in.) in the lift of the ball resulted in chatter-free operation under normal conditions with both designs; however, when the system pressure was suddenly lowered, the cage shown in Fig. 41*b* was definitely superior. It should be noted that the stop in the top of the cage is a small cup which serves as a hydraulic cushion for the ball and reduces noise and wear.

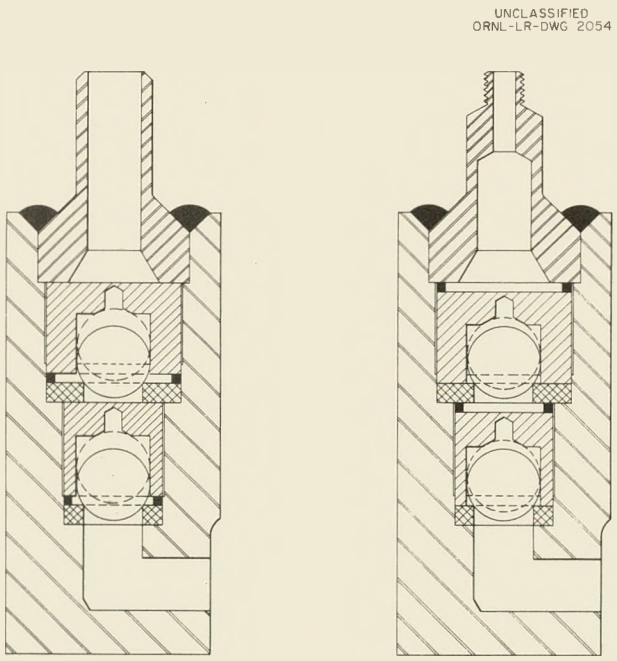

Fig. 40. Revised Inlet and Outlet for Pulsafeeder.

Operation of the pumping unit on the variable-frequency electrical power supply showed quiet, reliable performance at up to 82 strokes per minute – far in excess of the 40- to 50-stroke maximum for the HRE pumps.

In view of the success attained in the check-valve program, it was decided to convert the pump to 2000-psi service and to study the effect of increased compressibility and, at the same time, to look for unforseen problems which might be encountered on the HRT.

The hydraulic power unit from the D_2O system of the HRE and a small-bore (1-in.) oil cylinder already on hand provided a suitable power unit for the test. The only component which had to be replaced was the small pressurizer vessel which was not believed capable of withstanding the higher pressure. The pump head and check valves were designed for 1500-psi service and hence are considered safe on cold-water service.

The pump operated without difficulty at 71 strokes per minute, with a 5-hp 1750-rpm drive motor, and pumped water at an equilibrium temperature of 120°F. In Fig. 42, the lower curve represents the output of the pump after 1500 cc of oil was added to the hydraulic system to introduce a compressible volume more representative of a reactor system.

In order to supply HRT pumps with a minimum of development work, it appears that a duplex pump of the size tested would provide adequate flow and could be procured on relatively short notice. However, additional strength must be built into the heads so they can withstand the increased pressure, and a more substantial pumping unit should be provided. The D_2O pump from the HRE will be modified for 2000-psi service and tested as soon as possible. Specifications for a similar pump are almost ready to be submitted for bid so that a test pump may be available within a few months and reactor pumps by the first of the year.

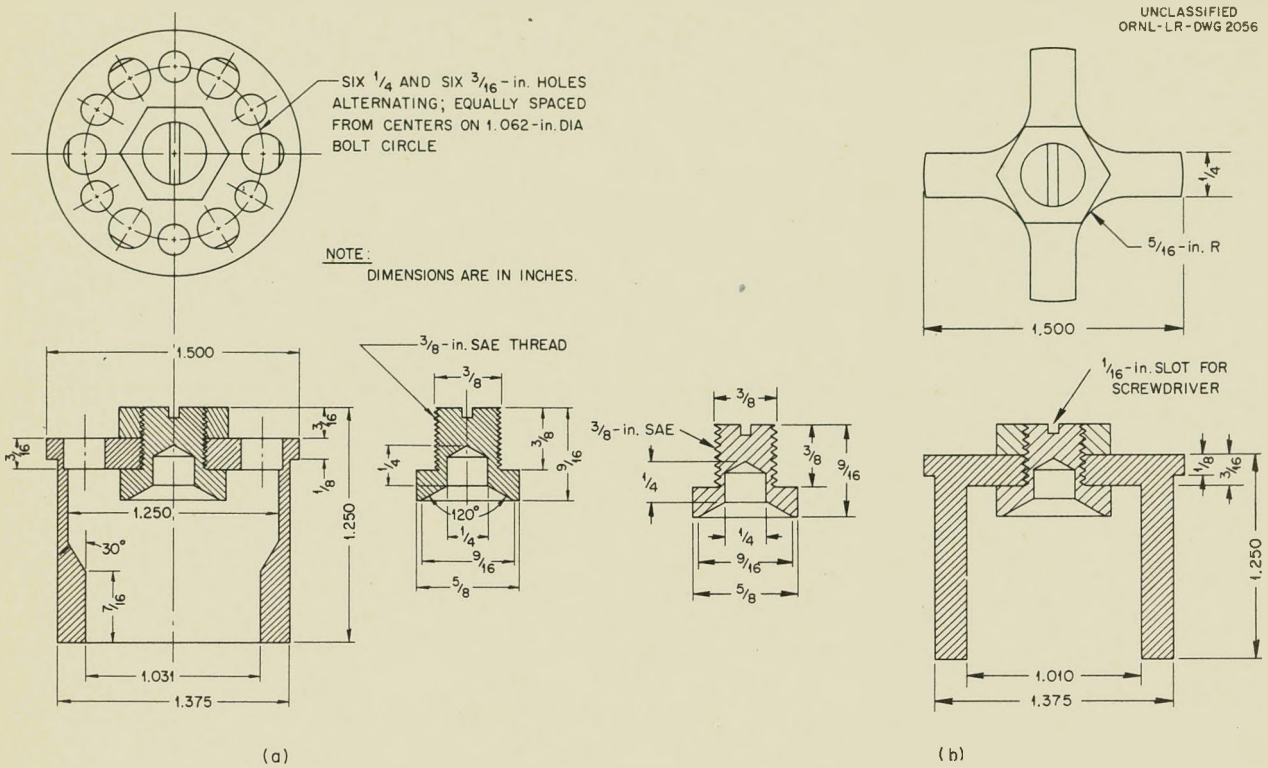

Fig. 41. Two Types of Ball-Guiding Cages for Pulsafeeder Check Valve.

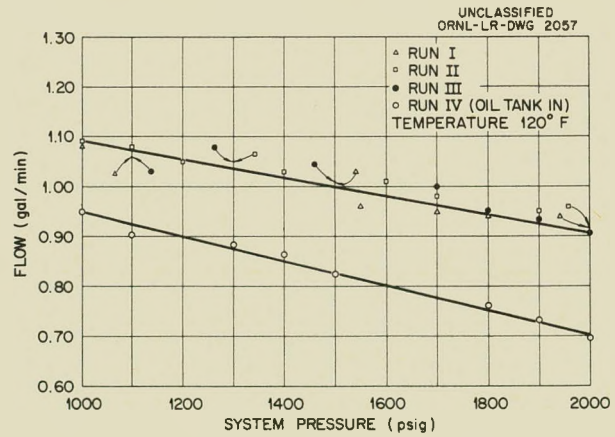

Fig. 42. Relationship Between System Pressure and Flow with Pump Operated at 71 Strokes per Minute at 120°F.

INSTRUMENTATION AND CONTROLS

J. N. Baird, Jr., Section Chief
A. M. Billings
D. G. Davis
R. L. Moore
J. L. Redford
D. S. Toomb, Jr.
W. P. Walker

HOMOGENEOUS REACTOR TEST INSTRUMENTATION

Control Panel

Two preliminary panel-board designs, one graphic and the other nongraphic, have been completed. The graphic panel has been laid out on cardboard to one-quarter scale, using miniature connector symbols, instrument photographs, and colored Scotch tape. A full-scale mock-up of the nongraphic panel has been completed; full-size instrument photographs have been mounted on a plywood panel that was erected inside a space bounded by pipe rails to simulate the ultimate intended floor area. A resumé of factors which affect panel selection is being prepared. Consideration of these data and the two panel layouts will determine which of the panels is more suitable for the HRT.

Several makes of pneumatic instrument systems have been ordered for test purposes. These instruments, which have plug-in air connections, may be removed from an instrument panel and replaced in a few seconds without disturbing anything else. The removed instrument may then be serviced. Because of these maintenance advantages, the use of pneumatic miniatures in either the graphic or the nongraphic panel, except for certain critical measurements, is recommended.

The control-room layouts have been examined, and provisions are being made on the first floor below for the installation of recording stations; in these stations, data-collecting instruments may be studied without interfering with the operator in the room above.

Preliminary inspection of the flow sheet has been completed, and the individual measuring elements are being investigated.

Control-Valve Program

Orders have been placed with two companies for type 347 stainless steel bellows for use at 2000 psi and 300°C. Breeze Corporations, Inc., Newark, New Jersey, which makes the more compact bellows of the two, plans to deliver six units by June 19. These bellows will take a maximum overload of 25% and can be used up to 2500 psi at the rated temperature. This overload factor of safety appears to be standard in the bellows industry. When built into a system, valves equipped with these bellows cannot be tested hydrostatically at higher pressures unless the valves are blanked off from the line or unless the bellows is externally pressurized. The bellows ordered from the Badger Manufacturing Company should be delivered by June 1. Bellows of both manufacturers will be cycled and life-tested.

Drawings and specifications for a prototype high-pressure leak-tight valve were sent out to 15 companies, many of which were contacted personnally. This 0.5-in. valve, for use at 2000 psi and 300°C, was designed in the Mechanical Design Section with the co-operation of the Instrumentation and Controls Section. In response to these inquires, nine companies returned bids which ranged in price from $1442 to $5000 for valves without bellows, and six companies submitted no bids. One valve is being purchased for evaluation from each of four manufacturers selected from the low-, medium-, and high-priced bids. Delivery times ranged from 8 to 16 weeks. These four valves will be operated by different means such as by hydraulic pistons, by pneumatic pistons, and by extra-large high-pressure pneumatic diaphragms.

Trim components suitable for use in this experimental valve are being fabricated in the ORNL shops and will be laboratory tested for leak-tightness and other characteristics. Valve trim specifications based on this experimentation will be written for subsequent valves.

An improved all-metal operator which employs a 68-sq in. stainless steel bellows has been designed for actuating the high-pressure valve in high-nuclear-radiation fields. Fabrication of this operator will soon be under way in ORNL shops, and, when completed, the operator will be cycled and life-tested.

The HRT soup system has been surveyed, and the requirements for each individual valve, including c_v, have been detailed.

Nuclear Instrumentation

A study of the nuclear instrumentation required for the HRT is now essentially complete. Emphasis was placed on improved reliability, ease of maintenance, and methods of mounting and adjusting the sensitivity of the chambers.

Four chambers are proposed for the reactor – two fission chambers and one compensated chamber for operational use, and one compensated chamber for use in transient experimentation. The use of Westinghouse fission chambers and sealed ORNL compensated chambers is recommended in order to eliminate the problem of maintaining a gas flow. In addition, process and personnel monitors will be required.

The elimination of safety rods from the reactor has reduced the electrical operational instrumentation to one Log N amplifier, one compensated power supply, two count-rate meters, and two recorders. Linear and logarithmic equipment has been selected which will meet the response requirements of transient experiments.

A multichannel radiation-monitoring unit has been ordered for evaluation as a substitute for the bulkier single-channel monitrons now in use.

Three alternate systems of mounting compensated and experimental chambers in the reactor are under investigation.

Waterproofing of Instrumentation

A 52-in.-dia 48-in.-high tank equipped with a standpipe 21 ft high and 14 in. in diameter has been relocated and is available to simulate HRT flooded-cell conditions. A large assortment of waterproof power wiring, connectors, and thermocouple wiring has been assembled and will be tested after submergence under 25 ft of water in this test facility.

General

An instrument flow sheet of the soup and the blanket systems has been completed, and an investigation of the individual transmitter requirements is under way.

51

Part III

GENERAL HOMOGENEOUS REACTOR STUDIES

ENGINEERING DEVELOPMENT

C. B. Graham, Section Chief

J. M. Baker
J. S. Culver
D. M. Eissenberg
L. F. Goode
R. Goodman
J. A. Hafford
P. H. Harley
R. J. Kedl
L. B. Lesem
R. Meza
L. W. Roane
W. L. Ross
I. Spiewak
R. E. Wascher
C. D. Zerby

GAS SEPARATORS

The initial runs on the experimental, intermediate-scale, 5000-gpm gas separator were described in the last quarterly report.[1] Additional runs have been made with the use of a spherical Pitot tube. The irregularity of the flow gave rise to poor reproducibility of velocities, which were consistent to only about 20%.

The long-radius elbow was replaced by a vaned-mitre elbow, which served to greatly improve void stability. With this modification, it was not possible to inject air directly into the void; so the maximum gas input to the separator was about 1000 cfm. Nearly all this gas was centrifuged into the void and removed in the gas takeoff. The amount of liquid entrainment in the gas stream was about 125 gpm, slightly less than that observed with the long-radius elbow. The quantity of entrainment does not appear to be very sensitive to gas-flow rate.

Flow patterns were again measured and appeared to be more consistent. Energy balances indicated that the recovery vanes were about 85% efficient.

Future investigations on this model will be aimed at modifying the gas takeoff to decrease local turbulences and to minimize the amount of entrainment.

HIGH-PRESSURE CATALYTIC RECOMBINER

Construction of components for the high-pressure recombiner loop is about 80% complete, and final assembly will be completed during the next quarter. The layout of the loop is shown in Fig. 43.

Preassembly testing of the ORNL pump, water jet, and boiler system at low pressure is under way. Some minor modifications in boiler operation have been suggested by these tests.

The main objectives of the experimental program[2] for the loop are to determine: the efficiency and life of the catalyst; its poisoning by halogens, uranyl sulfate, and possibly SO_3; the corrosion resistance of stainless steel at recombiner conditions; and the susceptibility to detonations when an explosive mixture is present.

In conjunction with this program, a high-pressure entrainment separator loop is being planned for evaluating wire-mesh demisters. The fabrication of this loop is awaiting development of a suitable high-pressure blower.

MAIN FUEL AND GAS CONDENSER HEAT EXCHANGERS

The Foster Wheeler Corp. has been selected to undertake the design and development of the major heat exchangers required for a 50-Mw system. Although contract negotiation has not been completed, both design and development are proceeding.

Figures 44, 45, and 46 are representative layouts of some of the fuel heat-exchanger designs studied to date. A noteworthy departure from previous designs, such as the HRE heat exchanger, is the reversed-head construction of the integral design shown in Fig. 44. This effects a reduction in channel holdup without the use of filler pieces. The horseshoe-shaped exchanger (Fig. 46) eliminates the pass-partition plate required in a conventional U-tube exchanger and has the added advantage of substantially reducing the size of the tube sheet and head forgings.

The two-drum unit appears to have operational characteristics superior to those of the integral unit, but requires more shielded volume for installation. The two-drum unit will have greater versatility, inasmuch as steam generation is more stable

[1] R. Goodman, J. A. Hafford, L. B. Lesem, and I. Spiewak, *HRP Quar. Prog. Rep. Jan. 31, 1954*, ORNL-1678, p 34.

[2] D. M. Eissenberg, *Proposed Experimental Program for High Pressure Recombiners*, memorandum, April 9, 1954.

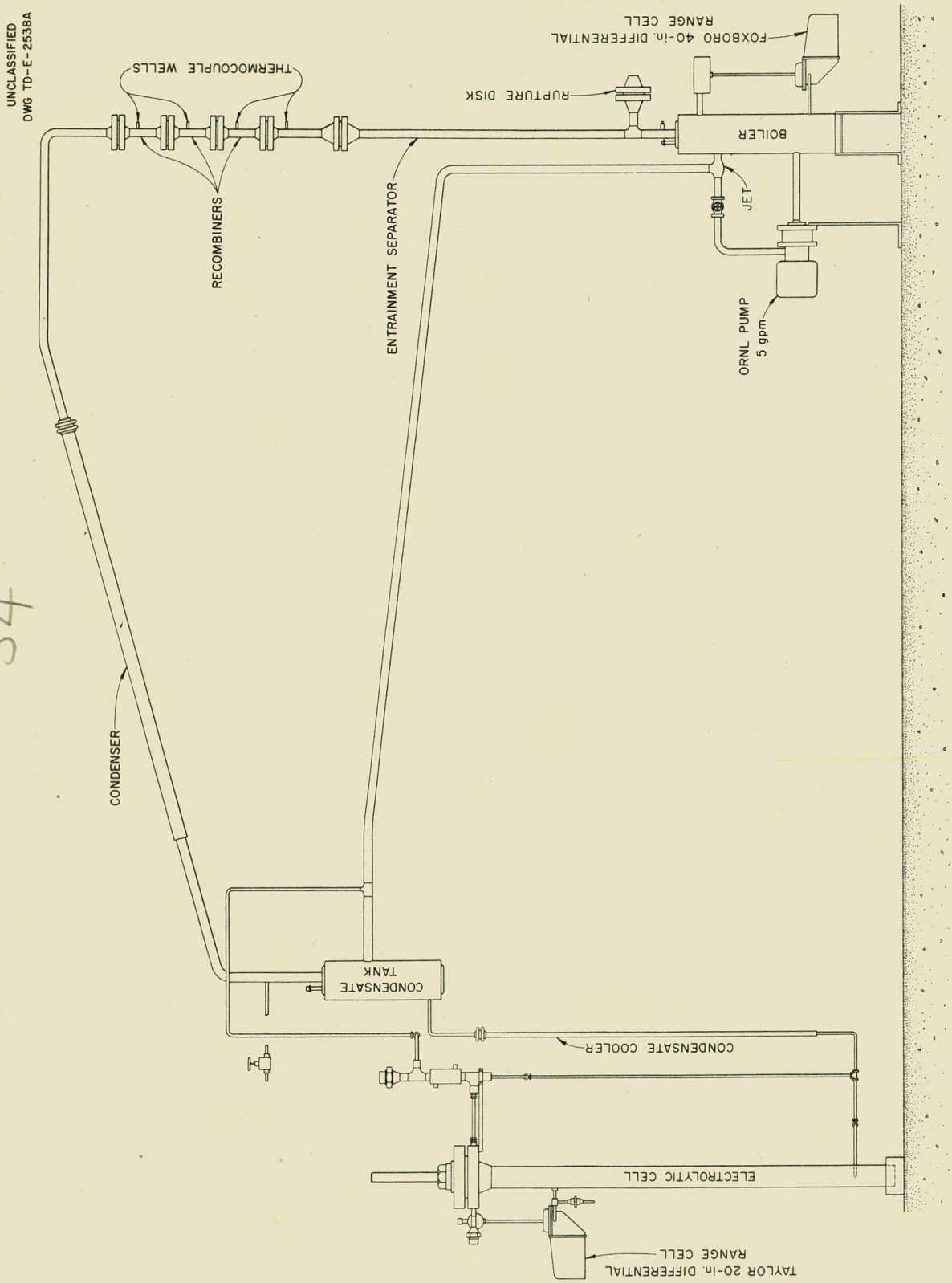

Fig. 43. High-Pressure Recombiner Loop.

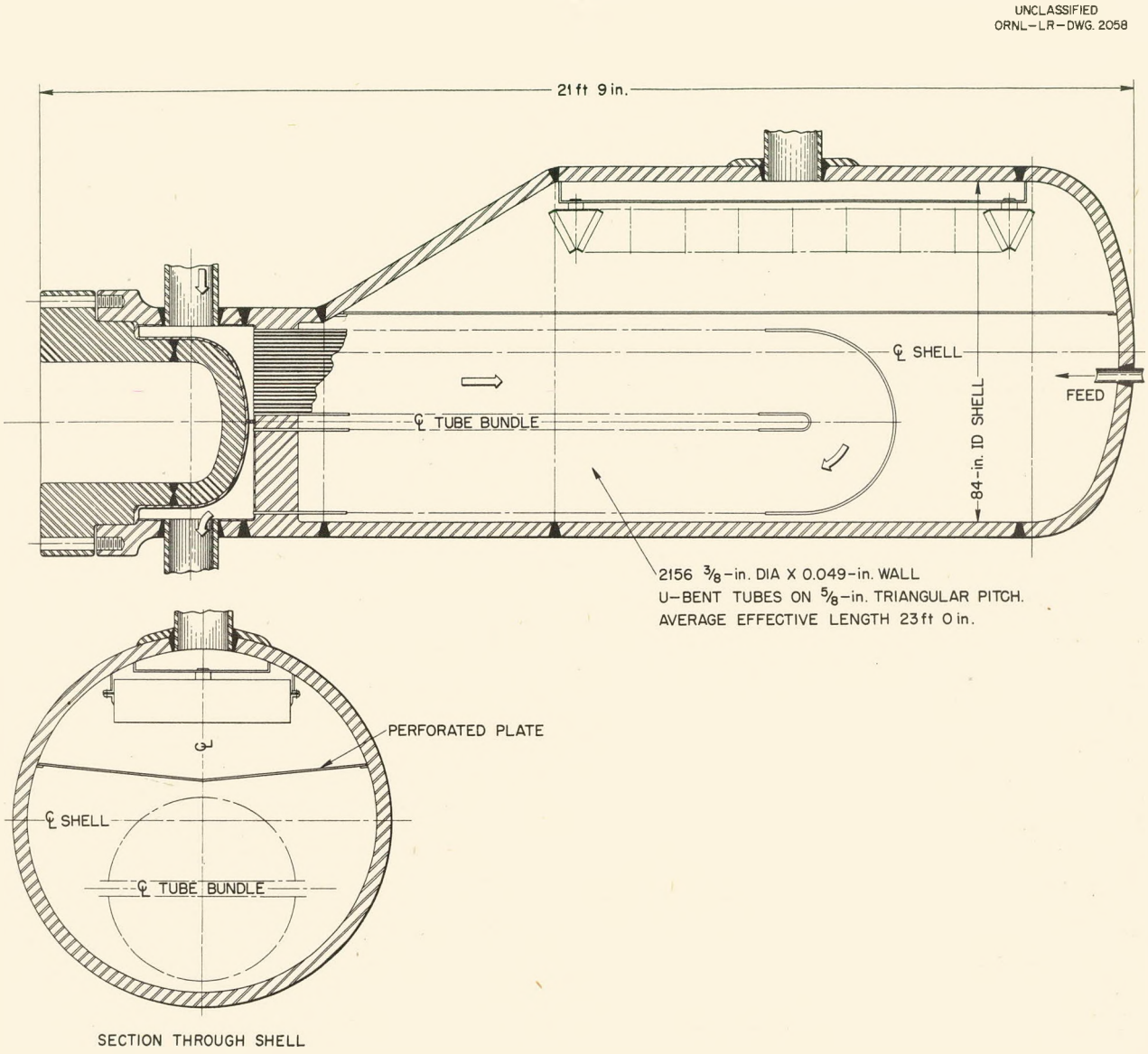

Fig. 44. 50-Mw Integral Heat Exchanger.

at power. Generation will be more stable over a wider range, and there will be greater assurance of high steam quality.

Basic design calculations for the gas cooler-condenser are being made; design study will be postponed pending better definition of system requirements.

The contractor has started development work on two problems: development of techniques in tube-joint welding, including manual welds and the study of automatic welding methods, and investigation of tube-testing methods which will ensure, insofar as practicable, the elimination of all faulty tubing prior to the fabrication of a heat exchanger. With respect to welded tube-joint development, a test-model heat exchanger, the first in a series of about four, is being designed. It will incorporate the most promising welds and will be used at ORNL under corrosive conditions.

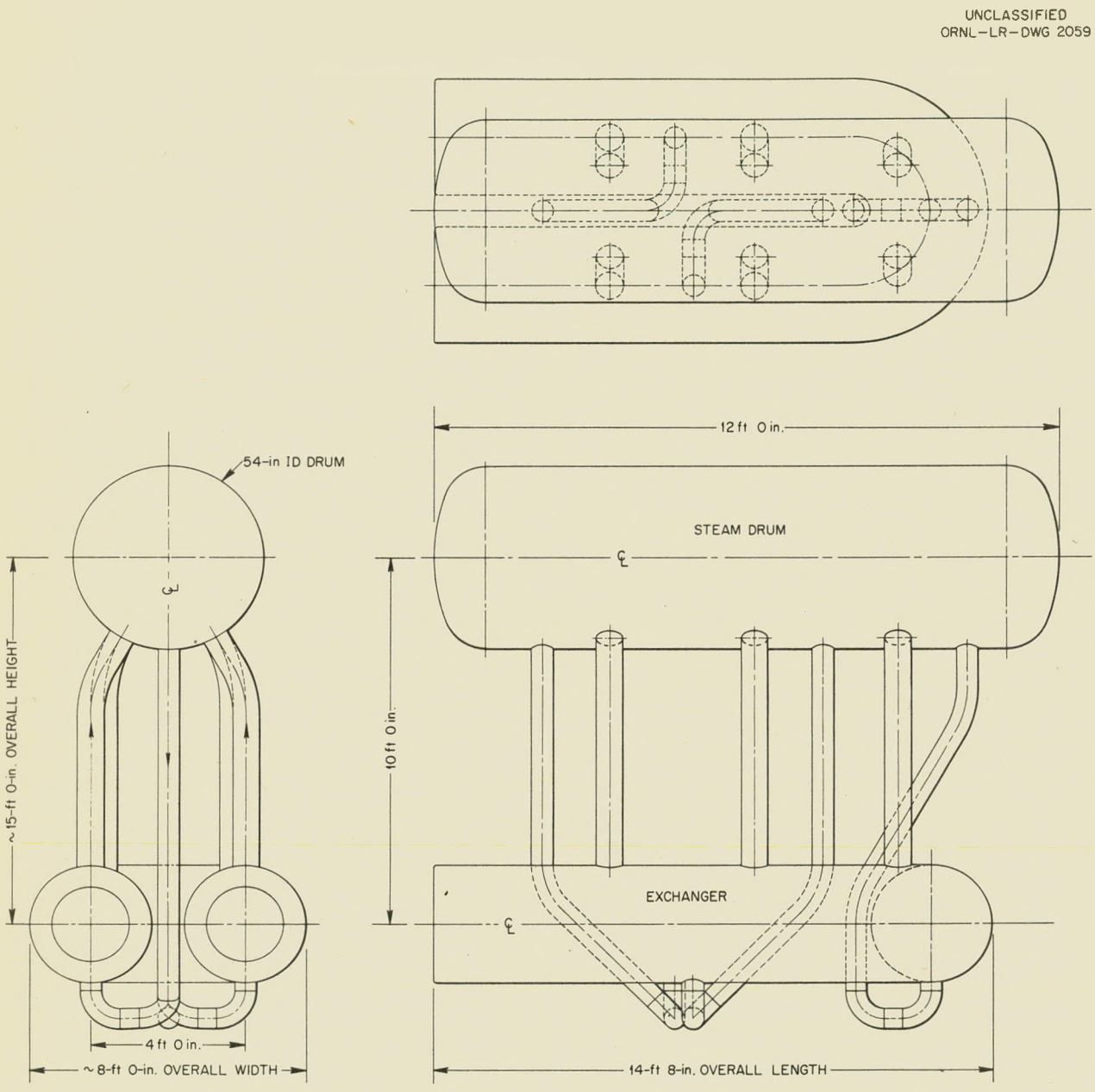

Fig. 45. 50-Mw Horseshoe Heat-Exchanger Assembly.

HEAT-EXCHANGER DEVELOPMENT

The tube-screening test outlined previously[3] is being continued. Three tube bundles have been exposed to 0.17 *M* UO_2SO_4 at 250°C, 16 to 70 fps, for 600 hr. These bundles are now being examined. Additional bundles which contain both duplicate and new samples will be run shortly.

A test installation is being constructed which will permit estimation of the magnitude of the inside scale coefficient of heat transfer of various tubes. The data thus obtained will be considered in the design of the main fuel heat exchanger.

[3] R. Goodman, J. A. Hafford, and I. Spiewak, *HRP Quar. Prog. Rep. Jan. 31, 1954*, ORNL-1678, p 37.

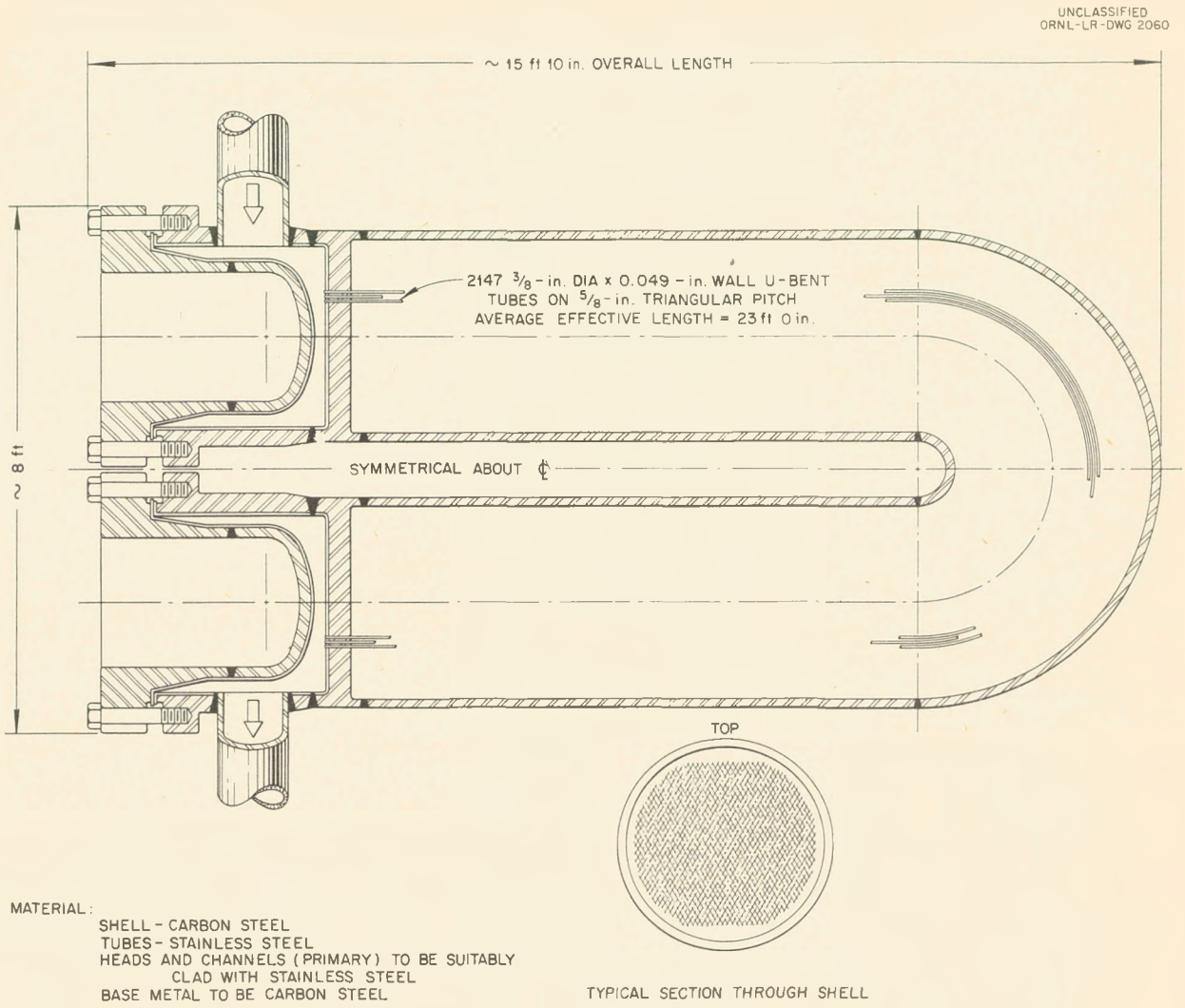

Fig. 46. 50-Mw Horseshoe Heat Exchanger.

WORTHINGTON CORPORATION PUMP DEVELOPMENT

A bearing-test assembly for proving certain aspects of the feasibility of a "pressure breakdown seal"[4,5] for a 20,000-gpm pump has been in operation for several months. Stellite-Graphitar and Stellite-Stellite bearing combinations have operated successfully.

Worthington engineers believe that large pumps which utilize pressure breakdown through a long radial bearing can be designed, fabricated, and operated satisfactorily.

4000-gpm LOOP

A rather large leak in the metal bellows of the system which maintains a pressure balance across the Inconel stator sleeve in the canned rotor pump was detected with a Consolidated helium leak detector. While steps are being taken to repair this leak, leak detection is progressing on the remainder of the loop. Auxiliary equipment for this work is being assembled, and personnel are being trained in its use.

[4] C. B. Graham *et al.*, *HRP Quar. Prog. Rep. July 1, 1952*, ORNL-1318, p 112.

[5] C. B. Graham *et al.*, *HRP Quar. Prog. Rep. Oct. 1, 1952*, ORNL-1424, p 65.

Essentially "reactor grade" fabrication techniques were used in the construction of the 4000-gpm loop. The system is being thoroughly leak-tested in an attempt to establish "tightness" specifications and testing procedures for large reactor systems which may be built in the future.

A low-head, wrought impeller is being purchased for the Byron Jackson 4000-gpm pump to replace the present cast, type 347 stainless steel impeller. This change will result in better simulation of future pumps.

SMALL GAS CIRCULATOR DEVELOPMENT

Both Westinghouse and Allis-Chalmers are preparing proposals for a gas circulator and test loop. These circulators are to be used for development of a high-pressure recombiner system for homogeneous reactors, with the possible addition of such a system to the HRT at a later date. The circulators are being designed for 20 cfm and 150 ft of head at 300°C and 2000 psi. The Allis-Chalmers circulator features fluid piston bearings and "top maintenance." Westinghouse has just started working on their design, and no information is yet available. Both companies will include in their proposals a completely instrumented loop for testing the gas circulators at design conditions.

ORNL 5-gpm PUMP

An operating endurance test of the ORNL 5-gpm pump has been under way for some time to determine the life expectancy of the various parts. So far, one pump has run for a total of 1800 hr, with water at 250°C. During the first period of operation, the pump was started and stopped 100 times. An examination of the pump after 100 hr and again after another 1000 hr showed no indication of unusual or severe wear. The same pump is in operation again and has operated an additional 700 hr. It will be stopped when it has completed a total of 1000 hr during this run; some indication of failure would, of course, necessitate a stoppage before the end of the 1000-hr period.

The particular stator used in the test described above has operated for a total of 3700 hr without failure. This stator has a Class A insulation on the windings and is cooled with copper water coils embedded in the stator iron laminations.

Because it is desirable to increase the head output of the pump for various purposes, a variable-frequency source was built and the pump was operated at 110 v at frequencies from 60 to 100 cycles. As predicted, it was found that the rotor rpm varied almost in direct proportion to the frequency. At a flow of 5 gpm, the pump generates 40 ft of head at 60 cycles, and 110 ft of head at 100 cycles.

CORROSION

E. G. Bohlmann, Section Chief

PUMP-LOOP CORROSION TESTS

J. C. Griess H. C. Savage

Pump-Loop Operation and Maintenance

H. C. Savage F. J. Walter

Loop Status. Thirteen dynamic-corrosion test loops are now in operation. The construction and installation of one additional loop, which incorporates features for special corrosion tests, are 90% complete. In general, each loop contains standard pin and coupon corrosion specimens. Several loops are also equipped for installation of gas-phase corrosion specimens.

Six loops are now completely shielded for protection of personnel against high-pressure leaks or ruptures. Present plans provide for shielding all 100A loops as rapidly as the manpower is available.

A brief summary of the status of each corrosion test loop is given below. Corrosion data and test results are given in the following section "Loop Test Results."

Loop A is operating at 315°C with 0.02 *m* uranyl sulfate which contains oxygen and 0.005 *m* sulfuric acid. During this quarter several short-term high-temperature runs have included gas-phase specimens and Zircaloy-2 and titanium impact specimens.

Loop B is being used to perform continuous-addition corrosion studies. A 1-gph pulsafeeder connected to the loop allows continuous, controlled-rate additions to the circulating solution.

During this quarter, the effects of the continuous addition of chromic sulfate and manganous sulfate on corrosion were studied. Also, one run was made in which the uranyl sulfate concentration was increased from 0 to 0.17 *m* by the slow addition of concentrated uranyl sulfate while the system was operating at 250°C.

A series of short-term tests for the evaluation of gas-phase corrosion in the presence of halogen-containing salts has been performed in Loop C.

During this quarter, the ½-in. and the ⅜-in., schedule-40, type 347 stainless steel bypasses in Loop C developed small cracks in bent sections of the pipe. Metallographic examination of these cracks showed pronounced evidence of transgranular cracking. A complete report on these cracks is given in the "Metallurgy" section of this report. Because of the cracking, representative parts of the loop, such as the 1-in. return line, the ½-in. bypass, and the ⅜-in. bypass, were removed and cross-sectioned for detailed examination. The corrosive attack in these sections of pipe was very small except in several highly turbulent sections. The inside walls of the pipe were covered with a black oxide film.

During this quarter, Loop D was used for a series of short-term runs at 250°C with various solutions, such as uranyl fluoride and uranyl sulfate, which contained radioactive samarium oxide. A run to test the corrosiveness of the HRE-decontamination solutions was also completed.

In Loop E, a 2100-hr run at 100°C with 0.02 *m* uranyl sulfate which contained 0.005 *m* sulfuric acid and 300 to 500 ppm of oxygen was completed. Loop E is now operating at 225°C with oxygen and 0.17 *m* uranyl sulfate.

Loop F is still being used for correlation tests on the in-pile type of corrosion-test coupons (see Figs. 61 and 62). The thermal spacer with a titanium face plate, which was installed in Loop F in order to investigate the possibility of crevice corrosion, was removed and dismantled for inspection. This thermal spacer consists of a standard Westinghouse model 100A, type 347 stainless steel thermal spacer with a titanium plate bolted to the side which is exposed to hot liquid. Several areas of relatively severe corrosion were observed on the type 347 stainless steel near two of the screw holes provided for attaching the face plate (Figs. 47 and 48). Microscopic examination indicated a corrosion pit depth of 0.024 to 0.034 in. in area 1. This thermal spacer has been used for approximately 835 hr under various conditions ranging from 1.34 *m* uranyl sulfate plus oxygen at 250°C to 0.17 *m* uranyl sulfate containing 0.01 *m* cupric sulfate plus oxygen at 250°C. The thermal spacer has been defilmed and installed in Loop H for additional testing. A second thermal spacer has been equipped with a titanium face plate and installed in Loop L.

The all-titanium Loop G has been operated during this quarter at 300°C and approximately 1400 psig

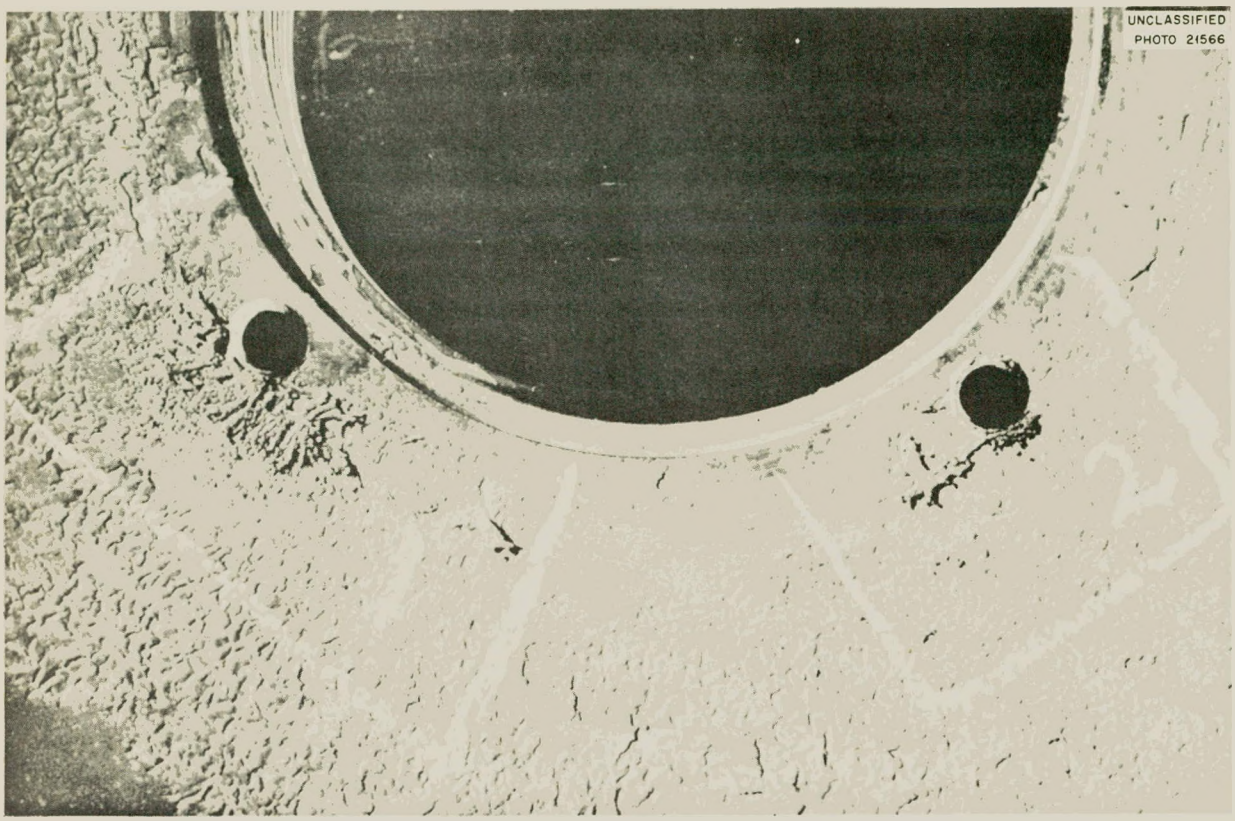

Fig. 47. Corrosion on Stainless Steel Side of Type 347 Stainless Steel to Titanium Interface (100A Thermal Spacer 425/AP20).

total pressure with 0.02 *m* uranyl sulfate containing oxygen and 0.005 *m* sulfuric acid.

During the start-up of run G-9 (oxygen and 1.34 *m* uranyl sulfate at 300°C), the titanium pressurizer ruptured under the bottom heater (Fig. 49). When the system reached 280°C, a leak was discovered at the 100A-pump back-plate valve. Approximately 1 liter of solution had leaked through the valve, and this resulted in complete drainage of the pressurizer (a loss of 0.5 liter of solution is sufficient to empty the pressurizer). The pressurizer heaters were shut off immediately after discovery of the leak (~7 min before the rupture). Recording-instrument charts indicated that the heaters (two 3000-w, radiant-type, clamshell heaters) had been operating for approximately 5 min after the pressurizer was empty. This condition probably caused an excessive pipe-wall temperature. Measurements of the pipe diameter in the heated section showed a general swelling which was indicative of yielding as the result of excessive temperature. The main-line temperature at the time of rupture was approximately 215°C.

A new titanium pressurizer is being fabricated for Loop G. This pressurizer will be equipped with Calrod heaters cast in 2S aluminum and with pressurizer-temperature cutouts.

During this quarter, Loop H has been operating at 225°C with oxygen and 1.34 *m* uranyl sulfate. During run H-30, the ¼-in.-OD, 0.035-in.-wall stainless steel mixing tube, which sprays solution through the top of the pressurizer to maintain vapor-liquid equilibrium, ruptured (Fig. 50). This tube was sectioned longitudinally and found to be badly corroded at the point of rupture (Fig. 51). The serious corrosion damage can probably be attributed to the high turbulence created by the Parker fitting immediately upstream. This loop is now operating at 225°C with oxygen and 1.34 *m* uranyl sulfate.

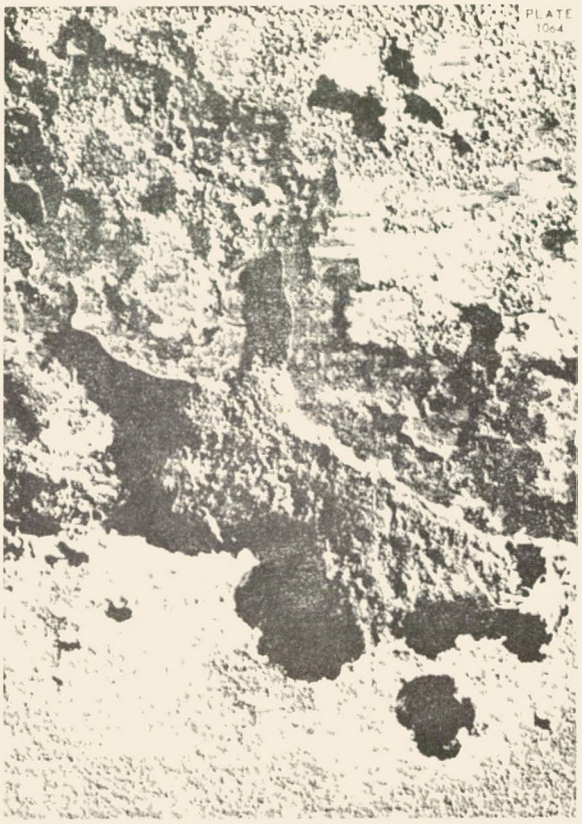

Fig. 48. Typical Pits in Stainless Steel of Area 1 of Fig. 47 After Defilming. 20X. Reduced 32%.

Loop I is being used for a series of long-term (~2000 hr) runs at 250°C with 0.04 *m* uranyl sulfate containing oxygen and 0.006 *m* sulfuric acid.

Loop J has been used for evaluating corrosion effects at 200°C with 0.02 *m* uranyl sulfate containing oxygen and 0.005 *m* sulfuric acid.

Loop K has not been operated during this quarter.

Loop L was used to evaluate the corrosion effects of 0.004 *m* uranyl sulfate containing oxygen and 0.015 *m* sulfuric acid at 250°C. One run at 250°C with oxygen and 0.015 *m* sulfuric acid has also been completed.

Loop M is still being used for corrosion tests of special samples such as heat-exchanger tube bundles and welded specimens.

Loop N (90% complete) was designed for operation with a high concentration of uranyl sulfate. An effort has been made to avoid highly turbulent regions except in a special removable test section which includes standard tees and elbows. This loop will be equipped with an all-titanium pump to eliminate the excessive corrosion usually observed in the highly turbulent volute regions of a Westinghouse model 100A pump. Facilities have been provided for the installation of crevice-corrosion specimens in addition to the standard pin and coupon specimens.

HRE Mock-up. The HRE mock-up in Building 9204-1 at Y-12 has been equipped with an all-titanium pump in order to eliminate excessive corrosion in the pump. The Westinghouse model 100A pump and the Lapp 1-gpm pulsafeeder are being operated with an Allis, Louis, Co. variable-frequency motor-generator set in order to reduce the velocity of the circulating liquid in the system. The system is operating at 250°C with oxygen and 0.43 *m* uranyl sulfate. The purpose of this operation is to evaluate the over-all corrosion rate of the system as a function of the bulk flow velocity.

Westinghouse Model 100A Pumps. The Inconel can in one Westinghouse model 100A pump failed during this quarter. Two pumps were repaired; this brought the total number of pumps repaired with stainless steel diaphragms to 16. To date, the 12 pumps with stainless steel diaphragms currently being used in corrosion-testing service have accumulated over 55,000 hr of service without a failure. One pump has accumulated over 10,000 hr of service.

Loop-Test Results

J. C. Griess R. E. Wacker

During the past quarter, additional data have been collected on the corrosion resistance of several alloys to uranyl sulfate solutions. The concentration range has been varied from 1 to 300 g of uranium per liter, and the temperatures have been varied from 200 to 320°C. Data on the corrosion resistance of stainless steel in 0.02 *m* (5 g of uranium per liter at 25°C) uranyl sulfate containing 0.005 *m* sulfuric acid have been essentially completed. At low flow rates, corrosion rates are measurable at all temperatures from 200 to 320°C, but even in the worst case the corrosion rate is only 1 mpy. At very high flow rates the corrosion rates are not much higher.

In 1.34 *m* uranyl sulfate (300 g of uranium per liter at 25°C), only preliminary data have been obtained with stainless steel, but the extent of corrosion is great at all flow rates. Both titanium

Fig. 49. Titanium Pressurizer on 100A Loop G After Rupture.

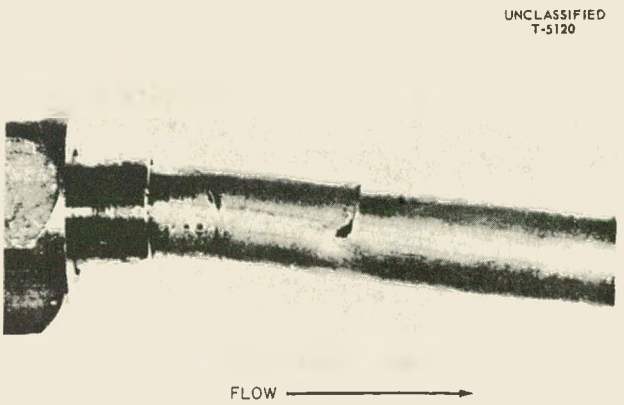

Fig. 50. Rupture of 0.25-in.-OD 0.035-in.-wall Type 347 Stainless Steel Tubing from 100A Loop H (Run H-30).

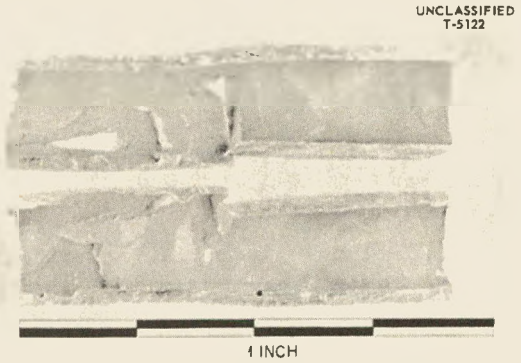

Fig. 51. Longitudinal Section at Point of Rupture of 0.25-in.-OD 0.035-in.-wall Type 347 Stainless Steel Tubing from 100A Loop H (Run H-30).

and zirconium, however, appear to be very resistant to 1.34 *m* uranyl sulfate, even at 275°C.

All the data collected on pin-type corrosion specimens are presented in tabular form, and the more pertinent data are discussed in the sections which follow.

General Corrosion Rates. In previous quarterly reports[1-5] all the corrosion data on pin-type specimens have been given in tabular form. The most recent data are given in Table 16. The presentation is the same as in the previous reports, and the usual precautions concerning the use of the data are mentioned again. The corrosion rates, as reported, represent average rates for the duration of the particular exposure. Most corrosion rates are not constant at low flow rates; hence discretion must be used in comparing one rate with another. The rates given in Table 16 have been calculated from weight losses of the various alloys. In all cases, unless otherwise noted, the corrosion specimens were cathodically treated in inhibited sulfuric acid to remove adhering oxide films before the final weighing was made.

Other pins which have received special metallurgical treatments have been tested but are not shown in the table. The results of these tests will be described and evaluated by the Metallurgy Group.

Corrosion of Stainless Steel by 0.02 *m* Uranyl Sulfate. A considerable amount of data has already been presented on the corrosion resistance of stainless steel to 0.02 *m* uranyl sulfate containing 0.005 *m* sulfuric acid. With the information gathered during the past quarter, the data are considered complete, and a summary of all the results is given below. Generally, all the austenitic stainless steels behaved in a similar manner under any set of conditions. At 300 and 320°C, however, type 309 SCb stainless steel corroded more rapidly at high flow rates than did the other steels, and, for that reason, the weight losses of type 309 SCb pins have been omitted from the averages which are plotted in the following graphs.

The pin data that have been obtained in regions of low flow rate (10 to 20 fps) are presented in Fig. 52. Each point represents the average weight loss of many pins, most of which were either type 347 or type 304 ELC stainless steel but some of which were types 304, 316, and 316 ELC. Note that in all cases the specimens lost most of their weight during the first 200 hr and then corroded at a low rate. If only the corrosion rate that was measured after the initial period is considered, a minimum rate was observed at 250°C and the highest rate was found at 320°C.

[1] J. C. Griess, J. M. Ruth, and R. E. Wacker, *HRP Quar. Prog. Rep. Jan. 1, 1953*, ORNL-1478, p 63.

[2] J. C. Griess and R. E. Wacker, *HRP Quar. Prog. Rep. March 31, 1953*, ORNL-1554, p 49.

[3] J. C. Griess and R. E. Wacker, *HRP Quar. Prog. Rep. July 31, 1953*, ORNL-1605, p 74.

[4] J. C. Griess and R. E. Wacker, *HRP Quar. Prog. Rep. Oct. 31, 1953*, ORNL-1658, p 45.

[5] J. C. Griess and R. E. Wacker, *HRP Quar. Prog. Rep. Jan. 31, 1953*, ORNL-1678, p 50.

TABLE 16. CORROSION RESULTS OF PIN-TYPE SPECIMENS

Run No.	Test Conditions: Solution	Uranium Concentration (g/liter)	Temperature (°C)	Time (hr)	Additions	Flow Rate (fps ± 10%)	Pin Material	No. of Pins	Corrosion Rate (mpy): Minimum	Average	Maximum
A-62[a]	UO_2SO_4	5	320	682	800 to 1500 ppm O_2, 0.005 *m* H_2SO_4	17	Type 304 ELC stainless steel	3	1.0	1.1	1.2
							Type 347 stainless steel	3	1.5	2.4	4.0
							Type 430 stainless steel	1		0.17	
							Type 416 stainless steel	1		8.9	
							Carpenter-20 stainless steel	1		4.2	
							Zircaloy-2	1[b]			
							Zirconium, crystal bar	1[b]			
							Titanium, RC-70	1[e]		0.25	
							Titanium, Ti-75A	1[e]		0.25	
							Platinum	1		0.12	
						76	Type 304 ELC stainless steel	5	0.80	1.3	1.6
							Type 347 stainless steel	5	2.3	3.7	6.8
							Type 304 stainless steel	2	2.5	3.7	4.9
							Type 316 ELC stainless steel	2	1.3	1.3	1.3
							Type 430 stainless steel	1		1.8	
							Type 416 stainless steel	1		9.2	
							Type 17-4 PH stainless steel	1		1.3	
							Type 322W stainless steel[c]	1		3.0	
							Miscro 4[d]	2	4.1	8.5	13
							Zircaloy-2	1[b]			
							Zirconium, crystal bar	1[b]			
							Zirconium–2 ½% tin	2[b]			
							Titanium, RC-70	1[e]		0.25	
							Titanium, Ti-75A	1[b]			
A-64	UO_2SO_4	5	320	157	800 to 1500 ppm O_2, 0.005 *m* H_2SO_4	17	Type 304 ELC stainless steel	8	1.9	3.2	3.7
							Type 347 stainless steel	9	2.5	5.1	6.2
							Type 309 SCb stainless steel	4	4.2	4.7	5.5
							Type 316 stainless steel	2	4.8	5.1	5.4
							Type 316 ELC stainless steel	2	2.3	3.0	3.7
							Type 310 stainless steel	2	5.0	5.2	5.3
							Platinum	1[b]			

TABLE 16. (continued)

Run No.	Test Conditions: Solution	Uranium Concentration (g/liter)	Temperature (°C)	Time (hr)	Additions	Flow Rate (fps ± 10%)	Pin Material	No. of Pins	Corrosion Rate (mpy): Minimum	Average	Maximum
A-64	UO_2SO_4	5	320	157	800 to 1500 ppm O_2, 0.005 *m* H_2SO_4	79	Type 304 ELC stainless steel	4	3.7	5.3	7.1
							Type 347 stainless steel	4	6.1	8.4	10
							Type 309 SCb stainless steel	2	12	13	13
							Type 316 ELC stainless steel	2	12	12	12
							Type 310 stainless steel	1		7.7	
A-65	UO_2SO_4	5	320	433	800 to 1500 ppm O_2, 0.005 *m* H_2SO_4	17	Type 304 ELC stainless steel	8	0.47	1.7	5.4
							Type 347 stainless steel	9	0.83	2.6	6.0
							Type 309 SCb stainless steel	4	0.94	2.6	3.6
							Type 316 ELC stainless steel	2	0.67	1.2	1.8
							Type 316 stainless steel	2	1.8	1.9	2.0
							Type 310 stainless steel	2	1.1	2.5	3.8
							Platinum	1		0	
						79	Type 304 ELC stainless steel	4	0.94	2.4	4.0
							Type 347 stainless steel	4	1.3	7.8	14
							Type 309 SCb stainless steel	2	15	16	16
							Type 316 ELC stainless steel	2	1.1	1.1	1.1
							Type 310 stainless steel	1		19	
							Platinum	1		0.28	
B-35	UO_2SO_4	40	250	187	1000 to 2000 ppm O_2, type 347 stainless steel shavings to contribute an excess of corrosion products	17	Type 304 ELC stainless steel	5	8.6	81	150
							Type 347 stainless steel	5	12	28	44
							Type 309 SCb stainless steel	2	29	40	51
							Type 316 ELC stainless steel	2	3.7	4.4	5.1
							Platinum	1[b]			
						75	Type 304 ELC stainless steel	5	200	250	310
							Type 347 stainless steel	4	220	260	300
							Type 309 SCb stainless steel	2	240	250	250
							Type 316 ELC stainless steel	2	230	290	340

TABLE 16. (continued)

Run No.	Test Conditions: Solution	Uranium Concentration (g/liter)	Temperature (°C)	Time (hr)	Additions	Flow Rate (fps ± 10%)	Pin Material	No. of Pins	Corrosion Rate (mpy): Minimum	Average	Maximum
B-36	UO_2SO_4	40	250	200	1000 to 2000 ppm O_2, $FeSO_4$[f]	16	Type 304 ELC stainless steel	4	24	66	96
							Type 347 stainless steel	4	22	29	36
							Type 309 SCb stainless steel	2	22	55	87
							Type 316 ELC stainless steel	2	9.0	49	89
							Platinum	1[b]			
						75	Type 304 ELC stainless steel	5	170	190	240
							Type 347 stainless steel	4	140	190	210
							Type 309 SCb stainless steel	2	210	230	240
							Type 316 ELC stainless steel	2	130	180	230
							Platinum	1[b]			
B-37[g]	UO_2SO_4	40	250	200	1000 to 2000 ppm O_2	17	Type 304 ELC stainless steel	5	0.09	0.33	0.60
							Type 347 stainless steel	5	0.09	0.22	0.43
							Type 309 SCb stainless steel	3	0.26	0.43	0.68
							Platinum	1		0.26	
						75	Type 304 ELC stainless steel	5	1.7	52	120
							Type 347 stainless steel	5	1.5	54	130
							Type 309 SCb stainless steel	3	22	87	170
							Platinum	1		1.1	
B-38	UO_2SO_4	40	250	113	1000 to 2000 ppm O_2, $Cr_2(SO_4)_3$[h]	17	Type 304 ELC stainless steel	5	43	71	190
							Type 347 stainless steel	5	41	57	100
							Type 309 SCb stainless steel	3	41	43	46
							Platinum	1[b]			
						75	Type 304 ELC stainless steel	2	310	340	360
							Type 347 stainless steel	2	360	370	380
							Type 309 SCb stainless steel	1		290	
							Type 430 stainless steel	2	270	280	280
							Titanium, RC-70	1[b]			
							Zircaloy-2	2[b]			
							Zirconium, crystal bar	1[b]			

TABLE 16. (continued)

Run No.	Test Conditions: Solution	Uranium Concentration (g/liter)	Temperature (°C)	Time (hr)	Additions	Flow Rate (fps ± 10%)	Pin Material	No. of Pins	Corrosion Rate (mpy): Minimum	Average	Maximum
B-38	UO_2SO_4	40	250	113	1000 to 2000 ppm O_2, $Cr_2(SO_4)_3$[h]	75	Zirconium–2½% tin	1[b]			
							Platinum	1[b]			
C-32, C-33, E-27	UO_2SO_4	5	100	3648	300 to 500 ppm O_2, 0.005 *m* H_2SO_4	20 to 30	Type 304 ELC stainless steel	2	0.01	0.01	0.01
							Type 347 stainless steel	2	0.01	0.01	0.01
							Type 347 stainless steel	4[i]	0.01	0.03	0.03
							Type 304 stainless steel	1		0.02	
							Type 304 stainless steel	2[i]	0.11	0.21	0.30
							Type 304 stainless steel[i]	2	0.01	0.02	0.03
							Type 17-4 PH stainless steel[c]	1		0.29	
							Type 416 stainless steel[c]	1		330	
							Type 322W stainless steel[c]	1		0.03	
							Miscro 4[d]	2[l]	0.28	0.29	0.29
							Stellite 98M2	2	1.0	1.1	1.2
							Stellite 1	2	0.04	0.06	0.08
							Stellite 3	2	1.0	1.3	1.6
							Stellite 6	2	0.01	0.04	0.06
							Haynes alloy No. 25	2	0.05	0.06	0.06
							Low-carbon Inconel	2[i]	0.06	0.17	0.27
							Inconel[l]	2[i]	0.30	0.75	1.2
							Inconel[m]	2[i]	3.3	3.8	4.3
							Inconel[n]	1[l]		0.28	
							Inconel X	2	0	0	0
							Inconel X, age hardened	2	0.02	0.41	0.80
							Hastelloy C	2	0	0	0.01
							Graphitar	2	0	0	0
C-34	UO_2SO_4	40	250	114	500 to 1000 ppm O_2, 50 ppm I as KI	11 to 13	Type 304 ELC stainless steel	8	7.3	36	89
							Type 347 stainless steel	8	9.7	31	44
							Type 309 SCb stainless steel	2	30	32	34
							Type 316 ELC stainless steel	2	66	75	83
							Type 430 stainless steel	2	5.4	8.7	12
							Titanium, RC-70	2[b]			
							Zirconium, crystal bar	2[b]			

TABLE 16. (continued)

Run No.	Test Conditions: Solution	Uranium Concentration (g/liter)	Temperature (°C)	Time (hr)	Additions	Flow Rate (fps ± 10%)	Pin Material	No. of Pins	Corrosion Rate (mpy): Minimum	Average	Maximum
C-35	UO_2SO_4	40	250	200	500 to 1000 ppm O_2, 25 ppm I as KI	11 to 13	Type 304 ELC stainless steel	8	4.5	40	100
							Type 347 stainless steel	8	24	27	32
							Type 309 SCb stainless steel	2	26	26	26
							Type 316 stainless steel	2	60	90	120
							Type 430 stainless steel	2	14	16	17
							Titanium, RC-70	2[b]			
							Zirconium, crystal bar	2[b]			
							Platinum	2[b]			
C-37	UO_2SO_4	40	250	200	1000 to 2000 ppm O_2, 50 ppm Cl as NaCl	15	Type 304 ELC stainless steel	5	5.6	17	32
							Type 347 stainless steel	5	15	25	31
							Type 309 SCb stainless steel	2	15	21	27
							Gold	1		11	
							Zircaloy-2	1[b]			
D-22	UO_2F_2	40	250	200	1000 to 1700 ppm O_2	15	Type 304 ELC stainless steel	4	6.4	8.2	11
							Type 347 stainless steel	4	6.0	7.8	10
							Type 309 SCb stainless steel	1		10	
							Type 316 ELC stainless steel	1		7.7	
							Type 310 stainless steel	1		13	
							Type 322W stainless steel	1		3.9	
							Type 17-4 PH stainless steel	1		5.0	
							Platinum	1[b]			
						69	Type 304 ELC stainless steel	4	65	82	120
							Type 347 stainless steel	4	63	73	79
							Type 309 SCb stainless steel	1		120	
							Type 316 ELC stainless steel	1		140	
							Type 310 stainless steel	1		68	
							Type 322W stainless steel	1		84	
							Type 17-4 PH stainless steel	1		77	
F-31	UO_2SO_4	40	250	~	300 to 400 ppm O_2, 0.01 *m* $CuSO_4$	12	Type 304 ELC stainless steel	7	1.5	1.8	2.8
							Type 347 stainless steel	6	5.4	19	32

TABLE 16. (continued)

Run No.	Test Conditions: Solution	Uranium Concentration (g/liter)	Temperature (°C)	Time (hr)	Additions	Flow Rate (fps ± 10%)	Pin Material	No. of Pins	Corrosion Rate (mpy): Minimum	Average	Maximum
F-32	UO_2SO_4	40	250	[a]	300 to 400 ppm O_2, 0.01 *m* $CuSO_4$	12	Type 304 ELC stainless steel	7	0.7	0.8	1.0
							Type 347 stainless steel	7	0.8	1.0	1.2
F-33	UO_2SO_4	300	250	[a]		9	Type 304 ELC stainless steel	4	55	66	76
							Type 347 stainless steel	4	19	20	22
							Type 309 SCb stainless steel	2	97	100	110
							Titanium, Ti-75A	1[b]			
							Zircaloy-2	1[b]			
							Platinum	1[b]			
H-27	UO_2SO_4	5	225	1315	900 to 2100 ppm O_2, 0.005 *m* H_2SO_4	13	Type 304 ELC stainless steel	4	0.88	0.91	0.93
							Type 347 stainless steel	5	0.92	1.0	1.1
							Type 316 ELC stainless steel	2	0.94	1.0	1.1
						51	Type 304 ELC stainless steel	4	2.4	6.0	8.0
							Type 347 stainless steel	4	7.5	7.9	8.8
							Type 316 ELC stainless steel	2	8.3	8.6	8.9
H-28	UO_2SO_4	300	225	200	1000 to 2000 ppm O_2	17	Type 304 ELC stainless steel	4	120	200	350
							Type 347 stainless steel	5	4.5	77	160
							Type 309 SCb stainless steel	2	220	240	250
							Type 316 ELC stainless steel	2	140	140	140
						64	Type 304 ELC stainless steel	4	530	650	730
							Type 347 stainless steel	5	490	650	760
							Type 309 SCb stainless steel	2	760	760	760
							Type 316 ELC stainless steel	2	610	620	630
H-29	UO_2SO_4	300	225	100	1000 to 2000 ppm O_2	17	Type 304 ELC stainless steel	4	450	530	630
							Type 347 stainless steel	5	420	460	540
							Type 309 SCb stainless steel	2	450	470	490
							Type 316 ELC stainless steel	2	350	360	370
						64	Type 304 ELC stainless steel	4	670	880	1100
							Type 347 stainless steel	5	920	1000	1300

TABLE 16. (continued)

Run No.	Test Conditions: Solution	Uranium Concentration (g/liter)	Temperature (°C)	Time (hr)	Additions	Flow Rate (fps ± 10%)	Pin Material	No. of Pins	Corrosion Rate (mpy): Minimum	Average	Maximum
H-29	UO_2SO_4	300	225	100	1000 to 2000 ppm O_2	64	Type 309 SCb stainless steel	2	580	780	970
							Type 316 ELC stainless steel	2	490	550	610
H-30	UO_2SO_4	300	225	192	1000 to 2000 ppm O_2	17	Type 304 ELC stainless steel	4	300	350	370
							Type 347 stainless steel	5	110	160	210
							Type 309 SCb stainless steel	2	370	390	400
							Type 316 stainless steel	2	180	190	200
						64	Type 304 ELC stainless steel	4	670	850	1000
							Type 347 stainless steel	5	600	780	890
							Type 309 SCb stainless steel	2	780	800	820
							Type 316 stainless steel	2	640	920	1200
I-6	UO_2SO_4	10	250	100	600 to 2000 ppm O_2,	18 to 19	Type 304 ELC stainless steel	6	8.8	10	12
through				400	0.006 *m* H_2SO_4			3	1.6	1.7	1.8
I-9				500				6	0.68	1.7	2.3
				1000				4	0.73	0.80	0.87
				1500				6	0.59	0.63	0.70
				2000				12	0.17	0.50	0.67
				3000				5	0.28	0.31	0.36
				3500				8	0.14	0.29	0.36
				100		27 to 28	Type 304 ELC stainless steel	6	4.8	12	16
				400				3	2.1	2.6	3.3
				500				6	2.0	2.8	3.8
				1000				4	1.1	1.3	1.9
				1500				6	0.77	0.96	1.3
				2000				12	0.20	0.92	2.1
				3000				5	0.13	0.38	0.67
				3500				8	0.13	0.37	0.46
				100		38 to 42	Type 304 ELC stainless steel	6	17	20	31
				400				3	2.7	4.2	6.2
				500				6	3.4	5.0	11
				1000				4	1.2	1.5	2.1

TABLE 16. (continued)

Run No.	Test Conditions: Solution	Uranium Concentration (g/liter)	Temperature (°C)	Time (hr)	Additions	Flow Rate (fps ± 10%)	Pin Material	No. of Pins	Corrosion Rate (mpy): Minimum	Average	Maximum
I-6 through I-9	UO_2SO_4	10	250	1500	600 to 2000 ppm O_2, 0.006 *m* H_2SO_4	38 to 42	Type 304 ELC stainless steel	6	1.2	1.7	3.9
				2000				11	0.28	4.2	12
				3000				5	0.52	0.76	1.1
				3500				8	0.25	0.85	1.7
J-34	UO_2SO_4	5	200	2475	700 to 1300 ppm O_2, 0.005 *m* H_2SO_4	16	Type 304 ELC stainless steel	6	0.94	1.1	1.2
							Type 347 stainless steel	5	1.1	1.2	1.3
							Type 430 stainless steel	1		1.3	
							Titanium, Ti-75A	1[e]		0.04	
							Zircaloy-2	1[e]		0.02	
						75	Type 304 ELC stainless steel	6	10	11	13
							Type 347 stainless steel	5	11	14	20
							Type 430 stainless steel	1		7.2	
							Titanium, Ti-75A	1[e]		0.08	
							Zircaloy-2	1[e]		0.03	
L-24	UO_2SO_4	1	250	969	800 to 2300 ppm O_2, 0.015 *m* H_2SO_4	14	Type 304 ELC stainless steel	4	1.5	3.0	4.5
							Type 347 stainless steel	3	6.4	7.2	7.8
							Type 309 SCb stainless steel	2	2.5	2.7	2.8
							Type 316 ELC stainless steel	1		7.1	
							Type 304 stainless steel	1		7.7	
							Type 310 stainless steel	1		3.7	
							Type 316 stainless steel	1		1.8	
							Carpenter-20 stainless steel	1		5.6	
						31	Type 304 ELC stainless steel	4	4.9	5.6	6.1
							Type 347 stainless steel	6	5.0	7.4	8.8
							Type 309 SCb stainless steel	3	3.5	5.6	9.1
							Type 316 ELC stainless steel	2	6.9	8.5	10
							Type 304 stainless steel	3	9.6	12	16
							Type 310 stainless steel	2	12	13	14
							Type 316 stainless steel	1		41	
							Carpenter-20 stainless steel	2	27	32	37

TABLE 16. (continued)

Run No.	Test Conditions						Pin Material	No. of Pins	Corrosion Rate (mpy)		
	Solution	Uranium Concentration (g/liter)	Temperature (°C)	Time (hr)	Additions	Flow Rate (fps ± 10%)			Minimum	Average	Maximum
L-24	UO_2SO_4	1	250	969	800 to 2300 ppm O_2, 0.015 m H_2SO_4	31	Miscro 4[d]	1		9.3	
							Zircaloy-2	1[b]			
						75	Type 304 ELC stainless steel	4	56	58	59
							Type 347 stainless steel	5	31	53	60
							Type 316 ELC stainless steel	1		96	
							Type 304 stainless steel[p]	1		3.4	
							Carpenter-20 stainless steel	1		110	
							Miscro 4[d]	1		9.9	
L-25		0	250	148	800 to 2300 ppm O_2, 0.015 m H_2SO_4	15	Type 304 ELC stainless steel	4	9.0	34	45
							Type 347 stainless steel	3	46	49	53
							Type 309 SCb stainless steel	2	10	11	11
							Type 304 stainless steel	1		68	
							Type 310 stainless steel	1		13	
							Type 316 stainless steel	1		45	
							Carpenter-20 stainless steel	1		32	
							Stellite 98M2	1		140	
						27	Type 304 ELC stainless steel	3	16	27	34
							Type 347 stainless steel	3	23	43	55
							Type 309 SCb stainless steel	1		13	
							Type 316 ELC stainless steel	1		96	
							Type 304 stainless steel	1		95	
							Type 310 stainless steel	1		13	
							Carpenter-20 stainless steel	1		36	
							Titanium, RC-70	1[b]			
							Zirconium, crystal bar	1[b]			
							Zirconium–2½% tin	1[e]		0.69	
						75	Type 304 ELC stainless steel	3	43	51	58
							Type 347 stainless steel	3	64	67	73
							Type 309 SCb stainless steel	1		25	
							Type 316 ELC stainless steel	1		150	

TABLE 16. (continued)

Run No.	Test Conditions: Solution	Uranium Concentration (g/liter)	Temperature (°C)	Time (hr)	Additions	Flow Rate (fps ± 10%)	Pin Material	No. of Pins	Corrosion Rate (mpy): Minimum	Average	Maximum
L-25		0	250	148	800 to 2300 ppm O_2, 0.015 *m* H_2SO_4	75	Type 310 stainless steel	1		35	
							Carpenter-20 stainless steel	1		80	
							Titanium, RC-70[b]	1			
							Zirconium, crystal bar[b]	1			
							Zirconium–2½% tin[b]	1			
							Stellite 98M2	1		350	

[a]There were no specimens in run A-63.

[b]These pins were not defilmed; all showed weight gains due to deposition of iron and chromium oxides.

[c]Precipitation hardened.

[d]This alloy was obtained from the Michigan Steel Casting Company and had the following composition (the balance being iron):

	(wt %)
Ni	0.15
Cr	13.1
C	0.07
Si	1.41

[e]These pins were not defilmed; hence the actual corrosion rate would be somewhat higher.

[f]During the first 150 hr of this run, about 3 liters of a uranyl sulfate solution (40 g of uranium per liter) containing 6.5 g of iron as ferrous sulfate was pumped into the loop to determine whether or not the continuous addition of a corrosion product to the system would influence the weight losses of the specimens.

[g]This run was started with the loop containing water and oxygen. During the first 100 hr, concentrated uranyl sulfate was continuously pumped into the system until a uranium concentration of 40 g of uranium per liter was reached. The loop was then operated for an additional 200 hr.

[h]During the first 100 hr of this run, about 5 liters of a uranyl sulfate solution (40 g of uranium per liter) containing 0.5 g of chromium per liter as chromic sulfate was pumped into the loop.

[i]These spins were included in the run for only 2648 hr.

[i]Cast.

[k]This pin was included in the run for only 1000 hr.

[l]Metal reduced 90% by swaging.

[m]Metal reduced 90% by swaging, annealed at 1900°F in H_2 atmosphere for 10 min, and furnace cooled.

[n]A 20-mil sheet from Westinghouse was rolled into a pin shape and ran for only 2110 hr.

[o]These pins were exposed to the following conditions:
3% Na_3PO_4 at 100°C for 5 hr,
5% HNO_3 at 100°C for 24 hr,
H_2O + 200-psi He at 250°C for 24 hr,
UO_2SO_4 solution at 250°C for 24 hr,
allowed to stand in UO_2SO_4 solution at room temperature for 48 hr,
UO_2SO_4 solution at 250°C for 176 hr.

[p]Sensitized by heating in hydrogen at 1000°F for 24 hr.

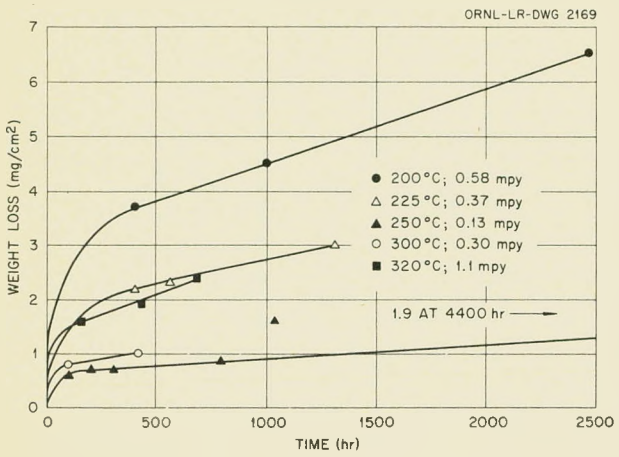

Fig. 52. Corrosion of Stainless Steel in 0.02 *m* UO_2SO_4 Containing 0.005 *m* H_2SO_4 and Approximately 1000 ppm of Oxygen (Flow Rate, 10 to 20 fps).

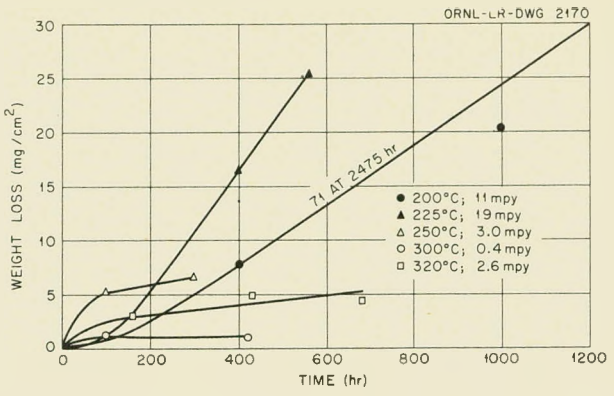

Fig. 53. Corrosion of Stainless Steel in 0.02 *m* UO_2SO_4 Containing 0.005 *m* H_2SO_4 and Approximately 1000 ppm of Oxygen (Flow Rate, 75 to 80 fps).

In practically all the experiments in 0.02 *m* uranyl sulfate, pins were included in the main line of the loop, where the flow rate was about 75 fps. Specimens exposed under these conditions were subjected to probably the most severe conditions in the entire circulating system. The data obtained under these conditions are presented in Fig. 53, and indicate that at high flow rates the temperature range of 200 to 225°C was by far the worst. At high flow, a minimum corrosion rate was found at about 300°C.

Coupon data obtained with 0.02 *m* uranyl sulfate generally verified the pin data, but at 200°C the so-called "critical velocity" appeared to be time-dependent. The observed results are shown in Fig. 54. At temperatures of 250°C and above, the critical velocity was in excess of 50 fps and appeared to be independent of time.

A series of long-term runs in which the solution was 0.02 *m* uranyl sulfate containing 0.005 *m* sulfuric acid at 100°C has been concluded during the past quarter. A number of alloys which would presumably be exposed to reactor solutions at temperatures below 100°C were tested. The pin data can be seen in Table 16 (runs C-32, C-33, and E-27). Several specific results should be noted: (1) all the Stellites were reasonably good, but Stellite Nos. 1 and 6 were superior to No. 98M2, which is presently in general use for pump bearings; (2) of the three precipitation-hardened

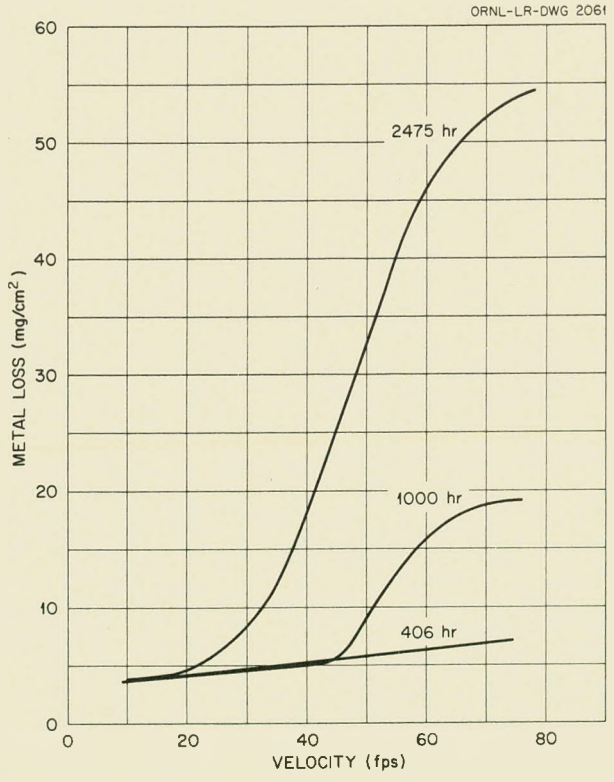

Fig. 54. Corrosion of Type 304 ELC Stainless Steel in 0.02 *m* UO_2SO_4 Containing 0.005 *m* H_2SO_4 and Approximately 1000 ppm of Oxygen at 200°C.

stainless steels tested, type 416 was completely worthless, whereas types 322W and 17-4 PH showed good corrosion resistance; (3) both Hastelloy C and chrome-plated stainless steel were completely stable at this temperature even though at higher temperatures (particularly at 250°C) they corrode rapidly; and (4) the corrosion resistance of Inconel was related to its grain size and its carbon content. Final evaluation of the Inconel is being made by the Metallurgy Group.

Corrosion of Type 304 ELC Stainless Steel by 0.04 *m* Uranyl Sulfate. A series of runs has been completed in which type 304 ELC stainless steel specimens were exposed to 0.04 *m* uranyl sulfate (10 g of uranium per liter at 25°C) containing 0.006 *m* sulfuric acid at 250°C. The runs were made in a multipass loop (Loop I), and 28 pins were exposed in each of three channels. The solution flowed past the pins in each channel at a different rate: 18, 28, and 40 fps. A set of coupons and 14 zirconium pins were placed in the fourth leg of the loop. At the end of each run (I-6 through I-9), some of the pins were removed from each leg and replaced with new ones; the coupons were replaced after each run. The pin data are shown in Tables 16 and 17. It is interesting to note that at all three flow rates the corrosion rate was approximately inversely proportional to the exposure time. Thus, after the first 100 hr, the specimens lost very little additional weight; this corresponded to a negligible corrosion rate. It should also be noted that the agreement between pins run for the same time at the highest flow rate was not nearly so good as for those exposed at lower flow rates. The indications were that if the solution velocity had been slightly higher the pins would have corroded at a high rate. The coupon data verified the pin data, with the critical velocity being in the range of 35 to 45 fps.

The zirconium specimens included in the above runs remained in the loop for the entire 3500 hr, after which the iron and chromium oxide scales on the surfaces of the pins were removed by the Virgo descaling method. Both the Zircaloy-2 and the zirconium–2.5% tin (Zircaloy-1) specimens were covered with thin, very tightly adhering, black films, whereas the crystal-bar zirconium had developed a white oxide over the first-formed black film.

Titanium-Loop Operation. A 529-hr run was made in the titanium loop (Loop G) in which the solution consisted of 0.02 *m* uranyl sulfate and 0.01 *m* sulfuric acid at 300°C. At the conclusion of this run, a small amount of yellow precipitate,

TABLE 17. SUMMARY OF CORROSION DATA FROM TYPE 304 ELC STAINLESS STEEL PINS, RUNS I-6 THROUGH I-9

Time (hr)	Number of Specimens	Weight Loss (mg)								
		At Velocity of 18 to 19 fps			At Velocity of 27 to 28 fps			At Velocity of 38 to 42 fps		
		Minimum	Average	Maximum	Minimum	Average	Maximum	Minimum	Average	Maximum
100	6	5.2	5.9	7.1	2.8	7.3	9.6	9.7	12.0	18.5
400	3	3.7	3.9	4.2	4.9	6.0	7.8	6.2	9.5	14.5
500	6	2.0	5.0	6.9	6.0	8.2	11.1	9.9	14.7	31.9
1000	4	4.3	4.7	5.1	6.4	7.9	11.1	7.0	9.1	12.6
1400	2	4.1	4.4	4.6	4.5	5.7	6.8	6.5	7.2	7.8
1500	6	5.2	5.6	6.2	6.8	8.5	11.7	10.2	14.9	34.8
2000	12	2.0	5.9	7.9	2.4	10.8	24.4	3.3	49.4*	137.6
3000	5	4.9	5.5	6.3	2.3	6.7	11.9	9.1	13.4	19.8
3400	1		3.4			6.8			7.1	
3500	8	2.9	6.0	7.5	2.7	7.7	9.5	5.1	17.5	35.5

*Average for 11 pins only. One pin was not included here because it was damaged in the holder.

apparently identical to that described previously,[2,5] was found in the system. The 0.01 *m* sulfuric acid was not sufficient to stabilize the solution completely. Because of the urgency for investigating higher uranium concentrations in a titanium system, further studies with dilute solutions had to be postponed.

After the loop was thoroughly cleaned, a 400-hr run was made in which the solution was 1.34 *m* in uranyl sulfate at a temperature of 275°C. Throughout this run the composition of the solution remained unchanged, and examination of the specimens at the conclusion showed no significant corrosion damage. The titanium pins had thin blue films, and the zirconium specimens (Zircaloys-1 and 2) developed thin black-gray films. The titanium impeller showed no change in weight or appearance.

The titanium loop is presently not in operating condition. (See the section "Pump Loop Operation and Maintenance" of this report.) After the loop has been repaired, it is planned to make a run with 1.34 *m* uranyl sulfate at 300°C. At this temperature the fluid will contain two liquid phases, which should represent the worst condition from the standpoint of corrosiveness of the aqueous phases.

Pretreatments. In the previous quarterly report[5] an experiment was discussed in which a loop was first pretreated with a very dilute chromic acid solution and then exposed to 0.17 *m* uranyl sulfate solution. The results were striking in that only the coupon which was exposed to the highest flow rate showed any appreciable attack; all other specimens showed only an insignificant weight loss.

In the method proposed for the run-in of a new in-pile loop, the interior surfaces of the loop are given a type of pretreatment. The procedure for the start-up of an in-pile loop is as follows: A 3% trisodium phosphate solution is circulated at 100°C for about 5 hr. After the system has been rinsed with water, a 5% nitric acid solution is circulated at 100°C for 24 hr. These two treatments serve to degrease the loop as well as to show the presence of materials other than stainless steel that might have been inadvertently included in the system. The loop is then operated at 250°C for 24 hr with water, pressurized with helium, in order to calibrate the loop heaters and instruments. If the loop is in satisfactory working order at this stage, it is proposed to charge the loop with the uranyl sulfate solution which will be used in the reactor and to operate the loop at 250°C for 24 hr out of the reactor. If an analysis of the uranyl sulfate solution shows no unusual concentrations of corrosion products or other ions, it is planned to cool the loop and transport it to its reactor position.

Since Loop F has been used to determine the degree of correlation between standard corrosion specimens and in-pile specimens,[4,5] the above procedure was used in runs F-31 and F-32. After the 24-hr run with 0.17 *m* uranyl sulfate containing 0.01 *m* cupric sulfate at 250°C, the solution was allowed to remain in the loop at room temperature for two days. The run was then continued at 250°C for 176 hr, making a total of 200 hr of exposure to uranyl sulfate solution at 250°C. At the end of both runs the corrosion specimens as well as the loop showed very low corrosion rates. The results were in close agreement with those obtained in the chromic acid pretreatment run,[5] and they show that the proposed run-in of an in-pile loop results in the formation of a temporarily protective film.

The pin data for runs F-31 and F-32 can be seen in Table 16, from which it is evident that corrosion had not proceeded very far. Had the specimens not received the pretreatment, the pins would have shown corrosion rates of about 25 mpy. The coupon data from both the in-pile and standard types agreed very well, and in no case was a characteristic critical-velocity region observed. However, on the standard coupons at flow rates of 50 fps and higher, small triangular-shaped pits developed in both runs. All the pits were oriented in such a way that the vertex of the triangle was on the upstream side. Figure 55 is a photograph of a coupon containing such pits. Figure 56 is a photomicrograph of a longitudinal section through one of the pits, and Fig. 57 is a photomicrograph of a transverse section through a similar pit. Metallographic examination of the steel showed no abnormalities in its microstructure that were related to pit locations.

A close examination of the surface where the pit density was high showed that the pits undercut the oxide film and the film then sloughed off. It seems reasonable to conclude that had the specimen been exposed longer, the entire specimen would have become free of film and the characteristic, film-free corrosion rate would have been observed. The presence of these pits rather clearly

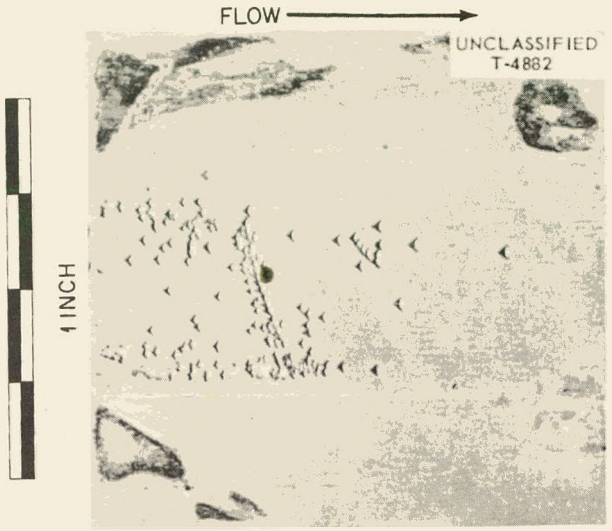

Fig. 55. Pits Formed in Type 347 Stainless Steel Specimen in Run F-31.

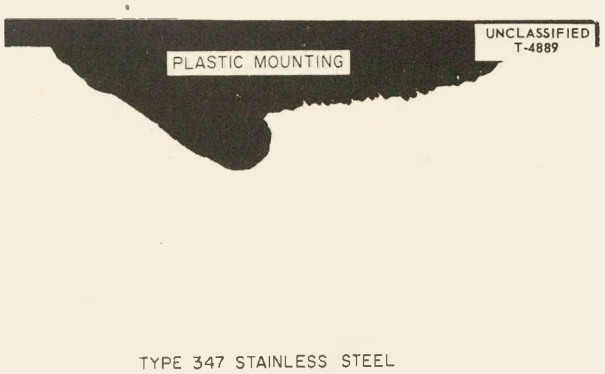

Fig. 56. Photomicrograph of Longitudinal Section Through One of the Triangular Pits in Type 347 Stainless Steel Specimen (Depth of Pit Is About 19 Mils). 50X. Reduced 31%.

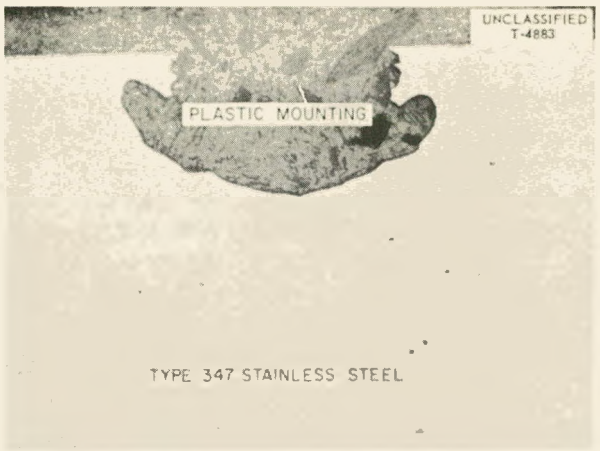

Fig. 57. Photomicrograph of Transverse Section Through One of the Triangular Pits in Type 347 Stainless Steel Specimen (Depth of Pit Is About 22 Mils). 50X. Reduced 31%.

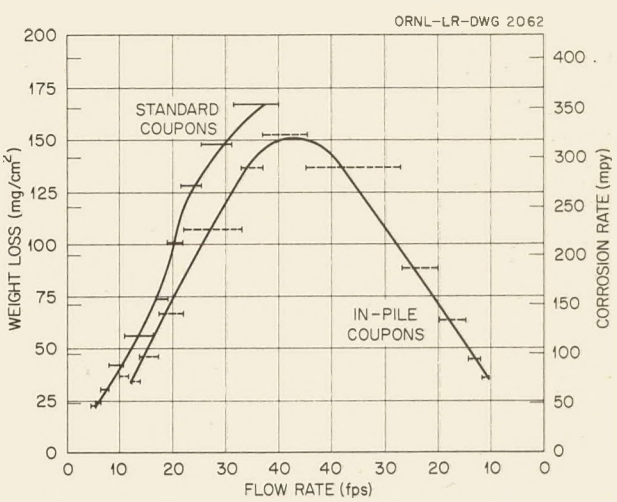

Fig. 58. Corrosion of Stainless Steel in 1.34 *m* UO_2SO_4 at 250°C as Indicated by Weight Loss (Run F-33).

demonstrates the questionable value of pretreatments in extending the critical velocity of a system.

In run F-33 the same run-in procedure that had been used in runs F-31 and F-32 was again used, but in run F-33 the uranyl sulfate concentration was 1.34 *m* instead of 0.17 *m*. Accidently, the pin weight losses were not obtained, but weight losses were obtained for both the in-pile and the regular coupons. The weight loss of specimens at different flow rates, as shown in Fig. 58, indicates that the agreement between the two types of specimens was satisfactory. In this run all the coupons had thick black films at all velocities, but the films were not protective. While the pretreatment did not give complete protection at the higher concentration, the corrosion rates were lower than expected and suggested some short-term effect of the pretreatment (see Ref. 3, Fig. 41, p 88).

As a matter of general interest, one other method of pretreating was attempted. In this particular run, B-37, the loop was filled with water and operated at 250°C overnight. Then, without cooling or stopping the pump, a concentrated uranyl sulfate solution was slowly pumped into the system so that after 100 hr of continuous pumping the solution in the loop contained 40 g of uranium per liter. The system was then run for an additional 200 hr at 250°C before it was cooled and the corrosion specimens were inspected. The pins exposed at low solution flow rate had developed very thin blue films and had lost very little weight. The same was true of all but the last coupon (flow rate 66 to 82 fps), which showed triangular pits identical in shape to those shown in Fig. 55. The pins exposed at high flow rates showed pitting to various degrees. If the duration of the run had been extended, both the pins and coupons exposed to high flow rates would have become film-free and would have corroded at a high rate.

The peculiar type of pitting described here has also been observed on the periphery of several impellers. In all cases the impeller had been used for the first time in a high-temperature oxygen-water system, and the pits usually developed during subsequent uranyl sulfate runs in which the uranium concentration was greater than or equal to 40 g of uranium per liter. In all cases the pits were oriented with respect to the flow in the manner shown in Fig. 55.

To summarize, it has been observed that the appearance of the triangular pits has been limited to situations in which stainless steel has been first exposed to a relatively noncorrosive solution which produced a temporary, protective film; when the stainless steel was then exposed to a more corrosive solution at a flow rate in excess of the critical velocity, the triangular pits formed. However, pretreatment by any of several methods may still be useful in minimizing the attack of the metal during film formation at velocities less than critical.

Miscellaneous. One run has been made in which 50 ppm of samarium as the oxide was added to 0.17 *m* uranyl sulfate, and the solution was circulated in a type 347 stainless steel loop at both 250 and 275°C to determine whether or not the samarium would remain in solution. The presence of samarium in solution was followed by a counting procedure, radioactive samarium having been added to the inactive samarium. Circulation of the solution at either 250 or 275°C with a bypass filter in the system did not result in a decrease in samarium concentration. A number of additions were then made to the system at 250°C. These additions included lanthanum nitrate (150 ppm La), uranyl fluoride (250 ppm F), ferrous sulfate (50 ppm Fe), sodium molybdate (250 ppm Mo), and a 200-lb partial pressure of carbon dioxide. None of these additions caused a change in either the samarium or the lanthanum concentration of the solution.

At the conclusion of the above-mentioned run, the corrosion specimens were left in the loop and 24-hr runs at 100°C were made with the following three solutions: (1) 10% sodium hydroxide, 2.5% sodium tartrate, and 2.5% hydrogen peroxide; (2) 5% nitric acid; and (3) 35% nitric acid. After each run the specimens were weighed and examined. None of the three solutions caused any change in weight or appearance. (These data are not shown in Table 16.) The above-mentioned three short runs were made because the solutions had been suggested as decontaminating solutions for the HRE, and it was of interest to determine how corrosive the solutions were to stainless steel and other alloys which had oxide coatings on their surfaces.

A series of runs has been made in order to determine the effect of small amounts of iodine- and chlorine-containing salts on the corrosion of stainless steel, titanium, and zirconium in 0.17 *m* uranyl sulfate at 250°C. In runs C-34 and C-36, 50 ppm of iodine was added to the system as potassium iodide; in C-35, 25 ppm of iodine was added. In run C-37, 50 ppm of chlorine as sodium chloride was added to the uranyl sulfate. In runs C-34 through C-37, samples were placed in the pressurizer as well as in the solution (except for run C-36). The solution samples were located in the usual position; the pressurizer specimens were placed in two different locations, above and below the entrance of the mixing line. Samples above the mixing line were exposed to only a gaseous atmosphere, while those below were exposed to the solution which was sprayed over the specimens. All runs were for 200 hr at 250°C.

The corrosion specimens in the solution showed no effect attributable to the presence of the halide ions. There was no pitting of the specimens and there was no change in the critical velocity of the systems. The steel specimens exposed in the gaseous region of the pressurizer showed severe

pitting when the systems contained iodine. There was a small amount of pitting in the spray region of the pressurizer, but the frequency and extent of pitting were very much less than in the gaseous region. Figure 59 is a photograph of a specimen exposed in the gaseous region and one exposed in the spray region in run C-35. Note that the specimen exposed in the spray shows no evidence of pitting, although a few shallow pits are visible under high magnification.

The addition of chloride ions to the uranyl sulfate in run C-37 caused a slight amount of pitting of the specimen in the gas region and none of the specimen in the spray region. In all the runs in which chloride or iodide ions were added to a system, neither titanium nor zirconium showed evidence of any measurable damage. Experiments are in progress to define in a more quantitative manner the nature of the gas-phase corrosion.

Run A-63, in which no corrosion specimens were used, was made to determine, qualitatively, the solubility of nickel and manganese sulfates in 0.02 *m* uranyl sulfate containing 0.005 *m* sulfuric acid at 320°C. In run A-62, which was made under the same conditions, the manganese concentration leveled off at 9 to 10 ppm after the first few days of operation and did not change for the duration of the run. Run A-63 was made in order to determine whether 200 ppm of nickel as nickel sulfate and 45 ppm of manganese as manganese sulfate would remain in the uranyl sulfate solution at 320°C. After the solution had been circulated for 12 days, the nickel concentration had not decreased, but had slowly increased as the result of the nickel added by the corrosion process. The manganese concentration, however, gradually decreased to 14 ppm at the end of the run and was still slowly decreasing when the run was terminated. It appeared that the manganese concentration would have approached a limit of about 10 ppm. The reason why the manganese concentration tends to level off at about 10 ppm is not apparent, but it may be related to the slow oxidation of manganese to manganese dioxide, in which case the 10 ppm would represent the equilibrium concentration of manganous ions in contact with manganese dioxide.

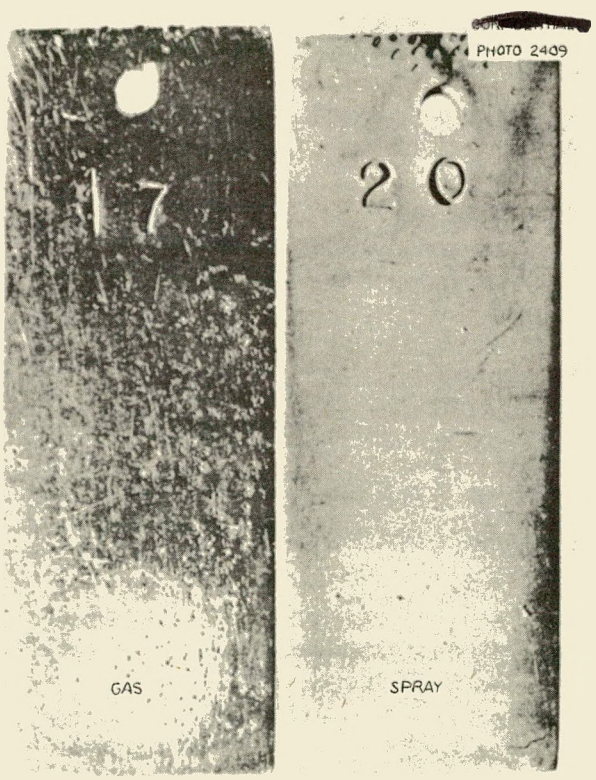

Fig. 59. Pitting of Stainless Steel in the Pressurizer in Run C-35; the Solution Contained 50 ppm of Iodine. 6.5X. Reduced 51.5%.

Platinum pins were included in a number of runs as a means of collecting oxide scale for chemical analyses. When platinum pins were included in a system, they developed a black film identical to that formed on stainless steel corrosion specimens exposed at low flow rates. When a platinum pin with its scale was removed from the loop, it was treated with hot perchloric acid to dissolve the scale, and the resulting solution was analyzed chemically. The analyses of such scales show that the compositions were very similar, regardless of the system in which the scale developed. Generally, the uranium concentration of such films varied between 1.4 and 4.0%, the iron amounted to 43 to 60%, and the chromium concentration was 1 to 9%. In all cases the nickel content of the films was less than 0.2%. There appeared to be no correlation between the loop conditions and the composition of the oxide films. Under identical operating conditions the range of composition has been approximately that given above. Furthermore, in two cases large amounts of loose oxide scale were found in the loop. The analyses of these scales were also within the limits given above.

Similarly, a number of steel specimens containing oxide films have been submitted for x-ray and electron-diffraction studies. In all cases except two, the major constituent of the film was alpha iron (and chromium) oxide. One of the two films, which did not contain alpha iron oxide, was composed of a hydrated iron oxide which was prepared at 225°C in 0.17 *m* uranyl sulfate; in the other case the same hydrated oxide was found and it was formed in 0.02 *m* uranyl sulfate at 200°C. However, other specimens prepared under the same conditions showed only alpha iron (and chromium) oxide. The exact nature of the oxide films is not certain at present, but additional information is being obtained.

Most of the data presented in Table 16 require no further discussion. In several cases, however, the significance of the data is not immediately apparent; for example, in run D-22 where 0.17 *m* uranyl fluoride was circulated at 250°C, the corrosion at all flow rates was two to three times lower than is usually observed with uranyl sulfate under the same conditions. No improvement was observed in the critical velocity of the system, and, in this respect, the results were disappointing; however, steel specimens suspended in the gas phase of the pressurizer did not show the evidence of pitting or heavy attack that was expected. The fact that zirconium, necessary for core-tank construction, is rapidly corroded by even dilute uranyl fluoride solutions has been the reason for the limited study of this system.

It has been shown previously[2,5] that the rapid introduction of relatively large amounts of corrosion products into a system, which takes place when a new loop is used for the first time, reduces the extent of corrosion and increases the critical velocity. In runs B-36 and B-38 ferrous sulfate and chromic sulfate, respectively, were pumped into the system during the runs in order to determine whether either the extent of corrosion could be decreased or the critical velocity increased by this method. The results presented in Table 16 clearly show that the rates of attack observed on pins were the same as those found in the absence of the ferric sulfate and chromic sulfate additions. Similarly, the coupons showed no change in either the rate of corrosion or the critical velocity.

Runs H-28 through H-30 represent those data that have been obtained with 1.34 *m* uranyl sulfate in a stainless steel loop. While the data are not consistent, they show clearly the magnitude of the corrosion rates that can be expected at the high uranium concentration. Corrosion by concentrated uranyl sulfate solutions at several temperatures is under test at present, and a new stainless steel loop fitted with a titanium pump is being constructed for experiments with concentrated solutions under controlled flow conditions.

Runs L-24 and L-25 were made in order to determine the effect of relatively large amounts of sulfuric acid on the corrosion rate of stainless steel. Run L-24 contained about 1 g of uranium per liter with the 0.015 *m* sulfuric acid, and run L-25 contained only the 0.015 *m* sulfuric acid. It should be noted that the duration of the runs was different, and, while the corrosion rates appear to be higher in L-25, the extent of damage was about the same in each case. Since all specimens had films in both cases, it seems probable that if run L-25 had been continued the weight losses of the specimens would not have changed very much and the two runs would have shown close agreement. It is thus concluded that in both cases the sulfuric acid was primarily responsible for the observed rates and that the presence of the small amount of uranium in run L-24 had little effect.

Data obtained in static systems on the corrosion of stainless steel in dilute sulfuric acid[6] showed the steel to be very severely attacked, much more so than in either of the above runs. The difference between the static and the dynamic tests could possibly be due to the oxygen being much more available to the steel in a circulating system than in a static one in which the oxygen could arrive at the steel surface only after diffusing through a thick layer of solution. The increased availability of oxygen in the dynamic system undoubtedly increased the rate of oxidation of ferrous ions (from the corrosion process) to ferric and hence indirectly increased the rapidity with which a protective film was formed on the steel. (At the high temperature, ferrous sulfate does not hydrolyze and hence does not contribute to film formation.)

The results obtained in 0.02 *m* uranyl sulfate are particularly interesting and significant in that they show very clearly the effect of temperature on the protectiveness of the oxide film on steel. Even at low flow rates it was possible to observe

[6] J. C. Griess and D. J. Sasmor, *HRP Quar. Prog. Rep. July 1, 1952*, ORNL-1318, p 22.

corrosion after the rapid initial attack. Undoubtedly the corrosion rate of steel at low flow rates in solutions more concentrated than 0.02 *m* is similar to that in a 0.02 *m* solution after the initial attack, but the extent of the initial attack is so great and varies so widely from specimen to specimen that it has not been possible to measure the long-term rate. At the 0.02-*m* level the extent of attack during the first few hundred hours was so small, and the agreement from specimen to specimen was so good, that it was not difficult to measure the low rate of attack reliably. The fact that there is a minimum corrosion rate between 250 and 300°C can be rationalized in the following manner: The protective film on the steel surface is composed of iron and chromium oxides which are formed by the hydrolytic precipitation of the ferric and chromic ions originating from the corrosion process. At all temperatures between 200 and 320°C the extent of precipitation is essentially complete, as shown by solution analyses, but the rate at which precipitation occurs is temperature-dependent. Thus the iron and chromium ions can diffuse further from the surface at a low temperature than they can at a high temperature before they precipitate. As a result of the slower rate of hydrolysis at a low temperature the film that is formed is porous and bulky and does not afford the same degree of protection afforded by a thinner, more compact film, such as the ones formed at a higher temperature. Consequently, if the rate of precipitation is slow enough and the rate of flow of the solution is sufficiently fast, the corrosion products may be swept from the surface before precipitation takes place. If this happens, the steel surface does not develop a film, and corrosion proceeds at a relatively high rate.

There are several points which support the diffusion hypothesis. First, the amount of film that is formed on steel surfaces is greater at low temperatures than at high ones. Furthermore, the films formed at low temperatures are generally less adherent, as shown by the fact that an appreciable amount of film can be removed by rubbing with cleansing tissue; films formed at high temperature are very tightly adherent and practically none can be removed by such treatment. Secondly, when platinum pins are exposed in a uranyl sulfate solution, the amount of iron and chromium oxides deposited on their surfaces is roughly inversely proportional to the temperature. At 300°C and above there has been no evidence of any film on the surface of the platinum pins indicating that the corrosion products precipitated before entering the main stream of the solution. Previously reported data[4] at higher uranium concentrations have shown that as the temperature is increased the critical velocity also increases, again indicating the more rapid formation of a protective film at higher temperatures.

In the case of 0.02 *m* uranyl sulfate, a minimum was found at 250 to 300°C at both velocities. At higher temperatures the corrosion rate increased, and the increased corrosion rate was closely associated with the oxidation of chromium to the soluble hexavalent state. Removal of chromium from the film apparently decreased the effectiveness of the protective oxide film and allowed a slightly higher corrosion rate. The fact that type 309 SCb stainless steel corroded faster than the other steels may have been due to the large percentage of chromium in this steel (type 309 SCb stainless steel contains 22 to 24% chromium). Hence, increasing the temperature is favorable from the standpoint of increasing the rate of hydrolysis of both ferric and chromic ions but, at the same time, is unfavorable because of the oxidation of chromium to a soluble state. The optimum temperature range from the standpoint of corrosion is 250 to 300°C.

Work presently in progress is being directed toward obtaining data, similar to those reported at the 0.02-*m* level, at higher concentrations. In addition, it is planned to further test zirconium and titanium under a number of different conditions, particularly at high uranium concentrations. A program of testing welded samples supplied by fabricators of component parts for the reactor will be started in the near future.

IN-PILE LOOP

G. H. Jenks H. C. Savage

Loop Package Testing and HB-4 Mock-Up

G. H. Jenks H. C. Savage
R. A. Lorenz D. T. Jones

In-Pile Development Loops. Since the previous quarterly report, two test runs with a solution containing 0.17 *m* uranyl sulfate and 0.01 *m* copper sulfate have been completed in an in-pile development loop. As previously reported, the operation of this loop has been entirely satisfactory. In both runs, type 347 stainless steel corrosion

82

ORNL-LR-DWG 2063

VOLUMES*

COMPONENT	VOLUME IN COMPONENT (cc)	FLUID VOLUME WHEN COLD (cc)	FLUID VOLUME WHEN HOT (cc)
BACK OF PUMP	115	115	115 AT 60°C
PUMP SCROLL	107	107	107 AT 250°C
CORE	300	300	300 AT 250°C
PRESSURIZER	550	54	300 AT 280°C
LOOP PIPE			
3/8 in. Sch. 40	443	443	443 AT 250°C
TOTAL	1510	1019	1265

CAPACITIES OF HEATERS AND COOLERS

HEATER OR COOLER	MINIMUM (watts)	MAXIMUM (watts)
PRESSURIZER LINE HEATER	0	1500 AT 220 VOLTS
LOOP HEATER	0	2500 AT 220 VOLTS
LOOP COOLER	600 AT 0.04 gpm	1780 AT 3 gpm
PUMP COOLER	750 AT 0.25 gpm	800 AT 3 gpm
HEATER JACKET ON PRESSURIZER	0	350 AT 110 VOLTS

LINE SIZE

COMPONENT	LINE SIZE (MATERIAL 347 STAINLESS STEEL)
MAIN LOOP	3/8 in. Sch. 40 PIPE
CORE WALL	2 in. Sch. 40 PIPE
PRESSURIZER	1¼ in. Sch. 80 PIPE
PRESSURIZER LINE	½ in. BWG 20 TUBING
PUMP DRAIN	0.090 in. OD – 0.050-in. ID TUBING
LOOP DRAIN	0.090 in. OD – 0.050-in. ID TUBING
GAS ADDITION LINE	0.060 in. OD – 0.020-in. ID TUBING
PRESSURE LINE	0.080 in. OD – 0.040-in. ID TUBING
PRESSURIZER LINE HEATER	¼ in. BWG 18 TUBING

PRESSURES

COMPONENT	MAIN STREAM (250°C)	PRESSURIZER (280°C)
STEAM	577 psi	930 psi
O_2	100 psi	70 psi
$2H_2 + O_2$	100 psi	12 psi
TOTAL	777 psi	1012 psi

FLOW RATES*

COMPONENT	FLOW RATE	VELOCITY
MAIN LOOP	5.8 gpm	9.74 ft/sec
PRESSURIZER LINE	6 cc/sec	1.20 ft/sec
PRESSURIZER LINE HEATER	6 cc/sec	10.4 ft/sec
PRESSURIZER (300 cc)	6 cc/sec	0.0397 ft/sec
SAMPLE HOLDER (Maximum)	5.8 gpm	51.0 ft/sec

*LOOP AT OPERATING TEMPERATURE AND PRESSURE.

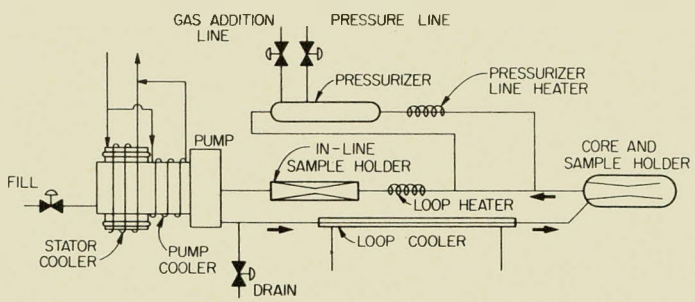

AREAS

SECTION OF LOOP	AREA (cm^2)
MAIN LINE AT 250°C	2000
PRESSURIZER AT 280°C	400

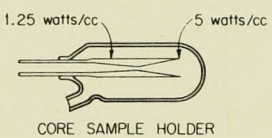

RESIDENCE TIME

COMPONENT	RESIDENCE TIME (sec)	IN-PILE ΔT (°C)	OUT-PILE ΔT (°C)
LOOP COOLER	0.359	1.26	1.26
CORE	0.82	0.530	0.0
LOOP HEATER	0.1603	0.460	1.26
PUMP SCROLL	0.292	0.566	0.566
PRESSURIZER HEATER	0.117	30.0	30.0
PRESSURIZER LINE	3.4	0.0	0.0
PRESSURIZER	50.		
COMPLETE LOOP	2.32		
COMPLETE PRESSURIZER	56.0		

SAMPLE HOLDERS

SAMPLE HOLDER	MATERIAL IN-PILE	ΔP** (5.8 gpm)
IN-LINE	ZIRCALOY-2	16.2 ft
CORE	ZIRCALOY-2	20.5 ft

*VOLUMES VARY SLIGHTLY IN DIFFERENT LOOPS DUE TO MINOR CHANGES.
**EACH SAMPLE HOLDER IS CALIBRATED BEFORE INSTALLATION IN THE LOOP. SOME VARIATION OF ΔP IS OBSERVED.

Fig. 60. Schematic Diagram and Physical Data for In-Pile Corrosion Test Loop.

test coupons[7] were exposed to the circulating solution. A schematic diagram of the in-pile loop is given in Fig. 60, along with pertient physical data, and Figs. 61 and 62 are photographs of the tapered corrosion-specimen sample holders.

The initial uranyl sulfate test run, No. AA-3, was preceded by a period of loop testing with water, a degreasing run with 3 wt % trisodium phosphate solution, and a run with 5% nitric acid solution. The loop corrosion specimens were

[7] C. D. Zerby *et al.*, *HRP Quar. Prog. Rep. Oct. 31, 1953*, ORNL-1658, Fig. 47, p 73.

UNCLASSIFIED
PHOTO 21363

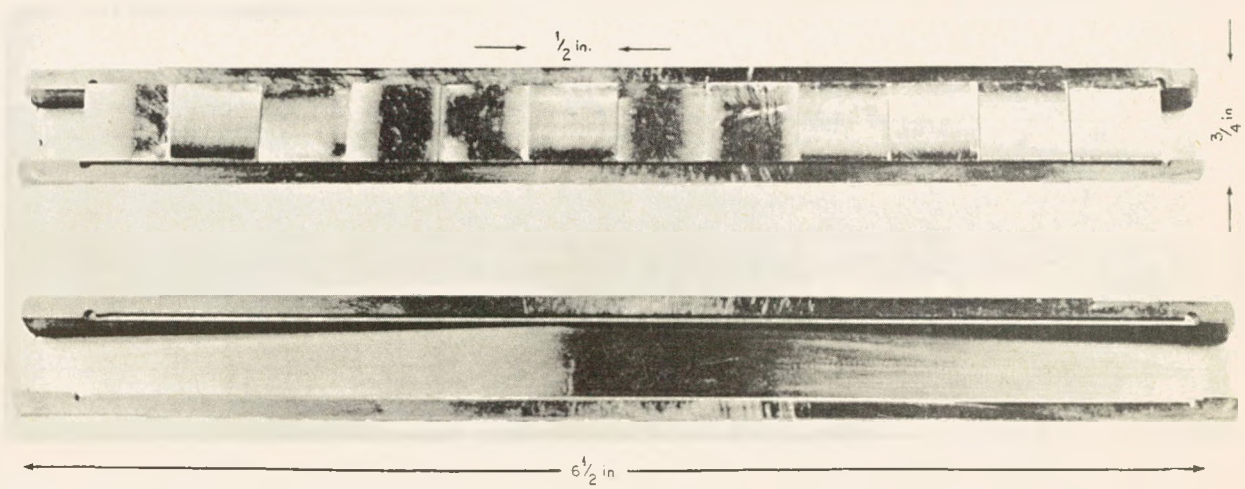

Fig. 61. Corrosion Test Coupons and Tapered Holder, In-Pile Loop.

UNCLASSIFIED
PHOTO 21389

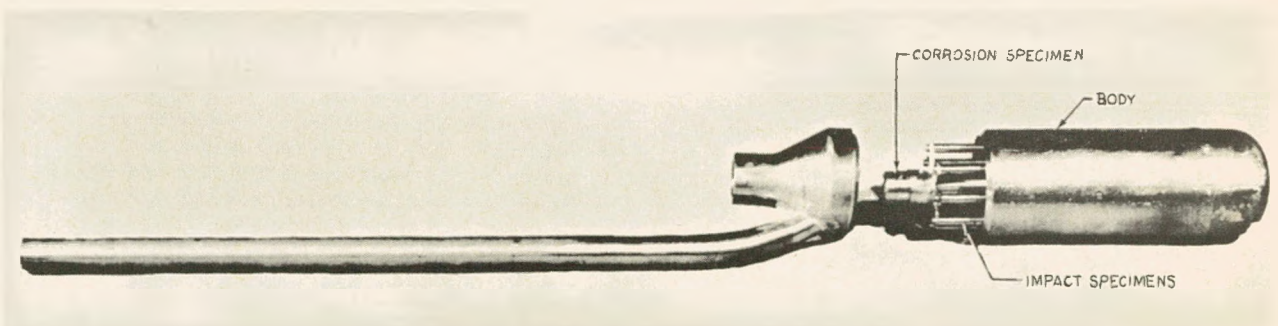

Fig. 62. Core Assembly, In-Pile Loop, Before Final Welding.

exposed to these solutions in addition to the 0.17 *m* uranyl sulfate solution. A complete operating history of the initial run is given in Table 18.

During the initial run with uranyl sulfate solution, it was possible to follow the generalized corrosion of the loop by using the decrease in oxygen partial pressure to calculate the quantity of oxygen consumed. The measurements of oxygen partial pressure were checked periodically by means of gas analyses of liquid samples withdrawn from the loop. The pump used in the development loop was the small, ORNL, totally enclosed, canned-rotor pump developed for use in the in-pile loops and has been described in previous quarterly reports. This particular pump contained Graphitar No. 14 bearings and a chrome-plated journal. Some wear of the Graphitar bearings was evidenced by the gradual increase of carbon dioxide gas in the loop during the course of the run. The average generalized corrosion rate of the system, based on the oxygen consumption (~320 cc at STP), was 0.95 mpy for the 215-hr run. This was in exact agreement with the average generalized corrosion rate of 0.95 mpy based on the nickel analysis of the solution. This agreement indicates the feasibility of following the corrosion rate in the loop, as installed in the LITR, by means of oxygen partial-pressure measurements, provided no oxygen is consumed in oxidizing the graphite material of the bearing to carbon dioxide. The oxidation of the graphite is one of two weaknesses of the present Graphitar bearings in the small in-pile circulating pump, since about half the oxygen used was converted to carbon dioxide. The second drawback to the Graphitar No. 14 bearings is the presence of small varying quantities of chloride in the bearing material (0.1 to 0.4%). The status of the pump bearings is discussed in more detail in the following sections of this report.

The corrosion test coupons contained in tapered titanium holders (Figs. 63 and 64) were removed, and the corrosion rates as a function of velocity for the coupons in both the in-line and the core positions are shown in Table 19. From these

TABLE 18. IN-PILE DEVELOPMENT LOOP, RUNS AA-1 THROUGH AA-3

Solution	Time (hr)	Temperature (°C)	Gas
Water	45	150 to 200	Helium (~500 ppm)
5 wt % HNO_3	48	100	Helium (~50 ppm)
0.17 *m* UO_2SO_4 + 0.01 *m* $CuSO_4$	215	250	Oxygen (200 to 700 ppm)

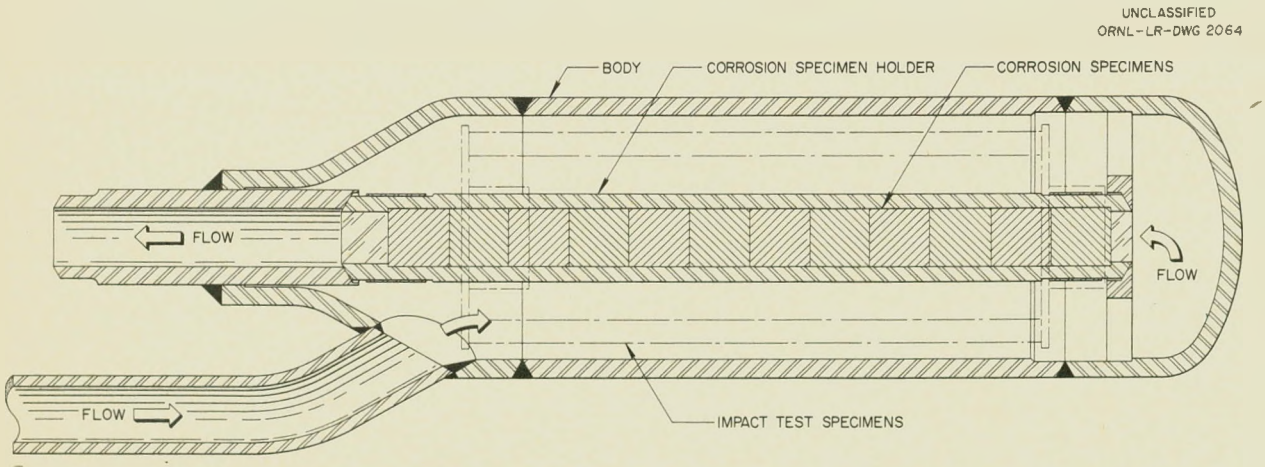

613 090

Fig. 63. Core-Sample-Holder Assembly, In-Pile Loop.

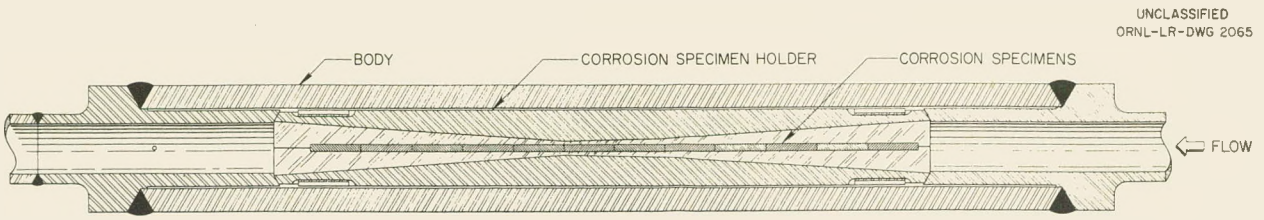

Fig. 64. In-Line Sample-Holder Assembly, In-Pile Loop.

TABLE 19. CORROSION OF IN-PILE LOOP, TYPE 347 STAINLESS STEEL COUPONS, RUNS AA-1 THROUGH AA-3

Velocity Range (fps)	Weight Loss (mg/sq cm)	Average Corrosion Rate (mpy)
	In-Line Position	
8.7–10.1	0.25	0.51
10.1–12.2	0.31	0.64
12.2–15.4	0.25	0.51
15.4–19.9	0.25	0.51
19.9–29.5	0.25	0.51
29.5–33.8	0.25	0.51
33.8–39.8	0.22	0.45
39.8–24.7	0.25	0.51
24.7–17.4	0.22	0.45
17.4–13.2	0.22	0.45
13.2–10.5	0.22	0.45
10.5– 9.4	0.19	0.39
	Core Position	
8.2– 9.6	0.27	0.58
9.6–11.5	0.25	0.51
11.5–14.4	0.22	0.45
14.4–19.0	0.19	0.39
19.0–28.8	0.22	0.45
28.8–32.8	0.16	0.32
32.8–40.3	0.37	0.77
40.3–23.5	0.12	0.26
23.5–16.8	0.22	0.45
16.8–12.9	0.25	0.51
12.9–10.3	0.22	0.45
10.3– 8.3	0.56	1.2

data it is seen that the corrosion rates are less than 1 mpy and that there was no effect of velocity on corrosion from approximately 8 fps to approximately 40 fps. This is consistent with data previously reported[8] for coupons that were given a similar pretreatment (water at 250°C, TSP solution, and nitric acid) prior to operation with uranyl sulfate solution.

In order to check the effect of pretreatment on corrosion rates, new, type 347 stainless steel corrosion-sample specimens in tapered titanium holders were installed in the development loop, and the second test run, AA-4, with a solution containing 0.17 *m* uranyl sulfate and 0.01 *m* copper sulfate was made with no pretreatment of the sample units. The operating conditions were 250°C with 650 to 160 ppm of dissolved oxygen, and the duration of the run was 200 hr. The average generalized corrosion rate based on oxygen consumption was 1.8 mpy. Based on solution nickel analysis, the average generalized rate was 1.2 mpy. In the second run the agreement between the two methods for determining over-all corrosion rate is not so good as in the initial run. It is uncertain whether the lack of agreement is due to error in oxygen partial-pressure measurements, error in the nickel analysis, or to some unknown factor. The generalized rate was higher in the second run because of the large increase in the corrosion of the exposed corrosion specimens, as shown in Table 20. From Table 20 it is seen that the maximum corrosion rate of the in-line sample units is 190 mpy, whereas the maximum corrosion rate of the coupons in the core position is 67 mpy. Both units theoretically should have the same flow; however, a possible explanation for this discrepancy is that a part of the total flow bypassed the sample units at the junction of the sample holder with the return line (see Fig. 63). All in-pile core assemblies are now being carefully checked for proper fit in order to ensure a tight seal at this point.

At the end of the second run in the development loop, a solution analysis showed a chloride ion

[8] J. C. Griess and R. E. Wacker, *HRP Quar. Prog. Rep. Jan. 31, 1954*, ORNL-1678, p 60-3.

TABLE 20. CORROSION OF IN-PILE LOOP, TYPE 347 STAINLESS STEEL COUPONS, RUN AA-4

Velocity Range (fps)	Weight Loss (mg/sq cm)	Average Corrosion Rate (mpy)
	In-Line Position	
8.8–10.2	1.6	3.5
10.2–12.5	2.0	4.4
12.5–14.9	3.9	8.6
14.9–20.2	8.8	20
20.2–30.5	15.2	34
30.5–35.4		
35.4–41.6	86.8	190
41.6–25.4	27.6	61
25.4–17.8	11.5	25
17.8–13.5	3.7	8.1
13.5–10.8	2.6	5.8
10.8– 9.5	1.2	2.8
	Core Position	
7.9– 9.5	1.3	3.0
9.5–11.3	2.7	5.9
11.3–14.3	4.5	9.9
14.3–18.5	9.0	20
18.5–28.3	13.4	30
28.3–32.7	18.2	40
32.7–39.2	30.1	67
39.2–23.4	18.0	40
23.4–16.4	10.5	23
16.4–12.4	7.9	17
12.4– 9.9	4.0	8.8
9.9– 8.6	1.5	3.2

concentration of 14 ppm. This chloride was presumed to have come from the Graphitar bearings; therefore operation of the development loop was temporarily suspended until a pump with improved bearings could be assembled. It was subsequently decided to install an Allis-Chalmers hydrodynamic-bearing pump in this loop for a test, as will be discussed in a following section of this report.

The initial model of the in-pile circulating loop built by the Engineering and Development Section of the REED has been incorporated in the over-all test program of the in-pile loop by the Corrosion Section. Two test runs with a solution containing 0.17 *m* uranyl sulfate solution with 0.01 *m* copper sulfate that were made in this loop have been reported previously.[9]

The third test run in the development loop was started as a test of the effect on corrosion of pretreatment with oxygenated water at 250°C. After 100 hr of operation with oxygenated water at 250°C, the core sample holder was opened and half of the corrosion specimens were removed and replaced with new specimens. The projected program was to operate the loop for 1000 hr at 250°C with 0.17 *m* uranyl sulfate solution. However, it was also decided to use the loop to test one of the in-pile pumps equipped with all-metal bearings (Stellite 98M2 to Stellite 98M2) in an effort to develop replacement bearings for the Graphitar No. 14.

As a preliminary check of pump and loop operation, the pump with all-metal bearings was installed and operated for 20 hr with water at 200°C in the line and at 230°C in the pressurizer. A 0.17 *m* uranyl sulfate solution containing 0.013 *m* copper sulfate and 5 mole % excess sulfuric acid was then added to the loop, along with oxygen, and a run, HT-5, of 350-hr duration was made. Analyses of solution samples taken periodically during the run gave somewhat erratic results. The highest concentration of cobalt (from the Stellite 98M2 bearings) that was reached was approximately 260 ppm after 150 hr of operation, and the concentration subsequently dropped to approximately 100 ppm. The decrease in cobalt concentration may have resulted from the removal of cobalt from solution by the formation of a uranium-cobalt sulfate[10] compound, which was previously identified in the Westinghouse model 100A pump test loops. The complete operating histories for runs HT-3 through HT-5, which cover the period of exposure of the sample units except for those replaced with new units after 100 hr of operation with oxygenated water at 250°C, are given in Table 21.

The type 347 stainless steel sample units in the core position were removed for examination. The corrosion data are given in Table 22. The sample units were coated with a loosely adhering yellow film on top of the normal tightly adhering protective type film usually found on coupons exposed to pretreatment with water at elevated temperatures. This yellow precipitate was found to contain uranium and cobalt. The corrosion rates of the

[9] C. D. Zerby *et al.*, *HRP Quar. Prog. Rep. Jan. 31, 1954*, ORNL-1678, p 67.

[10] J. C. Griess and R. E. Wacker, *HRP Quar. Prog. Rep. July 31, 1953*, ORNL-1605, p 94.

TABLE 21. LOOP OPERATION, RUNS HT-3 THROUGH HT-5

Run No.	Solution	Temperature (°C)	Time (hr)	Gas
HT-3	H_2O	250	100	Oxygen
	Replaced half of the core-corrosion-sample specimens			
HT-4	H_2O	200	20	Helium
HT-5	0.17 *m* UO_2SO_4 solution with 25 mole % H_2SO_4, 0.01 *m* $CuSO_4$	230	30	Oxygen
	0.17 *m* UO_2SO_4 solution with 5 mole % H_2SO_4, 0.013 *m* $CuSO_4$	250	320	Oxygen

TABLE 22. CORROSION OF IN-PILE LOOP, TYPE 347 STAINLESS STEEL COUPONS, RUNS HT-3 THROUGH HT-5

Velocity Range (fps)	Weight Loss (mg/sq cm)	Average Corrosion Rate (mpy)
	Core Position	
10.1–11.7	5.5*	7.0
11.7–14.1	5.3*	6.7
14.1–17.8	5.6*	7.1
17.8–23.1	6.4*	8.1
23.1–35.8	7.7*	9.7
35.8–41.3	7.3*	9.2
41.3–49.9	7.6*	9.6
49.9–29.1	0.87	1.1
29.1–20.5	0.53	0.67
20.5–15.6	0.56	0.71
15.6–12.4	0.53	0.67
12.4–11.8	0.47	0.59

*These coupons installed after run HT-3. All others exposed in runs HT-3 through HT-5. See Table 21.

coupons are low, and there was no apparent velocity effect.

The results of the chemical analyses of solution samples taken during the run are plotted in Fig. 65, and it can be seen that they are somewhat erratic. The decrease in the cobalt in solution from a high concentration of approximately 260 ppm to approximately 100 ppm after some 150 hr of operation is presumed to be the result of the formation of the uranium-cobalt sulfate compound. An almost identical situation was noted later in the initial run with uranyl sulfate solution in the in-pile mock-up (described elsewhere in this report). The over-all corrosion rate of the loop, based on the final nickel analysis (~85 ppm), is approximately 0.4 mpy.

New sample units are now being installed in the core position. The solution velocity past the corrosion test coupons will be increased by increasing the pump speed by means of a variable-frequency motor-generator set. The two primary objectives are to increase the solution velocity past the corrosion test coupons to a value considered high enough (60 to 80 fps) to produce bare-metal attack on corrosion samples that have a protective film formed by pretreating with oxygenated water at 250°C and to test the performance of the all-metal bearings at increased pump speeds.

In-Pile HB-4 Mock-up. During the past quarter a mock-up of the complete in-pile loop installation was built. Figures 66, 67, 68, and 69 are photographs of the in-pile mock-up located in Building 9204-1, Y-12 Area. The initial corrosion test loop, serial No. CC, installed in the mock-up is essentially as previously described. However, a flow diagram of the loop, together with pertinent physical data, is shown in Fig. 69.

In addition to the corrosion test loop, the in-pile mock-up contains all the auxiliary equipment to be installed at the LITR and a duplicate of the loop- and system-control panel. Initial testing of the loop involved pressure checks, leak checks, and instrument calibration. Loop operation was very satisfactory, and a pressure-temperature calibration of the system against steam-pressure data indicated a "total error" between the indicated pressurizer temperature (280°C) and absolute steam pressure (930 psia) of less than 10 psi. Loop flow measurements gave a flow rate in the main stream of 5.5 gpm at 30°C and a flow rate through the pressurizer of approximately 7 cc/sec at 30°C. The loop contained type 347 stainless steel corrosion test

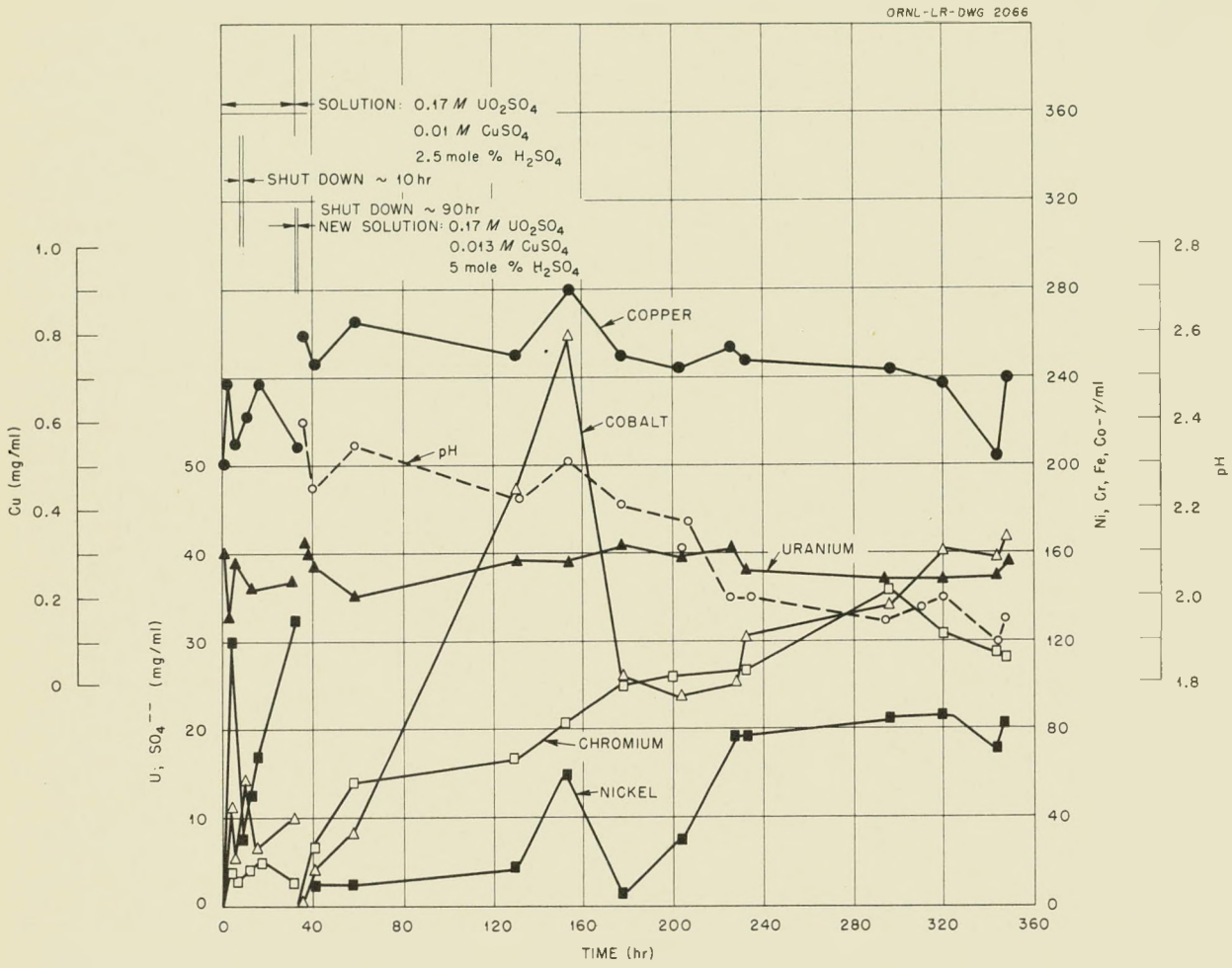

Fig. 65. Solution Analyses, Run HT-5, In-Pile Loop (Iron Less Than 5 ppm; No Cl^- Detected).

coupons in tapered titanium coupon holders in both the in-line and core positions. The corrosion test coupons and the holder are shown in Fig. 62. In addition, seven specimens of Zircaloy-2 machined with notches, as required for impact testing after exposure to uranyl sulfate solutions, were installed in the core position along with the corrosion test specimens. Thus this test loop is a duplicate of the in-pile loops and test specimens that are to be operated in the LITR to evaluate metal corrosion rates under conditions of nuclear irradiation. In the test loop to be installed in the LITR, the corrosion coupon holders will be made of Zircaloy-2 to reduce the absorption of neutrons and to allow a maximum neutron flux at the corrosion test specimens. Figure 62 is a view of the core assembly before final welding, and it shows the corrosion test specimen assembly with impact specimens.

The present procedure is to test-run two or three in-pile corrosion loops in the mock-up in order to ensure satisfactory operation of all the system components prior to installation of a loop in the LITR. These loops are also being used in obtaining out-of-pile corrosion data on the in-pile type of coupons, and they will be used as test assemblies in the dismantling facilities in the hot cell being fabricated at X-10. The personnel involved in testing and operating the mock-up are gaining valuable operating experience, and they will be assigned to the operation of the in-pile loop in the LITR.

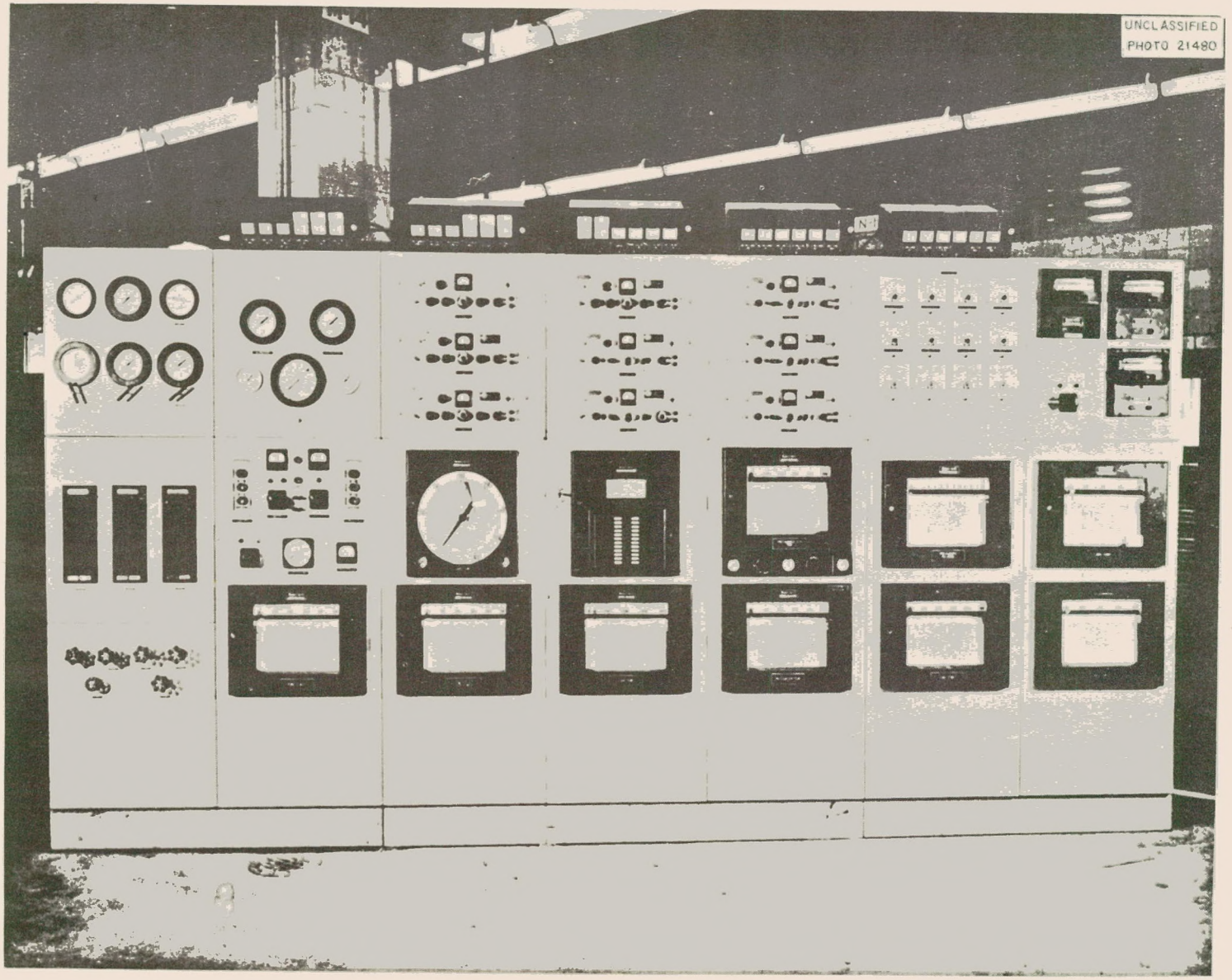

Fig. 66. Control Panel, In-Pile Mock-up.

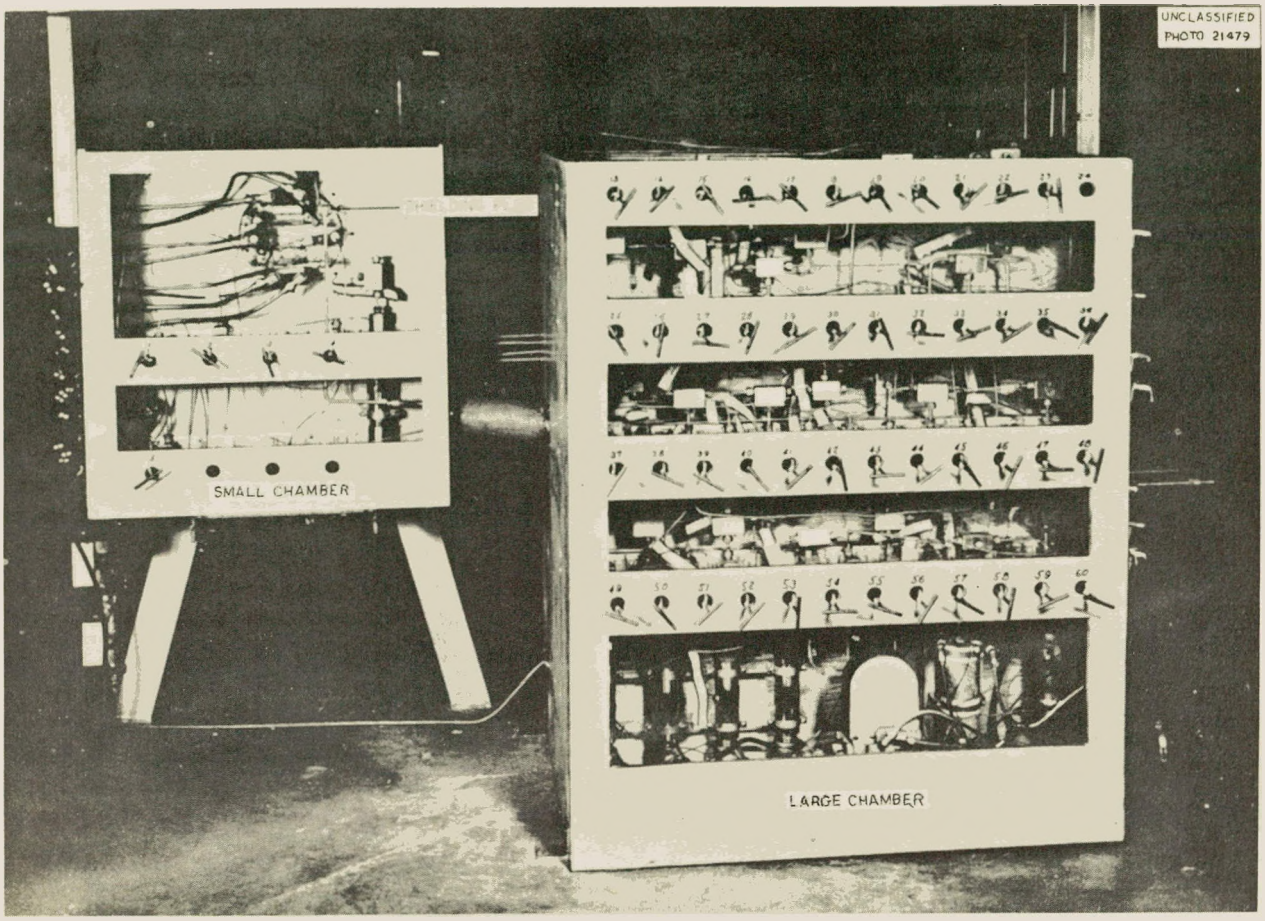

Fig. 67. Equipment Chambers, In-Pile Mock-up.

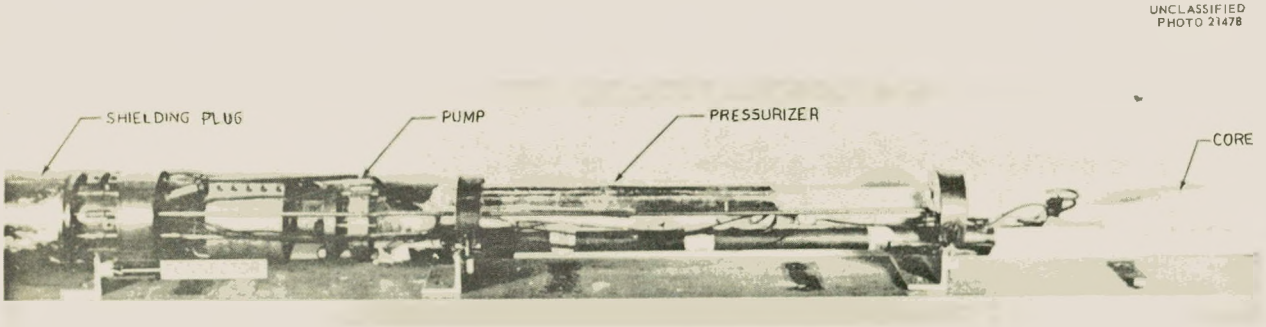

Fig. 68. Corrosion Test Loop, In-Pile Mock-up.

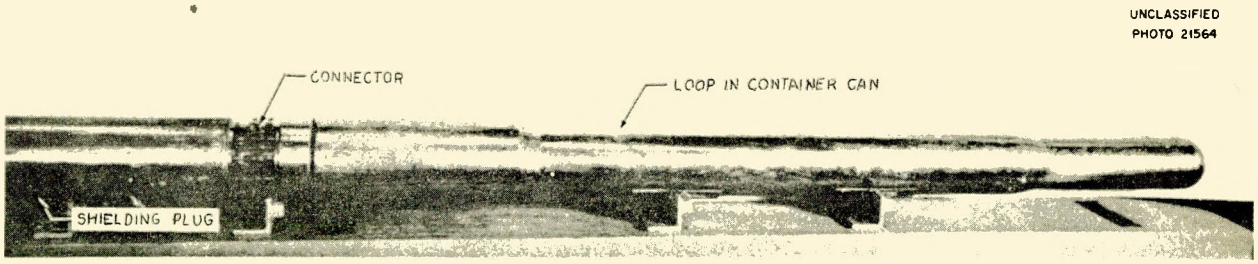

Fig. 69. Corrosion Test Loop with Container Can, In-Pile Mock-up.

All corrosion test loops will be assembled and tested in the in-pile mock-up before they are installed in the LITR. The loop assembly will include a completely canned-loop and shielding-plug assembly with all electrical leads, thermocouples, water, air, and high-pressure tubing lines. Cannon multipoint-disconnect plugs mounted in the small-equipment chamber will allow the assembly to be unplugged at the mock-up and to be plugged into identical disconnects in the small-equipment chamber at the LITR. Thus the canned loop and shielding plug can be removed from the mock-up after being tested and can be transported by means of a carrier to the LITR and then placed in hole HB-4. All service connections in the small-equipment chamber are then made by means of the disconnect plugs and by autoclave-type tubing fittings on the high-pressure tubing lines to the loop.

One run, BB-2, of 200-hr duration has been completed in the in-pile mock-up with a 0.17 *m* uranyl sulfate solution containing 0.13 *m* copper sulfate at 250°C and a dissolved oxygen concentration of approximately 500 ppm. The over-all system corrosion rate, based on the nickel analysis of the final solution (220 ppm), was approximately 2 mpy. No corrosion rate based on oxygen consumption was possible because both hydrogen and oxygen were added to the loop daily during the run in an effort to test the effectiveness of the copper sulfate as an internal catalyst for the recombination of hydrogen and oxygen.

The corrosion test coupons were removed and weighed at the end of the run, and the results are shown in Table 23. The corrosion of the coupons is low as was to be expected on the basis of previous runs in other in-pile loops and of in-pile-type coupons tested under similar conditions in a Westinghouse model 100A dynamic corrosion test loop (Loop F), described in the section "Loop Test Results." Figure 70 is a plot of the results of chemical analyses of solution samples taken during the run. The behavior of the cobalt in solution (from the Stellite 98M2 journal bushings)

TABLE 23. CORROSION OF IN-PILE LOOP, TYPE 347 STAINLESS STEEL COUPONS, RUN BB-2, IN-PILE MOCK-UP

Velocity Range (fps)	Weight Loss (mg/sq cm)	Average Corrosion Rate (mpy)
	In-Line Position	
8.9–10.4	0.62	1.5
10.4–12.7	0.56	1.3
12.7–15.7	0.50	1.2
15.7–20.4	0.44	1.0
20.4–29.9	0.34	0.81
29.9–34.0	0.28	0.66
34.0–40.2	0.25	0.59
40.2–25.4	0.31	0.73
25.4–17.9	0.34	0.81
17.9–13.6	0.44	1.0
13.6–10.9	0.50	1.2
10.9– 9.5	0.60	1.4
	Core Position	
9.0–10.5	0.44	1.0
10.5–12.7	0.53	1.2
12.7–16.0	0.47	1.1
16.0–20.7	0.53	1.2
20.7–31.3	0.38	0.88
31.3–35.8	0.38	0.88
35.8–42.9	0.40	0.95
42.9–26.1	0.40	0.95
26.1–18.4	0.38	0.88
18.4–14.0	0.47	1.1
14.0–11.2	0.50	1.2
11.2– 9.8	0.60	1.4

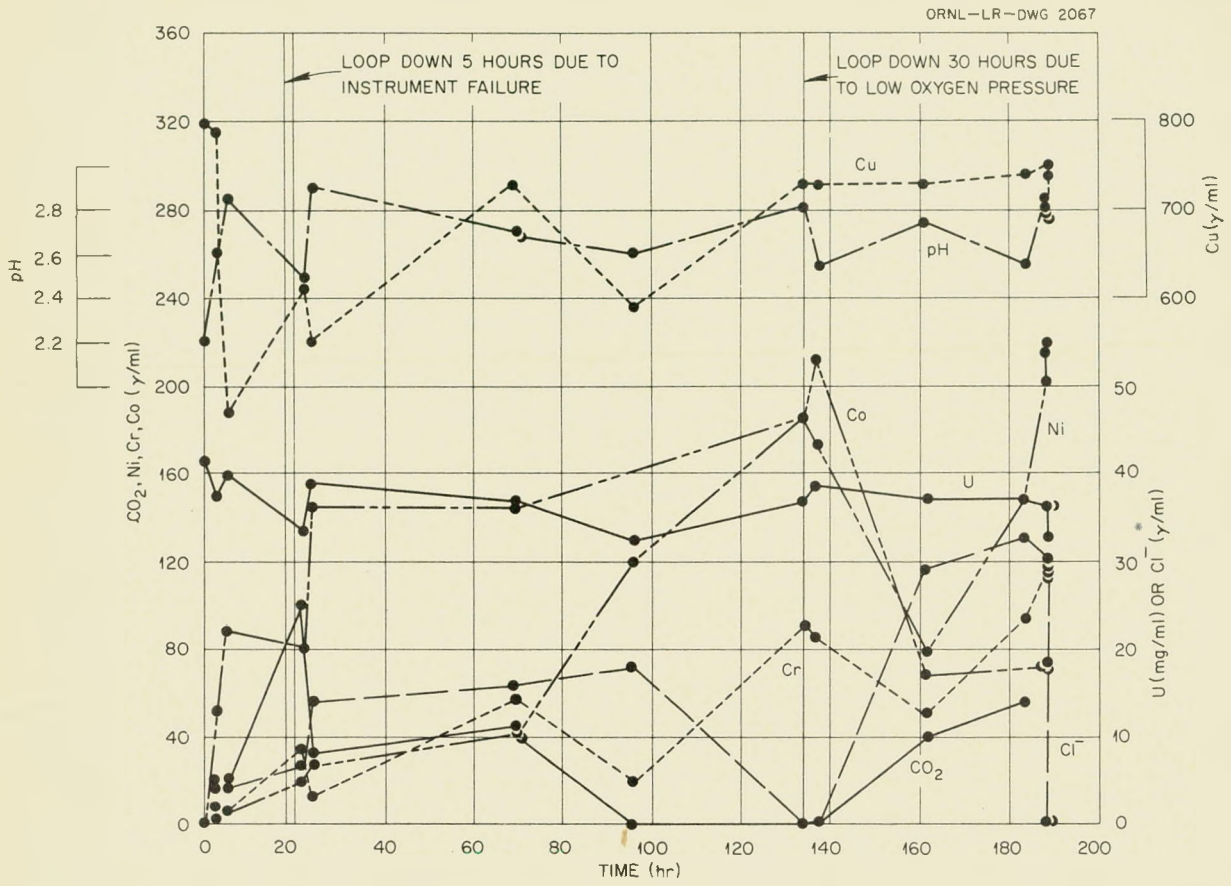

Fig. 70. Solution Analysis, Run No. 2, Loop BB, In-Pile Mock-up.

is almost identical to that of run HT-5 (see Fig. 65) in that it reaches a high concentration of approximately 240 ppm after about 140 hr of operation and then decreases to approximately 70 ppm. This is assumed, as in run HT-5, to result from the formation of the cobalt-uranium sulfate compound. Additional evidence of this compound was a yellowish coating on the lower surface of the pressurizer. The coating was similar in appearance to the substance previously identified as the cobalt-uranium sulfate.

As mentioned previously, stoichiometric additions of hydrogen and oxygen gas to the loop were made daily in an effort to evaluate the copper sulfate catalyst. The rate of addition of the gases was comparable to that expected from the dissociation of water under the operating conditions of the loop in the LITR (~8 cc/sec at STP). Equilibrium partial pressures of the hydrogen and oxygen were measured during and after the additions. The first test of the equilibrium partial pressure gave a result almost identical to the calculated expected pressure (~12 psi). However, equilibrium partial pressures of the hydrogen and oxygen increased to a high of approximately 50 psi in subsequent tests. The equilibrium partial pressures will be rechecked in the next loop to be installed in the in-pile mock-up.

The tests were discontinued and the loop was shut down and dismantled for a complete examination after 200 hr because leaks had occurred in both the tubing lines used to add the hydrogen and oxygen. The tubing was type 347 stainless steel with a 0.060-in. OD and a 0.020-in. ID. The reason for the tubing failure is unknown and is being investigated by the Metallurgy Section. However, it is known that the tubes contained uranyl sulfate solution at rather high temperatures. The uranyl

sulfate solution was forced into the tubes between the periods of gas flow, and, since the tubes passed close to the loop-pressurizer heater (~285°C), the lines could have been at a high temperature, which could have resulted in possible uranium precipitation (due to oxygen depletion) and corrosion. In addition, the uranyl sulfate solution contained chloride (~30 ppm at the end of the run), which is presumed to have come from the Graphitar No. 14 pump bearings. It should be pointed out that these two tubing lines are being used only in test work and are not a part of the in-pile installation. All high-pressure tubing connecting the loop to the small-equipment chamber is kept full of water and/or is maintained at low temperature during operation. However, the cause of this type of failure is being investigated, and additional precautions will be taken as indicated.

A second in-pile corrosion test loop, serial No. CC, has been completed and is now being installed in the in-pile mock-up for additional testing of the system.

In-Pile Pumps. The circulating pump used in the in-pile corrosion test loop is the 5-gpm, canned-rotor-type, ORNL pump described in previous quarterly reports. Figure 71 is a photograph of the pump parts. The Graphitar No. 14 bearings in this pump became the subject of some concern after it was found that the material being used contains small amounts of chloride. In test runs made to date, solution analyses have shown chloride concentrations in solution that ranged up to approximately 30 ppm. In addition, any Graphitar reaching the circulating solution consumes oxygen to form carbon dioxide, and this results in uncertainties in the corrosion rates as measured by oxygen partial pressures. In an effort to improve the situation, a pump with Stellite 98M2 bearings in place of the Graphitar No. 14 has been under test. Results of one test run with 0.17 *m* uranyl sulfate solution containing 0.013 *m* copper sulfate at 250°C for 350 hr indicate satisfactory operation of the Stellite 98M2 bearings against the Stellite 98M2 journal bushings.

It is now apparent from results obtained from runs in both the development loop and the in-pile mock-up that slight corrosion and/or wear of the Stellite 98M2 used in the pump result in cobalt going into

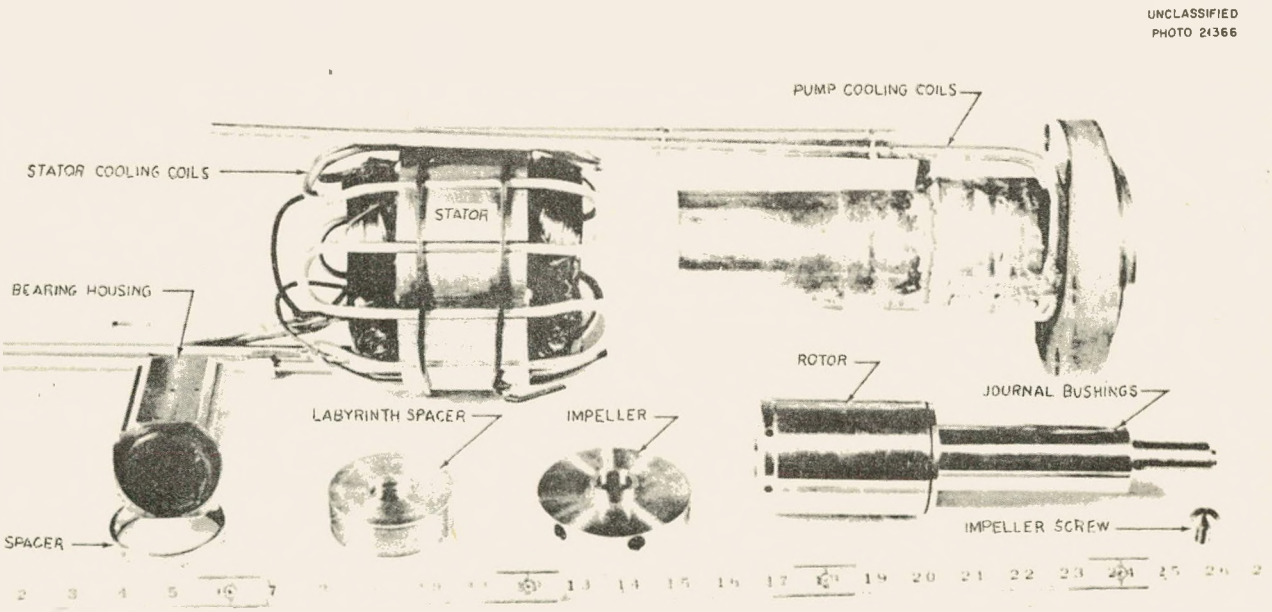

Fig. 71. Circulating Pump, In-Pile Loop.

solution (see Figs. 65 and 70). The presence of cobalt is undesirable but probably tolerable for short-term runs. Other bearing combinations will be tested in an effort to improve this condition, and, in this connection, an Allis-Chalmers hydrodynamic bearing pump is now under test as a possible future replacement for the sleeve-and-journal type of bearings.

From previous corrosion data obtained in the 100-gpm circulating loops, it appears that the cobalt from the Stellite 98M2 bearings may be due to corrosion rather than to wear. In the Westinghouse pumps, where Stellite 98M2 is the standard journal-bushing material, the cobalt concentration in solution stays below approximately 5 ppm. It is thought that the in-pile pumps may be operating at a higher bearing temperature, which results in a higher corrosion rate of the Stellite 98M2. Tests are under way in which the bearing temperatures are lowered by increased circulation of liquid around the bearings.

Arrangements have been made for the purchase, after development, of two pumps for possible use in the MTR loops. The Byron Jackson Co. will furnish one pump; the Allis-Chalmers Mfg. Co. will furnish the other. The general purchase specifications were the following:

Maximum external diameter	3½ in.
Maximum length	24 in.
Suction pressure	2000 psi
Operating temperature	300°C
Capacity	5 gpm against a 40-ft head
Rotor	Canned
Bearings	Other than graphite

The Byron Jackson pump is 3½ in. in diameter, 19 in. in length, and of two-stage construction. The bearings are of aluminum oxide, and the shaft is hard-faced with Stellite 6. The motor and bearings are water-cooled. The motor operates on 60-cycle, 3-phase current.

The Allis-Chalmers pump is 3½ in. in diameter, 11 in. in length, and utilizes fluid-piston bearings that operate at the temperature of the circulating liquid. The windings also operate at the system temperature. Two-stage construction is employed. The pump shaft will probably be of type 17-4 PH and the other parts will be of type 347 stainless steel. Allis-Chalmers will supply test parts which will be treated with water and with nitric acid at 250°C, since it is believed that this pretreatment will minimize the possibility of bearing seizure at startup of the pump. Final drawings will be ready by April 22.

LITR Installation

G. H. Jenks D. T. Jones

The stainless steel beam-hole liner and the two equipment chambers have been installed in permanent locations. All valves and interconnecting tubes are in the large chamber. Before installation, the valves were prepared according to the procedure previously described.[11] The interconnecting tubes were cleaned and pressure tested in the following manner. Each tube was first assembled in the chamber; then it was disconnected and pressure tested to 5000 psi with distilled water. The tube was next steam cleaned with 35-psi steam, washed with distilled water, and reassembled in the system.

All the service headers (air, off-gas, process water, demineralized water, etc.) have been installed, and work is progressing on connecting these services with the equipment chambers.

Several unsuccessful attempts have been made to install the neutron shutter. Difficulty has been encountered in placing the operating tubes so that they clear the top spider and do not interfere with normal maintenance of the LITR. Corrective alterations have been made in the tubing, and installation will be attempted again during the April 20 shutdown.

The housing that will shelter the emergency power supply is nearly complete. The hoist, track, and switches are installed and operating.

Loop Dismantling Facility

D. T. Jones A. R. Olsen

The installation of equipment in the dismantling cell is approximately 95% complete. Preliminary tests have been made of the performance of the various components, and, in general, the performance was found to be satisfactory, although a few minor adjustments were required. An adequate dust-collection system is not yet installed; however, when one is installed, the cell will be ready for a complete dummy operation.

Tests of the equipment will be carried out during April, and the procedure for dismantling and inspecting subassemblies from the loop will be

[11] G. H. Jenks *et al.*, *HRP Quar. Prog. Rep. Jan. 31, 1954*, ORNL-1678, p 63.

planned. This work will be done in cooperation with members of the Solid State Division.

Examination Facility

D. T. Jones A. R. Olsen

The new examination facility mentioned in the last report[11] has been expanded to take care of larger pieces of equipment. An outside loading door has been added, and the decision has been made to use an Electro Arc metal disintegrator as the cutting tool. All objects cut with this tool will be completely submerged in a liquid. Three vises of various sizes will be provided for holding the objects, and the cell will be serviced by an existing overhead crane through removable steel covers. Visual observation will be through liquid-filled windows and through existing periscopes of up to 20X magnification.

Efforts are being made to make the facility as versatile as possible, but special setups or clamps may be required for odd-shaped equipment.

LABORATORY CORROSION STUDIES

E. L. Compere

Vapor-Phase Corrosion of Type 347 Stainless Steel Over Oxygenated 0.1 *m* Uranyl Sulfate Solution at 250°C

E. L. Compere J. L. English

A very limited amount of quantitative static-corrosion data has been accumulated on the behavior of type 347 stainless steel in the vapor phase above uranyl sulfate solutions at elevated temperatures. Information of a qualitative nature with regard to this type of attack has been obtained from visual observation of the vapor-exposed surfaces in the 225-ml stainless steel autoclaves used for high-temperature testing of uranyl sulfate solutions. However, with the exception of a series of static tests to determine the effect of chloride additions to uranyl sulfate solutions on vapor-phase corrosion attack of stainless steel, there has been a paucity of information on the extent of vapor-phase corrosion above chloride-free uranyl sulfate solutions at elevated temperatures.

It has been noted that in the autoclaves used for routine corrosion testing with uranyl sulfate solutions the newly machined stainless steel surfaces, which are exposed in the vapor above the solutions, gradually darken in color and appear to be attacked quite uniformly. In general, the oxide film formed on the vapor-exposed surfaces appears to be considerably thinner than the film formed on solution-immersed surfaces. Furthermore, no significant corrosion damage has been observed around such metal-to-metal contact areas in the vapor phase as the metal junction between surfaces contacted by the O-ring stainless steel gasket used to seal the contents of the autoclave.

A very pronounced "water-line" attack has been found frequently in the test autoclaves. This form of corrosion damage is characterized by a continuous or near-continuous band of severe localized corrosion near or at the interface between the solution and the vapor phases. An example of water-line attack in a type 347 stainless steel test autoclave is shown in Fig. 72. The time required to produce water-line attack in stainless steel

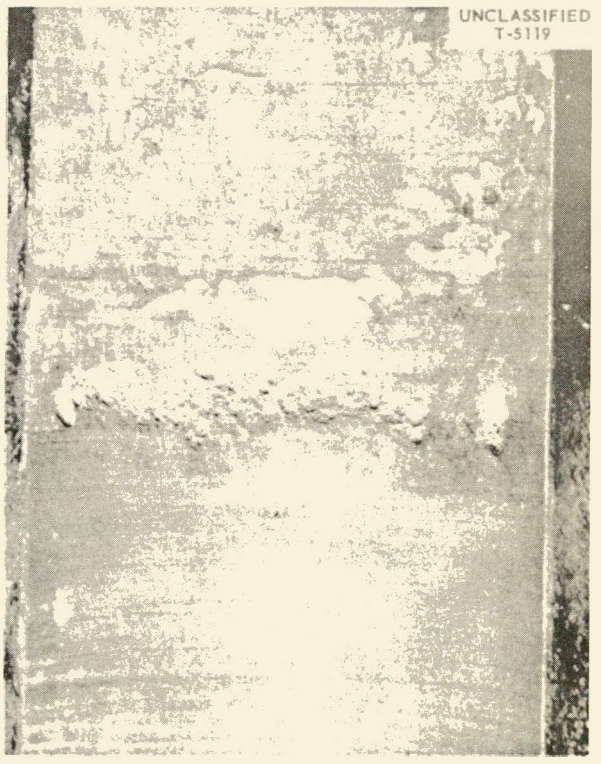

Fig. 72. An Example of Severe Water-Line Corrosion Attack in a Type 347 Stainless Steel Autoclave After 9736 hr of Service with Uranyl Sulfate Solutions at 250 and 300°C. (Blister-like formation is actually a large irregular cavity.) 2X. Reduced 13%.

autoclaves containing uranyl sulfate at high temperatures is quite variable. Recent test results have indicated that the attack may be produced in less than 100 hr in highly concentrated uranyl sulfate (~5 *m*) at 300°C. Normally, the time required to produce a noticeable water-line attack in an uneventful test series with oxygenated and mildly concentrated uranyl sulfate solutions at 250°C may vary from three to six months and longer. On occasion, when water-line corrosion has been observed in the autoclaves, the maximum penetration by this type of attack has been estimated at nearly 50 mils.

Although the present study on vapor-phase corrosion is not concerned specifically with water-line effects, a static-corrosion program has been undertaken in order to examine closely this form of attack. Titanium metal, as well as type 347 stainless steel, will be included in the investigation.

In the present study, corrosion test specimens of type 347 stainless steel were subjected to solution and to vapor-phase exposure for 913 hr in oxygenated 0.17 *m* uranyl sulfate solution at 250°C. The specimens, 3.18 cm in diameter by 0.45 cm in thickness, were prepared for test by abrading successively on No. 80, 120, 320, and 3/0 grit papers. The final preparation consisted of polishing on a metallographic wheel. A highly polished surface was desired on the specimens in order to facilitate the subsequent microscopic examination for signs of corrosion attack. Duplicate specimens were exposed in the solution and in the vapor phase above the solution. A single autoclave was used for the test.

The corrosion environment was 0.17 *m* uranyl sulfate with a SO_4/U ratio of 0.995. The chloride content in the solution was 1.6 μg/ml. Sufficient 30% hydrogen peroxide was added to the solution at the start of each run to generate an estimated oxygen partial pressure of 150 psia at 250°C by thermal decomposition of the room-temperature reaction product, uranyl peroxide (UO_4).

The final corrosion rates for the defilmed solution-exposed specimens were 0.39 and 0.42 mpy; the defilmed corrosion rates for the two vapor-exposed specimens were 0.04 and 0.06 mpy. Pitting corrosion was found on the latter specimens, however.

Mild pitting attack on the vapor-exposed specimens was first observed at the end of 426 hr. The frequency of the attack increased markedly with continued exposure. The pits were quite shallow, and microscopic examination, after removal of the corrosion products at the end of the test, disclosed that the maximum penetration by pitting did not exceed 1 mil.

The nature of the attack is shown in Fig. 73. Although the pits were small, they could be detected readily with the naked eye. A small group of pits, approximately 12 in number, was found on one face of a vapor-exposed specimen. These pits were oriented in a stringer-like fashion in a direction parallel with the radius of the specimen and were considerably deeper than the previously described shallow pits; the maximum pit depth was nearly 5 mils. The particular alignment of these pits suggested that the attack may have resulted from an accelerated corrosion caused by contact of the specimen with the stainless steel wire hanger. No such effect was noted on any of the other specimens.

The solution-exposed specimens exhibited a very mild intergranular attack when examined microscopically after removal of the bulky corrosion films; otherwise, the attack was of a uniform type. The grain-boundary attack was just visible at a magnification of 500X, as shown in Fig. 74. The intensity of the attack was too slight to permit an accurate depth measurement.

The corrosion rate for the stainless steel surface contacted by the uranyl sulfate solution at 250°C

Fig. 73. Pitting of Type 347 Stainless Steel Exposed for 913 hr in the Vapor Phase Above Oxygenated 0.17 *m* Uranyl Sulfate Solution at 250°C. 500X. Reduced 32%.

was 0.25 mpy as calculated from the final and corrected dissolved-nickel content (90 μg/ml) of the solution. The rate of increase of nickel in the uranyl sulfate solution is plotted in Fig. 75. The nickel values are expressed as milligrams of nickel per square decimeter of wetted stainless steel surface at 250°C.

A comparison between the defilmed weight losses on the solution- and the vapor-exposed specimens shows that the magnitude of vapor-phase attack was about 8% of the corrosion measured on the solution-exposed specimens.

Corrosion of Zircaloy-2 at 250°C in Oxygenated 0.02 *m* Uranyl Sulfate Solution Containing Fluoride Additions

J. L. English

A proposal made by personnel of the Vitro Corporation of America for the chemical processing of an enriched uranyl sulfate homogeneous reactor fuel solution involves the use of calcium fluoride as an ion-exchange medium.[12] The chemical separation process was concerned originally with the removal of fission products, especially the rare earths, and possibly plutonium and corrosion products from the uranyl sulfate solution. These objectives were to be realized without any modification of the fuel solution, such as changing the uranium or sulfate concentrations. Laboratory-column tests at 100°C by Vitro personnel showed that calcium fluoride exhibited a high degree of efficiency for the removal of the rare earths from a 0.02 *m* uranyl sulfate solution. Negligible amounts of uranium and only small amounts of sulfate (about 8%) were removed in the ion-exchange process. However, owing to the increased solubility of calcium fluoride in uranyl sulfate at 100°C, the effluent from the column was found to contain from 0.8 to 1.3 g of calcium and approximately 0.4 g of fluoride per liter. The presence of this quantity of fluoride ion in a uranyl sulfate fuel solution operating at a temperature of 250°C and higher would undoubtedly create serious concern because of its corrosive effect on reactor construction materials. In view of the potential corrosion hazard, the original Vitro proposal was modified for the express purpose of reducing the amount of fluoride contamination in the processed fuel solu-

[12] Vitro Corporation of America, *Homogeneous Reactor Processing. Decontamination of UO_2SO_4 Solutions. Project Summary*, KLX-1617 (July 31, 1953).

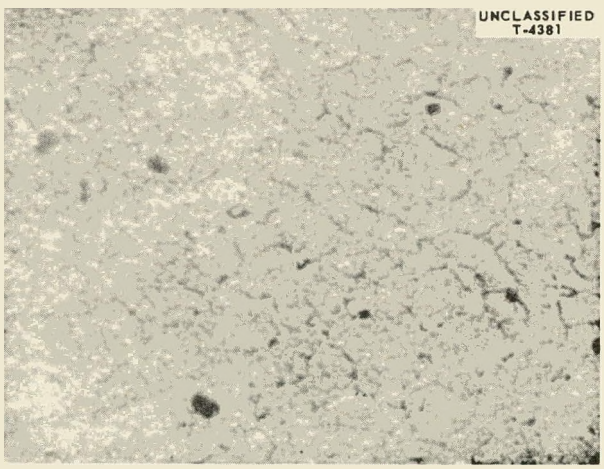

Fig. 74. Mild Intergranular Attack on Type 347 Stainless Steel Exposed for 913 hr at 250°C in Oxygenated 0.17 *m* Uranyl Sulfate Solution. 500X. Reduced 31%.

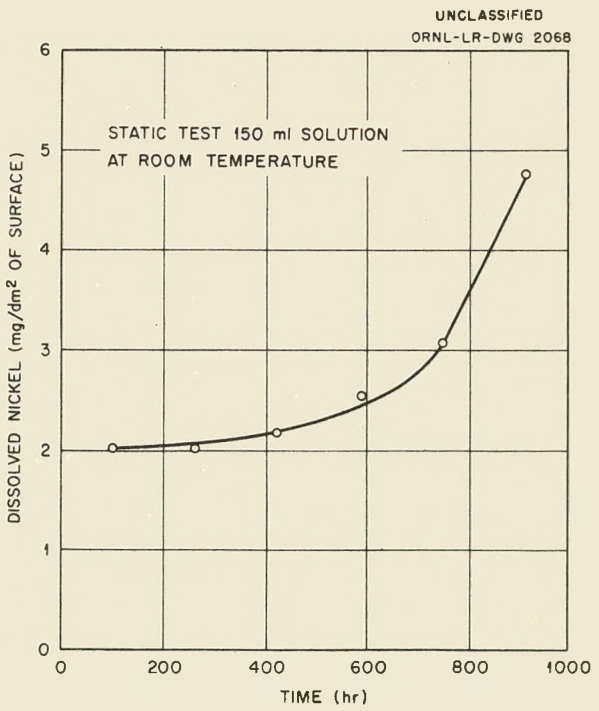

Fig. 75. Increase of Dissolved Nickel in Oxygenated 0.17 *m* Uranyl Sulfate Solution Contained in a Type 347 Stainless Steel Autoclave at 250°C.

tion.[13] In one modification, a thorium sulfate slurry is added to the fuel solution before its entry to a calcium sulfate precipitation column where the fluoride would be removed as thorium fluoride; the resultant fluoride contamination in the fuel solution after this treatment would not exceed 60 ppm. In an alternate modification, the effluent which comes from the calcium fluoride column and which contains 400 ppm of fluoride would be evaporated to dryness and heated for 1 hr at 300°C before being returned to the fuel system. This treatment, although fairly costly, would be expected to keep fluoride contamination in the fuel solution to less than 1 ppm.

A corrosion-testing program was conducted to determine the threshold level, if any, of fluoride concentration with regard to the extent of corrosion damage on reactor construction materials. Zircaloy-2 was selected as the first metal to be examined because of its proposed use as a construction material for the core tank of a large-scale homogeneous reactor.[14] The environment for the corrosion tests was oxygenated 0.02 *m* uranyl sulfate solution with 25 mole % excess sulfuric acid added to prevent hydrolytic precipitation of the uranyl ion at the test temperature, 250°C. The tests were run in nitric acid-pretreated stainless steel autoclaves for periods of from 24 to 1000 hr, depending upon the behavior of a particular test system.

Additions of solid uranyl fluoride, UO_2F_2, were made to the dilute uranyl sulfate solution in amounts calculated to give fluoride concentrations of 50, 200, 400, and 600 ppm; chemical analyses showed that the solutions contained 43, 153, 427, and 647 ppm of fluoride, respectively. The total uranium concentration in each test solution was maintained at 0.02 *m* by careful proportioning of a concentrated uranyl sulfate stock solution and the uranyl fluoride salt to give the desired fluoride concentration. All solutions contained 25 mole % excess sulfuric acid, including a fluoride-free 0.02 *m* uranyl sulfate solution which was run for a control test. Also included among the corrosion media was a 0.02 *m* uranyl fluoride solution (~785 ppm of fluoride). The solutions were pressurized with approximately 150 psia of oxygen at temperature by the hydrogen peroxide-addition technique.

The corrosion specimens were machined from 0.6-cm-dia Zircaloy-2 rod (Item No. 333). The final specimen size was 0.55 cm in diameter by 2.55 cm in length; the nominal surface area per specimen was 4 sq cm. The chemical composition of the alloy, in weight per cent, was as follows: Sn, 1.1; Cr, 0.034; Fe, 0.2; Ni, 0.044; N, <0.001; C, <0.01; and Zr, balance. Duplicate specimens were exposed in both the solution and vapor phase in each test solution.

The corrosion data are included in Table 24. The defilming treatment for removal of corrosion products consisted in immersing the specimens in a bath of Virgo salts for 15 min at 510°C, quenching in water, and exposing for single 3-min periods in 10% HCl and 10% HNO_3 solutions at 70 to 80°C, respectively. Previous work with uncorroded Zircaloy-2 specimens showed a negligible attack on the alloy when they were subjected to this treatment.

It should be emphasized that this defilming technique was not entirely effective in all cases for the complete removal of corrosion films or scales from the specimens. The films in certain cases proved to be extremely tenacious and of a nature which suggested the use of a harsh pickling treatment to effect complete removal. Some of the metal-thickness-loss values presented in Table 24 may be somewhat on the optimistic side because of the difficulty encountered in film removal. Nevertheless, the metal-loss values were considered to be sufficiently representative of the effect produced by increasing fluoride concentration in the test solutions.

The specimens tested in the solutions containing 43 ppm of fluoride continued to show significant weight gains after repeated exposures to the defilming treatment with Virgo salts. The films on the specimens in solution and vapor exposures were quite adherent and uniform and did not appear to flake from the specimens during the tests. In order to obtain some estimate of the magnitude of corrosion attack, it was assumed that the corrosion product was ZrO_2 and that it did not flake off during the test. The final as-removed weight gains were expressed in terms of the weight of zirconium metal consumed in the production of the specific quantity of oxide, and the estimated metal thickness losses were determined from these values.

[13] D. E. Ferguson *et al.*, *HRP Quar. Prog. Rep. Jan. 31, 1954*, ORNL-1678, p 100-2.

[14] A. M. Weinberg *et al.*, *Five-Year Program for Nuclear Power Development At Oak Ridge National Laboratory*, ORNL CF-53-10-222 (Oct. 30, 1953).

TABLE 24. CORROSION OF ZIRCALOY-2 AT 250°C IN OXYGENATED 0.02 *m* URANYL SULFATE SOLUTIONS CONTAINING FLUORIDE ADDITIONS AND 25 mole % EXCESS SULFURIC ACID

Test No.	Specimen Exposure	Time (hr)	Fluoride Content (ppm)		Weight Loss (mg/sq cm)		Estimated Metal Loss (mils)	Appearance of Specimen after Defilming
			Initial	Final	As-removed	Defilmed		
2524-1	Solution	1000	0	0	0.10	0.23	0.01	Shiny dark-gray surfaces; uniform corrosion attack
2524-2	Solution	1000	0	0	+0.08	0.10	<0.01	Shiny dark-gray surfaces; uniform corrosion attack
2524-3	Vapor	1000	0	0	+0.08	0.10	<0.01	Shiny blue-gray surfaces; uniform corrosion attack
2524-4	Vapor	1000	0	0	+0.05	0.08	<0.01	Shiny blue-gray surfaces; uniform corrosion attack
2525-1	Solution	1000	43	48	+1.30	+0.88	0.07*	Semidull; white corrosion products (30X)
2525-2	Solution	1000	43	48	+1.13	+1.05	0.06*	Semidull; white corrosion products (30X)
2525-3	Vapor	1000	43	48	+0.95	+0.78	0.05*	Shiny blue-black color; white corrosion products (30X)
2525-4	Vapor	1000	43	48	+0.96	+0.68	0.05*	Shiny blue-black color; white corrosion products (30X)
2530-1**	Solution	1000	43	55	+0.88	+0.60	0.05*	Dull; gray-white corrosion products
2530-2	Solution	1000	43	55	+0.90	+0.83	0.05*	Dull; numerous circumferential "cracks"
2530-3	Vapor	1000	43	55	+0.43	+0.35	0.02*	Semidull color; gray corrosion products
2530-4	Vapor	1000	43	55	+0.55	+0.48	0.03*	Semidull color; suspected pitting
2526-1	Solution	137	153	156	+5.93	0.30	0.02	Gray-white spotty film; roughened surfaces
2526-2	Solution	137	153	156	+6.23	0.20	0.01	Gray-white spotty film; roughened surfaces
2526-3	Vapor	137	153	156	0.43	1.55	0.09	Gray-white spotty film; random pitting; roughened
2526-4	Vapor	137	153	156	+0.13	0.10	<0.01	Gray-white spotty film; random pitting; roughened
2527-1	Solution	24	427	369	+5.18	8.40	0.50	Gray-white color; surfaces very rough
2527-2	Solution	24	427	369	+4.30	12.55	0.75	Gray-white color; surfaces very rough
2527-3	Vapor	24	427	369	23.98	37.75	2.25	Spotty corrosion scale; heavily roughened surfaces
2527-4	Vapor	24	427	369	8.00	30.08	1.80	Spotty corrosion scale; heavily roughened surfaces
2528-1	Solution	24	647	613	+28.30	49.05	2.93	Semidull gray (bare metal); heavily roughened
2528-2	Solution	24	647	613	+25.07	48.23	2.88	Semidull gray (bare metal); heavily roughened
2528-3	Vapor	24	647	613	22.80	23.32	1.39	Dull gray color; severe semilocalized attack
2528-4	Vapor	24	647	613	20.98	21.23	1.27	Dull gray color; severe semilocalized attack

*Estimated metal loss calculated from as-removed weight gain.
**Test run in platinum-lined autoclave.

TABLE 24. (continued)

Test No.	Specimen Exposure	Time (hr)	Fluoride Content (ppm)		Weight Loss (mg/sq cm)		Estimated Metal Loss (mils)	Appearance of Specimen after Defilming
			Initial	Final	As-removed	Defilmed		
2529-1	Solution	24	785	706	+19.33	59.75	3.57	Semidull gray (bare metal); severely roughened surface
2529-2	Solution	24	785	706	+10.95	60.20	3.59	Semidull gray (bare metal); severely roughened surface
2529-3	Vapor	24	785	706	69.03	69.43	4.15	Dull gray color; very severe semilocalized attack
2529-4	Vapor	24	785	706	30.50	64.83	3.87	Dull gray color; very severe semilocalized attack

Sufficient evidence has been presented by this series of tests to preclude the use of Zircaloy-2 at 250°C in oxygenated 0.02 *m* uranyl sulfate solutions containing 43 ppm, and higher, of fluoride ion. Although the magnitude of metal-thickness-loss values was not significant for specimens exposed in solutions containing 43 ppm of fluoride, 0.02 to 0.07 mil in 1000 hr, the condition of the Zircaloy-2 surfaces at completion of the tests warranted serious concern. All specimens exhibited considerable corrosion-product formation, and, in one instance, an intense localized corrosion resembling a "crack-type" of attack was observed along the machining grooves on a vapor-exposed specimen. At fluoride concentrations of 427 ppm and above, metal-thickness losses in 24-hr periods ranged from 0.5 to 4.2 mils.

A significant observation was made during the tests with Zircaloy-2 specimens exposed in the solutions containing 43 ppm of fluoride. After 72 hr of test, small, black, hard globules were randomly scattered on the surfaces. The globules remained during the 1000-hr test period. Prior to defilming, a few of the deposits were removed carefully and submitted for spectrographic examination. The major constituents and their relative concentration, in weight per cent, in the deposit were as follows: Al, 0.3; Cr, 6.0; Fe, 0.6; Mo, 0.6; Zr, <0.3; and U, >5.0. Similarly, a portion of the corrosion film was removed from a Zircaloy-2 solution-exposed specimen after 24 hr in a solution containing 647 ppm of fluoride (No. 2528-1) and was submitted for spectrographic and x-ray diffraction analyses. The spectrographic results, in weight per cent, were: Al, <0.05; Cr, 0.1; Fe, 0.05; Mo, <0.05; Zr, 5.0; and U, present. The x-ray diffraction patterns showed a compound of the following probable composition in weight per cent: ZrO_2, 40 to 80; U_3O_8, 20 to 40; and unidentified, 5 to 15.

Figures 76 through 83 are photographs of the test specimens. The specimens in Figs. 76, 77, and 78, photographed after 676 hr of test, show much the same appearance as the surfaces of those exhibited after 1000 hr of test. Figure 83 shows an enlarged view of the type of corrosion attack found on a solution-exposed specimen after 1000 hr in 0.02 *m* uranyl sulfate solution containing 43 ppm of fluoride.

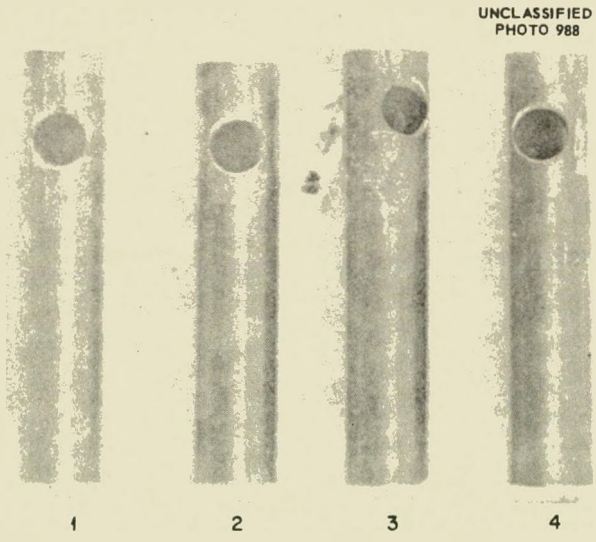

Fig. 76. Zircaloy-2 Specimens After 676 hr at 250°C in Oxygenated 0.02 *m* Uranyl Sulfate Solution; Control, No Fluoride Added. (Test 2524; specimens 1 and 2 in solution, 3 and 4 in vapor.) 3X. Reduced 25%.

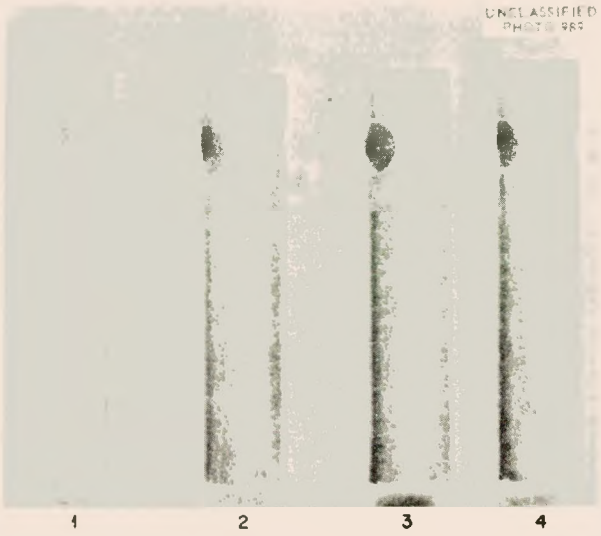

Fig. 77. Zircaloy-2 Specimens After 676 hr at 250°C in Oxygenated 0.02 *m* Uranyl Sulfate Solution Containing 43 ppm of Fluoride. (Test 2525; specimens 1 and 2 in solution, 3 and 4 in vapor.) 3X. Reduced 27%.

Fig. 79. Zircaloy-2 Specimens After 137 hr at 250°C in Oxygenated 0.02 *m* Uranyl Sulfate Solution Containing 153 ppm of Fluoride. (Test 2526; specimens 1 and 2 in solution, 4 in vapor.) 3X. Reduced 30%.

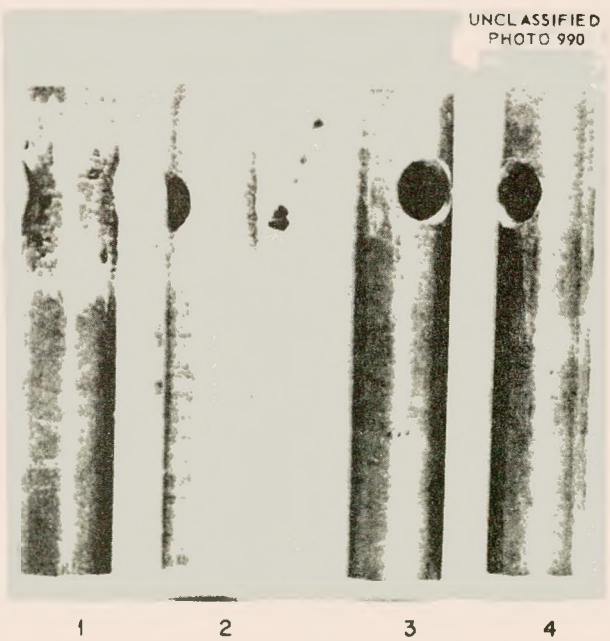

Fig. 78. Zircaloy-2 Specimens After 676 hr at 250°C in a Platinum-Lined Autoclave Containing Oxygenated 0.02 *m* Uranyl Sulfate Solution with 43 ppm of Fluoride. (Test 2530; specimens 1 and 2 in solution, 3 and 4 in vapor.) 3X. Reduced 15%.

Fig. 80. Zircaloy-2 Specimens After 24 hr at 250°C in Oxygenated 0.02 *m* Uranyl Sulfate Solution Containing 427 ppm of Fluoride. (Test 2527; specimens 1 and 2 in solution, 3 and 4 in vapor.) 4X. Reduced 37.5%.

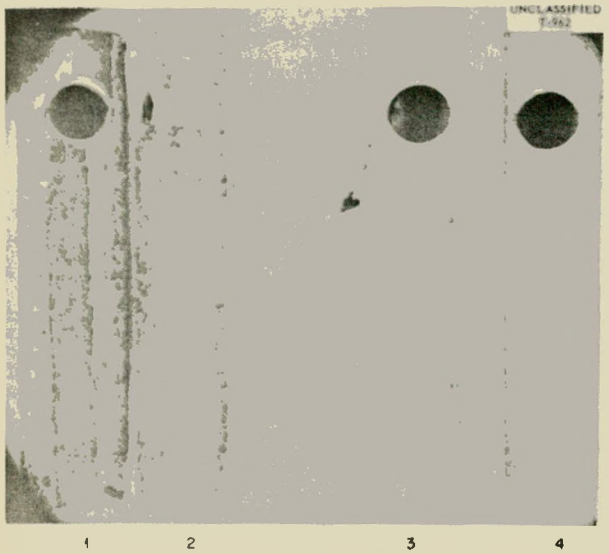

Fig. 81. Zircaloy-2 Specimens After 24 hr at 250°C in Oxygenated 0.02 *m* Uranyl Sulfate Solution Containing 647 ppm of Fluoride. (Test 2528; specimens 1 and 2 in solution, 3 and 4 in vapor.) 4X. Reduced 40%.

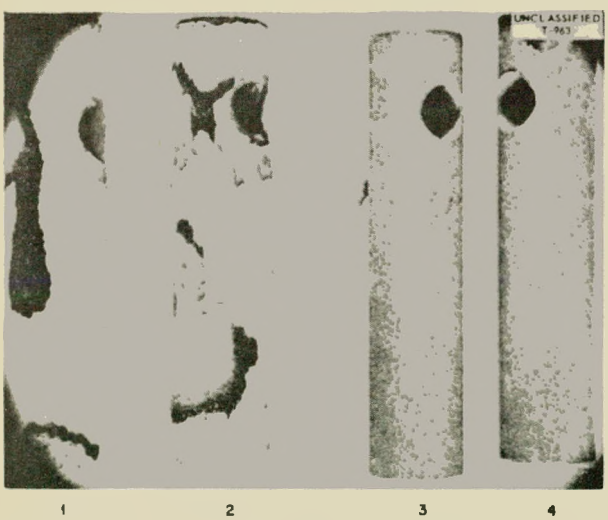

Fig. 82. Zircaloy-2 Specimens After 24 hr at 250°C in Oxygenated 0.02 *m* Uranyl Sulfate Solution. (Test 2529; specimens 1 and 2 in solution, 3 and 4 in vapor.) 4X. Reduced 43%.

Fig. 83. Stringer Type of Pitting in Zircaloy-2 After 1000 hr at 250°C in 0.02 *m* Uranyl Sulfate Solution Containing 43 ppm of Fluoride. (Test 2530-2; solution exposed.) 16X. Reduced 12%.

Corrosion of Titanium, Zircaloy-2, and Type 347 Stainless Steel at 300°C in Oxygenated 5 *m* Uranyl Sulfate Solution

E. L. Compere J. L. English

In recent months, a considerable effort at ORNL has been directed to a study of the design of a large-scale homogeneous reactor which will produce power and low g/T plutonium. The major interest is centered upon a two-region reactor consisting of a fuel solution of enriched uranyl sulfate surrounded by a blanket of a concentrated uranyl sulfate solution. The concentration in the blanket may be 300 g of uranium per liter, or higher. The possibility that the uranium content in the blanket solution may exceed 300 g of uranium per liter prompted an examination of the corrosion behavior of type 347 stainless steel, titanium, and Zircaloy-2 in a concentrated uranyl sulfate solution at elevated temperature.

The test conditions selected were a temperature of 300°C and a uranyl sulfate concentration of approximately 5 moles per 1000 g of water (the actual uranium content in the test solution by analysis was 923 g/liter). This particular temperature-concentration combination was taken from the phase diagram for the system UO_2SO_4-H_2O as established by Secoy[15] and by Jones and Marshall.[16] It was selected so that at 300°C the system would be slightly below the region of two-liquid-phase separation. The conditions thus crudely represented the type of corrosive environment that would exist in the heavy phase when the two-liquid-phase region was reached. Although it is not proposed to operate reactors in the two-liquid-phase region, the conditions of that region could be reached unintentionally by a not too extreme fluctuation in temperature and uranyl sulfate concentrations. The test conditions also represented a completely unexplored environment with respect to the corrosion behavior of promising reactor materials of construction.

The test solution was prepared by the evaporation of a uranyl sulfate stock solution containing 580 g of uranium per liter to a volume which was estimated to result in a 5 *m* uranyl sulfate solution. The actual concentration in the evaporated solution was determined by analysis to be 923 g of uranium per liter; the sulfate-to-uranium ratio was 1.008. Upon cooling below 100°C after the evaporation process, a solid formed in the solution, which, according to the two-component phase diagram of Jones and Marshall,[16] was $UO_2SO_4 \cdot 3H_2O$. Heating slightly above 100°C was sufficient to redissolve the hydrated solid in the solution.

The type 347 stainless steel corrosion specimens were cut from 0.048-cm-thick (0.019-in.), hot-rolled, annealed, and pickled sheet. The nominal surface area per specimen ranged from 14.3 to 16.0 sq cm. One set of six specimens was placed in the solution phase, and sets of four specimens each were exposed to the solution-vapor interface and to the vapor phase above the solution. After the initial 24-hr exposure period, duplicate specimens of machined titanium 75A and Zircaloy-2 were placed in the solution, as were two additional specimens of type 347 stainless steel for water-line exposure.

[15] C. H. Secoy, *J. Am. Chem. Soc.* 72, 3343 (1950).

[16] E. V. Jones, *HRP Quar. Prog. Rep. March 15, 1952*, ORNL-1280, p 180; W. L. Marshall, *HRP Quar. Prog. Rep. March 15, 1952*, ORNL-1280, p 190.

A 350-ml volume of the 5 *m* uranyl sulfate solution was placed in a stainless steel autoclave in which the specimens were supported in their respective positions. The sealed system was then pressurized with 150 psig of oxygen at room temperature. The temperature of the test was controlled at 300 ± 5°C. Test runs of 24, 24, 52, and 100 hr have been made thus far for a total exposure of 200 hr on most of the specimens. The test solution was replaced at the start of each run.

The accumulated corrosion data for 200 hr of test are presented in Table 25. Specimens were removed at periodic intervals for defilming and for measuring actual metal-weight losses. Solution-exposed specimens of type 347 stainless steel exhibited metal-thickness losses between 0.09 and 0.13 mil (based on defilmed weight losses) for a 200-hr exposure period; corrosion attack was of a uniform type. Estimated metal-thickness losses on the defilmed vapor-exposed specimens were 0.02 to 0.03 mil after 100 hr; no pitting was observed on the specimens. The most severe corrosion was found on surfaces which were exposed at the interface between the solution and the vapor phase. Large areas of semilocalized attack, as well as severe pitting attack, were evident. Pits as deep as 7 mils were measured, which represented a 37% penetration of the 19-mil specimen thickness, in somewhat less than 200 hr. A photograph of the water-line attack is shown in Fig. 84. Zircaloy-2 and titanium 75A specimens exhibited negligible or near-negligible attack after 176 hr in the 5 *m* uranyl sulfate solution at 300°C. Very thin, adherent, and lustrous films developed on the specimens during this period, and the surfaces were completely free from any pitting corrosion.

At the completion of each run and after cooling to room temperature, an extremely hard layer of solid material was found in the bottom of the autoclave. This material was removed by chipping and was partially redissolved, with great difficulty, in a small quantity of hot water. An analysis was run for uranium and sulfate contents on both the solid material and the solution above the solids after a test run of 52 hr. The results appear in Table 26. The liquid has been resubmitted for analysis because a SO_4/U ratio of 0.912 is not compatible with a pH of 0.7, or with any previous experience.

TABLE 25. CORROSION OF VARIOUS METALS AT 300°C IN OXYGENATED 5 *m* URANYL SULFATE SOLUTION

Test No.	Material	Specimen Area (sq cm)	Specimen Position	Total Time (hr)	Weight Loss (mg/sq cm)		Corrosion Rate (mpy)	Estimated Metal Loss (mils)	Specimen Appearance under 30X and 300X Magnification
					As-removed	Defilmed			
2544-6	Type 347 stainless steel	14.5	Solution	24	0.46	2.28	41.2	0.11	Dull light-gray color; uniform attack; no pits*
2544-5	Type 347 stainless steel	15.5	Solution	28	0.55	2.53	22.9	0.13	Dull light-gray color; uniform attack; no pits*
2544-4	Type 347 stainless steel	15.9	Solution	100	+0.02	1.58	6.9	0.08	Dull light-gray color; uniform attack; no pits*
2544-3	Type 347 stainless steel	15.5	Solution	200	+0.08	1.86	4.0	0.09	Dull light-gray color; uniform attack no pits*
2544-2	Type 347 stainless steel	15.9	Solution	200	0.28				Bulky, gray-black corrosion film; no pits
2544-1	Type 347 stainless steel	15.9	Solution	200	0.20				Bulky, gray-black corrosion film; no pits
2544-14	Type 347 stainless steel	15.2	Water line	24	0.02	0.74	13.5	0.04	Light-gray color; slight surface roughening at water line*
2544-11	Type 347 stainless steel	15.4	Water line	100	0.57	1.84	8.0	0.09	Light-gray color; heavily roughened at water line; shallow pits*
2544-9	Type 347 stainless steel	14.6	Water line	200	0.57				Dull-black mottled film; definite water-line attack
2544-7	Type 347 stainless steel	15.2	Water line	200	0.74				Dull-black mottled film; definite water-line attack
2544-19	Type 347 stainless steel	56.5	Water line	176	0.37				Severe water-line attack; 4- to 7-mil heavy pitting
2544-20	Type 347 stainless steel	56.3	Water line	176	1.05				Severe water-line attack; 4- to 7-mil heavy pitting
2544-13	Type 347 stainless steel	15.6	Vapor	24	0.00	0.66	12.0	0.03	Lustrous light-gray color; unfiorm attack*
2544-12	Type 347 stainless steel	14.8	Vapor	100	+0.13	0.43	1.9	0.02	Semilustrous light-gray color; uniform attack*
2544-10	Type 347 stainless steel	14.3	Vapor	200	0.02				Semilustrous thin film; interference colors; no pits
2544-8	Type 347 stainless steel	15.1	Vapor	200	0.00				Semilustrous thin film; interference colors; no pits
2544-15	Titanium, Ti-75A	6.2	Solution	176	0.05				Lustrous blue and golden-brown film; no pits
2544-16	Titanium, Ti-75A	6.2	Solution	176	0.05				Lustrous blue and golden-brown film; no pits
2544-17	Zircaloy-2	4.8	Solution	176	0.00				Lustrous purple-gray thin film; no pits
2544-18	Zircaloy-2	4.8	Solution	176	0.00				Lustrous purple-gray thin film; no pits

*Specimens examined microscopically after removal of corrosion film.

Examination for Iodide in the Vapor Condensate from an Iodide-Containing 0.17 *m* Uranyl Sulfate Solution at 250°C

E. L. Compere J. L. English

An 800-ml volume of an oxygenated 0.17 *m* uranyl sulfate solution containing an added total iodide content of 23 μg/ml (as KI) was heated to 250°C in a newly machined type 347 stainless steel autoclave and allowed to remain at this temperature for 1 hr. The solution was initially pressurized with 150 psig of oxygen at room temperature. After 1 hr at 250°C, a ¼-in.-OD stainless steel line exiting from the vapor phase above the solution was opened slightly by means of a needle-point valve, and the escaping vapors were condensed in a coil-type, water-cooled condenser.

Fig. 84. Water-Line Corrosion on Type 347 Stainless Steel After 100 hr at 300°C in Oxygenated 5.0 *m* Uranyl Sulfate Solution. (Test 2544-20.) 10X. Reduced 30%.

After a 14-ml volume of the condensate was collected, the valve was closed and the uranyl sulfate solution was cooled to room temperature. A starch test on a few milliliters of the vapor condensate immediately confirmed, by the formation of the characteristic blue starch-iodine color, the existence of free iodine in the presence of a soluble iodide ion. Chemical analysis showed 154 μg of total iodine per milliliter, including 112 μg of iodine per milliliter, and thus, by difference, 42 μg of free iodine per milliliter. The final iodide-plus-iodine content in the 0.17 *m* uranyl sulfate solution after cooling to room temperature was 27 μg/ml.

No corrosion specimens were included in the test. However, at the completion of the run, a ring of dark-brown, crystalline-appearing corrosion products was observed on the wall of the stainless steel autoclave. The products were located predominantly in the region of the solution-vapor interface. Qualitative chemical tests for the detection of iodide and/or iodine in the residue produced negligible results. A spectrographic analysis showed the corrosion products to be of the following composition in weight per cent: Fe, >10; Cr, 5; Ni, 2; Si, 0.5; Nb, 0.1; and Mn, 0.05.

TABLE 26. CHEMICAL ANALYSIS OF SOLID AND LIQUID PHASES RESULTING FROM COOLING A 5 *m* URANYL SULFATE SOLUTION AFTER 52 hr AT 300°C

	Solid (mg/g)		Liquid (mg/ml)	
	(1)	(2)	(1)	(2)
Uranium	578.8	577.3	474.0	476.9
Sulfate	233.8	241.8	175.3	174.6
Water	103.0			
Solution pH			0.7	
SO_4/U			0.912	
Av empirical formula,* $(UO_2)_{1.00}(SO_4)_{1.02}(H_2O)_{2.35}$				

*Except for water content and difficult solubility, the solid appears to be the uranyl sulfate trihydrate expected from the phase diagram.

Since this preliminary experiment has definitely confirmed the presence of iodine and iodide in condensate removed from the vapor phase above an iodide-containing uranyl sulfate solution at 250°C, a static-corrosion-test program will be undertaken to determine the corrosivity of such a vapor phase toward reactor-construction materials.

Results of Tests with Boiling 65% Nitric Acid and Types 304L and 347 Stainless Steel Tubing and Plate

J. L. English

Six samples of types 304L and 347 stainless steel tubing and plate were subjected to the boiling 65% nitric acid test (Huey test) as recommended in ASTM designation A 262-52T.[17] The Huey test has been found to be a very useful method for determining the quality of corrosion-resistant steels, especially with regard to the susceptibility of the steels to intergranular corrosion attack as affected by heat treatment. The data obtained from such a test, however, should not be used to predict the corrosion behavior of a particular alloy in a corrosion environment other than that specified by the test.

The Huey test consists of the exposure of suitably prepared specimens in boiling 65 ± 0.2 wt % nitric acid for five consecutive 48-hr periods. Fresh nitric acid solution is used for each of the 48-hr periods. The maximum permissible corrosion rates for various stainless steel alloys have tentatively been established as follows (rates are for each 48-hr period):

Type of Stainless Steel	Corrosion Rate (mils/month)
304 and 316[18]	1.5
304 (after 1 hr at 1250°F)[18]	2.0
347 (sensitized)[19]	2.0

Materials which meet the above specifications for each 48-hr period are classed as acceptable; those which do not meet these specifications are rejected.

The present investigation was limited to stainless steel alloys which were used or were considered for use in the fabrication of HRT components. The alloys were procured from three industrial fabricators or from producers of stainless steel tubing and plate. Five of the six materials were seamless or welded $\frac{5}{8}$-in. tubing, and one material was $\frac{1}{4}$-in.-thick plate. The products supplied by each of the three sources were as follows:

Source	Type of Stainless Steel
1	(a) 304L welded tubing (b) 347 welded tubing
2	(a) 304L welded tubing (b) 347 welded tubing (c) 347 seamless tubing
3	(a) 347 plate

The chemical compositions of the stainless steel alloys are reported in Table 27. The results of analyses performed at ORNL under the supervision of W. F. Vaughn of the Analytical Chemistry Division are compared with chemical analyses submitted by the vendor when such analyses were available. Two major discrepancies were noted in this comparison: a type 304L stainless steel welded tubing was found by laboratory analysis to be straight type 304 stainless steel, and a type 347 stabilized grade of seamless stainless steel tubing was found by laboratory analysis to be a nonstabilized grade (insufficient niobium).

The results of the boiling nitric acid tests are included in Table 28. Each type of material was tested in four conditions as follows: as-received, sensitized 1 hr in air at 1200°F, annealed 0.5 hr in air at 1950°F, and annealed and sensitized as described in 2 and 3. All specimens, including those in the as-received condition, were tested with pickled surfaces. A pickling operation was found to be necessary to remove the scale formed during the various heat treatments. The pickling treatment consisted of 10 to 20 min of immersion in 1:1 HCl at 65 to 70°C and 3 to 5 min of immersion in 20% HNO_3–3% HF (by weight) solution at 60 to 65°C. After the pickling treatment, the specimens were rinsed in a dilute alkaline solution, rinsed in water, vapor degreased in benzene, dried, and weighed to the nearest 0.2 mg.

Photographs were taken of all specimens at a magnification of 200X after the first, second, third, and fifth 48-hr exposure periods. At completion of the fifth period, the specimens were submitted for a complete metallographic examination.

[17] Report of Subcommittee IV on Methods of Corrosion Testing, *Am. Soc. Testing Materials, Proc.* 33, Part I, 187 (1933).

[18] M. A. Streicher, *ASTM Bull.* No. 195, 64 (Jan. 1954).

[19] F. L. La Que, in *Symposium on Evaluation Tests for Stainless Steels*, ASTM Special Technical Publication No. 93, p 5, 1950.

TABLE 27. CHEMICAL COMPOSITIONS OF STAINLESS STEEL TUBING TESTED IN BOILING 65% NITRIC ACID

Stainless Steel Type	Source	Material Form	Analyzed by	Analysis (%)						
				Cr	Ni	C	Mn	Si	Fe	Other Elements
304L	1	Welded	Vendor							
304L*	1	Welded	ORNL	18.2	9.0	0.07	0.64	0.64	Balance	
304L	2	Welded	Vendor	19.0	10.0	0.03	1.03	0.56	Balance	Cu, 0.23
304L	2	Welded	ORNL	19.1	9.5	0.02	0.88	0.60	Balance	
347	1	Welded	Vendor							
347	1	Welded	ORNL	18.1	11.2	0.07	1.05		Balance	Nb, 0.88
347	2	Welded	Vendor	18.6	10.4	0.06	1.58	0.53	Balance	Nb, 0.71; Ta, 0.1
347	2	Welded	ORNL	18.4	11.0	0.07	0.93		Balance	Nb, 0.79
347	2	Seamless	Vendor	18.6	12.6	0.06	1.79	0.40	Balance	Nb and Ta, 0.91
347**	2	Seamless	ORNL	17.6	12.0	0.07	1.03		Balance	Nb, 0.02
347	3	Plate	Vendor	18.0	10.5	0.06	1.26	0.54	Balance	Nb, 0.74

*ORNL analytical results show this material to be straight type 304 stainless steel rather than an extra-low carbon grade. Five carbon determinations resulted in values of 0.074, 0.073, 0.075, 0.072, and 0.076%.

**ORNL analyses show an unstabilized grade of stainless steel.

The two preliminary conclusions that may be drawn from the data in Table 28 are as follows: (1) In the absence of a chemical analysis, the Huey test will quickly distinguish extra-low carbon and stabilized grades of stainless steel from straight or nonstabilized grades (based on results after a sensitization treatment). (2) Extra-low carbon and stabilized grades of stainless steels may not respond in the expected manner to certain heat treatments and therefore may not behave properly in the boiling nitric acid test. A complete report will be issued at a later date on the results of this investigation.

Corrosion of Zircaloy-2 in Water and Steam at Elevated Temperatures

J. L. English

Several attempts were made to effect the disintegration of crystal-bar zirconium and Zircaloy-2 in high-temperature water containing nitrogen and in superheated steam enriched with nitrogen gas. It has been reported that nitrogen in high-temperature water or superheated steam causes a rapid acceleration in the corrosion of crystal-bar zirconium.[20]

Tests were conducted at 315°C (600°F) and at 400°C (750°F), and the distilled water had the composition, resistivity, and pH listed below.

Resistivity at room temperature, ohm-cm	520,000
Copper, ppm	<0.1
Chloride, ppm	0.1
Iron, ppm	<0.1
Fluoride, ppm	<0.1
Sulfate, ppm	20
pH	5.3

The tests at 315°C were run in distilled water in a stainless steel autoclave. The sealed system was pressurized with 150 psig of nitrogen at room temperature. The dissolved nitrogen in the water at 315°C was estimated to be between 650 and 850 ppm.[21]

The test at 400°C was run by passing water vapor, saturated with nitrogen gas, into a tube furnace controlled at 400 ± 10°C. The temperature control was obtained by means of a thermocouple inserted in the furnace and located in the immediate proximity of the zirconium specimen.

The crystal-bar zirconium specimen was machined from 0.63-cm-dia bar. The final size was 0.5 cm in diameter by 3.5 cm long for an apparent surface

[20] J. Chirigos and D. E. Thomas, *The Mechanism of Oxidation and Corrosion of Zirconium*, WAPD-53 (April 11, 1952), p 19.

[21] H. A. Pray, C. E. Schweickert, and B. H. Minnich, *The Solubility of Hydrogen, Oxygen, Nitrogen, and Helium in Water at Elevated Temperatures*, BMI-T-25 (May 15, 1950).

TABLE 28. RESULTS OF BOILING 65% NITRIC ACID TESTS ON TYPES 304L AND 347 STAINLESS STEEL TUBING AND PLATE

Test No.	Type of Stainless Steel	Source	Form	Material* Condition	Specimen Area (sq cm)	Corrosion Rate Per 48-hr Period (mils/month)					Average Corrosion Rate Over Five Periods (mils/month)
						First Period	Second Period	Third Period	Fourth Period	Fifth Period	
756-5	304L**	1	Welded tubing	AR	12.1	1.6	1.6	1.3	1.3	1.3	1.4
756-6	304L	1	Welded tubing	AR-S	13.4	26.7	58.5	48.2			44.5 (3 periods)
756-7	304L	1	Welded tubing	AR-A	13.4	1.2	1.1	1.0	1.1	1.1	1.1
756-8	304L	1	Welded tubing	AR-A-S	13.4	3.2	5.5	14.7	59.7		20.8 (4 periods)
756-21	304L	2	Welded tubing	AR	13.4	0.7	0.6	0.7	0.7	0.8	0.7
756-22	304L	2	Welded tubing	AR-S	13.4	2.2	2.6	2.8	3.4	3.8	3.0
756-23	304L	2	Welded tubing	AR-A	13.4	1.0	0.7	0.6	0.6	0.6	0.7
756-24	304L	2	Welded tubing	AR-A-S	13.4	0.8	0.8	0.8	0.9	0.9	0.8
756-1	347	2	Welded tubing	AR	13.4	0.9	1.0	1.0	1.0	1.0	1.0
756-2	347	2	Welded tubing	AR-S	13.4	5.2	4.8	4.3	4.2	4.0	4.5
756-3	347	2	Welded tubing	AR-A	13.4	0.7	0.7	0.6	0.7	0.9	0.7
756-4	347	2	Welded tubing	AR-A-S	13.4	1.2	1.7	1.9	2.0	2.1	1.8
756-9	347***	2	Seamless tubing	AR	13.4	1.0	1.3	1.4	1.5	1.6	1.4
756-10	347	2	Seamless tubing	AR-S	13.4	43.5	64.1	62.8			56.8 (3 periods)
756-11	347	2	Seamless tubing	AR-A	13.4	1.2	1.2	1.2	1.2	1.3	1.2
756-12	347	2	Seamless tubing	AR-A-S	13.4	34.0	154.4				94.2 (2 periods)
756-13	347	3	Plate	AR	17.9	0.5	0.6	0.7	0.7	0.8	0.7
756-14	347	3	Plate	AR	17.9	0.5	0.5	0.6	0.7	0.7	0.6
756-15	347	3	Plate	AR-S	17.9	1.1	1.0	0.9	1.3	1.6	1.2
756-16	347	3	Plate	AR-S	17.9	1.2	1.2	1.0	1.4	1.8	1.3
756-17	347	3	Plate	AR-A	17.9	3.4	2.9	2.2	2.6	2.5	2.7
756-18	347	3	Plate	AR-A	17.9	3.1	2.6	2.2	2.4	2.4	2.5
756-19	347	3	Plate	AR-A-S	17.9	0.8	0.9	0.8	0.8	0.8	0.8
756-20	347	3	Plate	AR-A-S	17.9	0.8	0.8	0.8	0.9	0.9	0.8
756-25	347	1	Welded tubing	AR	13.4	1.6	1.6	1.3	1.2	1.1	1.4
756-26	347	1	Welded tubing	AR-S	13.4	8.6	9.2	6.2	5.4	4.7	6.8
756-27	347	1	Welded tubing	AR-A	13.4	0.7	0.6	0.6	0.7	0.6	0.6
756-28	347	1	Welded tubing	AR-A-S	13.4	2.0	2.3	2.3	2.6	2.4	2.3

*Material conditions were as follows: AR, as-received condition; AR-S, as-received, sensitized for 1 hr in air at 1200°F, air-cooled, and pickled; AR-A, as-received, annealed for 0.5 hr in air at 1950°F, air-cooled, and pickled; AR-A-S, as-received, annealed and sensitized (as above), and pickled.
**Laboratory analyses show this material to be a straight type 304 grade stainless steel (Table 27).
***Laboratory analyses show that this material was not stabilized (Table 27).

area of 7.2 sq cm. The Zircaloy-2 specimens, containing 1.1% Sn, 0.2% Fe, 0.03% Cr, 0.04% Ni, and 0.01% C, were machined from annealed 0.55-cm-dia bar. The final size was 0.5 cm in diameter by 2.5 cm long for an apparent surface area of 4.7 sq cm. The corrosion data are given in Table 29. At the completion of the tests, the specimens exhibited lustrous, purple-gray, thin films, and there were no indications of destructive corrosion attack.

Small-Scale Dynamic-Corrosion Program

E. L. Compere G. E. Moore

DeRieux-McWherter Toroid Rotator I. This rotator has been described previously;[22] it is capable of rotating twenty 6-in.-dia toroids so that the bulk fluid flow is from 0 to 25 fps. The toroids themselves have been fabricated from $\frac{3}{8}$-in. pipe of type 347 stainless steel. Commercially available, $\frac{1}{4}$-in., type 347 stainless steel, Parker tubing fittings have been welded to the toroids in such a manner as to provide means of inserting sample pins into the circulating solution. By this method, corrosion pin specimens may be exposed to the circulating solution and can be removed or replaced at will. The toroid itself, of course, may be sectioned for inspection. By using high-speed photography and a Lucite toroid about half-filled with liquid, it has been shown that the liquid circulates within the toroid as a slug, and so the sample pins are alternately exposed to liquid and vapor phases. Four sample pins symmetrically arranged about each toroid seem to be satisfactory.

This rotator has been completed and has shown satisfactory performance, as previously reported.[23] Before actual tests may be undertaken, the furnace for heating the toroids must be fabricated; this is currently being done in the machine shop. The rotator has been used, however, during parts of the quarter to circulate slurries at room temperature.

This program has not been emphasized because of demands of other higher priority programs, including the In-Pile Loop Program.

Toroid Rotator II. The toroid rotator II is the small experimental model designed chiefly by R. A. Lorenz and patterned basically after the NACA toroid-circulating apparatus.[24] The rotator is capable of rotating up to four toroids at liquid velocities of at least 20 fps. It is thought that it may be able to circulate liquid at velocities of 40 fps by using only two toroids.

The toroids are wrapped with resistance wire and insulated so that the temperature may be controlled while the apparatus is in operation.

During the past few months, a series of runs has been carried out in which four toroids of type 347 stainless steel and containing corrosion-pin specimens of the same material were used. The solution was adjusted in each case to contain 0.17 *m* uranyl sulfate after the addition of the quantity of hydrogen peroxide calculated to yield 430 psi of oxygen at 250°C. These runs were at 20 fps bulk-liquid velocity.

Weight losses of the pin specimens from the earlier runs had appeared to be erratic.[23] This erratic behavior now appears to have been due to a very low oxygen pressure that was caused by use of a practically completely decomposed hydrogen peroxide solution as the source of oxygen. Four subsequent runs in which freshly standardized hydrogen peroxide was used have provided more consistent data. These runs gave periods of operation of 128, 304, 219, and 367 hr, respectively, with two single-pin and two four-pin toroids being used each time. Only the 219-hr run was conducted

[22] W. L. DeRieux and J. R. McWherter, *HRP Quar. Prog. Rep. March 31, 1953*, ORNL-1554, p 65.

[23] G. E. Moore, *HRP Quar. Prog. Rep. Jan. 31, 1954*, ORNL-1678, p 63.

[24] L. G. Desmon and D. R. Mosher, *Preliminary Study of Circulation in an Apparatus Suitable for Determining Corrosive Effects in Hot Flowing Liquids*, NACA RM E51D12 (June 1951).

TABLE 29. CORROSION OF CRYSTAL-BAR ZIRCONIUM AND ZIRCALOY-2 IN WATER AND STEAM AT ELEVATED TEMPERATURES

Material	Area (sq cm)	Medium	Temperature (°C)	Nitrogen Content (ppm)	Time (hr)	Weight Change (mg/sq cm)
Crystal-bar zirconium	7.2	Water	315	650 to 850	17	+0.1
Zircaloy-2	4.7	Water	315	650 to 850	14	+0.2
Zircaloy-2	4.5	Steam	400	Saturated	24	+0.1

continuously without equipment shutdown. However, shutdowns did not appear to have any significant effect. The results of these four runs are plotted in Fig. 85.

The average corrosion rate in the single-pin toroids was 660 mg/sq dm·day (5.5 mg/sq dm·day corresponds to 1 mpy). This may be compared with the average bare-metal corrosion rate of 1400 mg/sq dm·day observed under corresponding conditions (except at higher velocities) in the large-scale dynamic loop experiments. Apparently in the single-pin toroids the critical velocity above which bare-metal corrosion occurs and no protective film exists is exceeded at 20 fps. There appears to be some effect of turbulence or slug flow, since the four-pin toroids give lower values of 320 mg/sq dm·day at the same velocity. The consistency of values under each set of conditions appears to be adequate, as may be seen from Fig. 85. The correlation of loop and toroid conditions producing similar corrosion results will be developed. Liquid velocity, number of pins, and other conditions affecting turbulence appear to be important.

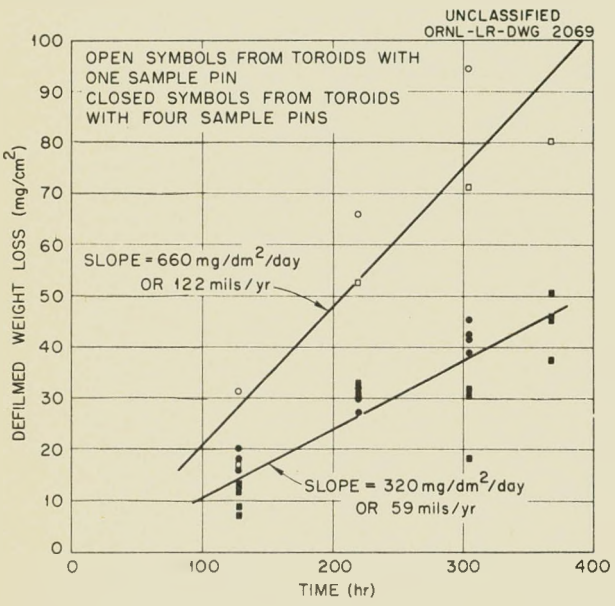

Fig. 85. Weight-Loss Data of Type 347 Stainless Steel Corrosion Pins in Toroid Experiments (40 g of Uranium per Kilogram of H_2O as UO_2SO_4; 250°C; 430 psi Oxygen Pressure at 250°C; Flow Velocity, 20 fps).

The toroids themselves, of course, undergo corrosion, as well as do the sample pins. The amount of corrosion of the toroid can be estimated from the amount of nickel present in the solution at the end of the experiment minus that due to the corrosion of the sample pins. The alloy contained 10.42 wt % nickel by analysis. The results of these calculations are given in Table 30. Since these toroids had all been operated previously with oxygenated uranyl sulfate solution at 250°C, even the first values shown in Table 30 represent a pretreated surface. These data show that the nickel pickup from the toroid walls decreased with time of operation, although a constant value was possibly being obtained at the longer operating times. The values range between 0.2 to 5.3 mg/sq dm·day for the single-pin toroids and 0.5 to 17 mg/sq dm·day for the four-pin toroids. These values are considerably less than those determined from the pin data (660 mg/sq dm·day for the single-pin and 320 mg/sq dm·day for the four-pin toroids). They probably indicate the presence of a protective film on the toroid walls.

TABLE 30. CALCULATED CORROSION RATES FOR TOROIDS BASED ON NICKEL ANALYSES

Run No.	Cumulative Operating Time (hr)	Calculated Weight Loss of Toroid (mg/sq dm·day)				Time Per Run (hr)	Estimated Corrosion Rate of Toroid (mg/sq dm·day)			
		Single-Pin Toroid		Four-Pin Toroid			Single-Pin Toroid		Four-Pin Toroid	
		A	B	A	B		A	B	A	B
1	128	28	28	52	89	128	5.3	5.3	9.7	17
2	432	38	7.1	10	52	304	3.0	0.6	0.8	4.1
3	651	7.1	2.6	4.6	6.6	219	0.8	0.3	0.5	0.7
4	1018	2.6	8.7		12.2	367	0.2	0.6		0.8

As stated earlier, the four-pin toroids appear to give lower pin corrosion rates than do the single-pin toroids. The reason for this effect is unknown, but it is to be investigated. Possible causes for the lower corrosion rates may be differences in surface-to-volume ratio or depletion of the solution; however, these causes do not seem to be very likely, since the corrosion rate appears to be independent of time. The reason may possibly be due to different degrees of turbulence in the two systems.

The results obtained so far certainly show the need for additional experiments, particularly to clarify the effect of the number of pins and of the velocity on the corrosion rates. These experiments are necessary before any correlation with dynamic loop results can be attempted, and they are scheduled next for investigation.

Three all-titanium toroids are being fabricated. They will probably be used with more concentrated or more acid solutions of uranyl sulfate in order to approximate better the conditions anticipated for the HRT blanket and other reactor systems.

Vapor-Phase Tests: Effect of Carbon Dioxide and of Chloride Ion on Type 347 Stainless Steel at 100°C

E. L. Compere G. E. Moore

Certain experiments by G. H. Jenks in connection with the In-Pile Loop Program had suggested the possibility that carbon dioxide (produced by oxidation of Graphitar No. 14 bearings) might cause increased vapor-phase attack on type 347 stainless steel over a 0.17 *m* solution of uranyl sulfate at 100°C. This possibility was investigated further by setting up static experiments in which duplicate type 347 stainless steel samples were exposed to the solution as well as to the vapor phase. The effect of cupric ion in solution was also studied.

Negligible corrosion in either phase occurred under these conditions during a 35-day test period. The presence of carbon dioxide and cupric ion had no apparent effect. Chloride ion at a concentration of 10 ppm for three weeks and then at 20 ppm for three weeks also showed negligible effect.

In all experiments the amount of standard hydrogen peroxide added was calculated to yield about 300 psi of oxygen pressure at 100°C. The bombs were first heated at 250°C and kept at that temperature for 1 to 2 hr in order to decompose the uranyl peroxide. The bombs were then transferred to an oven controlled at 100°C for the remainder of the test.

Originally, an approximately 0.17 *m* solution of uranyl sulfate was divided into two parts: one that was not treated further and another that was made about 0.01 *m* in cupric ion by the addition of copper sulfate. These two solutions provided the uranyl sulfate for the runs.

In those experiments in which carbon dioxide was to be present, the calculated weight of dry ice was added to the bomb just before sealing; this weight was such as to yield a calculated 100-psi carbon dioxide pressure at 100°C.

The specimens were examined after one week and again after an additional four weeks; a fresh solu- was used after each inspection. In general the vapor-phase specimens showed interference colors, while the solution-phase samples remained unchanged after the five weeks of exposure. No specimens in either phase showed visible attack, and only negligible weight changes were observed. These data are summarized in Table 31. Analytical results obtained on the solutions are also included.

The effect of chloride ion under these conditions was also investigated by the addition of nickelous chloride to each solution. An exposure of three weeks at about 10-ppm chloride and another three weeks at about 20-ppm chloride produced little apparent change in the vapor-phase specimens. The former conditions somewhat dulled the surface of the solution-phase specimens, whereas the three-weeks exposure to 20-ppm chloride darkened them considerably more. No measurable attack on the metal was observed, however. These data are also summarized in Table 31.

Hydrogen in Metals

E. L. Compere W. O. Harms
G. E. Moore

The behavior of titanium and other metals in a system containing atomic hydrogen is being considered with respect to hydride formation, embrittlement, and atomic hydrogen diffusion. Atomic hydrogen may be produced by corrosion or by decomposition of an aqueous solution.

The experimental apparatus was patterned after the one devised by Marsh.[25] In Marsh's apparatus, a cell of suitable metal-wall thickness and surface-to-volume ratio was connected to a pressure gage. Substantial pressure increases occurred on immersing the cell in suitable media, and these increases

[25] G. A. Marsh, *Corrosion* 10, 101 (1954).

TABLE 31. EFFECT OF CARBON DIOXIDE AND CHLORIDE AND COPPER IONS ON VAPOR- AND LIQUID-PHASE CORROSION OF TYPE 347 STAINLESS STEEL IN OXYGENATED URANYL SULFATE (34 g of uranium per kilogram of H_2O) AT 100°C

Experiment No.	Nominal CO_2 Pressure (psi)	Nominal Cu Concentration (m)	Coupon Weight Loss (mg/sq dm)		Analysis*				
			Vapor	Liquid	U (g/liter)	pH	Ni (ppm)	Cl (ppm)	Cu (mg/liter)
Nominal Chloride Concentration, 0 ppm									
After 7 days									
1	0	0	+0.7, +3.7	5.0, 3.8	34.22	2.50	28.0	1.1	
2	100	0	4.4, 0.7	3.7, 4.5	34.02	2.50	1.9	2.2	
3	0	0.01	2.7, +1.9	2.1, 5.3	33.51	2.50	8.8	1.7	530
4	100	0.01	0.0, 1.4	3.9, 5.6	35.07	2.50	4.9	1.3	560
After 35 days									
1	0	0	0.0, 1.2	2.8, 0.0	33.37	2.53	10.1	3.3	
2	100	0	2.9, 2.0	1.9, 1.3	32.29	2.53	0.8	6.8	
3	0	0.01	+0.7, 4.4	4.1, 2.6	34.04	2.49	0.6	2.3	510
4	100	0.01	0.0, 2.1	3.9, 0.2	34.22	2.45	2.1	2.4	540
Nominal Chloride Concentration, 10 ppm									
After 7 days									
1	0	0	0.7, 1.2	+1.4, 0.8	34.72	2.53	15.4	10.3	
2	100	0	+0.7, 0.0	3.7, 4.5	34.54	2.53	10.4	10.5	
3	0	0.01	0.7, +2.5	0.0, 0.7	37.64	2.47	12.1	9.8	580
4	100	0.01	2.1, 2.8	1.6, 0.2	37.71	2.50	17.0	9.6	460
After 21 days									
1	0	0	+1.4, +0.6	0.0, +1.5	33.86	1.95	9.3	11	
2	100	0	+2.2, +2.0	0.6, 0.0	33.82	2.15	9.7	10	
3	0	0.01	1.4, 0.6	4.1, 1.3	33.45	1.82	12.5	9	530
4	100	0.01	1.4, 0.0	3.9, 0.4	37.20	1.80	9.5	9	510
Nominal Chloride Concentration, 20 ppm									
After 7 days									
1	0	0	1.4, 0.0	0.0, 1.5	33.80	2.43	20.3	19	
2	100	0	1.5, 2.7	+0.6, 1.3	33.90	2.50	13.7	19	
3	0	0.01	0.7, 3.8	0.0, +0.7	34.81	2.52	5.6	19	520
4	100	0.01	+1.4, +0.7	3.1, +0.7	34.97	2.56	2.8	20	550
After 21 days									
1	0	0	0.0, +0.6	+1.4, +0.8	33.55	2.59	57.7	20	
2	100	0	3.7, 1.4	6.2, 3.9	33.45	2.50	22.0	21	
3	0	0.01	+2.7, +1.9	+1.4, 0.0	34.00	2.60	37.1	22	420
4	100	0.01	+1.4, +1.4	+0.8, +0.7	34.24	2.63	27.4	25	430

*Analysis after each test period. Solution renewed for each test period.

were interpreted as being the result of atomic hydrogen passing through the metal wall. For the present experiments, an approximately 1-in.-dia bar of cold-rolled carbon steel was chosen as the material for investigation. A 6-in. length of the bar was drilled lengthwise to provide a hole $\frac{5}{8}$ in. in diameter and about 5 in. deep. The thickness of the outside wall was therefore about $\frac{3}{16}$ in. Another length of the bar was machined to yield about a $\frac{5}{8}$-in.-dia rod which just fitted snugly into the drilled-out length and thus provided a practically volumeless crack between the two pieces of bar stock. A cap to which a pressure gage had been fitted by threading and soft soldering was then silver soldered to the cell. The upper portion of the cell was coated with paraffin to protect the silver-soldered joint and the pressure gage from the solution, even though the cell was immersed only 5 in. in the solution. An external area of about 106 sq cm (16.5 sq in.) was exposed to the solution.

No pressure buildup was observed with this apparatus during a three-day exposure to 2.4% hydrochloric acid at about 25°C. Since the rate of diffusion may be inversely proportional to the square of the thickness of metal, $\frac{1}{16}$ in. was removed from the diameter of the cell without it having to be disassembled; this produced a wall of approximately $\frac{5}{32}$-in. thickness. Again, no detectable buildup of pressure was observed during a four-day exposure to 2.4% hydrochloric acid at room temperature. At this time, the original pressure gage (3000-psi maximum) was replaced by a more sensitive one (300-psi maximum), and the experiment was continued. On the seventh day following this change, a pressure of 5 psig was observed, which continued to increase to 62 psig on the fifteenth day.

These results appear to be considerably different from those obtained by Marsh, who found a pressure buildup of 1000 psi in nine days with an induction period of only 1 hr. However, the results should be compared on the basis of volume of hydrogen diffused, for which sufficient, accurate data are not available. The induction period is probably the the time required to saturate the outer metal cylinder, and it would be expected to vary with the condition of the metal. Several other factors also probably contribute to the observed difference, such as differences in wall thickness and in material.

Somewhat similar experiments in which titanium cells are to be used will be undertaken as soon as the method has been adequately tested. Type 347 stainless steel, and probably also zirconium, will be studied.

The purpose of these experiments is to investigate the permeability to atomic hydrogen of metals of interest in reactor construction. A number of investigators[26,27,28] believe that atomic hydrogen may diffuse through substantial thicknesses of metal. When hydrogen atoms encounter imperfections in the metal lattice, they combine to form molecular hydrogen, whose diffusion rate is negligible compared with that of atomic hydrogen. Thus this entrapped hydrogen may build up to considerable pressure and cause blistering of the metal.[29]

The diffusion of atomic hydrogen through metals does not always take place under the conditions just described. This may be the case for titanium and zirconium, since these metals have known tendencies towards hydride formation.[30] In this event, metallographic examination may possibly reveal a hydride phase.

---

[26] L. S. Darken and R. P. Smith, *Corrosion* 5, 1 (1949).

[27] T. Skei, A. Wachter, W. A. Bonner, and H. D. Burnham, *Corrosion* 9, 163 (1953).

[28] D. P. Smith, *Hydrogen in Metals*, University of Chicago Press, Chicago, 1948.

[29] M. H. Bartz and C. E. Rawlins, *Petroleum Processing* 4, 898 (1949).

[30] D. T. Hurd, *An Introduction to the Chemistry of the Hydrides*, p 181, John Wiley and Sons, New York, 1952.

METALLURGY

E. C. Miller

DYNAMIC CORROSION OF WELDED AUSTENITIC-STAINLESS-STEEL SPECIMENS

W. J. Leonard W. O. Harms

Effects of Composition and Heat Treatment

The dynamic-corrosion resistance in uranyl sulfate solutions of austenitic-stainless-steel welds as affected by different heat treatments, which were described in the previous quarterly report,[1] was studied in more detail.

The ferrite content of the weld metal after various heat treatments for the three compositions studied, as determined by Magne-Gage measurements, is listed in Table 32. It is observed that heat treatments at 1625°F and higher promote solution of the ferrite in types 347 and 308L stainless steel welds and that Composition H welds (nominal 18% Cr, 13% Ni, 5% Mn, columbium stabilized) were fully austenitic in all heat-treated conditions.

Results of dynamic-corrosion tests on the pin specimens are given in Table 33. Film integrity was maintained on all pins which had received the 1000°F stress-relief anneal, while all except two of the 27 pins which had received a solution anneal at 1950°F showed bare-metal attack and high weight losses. Specimens given treatment E (1625°F for 2 hr, water quench, followed by 1000°F for 6 hr, air cool) showed improved corrosion resistance. Other treatments appeared to lessen or, at best, failed to improve the corrosion resistance relative to the as-welded condition except in the case of the type 308L stainless steel, where the as-welded specimens showed very poor resistance to attack.

Metallographic examination indicated no change in as-welded structure after treatment at 1000°F, whether this treatment was given alone or was preceded by heating to 1625°F for 2 hr and water quenching. The difference in microstructure after the stress relief at 1000°F and after the solution anneal at 1950°F is illustrated in Fig. 86. It should be noted that the high-temperature treatment effects an agglomeration and partial solution of the interdendritic network type of structure observed in as-welded specimens and those stress relieved at 1000°F. The microstructures of type 308L stainless steel were similar to those shown in Fig. 86. In all cases, there was no discernible difference between the microstructures of the as-welded specimens and those which were stress-relief annealed at 1000°F.

No definite correlation could be made between ferrite content and corrosion resistance in these studies. For example, type 308L stainless steel weld metal in the as-welded condition, which had poor corrosion resistance, contained a substantial amount of ferrite; in the solution-annealed condition

[1] W. O. Harms and W. J. Leonard, *HRP Quar. Prog. Rep. Jan. 31, 1954*, ORNL-1678, p 74.

TABLE 32. PERCENTAGE OF FERRITE IN AUSTENITIC-STAINLESS-STEEL WELDS AFTER VARIOUS HEAT TREATMENTS

Weld Metal	Heat Treatment						
	A	B	C	D	E	F	G
	As Welded	1000°F, 6 hr, Air Cool	1625°F, 2 hr, Furnace Cool	1625°F, 2 hr, Water Quench	1625°F, 2 hr, Water Quench; 1000°F, 6 hr, Air Cool	1950°F, 0.5 hr, Water Quench	1950°F, 0.5 hr, Furnace Cool
Type 347 stainless steel	8.0	8.0	7.5	7.5	7.4	4.0	3.5
Type 308L stainless steel	10.0	10.0	8.0	8.0	7.0	3.5	3.0
Composition H	0	0	0	0	0	0	0

TABLE 33. RESULTS OF DYNAMIC-CORROSION TESTS OF HEAT-TREATED, WELDED, AUSTENITIC-STAINLESS-STEEL SPECIMENS IN URANYL SULFATE SOLUTION WHICH CONTAINS 40 g OF URANIUM PER LITER FOR 400 hr AT 250°C AND 23 TO 26 fps

Type of Stainless Steel	Heat Treatment						
	A	B	C	D	E	F	G
	Average Defilmed Weight Loss (mg)*						
347, all-coated electrode weld	(4) 56 (0)	(3) 35 (0)	(5) 49 (1)	(4) 83 (1)	(5) 52 (1)	(4) 170 (4)	(3) 61 (0)
347, coated electrode and base metal	(3) 52 (0)	(3) 36 (0)	(4) 104 (2)	(2) 210 (2)	(1) 25 (0)	(3) 131 (2)	(2) 46 (0)
347, heliarc root pass and base metal	(3) 52 (0)	(3) 55 (0)	(2) 94 (1)	(3) 132 (2)	(1) 29 (0)	(2) 140 (2)	(3) 59 (0)
308L, all-coated electrode weld	(4) 146 (3)	(4) 26 (0)	(4) 119 (2)	(3) 102 (1)	(2) 48 (0)	(2) 226 (2)	(3) 73 (1)
308L, coated electrode and base metal	(2) 277 (2)	(2) 28 (0)	(1) 146 (1)	(3) 117 (1)	(2) 36 (0)	(4) 134 (4)	(2) 129 (1)
308L, heliarc root pass and base metal	(3) 86 (2)	(3) 32 (0)	(2) 94 (1)	(3) 76 (1)	(2) 63 (0)	(3) 135 (3)	(2) 128 (2)
Composition H, all-coated electrode weld	(6) 33 (0)	(4) 31 (0)	(3) 93 (1)	(4) 121 (1)	(2) 110 (0)	(3) 150 (3)	(3) 135 (2)
Composition H, coated electrode and base metal	(2) 30 (0)	(3) 46 (0)	(4) 90 (2)	(3) 91 (1)	(2) 114 (1)	(3) 110 (2)	(3) 122 (2)
347, heliarc root pass, diluted by Composition H and base metal	(2) 40 (0)	(2) 34 (0)	(2) 99 (1)	(2) 103 (1)	(2) 125 (1)	(3) 111 (2)	(2) 52 (0)

*The figures in parentheses to the left of the average weight loss indicate the number of specimens tested, and the figures in parentheses to the right of the average weight loss denote the number of specimens from which the oxide film and underlying metal were removed during the test.

the corrosion resistance was equally poor, yet the amount and distribution of the ferrite was vastly different. On stress-relieving the as-welded type 308L stainless steel sample at 1000°F, the corrosion resistance was greatly improved, but the amount and distribution of the ferrite remained the same. On the other hand, as-deposited Composition H weld metal, which contained no ferrite, was superior in corrosion resistance to as-deposited types 347 and 308L stainless steels which contained considerable ferrite and also appeared to remain more corrosion resistant in all the heat-treated conditions.

Corrosion of Special Flat-Plate Types of Specimens

Twenty special flat-plate types of corrosion specimens (see Fig. 87) have been tested in two runs (0.17 *m* uranyl sulfate, 250°C, 20 fps), and weight-loss data are now available for exposures of 200 and 400 hr. These data are given in Table 34.

The specimens in Holder B were 20% thicker than those in Holder A, and, since the holders themselves are identical, the former required a lower volume flow rate in order to produce a comparable mean solution velocity. It is observed that in the 400-hr run, specimens contained in Holder B lost considerably more weight than those in Holder A; there is no ready explanation for this behavior. Actually, the Reynolds number for flow conditions corresponding to those which obtained in Holder A is higher than that for Holder B; so the effect cannot be attributed to increased turbulence, at least as it is defined in terms of Reynolds numbers. Whatever the cause, the effect on specimens in Holder B after 400 hr served nicely to compare the various weld metals and combinations. It was of interest to note, for example, that the specimens containing Composition H welds showed the lowest weight losses among the welded specimens. The zones near weld-pass interfaces in these welds maintained protective oxide films (Fig. 87*a*), while on the intervening portions essentially bare-metal attack had occurred. A small amount of this type of behavior was observed on type 347 stainless steel welds, but type 308L stainless steel showed practically none (see Figs. 87*b* and 87*c*). Specimens were tested in 0.17 *m*

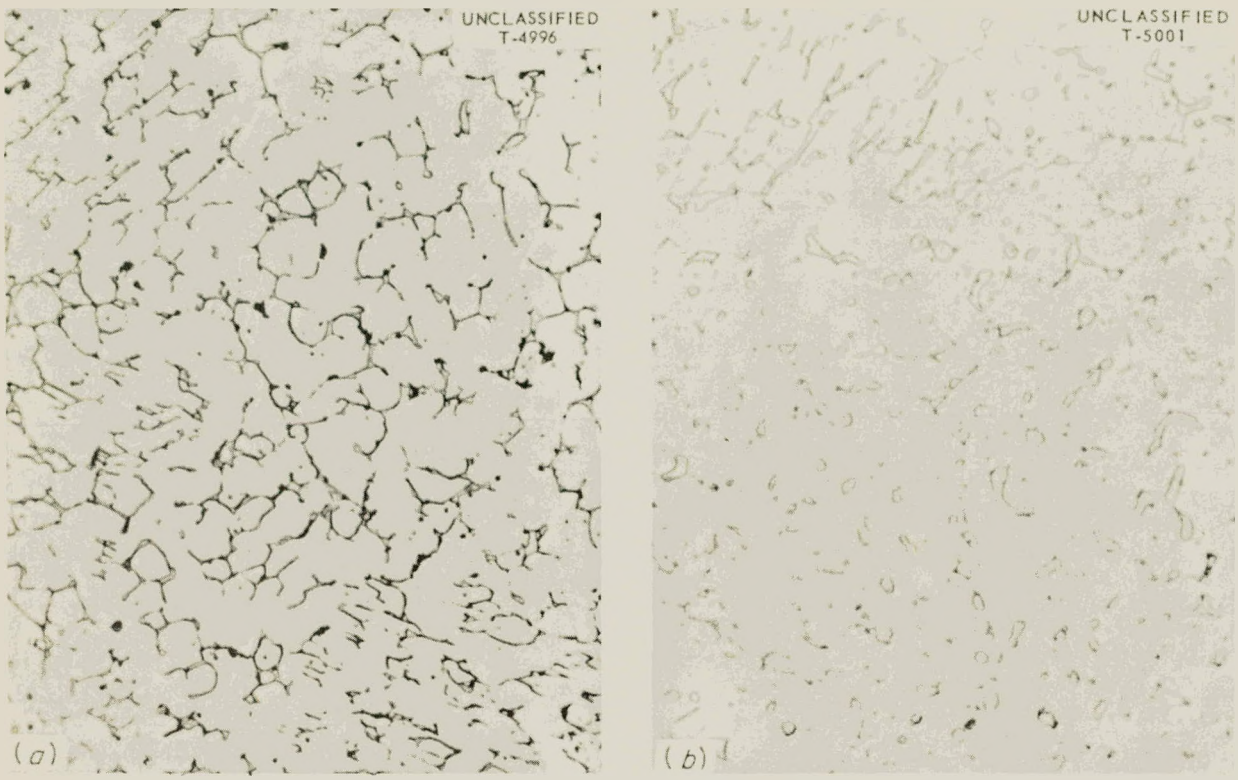

Fig. 86. Effect of Heat Treatment on the Microstructure of Type 347 Stainless Steel Weld Metal. (*a*) As-welded or stress-relieved at 1000°F. (*b*) Annealed at 1950°F for 0.5 hr and water quenched. 750X. Reduced 10%.

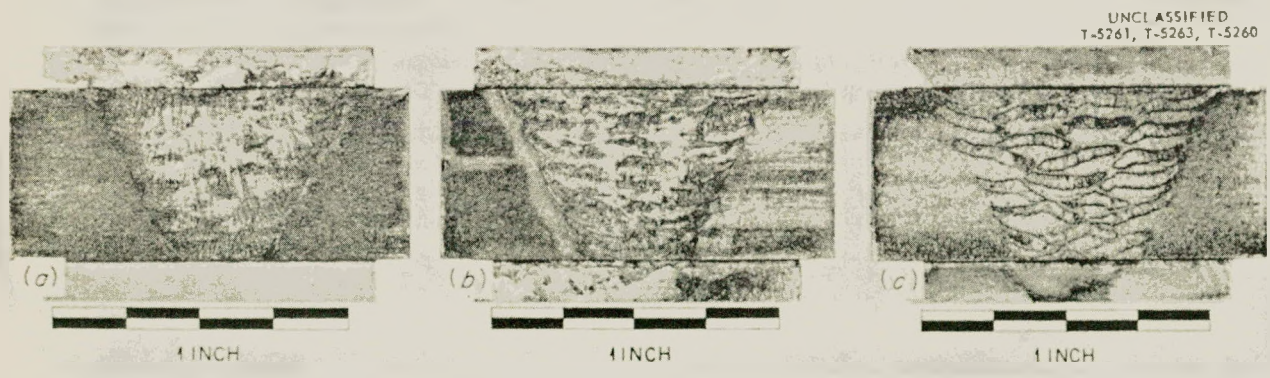

Fig. 87. Special Flat-Plate Welded Austenitic-Stainless-Steel Corrosion Specimens. (*a*) Type 304L joined by Composition H. (*b*) Types 304L (left) and 347 (right) joined by type 347. (*c*) Type 304L joined by type 308L.

TABLE 34. RESULTS OF DYNAMIC-CORROSION TESTS ON SPECIAL FLAT-PLATE-TYPE WELDED AND BASE-METAL AUSTENITIC-STAINLESS-STEEL SPECIMENS*

	Type of Stainless Steel		Ferrite in Weld (%)	Defilmed Weight Loss (mg)	
	Base Metal	Weld Metal		200 hr	400 hr
Holder A	347	None		83.0	115.4
	310	None		179.4	209.8
	347	347	8.0–8.5	73.9	111.7
	309-SCb	None		81.9	196.1
	347	Composition H	0	96.1	186.7
	304L	None		53.6	114.1
	347	308L	9.0–11.0	98.0	174.9
	304	None		55.7	190.9
	347	Composition H	0	90.9	199.8
	347	None		84.9	199.3
Holder B	347	None		67.8	307.2
	347-304L	Composition H	0	51.8	396.6
	304L	Composition H	0	40.1	438.4
	304L	Composition H	0	**	473.4
	304L	None		39.2	504.5
	304L	308L	9.0–11.0	56.8	921.2
	304L-347	308L	9.0–11.0	68.3	893.1
	304L-347	347	8.0–8.5	78.2	560.0
	304L	347	8.0–8.5	57.6	712.3
	347	None		83.0	339.7

*Specimens tested in 0.17 *m* uranyl sulfate, 250°C, 20 fps. Thickness of specimens in Holder B was 20% greater than those in Holder A. Welded specimens were tested in as-welded condition, and wrought specimens were tested in the solution-annealed condition.

**Weighing error.

uranyl sulfate solution for 400 hr at 250°C and 20 fps and were given standard cathodic defilming treatment in inhibited 5% H_2SO_4. Metallographic examination revealed that the portions which supported stable films contained many randomly dispersed carbide particles, while the remainder appeared quite homogeneous except for stringer-like interdendritic microconstituents usually observed in austenitic-stainless-steel welds.

MISCELLANEOUS INVESTIGATIONS

E. C. Miller W. O. Harms
T. W. Fulton

Service work for the other development and research groups has continued. This work includes investigations of failures, which occur in the various HRP testing facilities, and assistance in the design of experiments in which metallurgical variables are to be studied or where their control is desirable.

Stress-Corrosion Failures in Dynamic Loop C

After 7788.8 hr of operation under a variety of conditions, dynamic-corrosion Loop C was shut down because of the development of a leak on the inside of a 90-deg bend in a section of $\frac{3}{8}$-in. schedule-40 type 347 stainless steel welded tubing. Another failure occurred 11.2 hr after this section was replaced and operation was resumed; again, a leak had developed on the inside of a 180-deg bend of a $\frac{1}{2}$-in. section of schedule-40 type 347 stainless steel welded tubing.

Metallographic examination of these failures showed that transgranular cracking had occurred in both cases. In the first failure, considerable cracking was observed (see Fig. 88), but only one crack had penetrated both the tube wall and the oxide

film on the inside. The appearance of the cracks suggested that they started on the outside of the tube. It was learned that during a previous run, at 100°C for 1000 hr, tap water had been sprayed onto this tube for temperature control. The scale on the outside of the tube was analyzed and was found to be a boiler type of scale which contained considerable amounts of calcium and magnesium. The presence of 7 to 10 ppm chloride ion in Oak Ridge tap water may have figured in the transgranular stress corrosion. Evidence of cold work, such as that shown in Fig. 89, indicated that the section was not stress-relieved after bending.

Failure in the ½-in. tube showed characteristics similar to the earlier failure except that apparently only one branched crack (Fig. 90) had been operative in this penetration. Moreover, this section had not been exposed to tap water but had been covered at all times by a magnesia-base insulation material. In this case the evidence was not so clear that the initiation of cracking was on the outside of the tubing. The transgranular type of cracking which was observed in both failures is shown in Fig. 91, where some of the finer branching near the main crack which led to the second failure is illustrated.

Two sections of the ½-in. pipe – one from the U bend and the other from a straight section – were submitted to the HRP Static Corrosion Group for examination of corrosion characteristics by special laboratory tests. Specimens from each section were tested in three conditions for intergranular corrosion susceptibility with boiling nitric acid under the following conditions: (1) as-received and pickled; (2) sensitized for 2 hr at 1200°F, air cooled, and pickled; and (3) annealed for ½ hr at 1950°F, air cooled, and pickled. In addition, specimens in the as-received conditions were tested in boiling 42% magnesium chloride to determine relative susceptibility to transgranular cracking.

Results of the nitric acid tests showed that only the annealed specimen performed satisfactorily. Chemical analysis, however, showed that sufficient columbium was present to stabilize the alloy. These results are considered significant, since transgranular stress-corrosion failures in austenitic stainless steels sometimes originate as intergranular penetrations.

The magnesium chloride test showed that the specimens from the bent portion of the tube were

Fig. 88. Transgranular Cracks in ⅜-in. Type 347 Stainless Steel Tube from Dynamic Corrosion Loop C. The inside (uranyl sulfate side) of the tube wall is at the top of the photomicrograph. 50X. Reduced 31%.

Fig. 89. Evidence of Cold Work in Bent Section of 0.5-in. Type 347 Stainless Steel Tubing from Dynamic Corrosion Loop C. Note traces of slip planes within the grains. 750X. Reduced 28%.

considerably more susceptible to transgranular cracking than the straight-pipe specimen. The cracks in this environment originated on the outside of the tube.

The results of these investigations serve to emphasize (1) the necessity for stress-relief annealing after fabrication of austenitic-stainless-steel reactor components; (2) the desirability of subjecting HRP materials before use to suitable laboratory tests, such as, perhaps, the boiling nitric acid and magnesium chloride tests, to determine susceptibility to specific corrosion and stress-corrosion phenomena; and (3) the desirability of requiring chemical analyses and metallurgical histories of HRP materials.

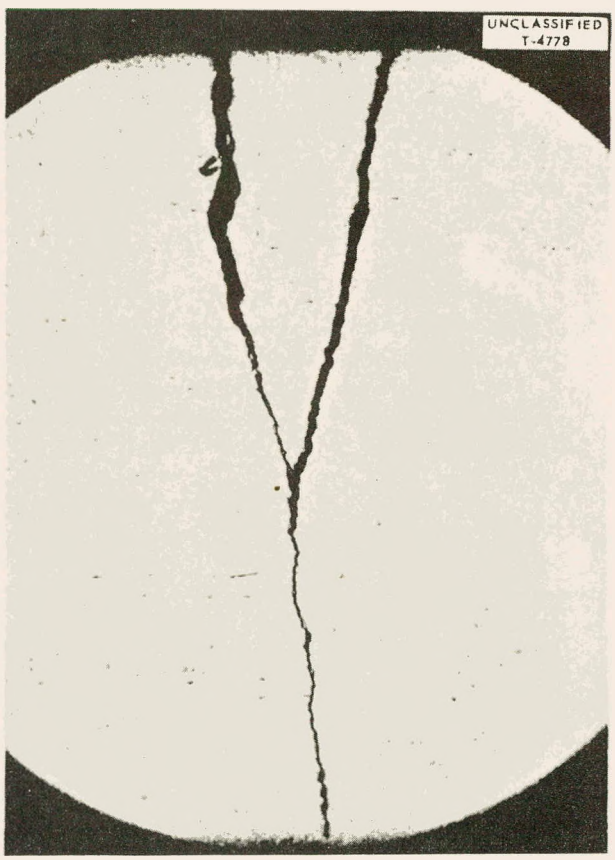

Fig. 90. Transgranular Cracks in 0.5-in. Type 347 Stainless Steel Tube from Dynamic Corrosion Loop C. The uranyl sulfate side of the tube wall is at the top of the photomicrograph. 50X. Reduced 32%.

Failure of Type 347 Stainless Steel Capillary Tubing in In-Pile Mock-up Loop

After 114 hr of operation of the in-pile mock-up loop Run BB-2, a leak developed in the 0.060-in.-OD 0.020-in.-ID type 347 stainless steel capillary tubing through which oxygen was added for gas-recombination tests. There was evidence that uranyl sulfate had entered this line. Shortly thereafter, three other leaks were discovered – one in the same oxygen line and two in a similar hydrogen-addition line. Both lines had been exposed to temperatures between 100 and 150°C and pressures up to 1000 psi.

Failures in both lines had occurred by transgranular cracking, as shown in Fig. 92. The presence of uranyl sulfate in the oxygen line suggested that cracking in this case was the result of the combined effects of corrosion and stress. In either case, the localized residual stress levels were probably quite high, since 0.060-in. capillary

Fig. 91. Transgranular Cracks Adjacent to Main Crack in 0.5-in. Type 347 Stainless Steel Tube from Dynamic Corrosion Loop C. 750X. Reduced 11%.

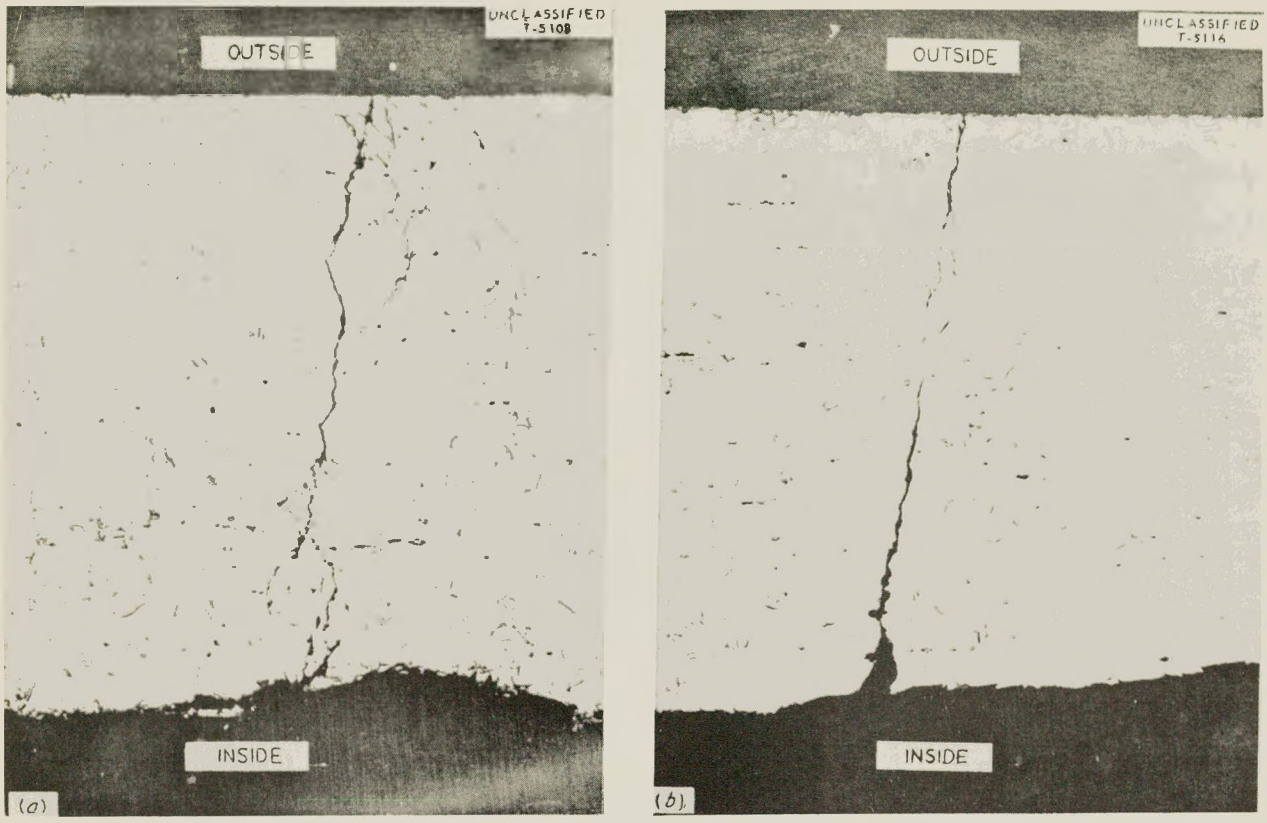

Fig. 92. Transgranular Failures in 0.060-in. Type 347 Stainless Steel Capillary Tubing from Gas Lines in In-Pile Mock-up Loop BB. (*a*) Oxygen line. (*b*) Hydrogen line. 250X. Reduced 31%.

tubing is often inelastically deformed in handling and on installation.

Failure of Type 316 Stainless Steel Parker Fitting Cap

A type 316 stainless steel hexagonal cap on a Parker fitting from dynamic-corrosion Loop H developed a pin-hole type of leak after an unknown time in service. Metallographic examination revealed that the failure had occurred as the result of intergranular attack on the alloy, as shown in Fig. 93, and appeared to have started on the uranyl sulfate side of the cap.

Failure of Letdown Valve in HRE Mock-up

A valve seat and plug from the letdown system of the HRE mock-up were submitted for metallographic examination after they had been removed because of excessive leakage. The operating history and detailed description of the valve components have been reported previously.[2]

The components were made of type 347 stainless steel with a Stellite 6 overlay in the seat and on the guide stem, and the plug was made of Stellite 6 only. The weld-deposited Stellite 6 in both the seat and the stem exhibited porosity and brittleness, but the plug was sound.

Samples of both the porous and the sound material were submitted for chemical analysis, and the results are listed in Table 35. It is to be noted that the porous material contained considerably less cobalt and tungsten, these deficits being reflected as an increase in iron concentration.

Metallographic examination showed that both the Stellite 6 and the type 347 stainless-steel-base alloy were attacked. There was evidence of shrinkage voids as well as of preferential attack on a particular microconstituent in the cast structure of the Stellite 6. This microconstituent is

[2]H. C. Savage, F. J. Walter, and R. A. Lorenz, *HRP Quar. Prog. Rep. Oct. 31, 1953*, ORNL-1658, p 44.

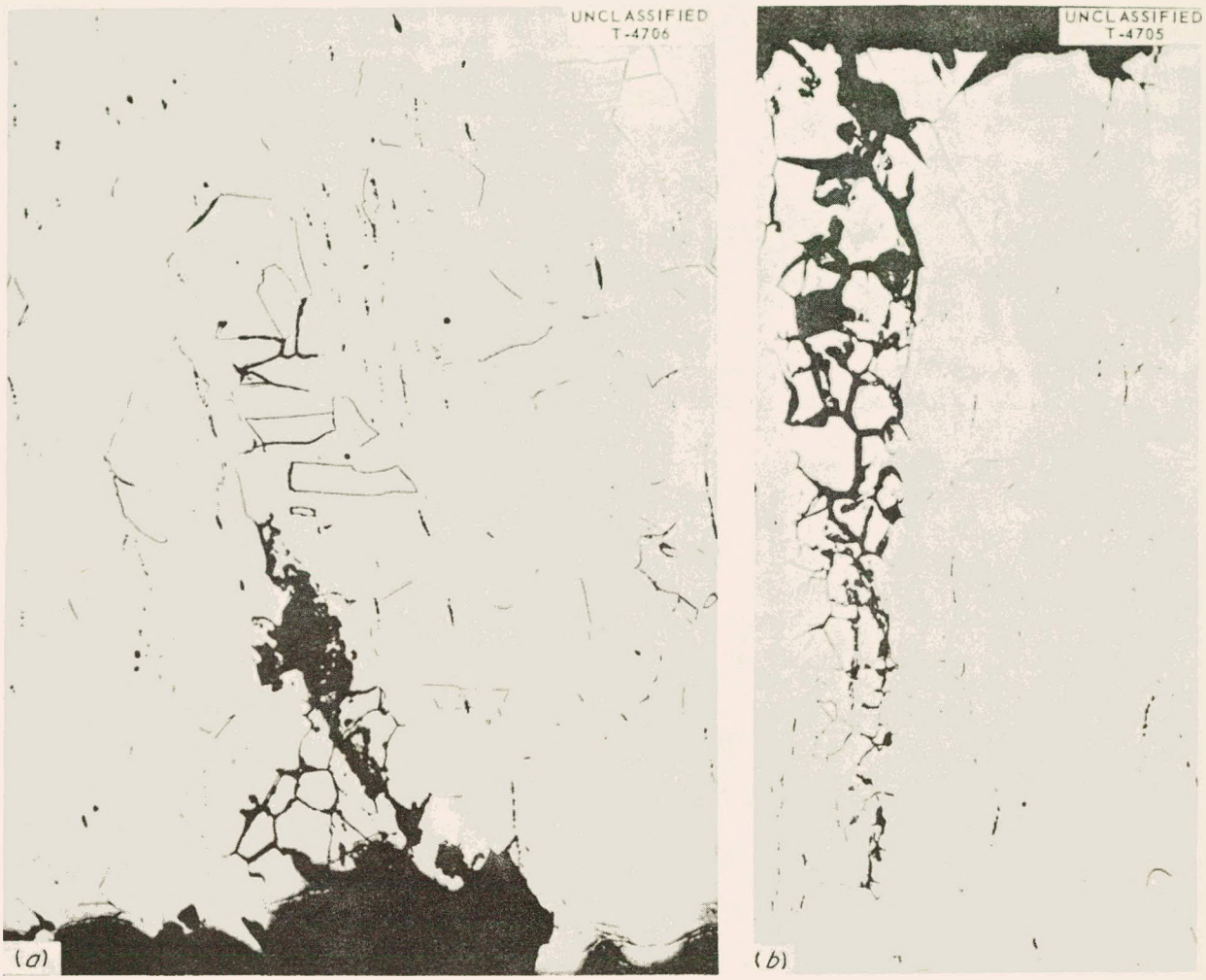

Fig. 93. Intergranular Attack Leading to Failure of Type 316 Stainless Steel Parker Fitting Cap in Dynamic-Corrosion Loop H. (*a*) Attack on uranyl sulfate side. (*b*) Termination of crack on air side. 250X. Reduced 16.5%.

TABLE 35. CHEMICAL ANALYSIS OF STELLITE 6 OVERLAY ON HRE MOCK-UP LETDOWN VALVE

Element	Sound Metal (wt %)	Porous Metal (wt %)
Co	59.1	46.6
Cr	27.50	28.47
W	5.26	2.74
Fe	1.66	9.06
Ni	0.84	1.29
Si	1.07	0.94

believed to be a complex carbide which contains cobalt, tungsten, and chromium and which is a peritectoid-type transformation product in the Co-Cr-W-C system. Corrosion appeared to have proceeded into the stainless steel alloy by an intergranular mechanism. Carbide precipitation was observed in grain boundaries of the type 347 stainless steel near the fusion zone, thus accounting for the intergranular attack. Carbon had apparently diffused from the Stellite to the base material during

welding, and precipitation as chromium carbides occurred on slow cooling through the sensitizing temperature range.

PROPERTIES OF TITANIUM AND ZIRCONIUM ALLOYS

W. J. Fretague

Commercial Titanium

Impact specimens are being prepared from a corrosion specimen holder made from RC-70 titanium (Heat 3102 REED Item 11). The history of this specimen holder was given in a previous quarterly report.[3] Specimens will be tested as soon as they are machined.

Notched slow-bend tests have been performed on a series of 0.204-in.-dia corrosion pins made from commercial titanium (Ti-75A-3 Item 49). The results obtained from these tests will serve as a guide in setting up the testing temperatures for titanium sheet specimens exposed in the HRE.

Specimens for slow-bend testing are being prepared from two special heats of commercial titanium. The one heat was prepared from selected sponge titanium by the Mallory-Sharon Titanium Corp. and was fabricated in the Metallurgy Division of ORNL to $\frac{3}{16}$-in. plate by the picture-frame technique. The other special heat was prepared and fabricated by Rem-Cru Titanium Corp. from selected purity sponge and is designated as RC-55 (Ingot T5-3671 REED Item 48).

Impact tests have been completed on eight multiple-break impact specimens. The thermal and mechanical history of these specimens prior to loop exposure by the Dynamic Corrosion Testing Group is given in an earlier quarterly report.[4] The loop history of these specimens is listed in Table 36, and the results of impact tests are plotted in Fig. 94.

A comparison of the impact data reported for commercial titanium (Ti-75A Item 24 Heat L782) exposed as outlined in Table 36 with the data for this same material reported previously[5] shows that the exposure to simulated HRE environments (in the absence of radiation), after various specimen pretreatments, had no noticeable effect on the impact behavior.

Zircaloy-2

Impact tests have been completed on the Zircaloy-2 specimens described in the previous quarterly report.[6] The loop history of the specimens is outlined in Table 37, and the resultant data are graphically presented in Fig. 95.

A group of seven multiple-break impact specimens of Zircaloy-2, which had been vacuum annealed at 750°C for 2 hr and furnace cooled prior to final machining, were impact tested in the temperature range from −195.8 to 300°C. The data obtained are presented in Fig. 96.

Comparison of the impact data for annealed Zircaloy-2 (Fig. 57) with that obtained from vacuum-annealed Zircaloy-2 specimens exposed to simulated HRE environments[6,7] shows no apparent effect on impact properties that can be attributed to the environments in which the specimens were exposed.

[3] W. J. Fretague, *HRP Quar. Prog. Rep. Jan. 31, 1954*, ORNL-1678, p 75-6.

[4] W. J. Fretague, *HRP Quar. Prog. Rep. Jan. 1, 1953*, ORNL-1478, p 88.

[5] W. J. Fretague, *HRP Quar. Prog. Rep. July 31, 1953*, ORNL-1605, Fig. 53, p 119.

[6] W. J. Fretague, *HRP Quar. Prog. Rep. Jan. 31, 1954*, ORNL-1678, p 76-8.

[7] W. J. Fretague, *HRP Quar. Prog. Rep. Oct. 31, 1953*, ORNL-1658, Table 13, p 80 and Fig. 50, p 82.

TABLE 36. LOOP HISTORY OF TITANIUM IMPACT SPECIMENS

Run No.	Specimen No.	Solution	Remarks
A-62	67, 68, 71, and 72	5 g of uranium per liter of UO_2SO_4 plus 0.005 *m* H_2SO_4 at 320°C for 682 hr	The solution contained 900 to 1500 ppm O_2 and flowed past the specimens at 3 to 5 fps
G-6	69, 70, 73, and 74	5 g of uranium per liter of UO_2SO_4 plus 0.010 *m* H_2SO_4 at 300°C for 529 hr	The solution contained approximately 1000 ppm O_2; during the run the specimens came loose from their holder and were rather badly battered

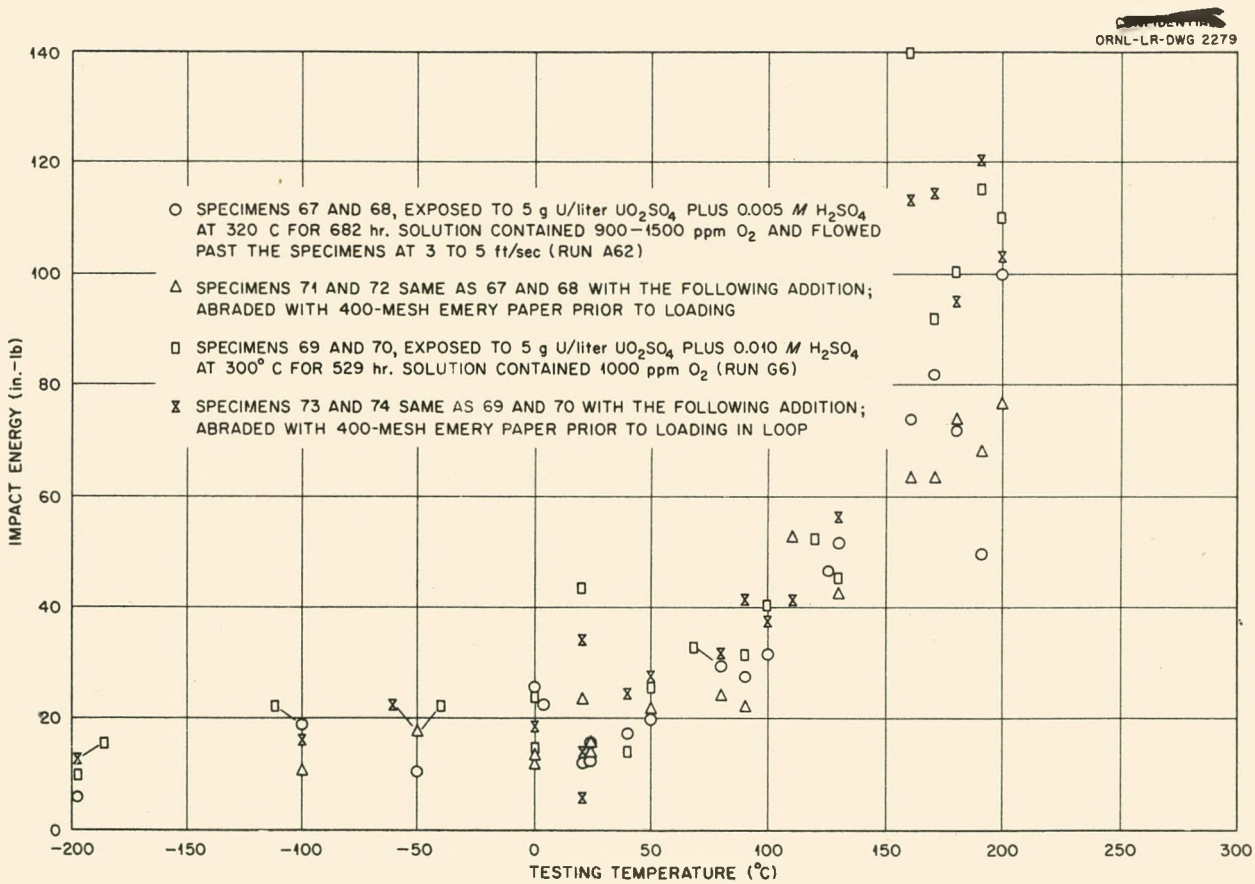

Fig. 94. Commercial Titanium (Ti-75A Item 24 Heat L782) 1-in.-dia Bar Swaged to Approximately 0.25 in., Rod Vacuum Annealed at 500°C for 1 hr and Furnace Cooled, Machined to Final Size, Reannealed in Vacuum at 600°C for 1 hr After Machining.

TABLE 37. LOOP HISTORY OF ZIRCALOY-2 SPECIMENS

Run No.	Specimen No.	Solution	Remarks
A-62	Z 2-1, Z 2-4, Z 2-10, and Z 2-11	5 g of uranium per liter of UO_2SO_4 plus 0.005 m H_2SO_4 at 320°C for 682 hr	The solution contained 900 to 1500 ppm O_2 and flowed past the specimen at 3 to 5 fps

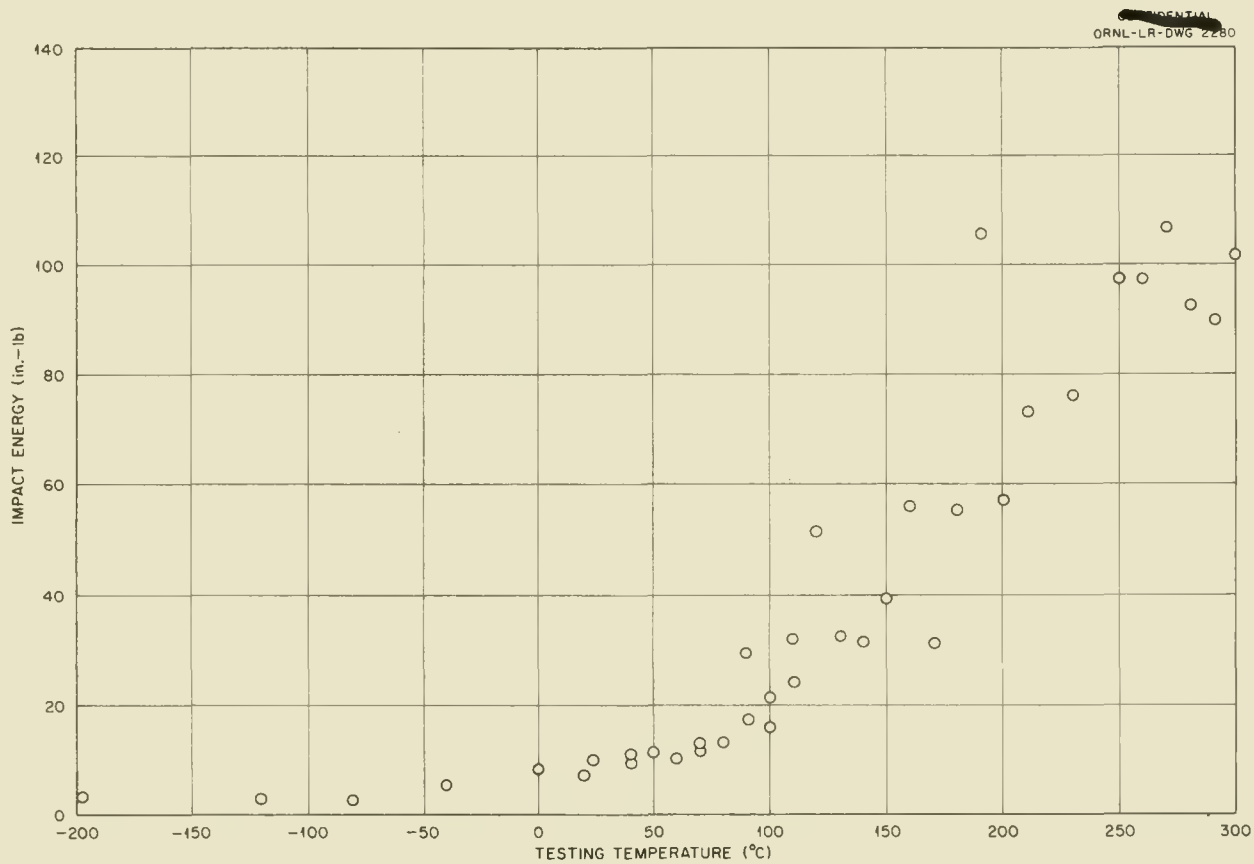

Fig. 95. Zircaloy-2, $\frac{3}{8}$-in. Rod Swaged to 0.217-in.-dia Rod, Sand Blasted, Pickled, Vacuum Annealed at 750°C for 2 hr, Furnace Cooled, and Machined to Final Specimen Size. Exposed to 5 g of uranium per liter of UO_2SO_4 plus 0.005 *m* H_2SO_4 at 320°C for 682 hr; solution contained 900 to 1500 ppm of oxygen; flow rate, 3 to 5 fps (Run A-62).

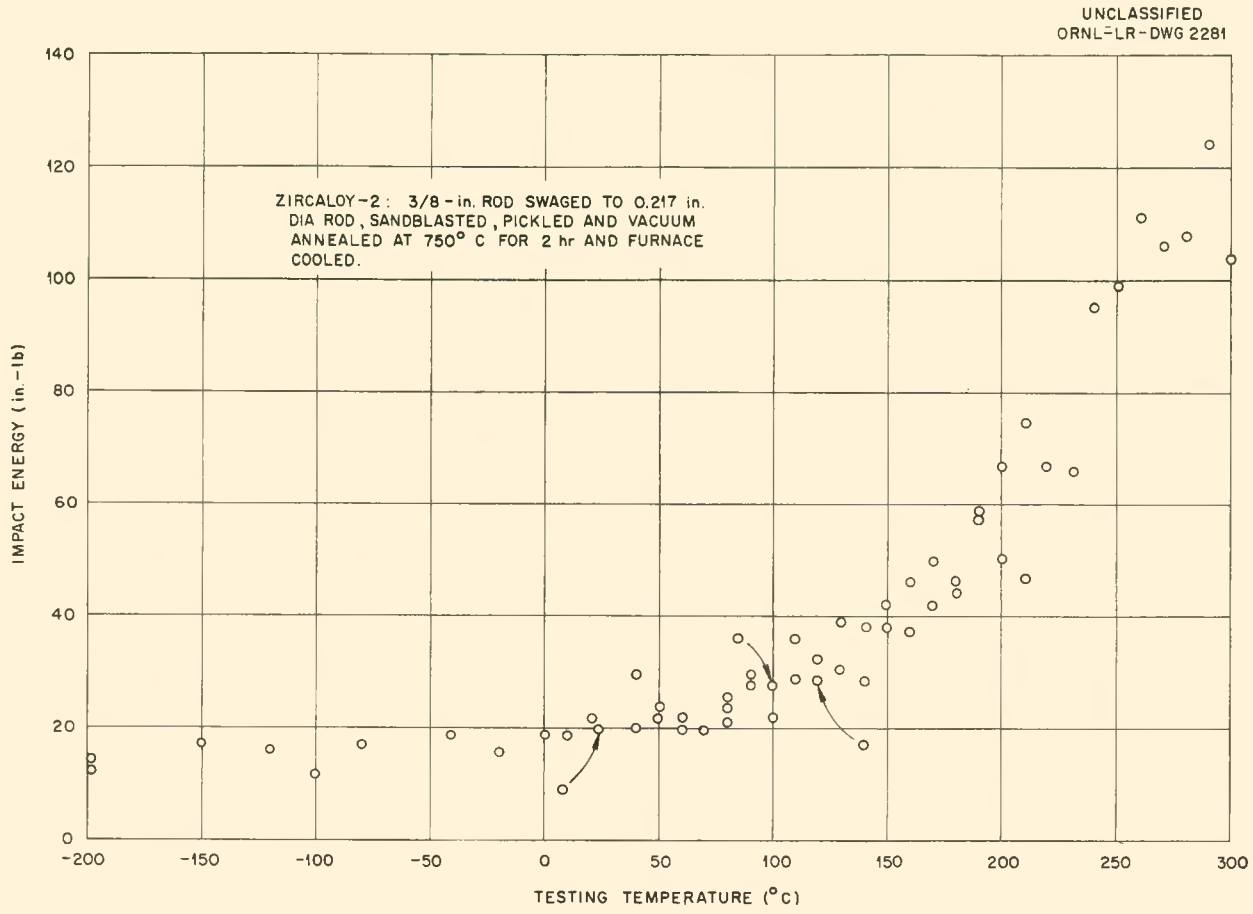

Fig. 96. Zircaloy-2, $\frac{3}{8}$-in. Rod Swaged to 0.217-in.-dia Rod, Sand Blasted, Pickled, Vacuum Annealed at 750°C for 2 hr, and Furnace Cooled.

INSTRUMENTATION AND CONTROLS

J. N. Baird, Jr., Section Chief

A. M. Billings
D. G. Davis
R. L. Moore
J. L. Redford
D. S. Toomb, Jr.
W. P. Walker

IN-PILE LOOP PROGRAM

Control information was assembled for a report which was prepared for the ORNL Reactor Experiment Review Committee. Operation of the loop and of the LITR as affected by conceivable misoperation and by instrument and component failure is considered in the report.

Wiring of the second instrument panel, which will be operated in the west room of the LITR, is practically complete.

COMPONENTS AND SYSTEMS TEST LOOPS

The engineering for instrumentation and controls of eight new-type slurry loops has been completed, and the construction of instrument panels for two loops is under way.

The instrumentation for the testing of the electrical heating system for an HRT pressurizer has been specified.

The construction of the instrument panel is under way for the high-pressure recombiner loop, an entrainment-separator test system, and four test loops for 400-gpm canned-rotor pumps.

A variable-frequency motor-generator set built by The Allis, Louis, Co. has been wired, tested, and placed in operation. The set is used to change the speed of induction motors, thereby providing a very flexible method for varying the pumping rates in test loops. The set has a rating of 31 kva at 75 cycles, which decreases to 6.5 kva at 15 cycles.

BOILING HOMOGENEOUS REACTOR STUDIES

R. N. Lyon, Section Chief

STEAM REMOVAL FROM THE BOILING HOMOGENEOUS REACTOR

The problem of maintaining a high fuel density in the core of a boiling reactor can be considered in two parts, that of transport of the vapor from the region in which it is generated to the surface of the core and that of subsequent removal of the vapor from the entraining liquid at the surface. Therefore both experimental work and theoretical work have been directed toward investigating the two parts of the problem separately in such a manner that the results can be assembled to provide information on the most satisfactory core arrangement.

VAPOR TRANSPORT IN THE CORE – NATURAL CONVECTION

P. C. Zmola H. A. MacColl
M. Richardson

The results of previous work, reported in preceding quarterly reports, indicate that core arrangements in which a gross circulation of the fuel fluid is established have substantially better vapor-transport properties than those in which no circulation is established and only natural vapor rise occurs. Accordingly, work initiated during this quarter has been directed toward the investigation of circulating systems. Either natural or forced circulation can be employed; experimental work has been with natural-circulation systems, but the essential results can also be applied to forced-circulation systems.

The $1\frac{1}{4}$ × 4-in. natural-circulation system descrived previously[1] has been run at 1, 2, and 3 atm pressure. Results from three representative runs, one for each pressure at comparable total power, are shown in Table 38. P and $\bar{f}$ are the power density and average vapor fraction, respectively, based on the entire test section (approximate volume, 4l). P_a and $\bar{f}_a$ are the power density and average vapor fraction, respectively, based on the active boiling height in the test section. It will be recalled that, for all except the highest power runs, boiling does not take place over the entire test-section height because of the increase in saturation temperature due to hydrostatic head. The recirculation factor n is the ratio of the circulating-flow rate to the net steam rate. The loss coefficient K reflects the number of velocity heads lost in each circulation pass, based on the exit-liquid velocity, and for this system is defined by the expression

$$Z_a \bar{f}_a (\rho_f - \rho_g) = \rho_f K \frac{U_f^2}{2g}$$

where

Z_a = active test-section height,

$\bar{f}_a$ = average vapor fraction based on the active boiling height,

ρ_f = liquid density,

ρ_g = vapor density,

U_f = liquid velocity at exit of test section,

g = gravitational acceleration.

Except for low-power runs, the value of K falls in the range of 1 or 2, which indicates that the principal flow loss is due to accelerating the liquid in the test section.

[1] R. V. Bailey, W. S. Brown, H. A. MacColl, M. Richardson, and P. C. Zmola, *HRP Quar. Prog. Rep. July 31, 1953*, ORNL-1605, pp 24-5; *HRP Quar. Prog. Rep. Oct. 31, 1953*, ORNL-1658, pp 16-17.

TABLE 38. REPRESENTATIVE RESULTS FROM $1\frac{1}{4}$ × 4-in. NATURAL-CIRCULATION APPARATUS

Power Density (kw/liter)		Average Vapor Fraction		Pressure (atm)	Velocity at Exit of Test Section (fps)		Recirculation Factor (n)	Loss Coefficient (K)
P	P_a	$\bar{f}$	$\bar{f}_a$		Liquid	Vapor		
9.9	15.3	0.41	0.62	1	10.8	39	130	0.9
10.2	13.75	0.32	0.43	2	8.3	24	145	1.2
9.1	11.7	0.32	0.45	3	7.5	16	160	1.5

In order to determine the influence of size and geometry on vapor transport, a second natural-circulation system is being constructed; it will have a test section 6 in. square and 4 ft high. Measurements which correspond to those obtained with the $1\frac{1}{4} \times 4$-in. system will be made. Operation will be at atmospheric pressure only.

Circulating systems from which significant data may be obtained are rather costly and require a considerable amount of time for construction. Apparatus for experiments with natural vapor rise is generally simpler. With the hope of setting at least a lower limit on the power-removal capability of a boiling system at high pressures, a 4-in.-dia natural-vapor-rise system capable of operating at pressures up to 1500 psi has been constructed. For simplicity, heat is added to the vessel wall so that surface boiling instead of volume boiling takes place. The boiling height is obtained from a radiogram of the vessel, and the corresponding nonboiling height is read from a sight glass. Runs made to date have been restricted to checking out the apparatus and to developing a satisfactory radiographic technique. In addition to tests with water, it is also intended to boil thorium oxide slurry in this system.

The extrapolation of vapor-transport properties of systems which operate at near-atmospheric pressures to the properties of a full-scale boiling reactor which might operate at pressures of 1000 psi and above is exceedingly difficult. While there is some hope of determining the influence of geometry by comparing results from various sizes of experimental systems operated at near-atmospheric pressure, the extrapolation of results from any one of these systems to high pressure cannot be performed within the limits necessary for design purposes. It is planned to operate a natural-circulation system, generally similar to the low-pressure circulation system referred to above, at high pressure to obtain vapor-transport information in this range. The specific features and operating range of this apparatus are as follows:

1. test-region geometry – provisions for running both 6 × 6-in. and 2 × 6-in. cross sections with heights of 2, 4, and 6 ft,
2. test-pressure range – 600 to 2400 psi,
3. maximum total power – approximately 2000 kw provided by electrical-resistance heating of liquid.

The measurements to be made for each run are:

1. density distribution in test region (obtained with gamma-ray attenuation densitometer),
2. circulation-flow rate,
3. steam-generation rate.

It is expected that this work will not be performed at the Laboratory; at the present time, negotiations are in progress to subcontract the construction and the performance of the initial experimental work.

FORCED CONVECTION

C. G. Lawson

During the past quarter, work has continued on a study of the feasibility of employing forced circulation in boiling reactors. Work has progressed along two lines:

1. an estimation of the power densities obtainable with a given pressure drop as a function of the reactor operating conditions and the reactor design,
2. the feasibility of using a centrifugal type of pump to increase the circulation rate of a system operating near saturation temperatures and pressures.

Pressure-Drop Determination

The pressure drop in a boiling reactor system was estimated in a manner similar to that employed by Bailey and Zmola[2] for their Model (1) natural-circulation systems. The model reported here is a circulating reactor which employs steam separators and a baffle to separate the fluid downcomer region from the riser region. The pump is inserted in the downcomer region downstream from the steam separators and the condensate return lines. Since the flow area at the separator inlet is from one-fifth to one-seventh the reactor cross section, it is assumed that the reactor itself acts as a header into the separators, and consequently the pressure drop in the reactor system is only slightly greater than the pressure drop across the separator inlet. The driving force available to supply this pressure drop, under steady-state conditions, would be supplied by the buoyant force that results from the difference in density in the riser and downcomer, as well as by the pump.

[2] R. V. Bailey and P. C. Zmola, *Preliminary Investigation of Power Removal from a Boiling Reactor*, ORNL CF-53-11-145 (Nov. 1953).

The equation which compares the velocity heads lost at the separator entrance with the available pressure is

$$(1) \qquad K\rho_2 \frac{V_2^2}{2g_c} = Z(\rho_f - \rho_a) + Z_p\rho_f ,$$

where

K = number of velocity heads lost at the separator inlet,

ρ_2 = density of the steam-liquid mixture entering the separator, lb mass/cu ft,

V_2 = velocity of the steam-liquid mixture entering the separator, fps,

g_c = gravitational conversion constant, ft/sec^2,

Z = reactor height, ft,

ρ_f = liquid density at the pump, lb mass/cu ft,

Z_p = pump head, ft (lb force)/lb,

ρ_a = average density in the riser section [assumed to be equal to $(\rho_f + \rho_2)/2$], lb mass/cu ft.

Since the liquid is subcooled and below saturation in H_2 and O_2 when it enters the downcomer, and since only about 25% of the circulation time is spent in the downcomer, it is assumed here, for simplicity, that no bubbles form in the downcomer. Actually, if it is assumed that the power density is uniform, the hydrostatic driving force is essentially unchanged if bubbles form in the downcomer, but the force is reduced if the liquid is still subcooled when it enters the riser.

If Eq. 1 is combined with the laws of conservation and if the steam-generation rate is expressed as average power density, it may be shown that

$$(2) \qquad \frac{Z_p}{Z} \times \frac{\rho_f}{2\rho_2} = \frac{\Delta\pi}{2Z\rho_2}$$

$$= \frac{KZ}{4g}\left[13.4P\left(\frac{A_D + A_R}{A_2}\right)\frac{v_{f_g}}{h_{f_g}}\right]^2 \left(\frac{\rho_f}{\rho_f - \rho_a}\right)^2 - \frac{\rho_f - \rho_a}{\rho_f} ,$$

with the restriction that $\rho_a \simeq (\rho_f + \rho_2)/2$ [actually $\rho_a = \left(\int_0^Z \rho(z)\, dz\right)/Z$], where

v_{f_g} = volume change on vaporization at the reactor operating pressure, cu ft/lb mass,

h_{f_g} = latent heat of vaporization at the reactor operating pressure, Btu/lb mass,

A_D, A_R = reactor downcomer and riser areas, respectively,

$A_D + A_R$ = total reactor cross-sectional area,

A_2 = total area of entrances to separators,

P = power density (average across total reactor cross section),

$\Delta\pi$ = pressure rise across the pump, lb force/sq ft.

Equation 2 is shown plotted in Fig. 97 with $(Z_p/Z) \times (\rho_f/2\rho_2)$ plotted vs

$$\frac{KZ}{4g}\left[13.4P\left(\frac{A_R + A_D}{A_2}\right)\left(\frac{v_{f_g}}{h_{f_g}}\right)\right]^2$$

and $\rho_f/(\rho_f - \rho_a)$ as a parameter.

The case where $(Z_p/Z) \times (\rho_f/\rho_2) = 0$ is such that natural circulation will be established. Negative values of $(Z_p/Z) \times (\rho_f/\rho_2)$ indicate that the desired operating conditions may be obtained and that there is additional pressure drop available for use in the circuit.

Since it is assumed that no slip of vapor through the liquid occurs, the results shown are overly pessimistic in low-velocity regions where natural circulation might be used.

The pressure drop across existing separators used by Babcock & Wilcox Co. was determined experimentally to correspond to a value of $K = 1$ for ideal conditions (laboratory tests) and $K = 1.7$ for field data.[3]

A graph which indicates the estimated power density vs the pressure rise across the pump for typical boiling reactors of different heights, operating under identical inlet and outlet conditions, is shown in Fig. 98. The reactor cross section is constant, K is assumed to be 2, and the outlet steam volume fraction is 0.5. The power density at

[3] Conference with R. U. Blaser, W. M. Moyer, and E. Coulter of the Babcock and Wilcox Company.

$\Delta\pi = 0$ is that obtainable in a natural-circulation system without a pump, although again the postulation of no slip probably gives values of power density which are too low in the region near $\Delta\pi = 0$.

If the reactor operates at some pressure other than 1000 psi, the variation in power density at the same void fraction and pressure rise across the pump will be due largely to the difference in the ratio of latent heat to specific volume of the steam. The factor by which the specific power will differ at pressures other than 1000 psi is shown in Fig. 99 and illustrated by the following data:

Pressure	Power / Power at 1000 psia
0	0
15	0.025
100	0.137
500	0.552
1000	1.00
1500	1.34
2000	1.69
2200	1.79
2400	1.86
2500	1.897
2600	1.904
2700	1.904
2800	1.88
2900	1.84
3000	1.74
3100	1.53
3200	0.730
3206.5	0.000

Pump-Feasibility Study

Primarily the pump-feasibility study has been directed toward determining whether sufficient net positive suction head (NPSH) can be obtained at the pump inlet to ensure the development of the required pressures without cavitation occurring in the pump and whether this can be accomplished with little additional complexity and core-solution holdup.

One method of increasing the NPSH is to subcool the liquid entering the pump in order to establish a net positive pressure between the pressure of the system and the vapor pressure of the liquid in the pump. By subcooling the condensate and returning it to the core downstream of the separator and upstream of the pump, it is possible to lower the temperature of the liquid entering the pump below saturation. Calculations have been made to determine the temperature drop so obtained, with the assumptions that there is no slip velocity between the liquid and vapor, that the condensate is subcooled to 80°C (176°F), and that no heat is added to the solution between the separator and the pump. The

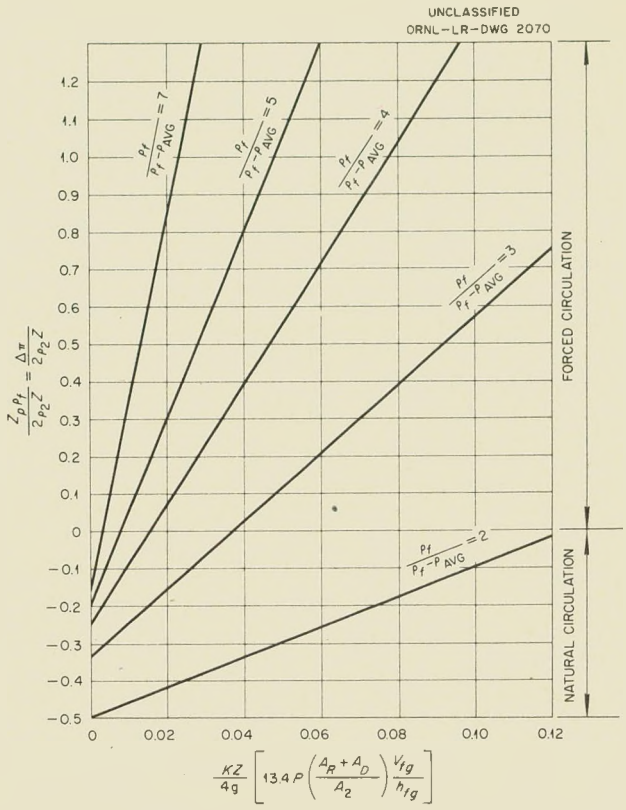

Fig. 97. Pressure Drops Through Boiling Reactors with Separators.

results of this calculation for a system operating at 1000 psia and 285°C (545°F) are shown in Fig. 100, where the temperature drop (°F) is plotted against the void fraction at the reactor outlet. The dotted line indicates the temperature drop obtained with no entrainment of steam in the liquid, and the solid line indicates the temperature drop obtained when 10% of the steam which enters the separator is entrained in the liquid which leaves the separator. The positive suction pressure which results from a given temperature drop is indicated on the right-hand ordinate of Fig. 100. With the suction pressures indicated, cavitation in the pump may be easily avoided at a system pressure of 1000 psia and a temperature of 285°C (545°F).

In addition to the pump itself, the proposed method of increasing the suction pressure requires the complication and condensate holdup inherent in a heat exchanger. Although the holdup may be important, the hot solution in the exchanger is con-

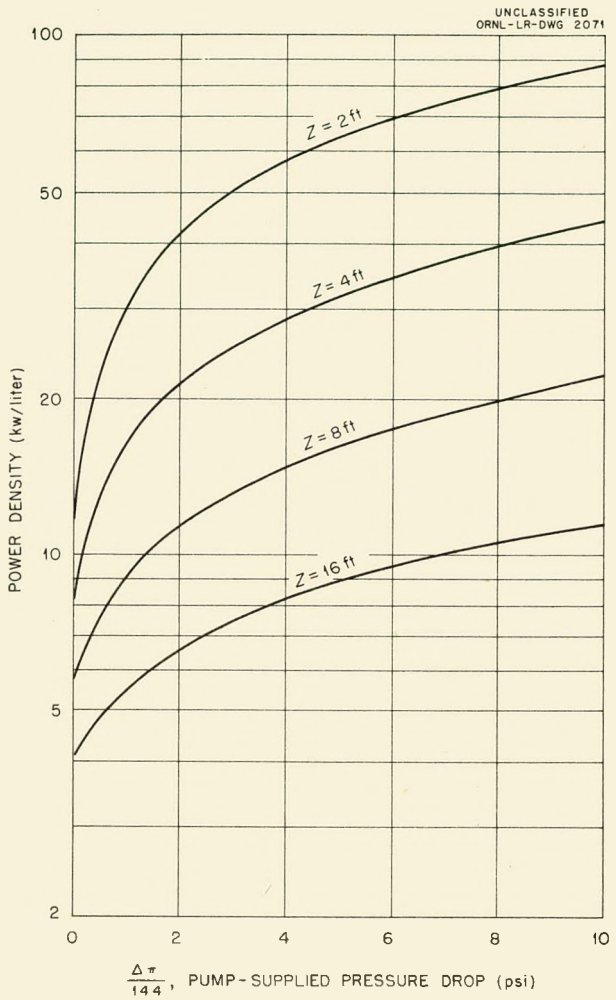

Fig. 98. Estimated Pressure Drop for a Typical Boiling Reactor (1000 psia Operating Pressure; Outlet Liquid Mixture Contains 50% Steam by Volume; Ratio of Outlet Area to Reactor Cross Section, 1 to 7; Head Loss Due to Circulation in Terms of Head Velocity Before Entering the Separator, 2).

densate which will contain little or no uranium. The advantage of a heat exchanger, apart from preventing pump cavitation, is that it permits removal of sensible heat as well as latent heat from the steam leaving the reactor. At 1000 psia, the liquid-sensible heat above 80°C is 61.5% as great as the latent heat. On this basis the power densities shown in Fig. 98 would be multiplied by 1.615 to obtain the actual (latent and sensible) heat removed from the reactor system. The value of the

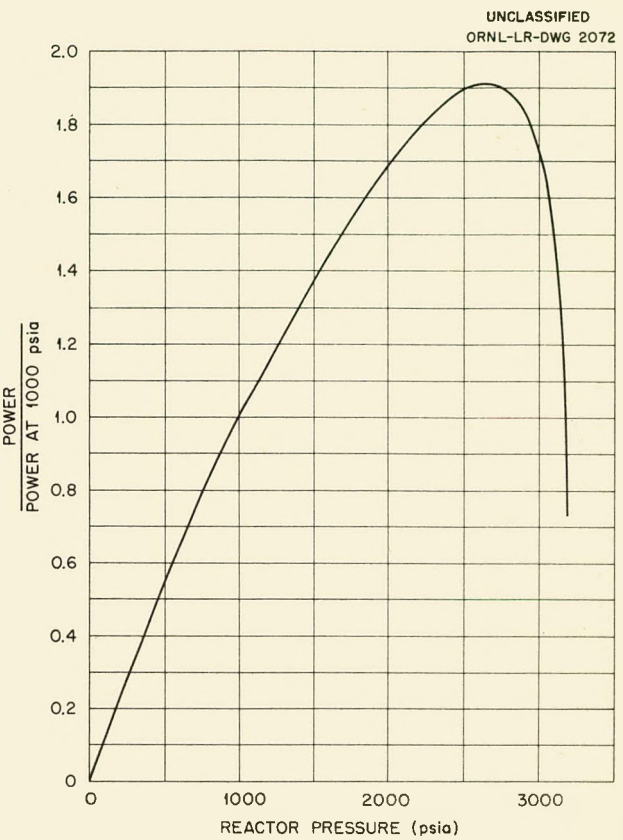

Fig. 99. Effect of Pressure on Specific Power.

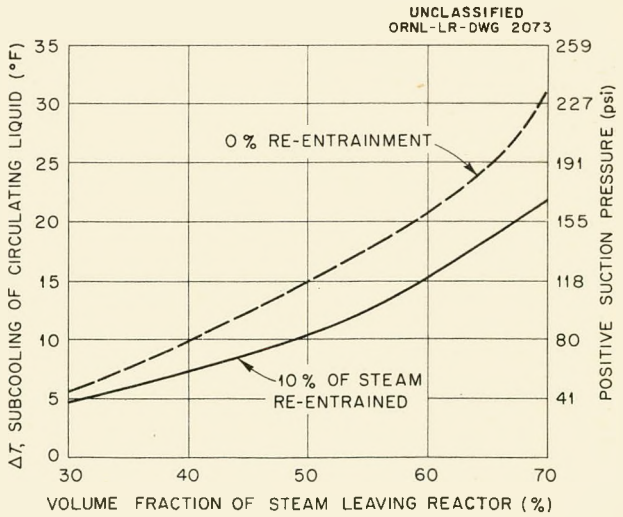

Fig. 100. Subcooling Obtainable, and Resulting Suction Pressure, When Condensate Is Cooled to 176°F Before Being Returned to Core (Core Pressure, 1000 psia).

additional heat is less, however, because of its lower availability.

Vapor Separation

Essentially all the work during this quarter on separation of vapor from liquid has been carried out at the Babcock & Wilcox Co. Research and Development Laboratories under a subcontract. So far, the work by that organization has been directed largely toward finding the points in the separator at which loss of head occurs and in investigating methods for reducing the head loss.

AQUEOUS SOLUTION AND RADIATION CHEMISTRY

HOMOGENEOUS REACTOR SOLUTIONS UNDER IRRADIATION

C. H. Secoy
H. O. Day
Q. V. Larson
M. D. Silverman
H. Stone
F. H. Sweeton
L. F. Woo
W. C. Yee

During the past quarter, studies of the corrosion of metals by homogeneous reactor solutions under reactor irradiation have been continued. In addition, several out-of-pile corrosion studies have been made in order to provide control conditions.

Two important changes have been made with regard to the experimental technique used. In previous investigations, the metal bombs had remained in a stationary position during the test period, and it was found that the deposit of corrosion material on the metal exposed to the vapor phase was heavier than that on the metal exposed to the liquid phase. In an attempt to eliminate this phenomenon and to enable more accurate corrosion rates to be calculated from the experimental data, the bomb is now rocked during the corrosion test. For out-of-pile bombs the rocking rate is about 40 times per minute, whereas for in-pile bombs the rate is about 9 times per minute. The second change is in the manner in which in-pile bombs are pressure-tested to ensure safe operation. This testing had previously been carried out with the bomb containing aerated water at 250°C or above. Inasmuch as this, in effect, meant that there was a small but unknown amount of pretreatment, the testing is now conducted at room temperatures by using water pressurized by high-pressure N_2 gas.

As in previous corrosion tests, the amount of penetration is calculated from the change in oxygen partial pressure in a bomb, and it is assumed that the corrosion is uniform over the surface and that there is no selective oxidation of any particular constituent of the alloy from which the bomb was constructed.

Stainless Steel

A total of three out-of-pile and three in-pile corrosion tests have been made with type 347 stainless steel bombs. The six bombs used in the tests were constructed from the same bar of stainless steel and were finished as identically as possible. The interiors of the bombs were polished mechanically to a mirror finish. No further treatment was made other than cleaning the surface with petroleum ether and acetone.

Out-of-Pile Tests. A new instrument capable of measuring the output voltages of six Baldwin cells is now in operation. In the measurement of the potentials, an accuracy that corresponds to ±0.02 psi can be obtained. However, the limiting errors due to instability and inaccuracy in a Baldwin cell are larger than this figure.

In an attempt to check on the corrosion, as given by oxygen-pressure data, two type 347 stainless steel pins were added to each bomb. These pins were weighed before the test, and they were weighed again following the test after having been stripped by the usual technique. If the data from the two methods are in agreement, this direct measurement will enable the pressure data to be used with more confidence.

The original test solution was of such a concentration of UO_2SO_4 and $CuSO_4$ that after addition of H_2O_2 solution the final concentration of the bomb contents was approximately 40 g of uranium per liter and 0.01 M in Cu^{++}. All tests were made at 250°C.

Test H-24. – The data from Test H-24 are presented in Figs. 103 and 104. At first, the rate of corrosion is relatively high – about 19 mpy. After the curve levels off somewhat, the corrosion rate decreases to about 0.1 mpy up to 6 days and further decreases to about 0.04 mpy between 21 and 33 days.

After operation for a little more than a day, it became necessary to unload another bomb from the thermostat. During this operation, the shaking was stopped for a few minutes and the temperature dropped a few degrees. After temperature equilibrium had been regained and the shaking was resumed, it was found that the pressure in Bomb H-24 had increased by approximately 3 psi. Since it was unlikely that corrosion had stopped, it was assumed that the reading on the Baldwin cell was 3 psi too high, and subsequent readings were corrected by this amount. Later, shaking was again interrupted and other increases of pressure were noted and corrected. Of the two curves in Fig. 104, the corrected one is labeled "normalized"; the original data are presented by the lower curve.

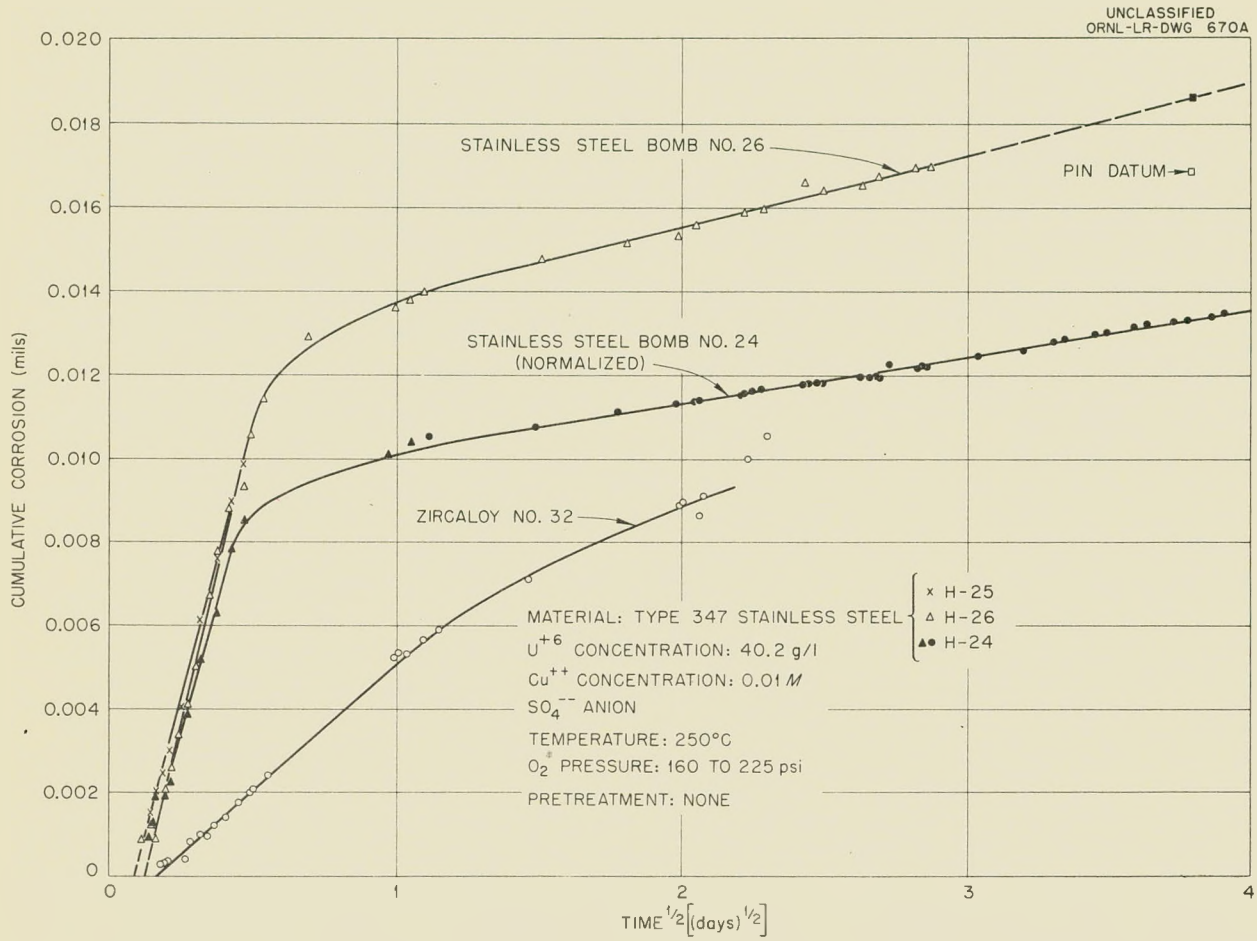

Fig. 103. Cumulative Corrosion Data for Tests H-24, H-25, and H-26.

Test H-25. – This test was run for only about 5½ hr. After the test was concluded, a leak developed in the capillary line, and further data were invalid because of the loss of oxygen. The corrosion values obtained during the run agree closely with the initial corrosion data from Test H-24 and, as will be shown later, from Test H-26.

Test H-26. – The corrosion values obtained in Test H-26 are given in Fig. 103. If the corrosion data from Test H-26 are compared with those from Test H-24, it may be seen that the initial rates agree closely and that the later rates are slightly higher for Test H-26. After the initial corrosion rate slowed down, the corrosion rate was about 0.2 mpy up to about 6 days, and from 6 to 16 days the rate was about 0.1 mpy.

None of the curves in Figs. 103 and 104 pass through the point of origin, because there was an error either in time or in the measurement of cumulative corrosion. Time was measured arbitrarily, starting with the loading of a cold bomb into a thermostat at 250°C. Here, a definite time error was introduced because it is not known at which temperature corrosion reached a measurable rate. The second error arises from the combination of a rapidly changing temperature and a high initial corrosion rate; under such conditions it is quite difficult to measure the initial oxygen pressure with precise accuracy. Fortunately, both of these errors are small, and it is hoped that they can be further reduced or eliminated.

The results of analyses made on the contents of bombs H-24 and H-26 are listed in Table 40. In both instances there was considerable CrO_4^{--} ion

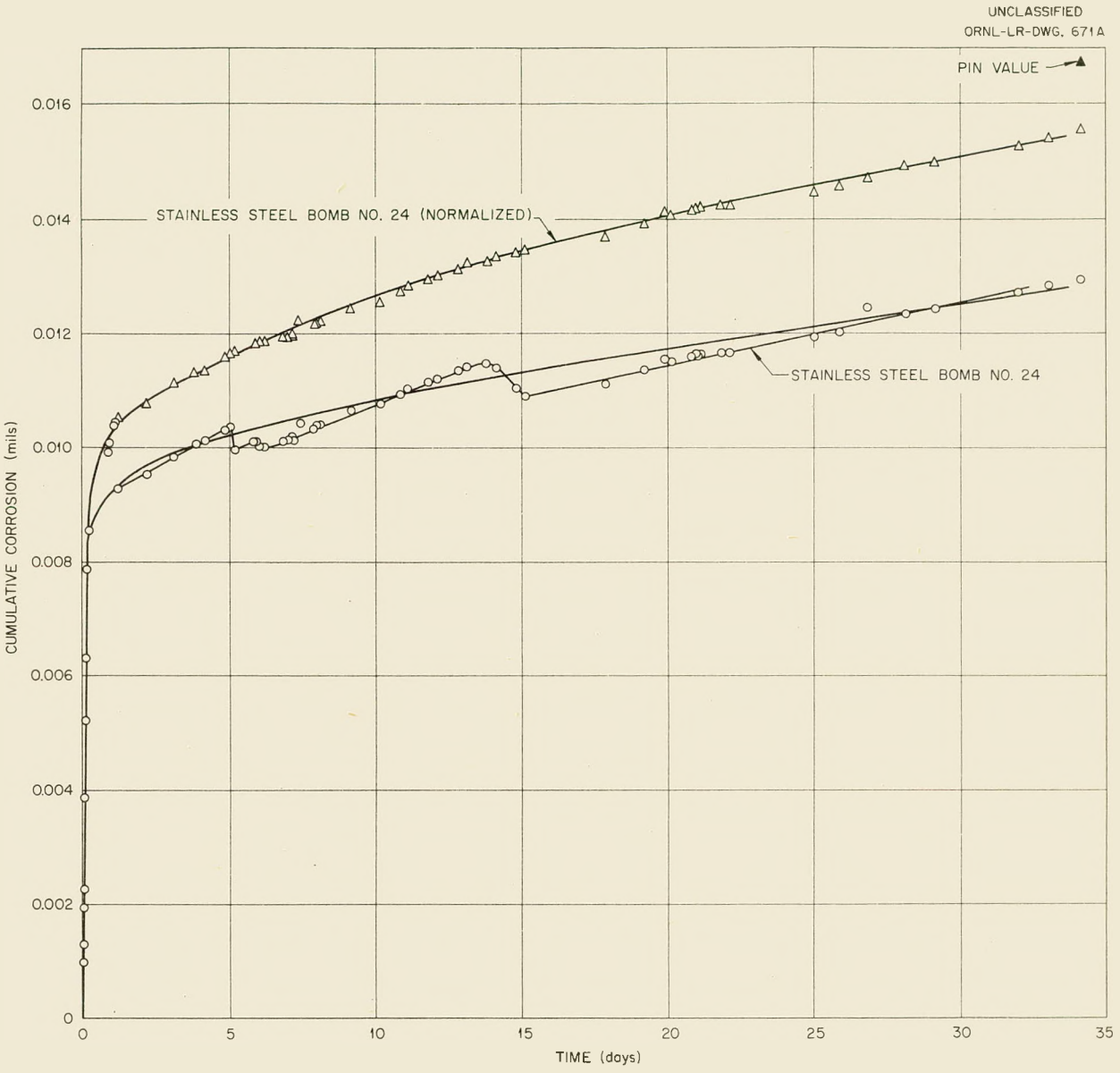

Fig. 104. Cumulative Corrosion Data for Test H-24.

present. The mathematical factor for converting pressure readings to corrosion penetration was calculated on the assumption that chromium goes to the Cr^{3+} rather than to the Cr^{6+} state. Therefore, because at least part of the chromium has gone to the Cr^{6+} state, the corrosion shown in Figs. 103 and 104 is too high. From the nickel analyses, it is possible to check on the corrosion as measured by oxygen consumption and corrosion-pin weight changes. A comparison of the corrosion results obtained by these three methods is given in Table 41.

The bombs from Tests H-24 and H-26 were cut lengthwise through the center. Figure 105 is a photograph of the sections. An examination of the halves revealed that the corrosion attack had been quite even over the surface except for a small area at the bottom. However, the appearance at the bottom of the bomb where the weld had been made was not quite the same. That slight difference

TABLE 40. ANALYSIS OF THE CONTENTS OF BOMBS H-24 AND H-26 AFTER COMPLETION OF CORROSION TEST

Species	Method of Analysis	H-24		H-26	
		Starting Concentration (mg/ml)	Final Concentration (mg/ml)	Starting Concentration (mg/ml)	Final Concentration (mg/ml)
U	Colorimetric	40.22	40.0	40.3	40.4
SO_4^{--}	Ion exchange		17.5		17.8
Cu^{++}	Colorimetric	0.637	0.61	0.638	0.63
Ni^{++}	Colorimetric – diphenylcarbazide		0.20		0.25
Ni^{++}	Colorimetric – dimethylglyoxime		0.20		0.25
Ni^{++}	Polarographic		0.207		0.238
Cl^-	Potentiometric titration		<0.005		<0.005
CrO_4^{--}	Colorimetric		0.37		0.30
pH			3.0		2.8

TABLE 41. COMPARISON OF METHODS OF CORROSION MEASUREMENT

	Corrosion (mils)	
	H-24	H-26
Pin data	0.017	0.017
Ni^{++} analysis	0.013	0.016
O_2 consumption data (assuming all Cr goes to Cr^{3+} state)		
Normalized curve	0.016	
Raw data	0.013	0.019
O_2 consumption data (assuming all Cr goes to Cr^{6+} state)		
Normalized curve	0.013	
Raw data	0.011	0.016

was not unexpected since the welding heat treated that area for a distance of 1 or 2 cm.

Gas samples, collected after completion of the tests, have not been analyzed.

In-Pile Tests. Three solutions of 93.2% enriched UO_2SO_4, about 39 g of uranium per liter in concentration, were tested in Bombs H-22, H-27, and H-28 in facility HB-6 of the LITR. The flux was about 4.8×10^{12} neutrons/sq cm·sec, and the fission density varied from 6.39 to 6.44 kw/liter. Five stainless steel pins were added to each bomb. The results will be discussed in the order in which the experiments were made.

Tests H-22 and H-28. – The results of irradiations of Bombs H-22 and H-28 are given in Fig. 106 together with the out-of-pile results for purposes of comparison. Both radiation time and nonradiation time are included in the time axis. In Fig. 107, the corrosion in Bombs H-22 and H-28 is plotted against radiation time at 250°C. Since experimental conditions had been made as identical as possible for all tests, there is no obvious explanation for the differences between these runs. The simplest explanation is that exact reproduction of conditions between runs is virtually impossible. Inasmuch as the reactor is on and off at various intervals between the times that measurements were made, it may also be that differences in corrosion are a function of reactor down time. However, it should be emphasized that the true explanation is not yet known.

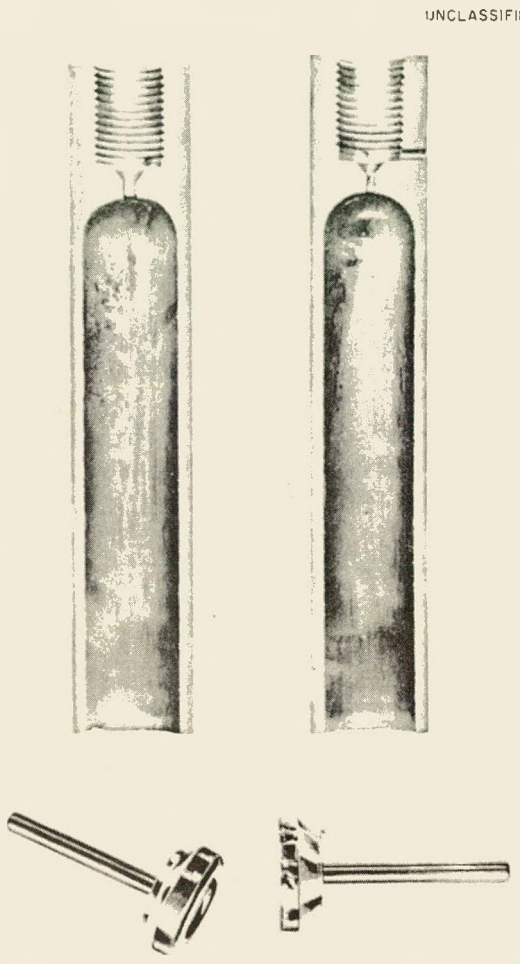

Fig. 105. Photographs of the Interiors of Two Out-of-Pile Tests.

Test H-27. – The results of Test H-27 are also plotted in Figs. 106 and 107. The test was terminated to avoid a depletion of oxygen which, in turn, would lead to a precipitation of uranium. The results from Test H-27 agree fairly closely with those from the two previous in-pile tests.

Pin-Weight Data from In-Pile Tests. – At the present time, the only pins which have been removed from the irradiated bombs and stripped are those from the bombs in Tests H-22 and H-28. The condition of the films on the in-pile pins was quite different from that on the out-of-pile pins; the films on the in-pile pins were much less adherent than those on the out-of-pile pins. Ninety per cent of the residual radioactivity of the pins taken from the pile was removed when the film was stripped off.

Since there was confusion as to the identity of the individual pins removed from the bombs in Tests H-22 and H-28 and since two of the pins were stripped to preserve the film, exact corrosion data for individual pins are not available. The corrosion on four pins in Test H-22 ranged from 0.038 to 0.074 mil, while the corrosion on four pins from Test H-28 ranged from 0.040 to 0.085 mil. These data compare favorably with the oxygen-pressure data of 0.061 and 0.063 mils for Test H-22 and Test H-28, respectively.

Analysis of the irradiated solutions has not been completed. Analysis of the contents of the bomb in Test H-22 indicated that there was a nickel concentration of 1.287 mg/ml. If it is assumed that the irradiated solution is completely recovered and equal to the original volume, there is a calculated corrosion of 0.065 mil, based on the analysis for nickel.

Figures 108 and 109 are photographs of the internal surfaces of the bombs used in Tests H-22 and H-28, respectively. Even though the surfaces, particularly those in Test H-28, were scratched in handling, there are readily observable differences between the results of the in-pile and out-of-pile tests, as indicated by a comparison of these figures with Fig. 105.

Summary of the Stainless Steel Corrosion Tests. It should be emphasized that the high corrosion rates exhibited in the in-pile tests do not necessarily mean that type 347 stainless steel cannot be used in a reactor which is intended to operate for a long period of time. The purpose of these tests was not to determine the conditions under which corrosion would be held to a minimum, but rather to determine whether the corrosion of type 347 stainless steel bombs, prepared under the simplest conditions of no pretreatment, would be different under in-pile conditions from that under out-of-pile conditions. On the basis of available data it must be definitely stated that radiation increases corrosion.

Zircaloy-2

Out-of-pile corrosion tests have been carried out on two Zircaloy-2 bombs, and no in-pile tests have been made. Because of experimental difficulties,

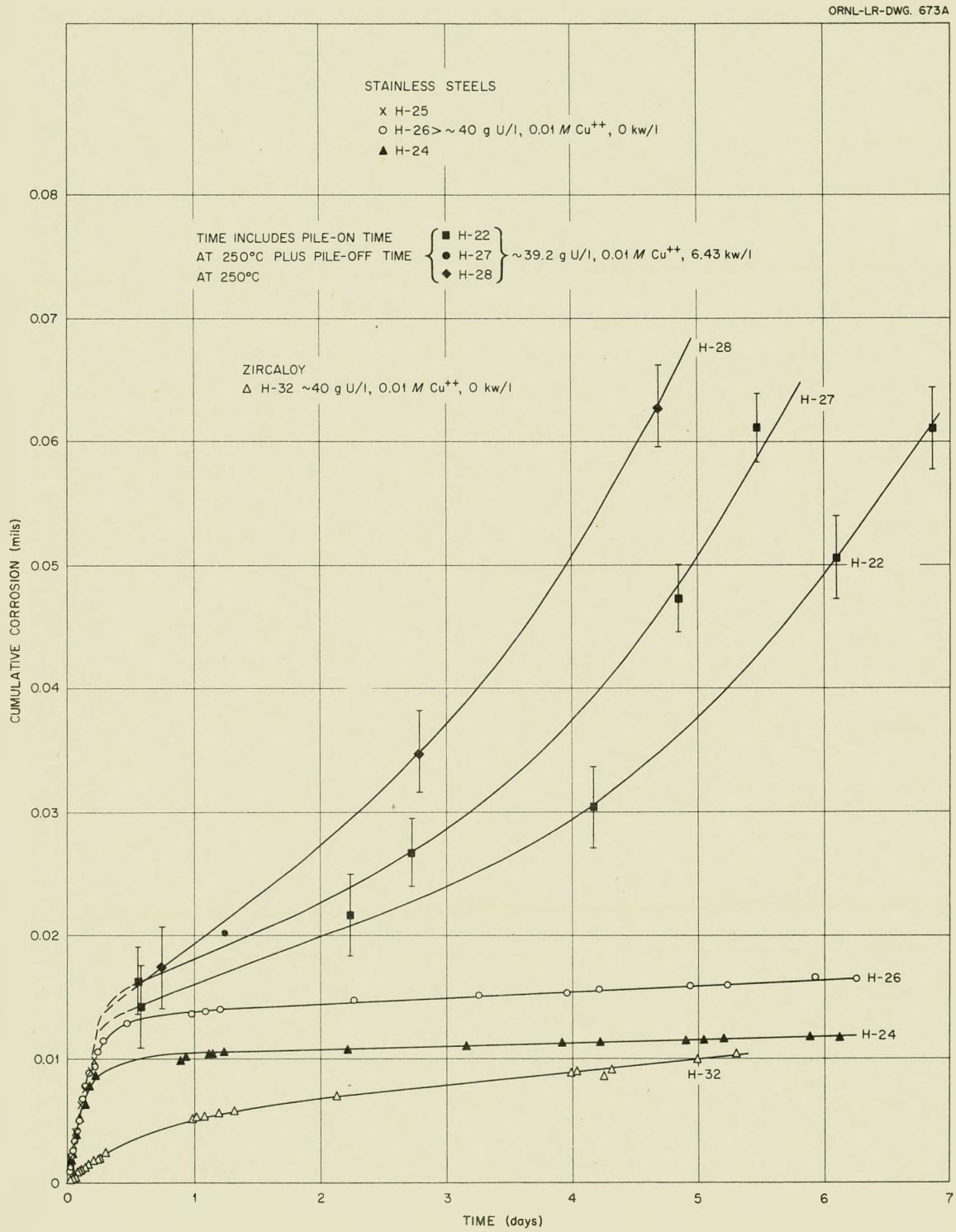

Fig. 106. Cumulative Corrosion Data for Tests H-22, H-24, H-26, H-27, H-28, and H-32.

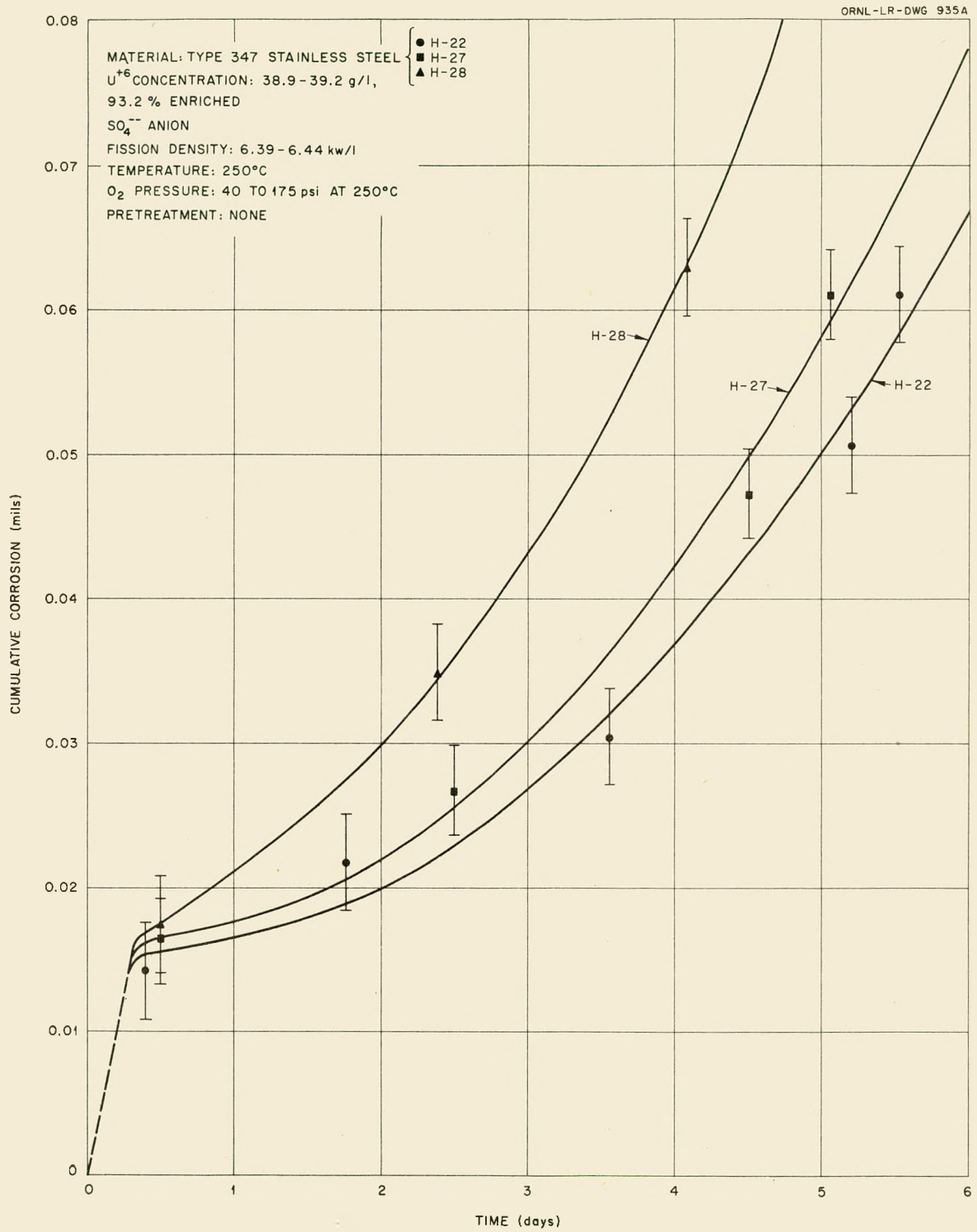

Fig. 107. Cumulative Corrosion Data for Tests H-22, H-27, and H-28.

UNCLASSIFIED

Fig. 108. Photograph of the Interior of Bomb H-22.

UNCLASSIFIED

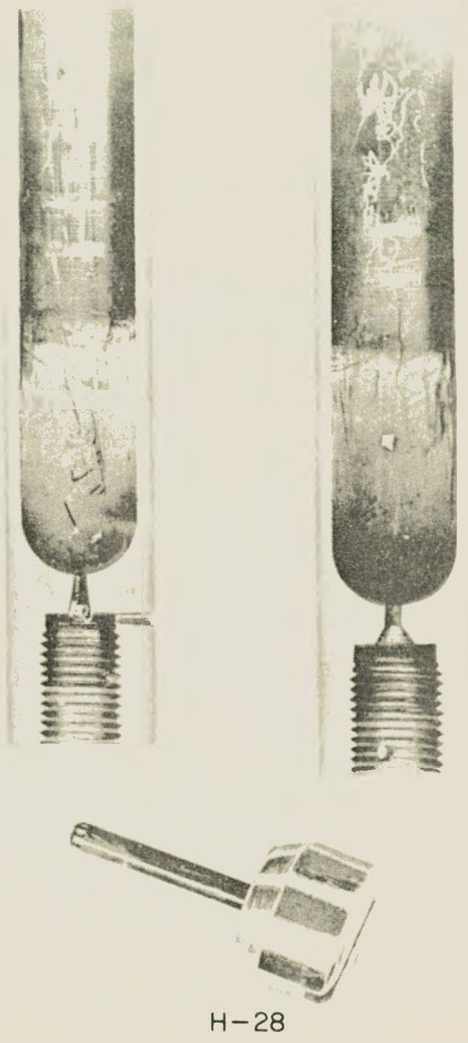

Fig. 109. Photograph of the Interior of Bomb H-28.

these first out-of-pile tests are not sufficiently accurate to serve as controls for in-pile tests.

Test H-32. – Out-of-pile tests with Zircaloy bombs were made with the same stock uranyl sulfate solution and under the same test conditions as those in the tests with stainless steel bombs.

Test H-32 was terminated after 5.3 days because of a leak in the capillary tubing. The data obtained up to that time are presented as the bottom curves in Figs. 103 and 106.

The bomb was sawed open in the usual manner, and it was observed that the Zircaloy was covered with an even, blue film. Metallographic examination is not yet complete.

Test H-33. – Quantitative oxygen pressure data were not obtained in this test because the internal circuits of the Baldwin cell failed immediately after the bomb was placed in the thermostat. A second Baldwin cell was attached to the bomb by use of the proper valves. The pressure values obtained from this cell were quite erratic, and the initial values are valid only if little or no oxygen was ever present in the bomb.

Nevertheless, the bomb was allowed to remain at 250°C for 14 days. Then it was removed from the thermostat and was found to contain only about six-tenths of the initial volume of the solution. Much of the uranium had precipitated. It was later found that the capillary tubing between the connecting valve of the faulty Baldwin cell and the valve attached to the second Baldwin cell had a small leak in the wall. Either the leak was very small or it did not develop until late in the run because several cubic centimeters of solution remained in the bomb. At any rate, it can be concluded that the Zircaloy bomb had been subjected to essentially reducing conditions for some time, possibly the full 14 days.

In order to estimate the amount of corrosion undergone by the Zircaloy bomb, the original weight of the bomb was compared to its weight after the test was completed. On the assumption that no ZrO_2 or SnO_2 had gone into the solution, the cumulative corrosion for 14 days was calculated to be 0.006 mil. Since part of this film could be precipitated uranium, this amount of corrosion could be excessive. However, this point has not yet been checked.

Analysis of the solution which remained revealed the presence of extremely large amounts of Ni^{++} – almost twice as much as that found in the stainless steel bombs. Since the nickel content is very low in Zircaloy-2, it is believed that the nickel may have come from the stainless steel swage fitting located at the end of the connecting capillary tubing. Thus there is the possibility that calculated corrosion rates may be erroneously interpreted when a bomb is constructed of an alloy different from that which makes up the connecting fitting. This might apply to titanium as well as Zircaloy-2 bombs, and the possibility of using titanium and Zircaloy fittings and tubing is being investigated.

The interior of the bomb in Test H-33 was covered by a uniform, green film. Metallographic examination is not yet complete.

THORIUM NITRATE RADIATION STUDIES

J. W. Boyle

The studies on gas production from the reactor irradiation of uranyl solutions showed that an appreciable quantity of nitrogen gas was liberated from the more concentrated solutions of uranyl nitrate.[1] This has caused some concern over the possible production of free nitrogen from solutions of thorium nitrate. Thorium nitrate, containing only low-cross-section N^{15}, is the only low-cross-section thorium compound sufficiently soluble in water which will give concentrations of thorium high enough for successful U^{233} breeding. Because of the cost of separating N^{15} from natural nitrogen, any N_2 formed during irradiation would have to be saved and reconverted to nitrate.

The major effort to date has been on the development of a reliable analytical technique for the measurement of the decomposition gases. A method of microanalysis for mixtures of H_2, O_2, N_2, NO, N_2O, NO_2-N_2O_4, CO, and CO_2 has been worked out; by this method 10^{-3} cc (at STP) of these components can be analyzed quantitatively, with an accuracy of 10%. Greater accuracy can be obtained with larger amounts. The oxides of nitrogen cause the most trouble. Nitrous oxide, the most inert gas of those listed, is difficult to measure quantitatively because of its physical and chemical similarity to CO_2 (a component always found in small quantities in irradiated aqueous solutions). Nitrogen dioxide and its dimer, nitrogen tetroxide, are considered together and are hereafter referred to as nitrogen dioxide. It is a reactive condensable gas which reacts with both mercury and stopcock grease and therefore is troublesome in the ordinary vacuum system which uses mercury to push the gases through the system. Nitric oxide reacts with oxygen; so it can be present only in the absence of oxygen.

A brief description will be given of the analysis of each component. As the mixture contains both condensable and permanent gases, the two are separated at the start and analyzed separately. In general, the permanent gases are present in much larger amounts than are the condensable gases.

A micro-introductor[2] has proved invaluable in analyzing both the permanent and condensable gases. It is a device for obtaining gas bubbles 10^{-4} cc (at STP) in volume or larger. The quantitative addition of any gaseous reagent is made by this apparatus.

[1] J. W. Boyle *et al.*, *Reactor Sci. Technol.* 3, No. 1, 32 (March 1953), TID-2008.

[2] J. C. P. Mignolet, *Trans. Faraday Soc.* 45, 271 (1949).

Permanent Gases

The permanent gases are those which are still gaseous, having a vapor pressure greater than 10^{-2} mm Hg, at –196°C (liquid nitrogen) and consist of H_2, O_2, N_2, CO, and NO.

Hydrogen. Experience has shown that there is an excess of oxygen over the equivalent amount of hydrogen present in gas samples from irradiated $Th(NO_3)_4$ solutions. The hydrogen content of the permanent-gas component is found by igniting the sample on a platinum filament at an incipient glow for several minutes. Hydrogen is burned to water and is condensed out in a cold trap. Therefore two-thirds of the pressure decrease is traceable to the hydrogen originally present.

Oxygen. The oxygen which remains after the hydrogen determination is made is found by adding a slight excess of hydrogen gas by means of the micro-introductor and reigniting on the platinum filament. The oxygen originally present is equal to one-third of the sum of the two ignitions – the ignition in the hydrogen determination plus the ignition after the introduction of hydrogen.

Nitrogen. Nitrogen is determined by difference after all the other gases have been measured. Thus errors in the determination of the other components will show up also in the nitrogen analysis. It is also evident that initial deaerating of samples is extremely important. Degassing blanks on several samples showed that less than 10^{-4} cc of $N_2 + O_2$ was present at the start.

Carbon Monoxide and Nitric Oxide. Experience has shown that these two gases are absent. Nitric oxide cannot coexist with oxygen, and inasmuch as large amounts of oxygen are formed from the decomposition of water, no nitric oxide, as such, exists in the gas samples. Carbon monoxide has not been detected in any of the samples so far but, if present, would be determined as CO_2 after the ignitions.

Condensable Gases

The condensable gases at –196°C are CO_2, N_2O, and NO_2. An instrument which has proved very useful in identifying condensable gases is the Pirani gage. The gas in question is condensed out completely (vapor pressure $< 10^{-4}$ mm Hg), and a plot of pressure (microamperes on the Pirani gage) vs temperature is taken. If the warming rate is not too fast (~ 1½ deg/min) and the volume of gas phase is not too large (a few cubic centimeters), then equilibrium between the vapor and solid is maintained and a saturated vapor-pressure curve which is characteristic of the gas is obtained. This is a physical method which leaves the material unaltered for further chemical test if desired. The Pirani gage used in this work is capable of measuring pressures from 10^{-4} to 0.5 mm Hg. A volume of 10^{-4} cc of gas at STP is sufficient to give a positive indication of the presence of a particular condensable gas if there is no interfering gas present. Interfering gases are those which have boiling points within 10 to 20 deg of each other, as, for example, carbon dioxide and nitrous oxide.

Carbon Dioxide–Nitrous Oxide. After the analysis of the permanent gases is complete, carbon dioxide and nitrous oxide are collected by fractional distillation – warming the cold trap in which they are contained from –196 to –130°C. At –130°C, nitrogen dioxide and water are completely condensed out, whereas nitrous oxide and carbon dioxide are gaseous. A vapor-pressure curve is prepared as outlined above, and if only carbon dioxide is present, it is evident from the curve; then all the condensable gas collected is carbon dioxide. If nitrous oxide is present alone or in mixture with carbon dioxide, the analysis cannot be completed by the vapor-pressure curve alone.

There are two possible ways to analyze the mixture. The basis for the first method is that nitrous oxide decomposes spontaneously, but at a measurable rate, when heated, whereas carbon dioxide is stable.

$$N_2O \xrightarrow{\Delta} N_2 + \tfrac{1}{2}O_2$$

There is a net increase in pressure – the increase being equal to the amount of oxygen formed, or one-half the amount of nitrous oxide originally present. The ignition, best at a red heat, should be carried to completion (until no further increase in pressure is noted), but prolonged heating should be avoided. The carbon dioxide can then be condensed out with liquid nitrogen at –130°C; this leaves an amount of nitrogen and oxygen equal to three times the net increase on ignition. A vapor-pressure curve on the condensed gas will show whether the destruction of nitrous oxide was complete and whether the condensed gas is carbon dioxide. If hydrogen is added, one-third of the permanent gases will react with the hydrogen, leaving the inert nitrogen unreacted.

In the second method, an excess of hydrogen is added initially and ignited on a platinum filament, with a cold trap present at –130°C.

(1) $CO_2 + H_2 \xrightarrow{\Delta} CO + H_2O$

(2) $N_2O + H_2 \xrightarrow{\Delta} N_2 + H_2O$

Because the water is condensed out as it forms, reaction 1 will continue to completion instead of reaching an equilibrium dependent upon temperature as in the water-gas reaction.[3] A higher temperature is needed for reaction 1 in contradistinction to the commercial water-gas reaction. Inasmuch as the volume change is the same for both reactions, nothing definitive is learned from this alone. If the gases are cooled to –196°C, neither carbon monoxide nor nitrogen can be condensed out. However, if oxygen is added and ignited, the carbon monoxide is oxidized back to carbon dioxide, whereas the nitrogen is unaffected. The carbon dioxide can then be condensed out and measured separately, and the volume of nitrogen can be determined by difference.

Nitrogen Dioxide. Because nitrogen dioxide reacts readily with stopcock grease and with mercury, it is difficult to determine the amount present before any reaction takes place. In an attempt to circumvent this difficulty, stopcock grease has been replaced with silicone grease and the nitrogen dioxide is converted to a less reactive gas before it comes in contact with mercury or mercury vapors.

Before the sample is broken open, the system is thoroughly evacuated and the mercury vapors are condensed out in a liquid-nitrogen trap. A second liquid-nitrogen trap in the mercury-free part of the system is used to entrap the condensable gases when the permanent gases are pumped over and analyzed. The nitrogen dioxide is allowed to vaporize into a reagent of cesium hydroxide[4] whereupon the following reactions occur:

$$3NO_2 + 2CsOH \longrightarrow 2CsNO_3 + NO + H_2O$$

$$4NO + 2CsOH \longrightarrow 2CsNO_2 + N_2O + H_2O$$

Further work is needed to check these reactions thoroughly, but they appear to be reliable for the few samples run so far. Unfortunately, 12 nitrogen dioxide molecules are needed to obtain one measurable nitrous oxide molecule, but a measurable product is obtained. The reaction should be carried out at room temperature because elevated temperatures cause side reactions which lead to the formation of nitrogen gas.

It is also possible to convert the nitrogen dioxide to nitric oxide and then to measure that gas.

Sample Analysis

The analysis of the gases, in cubic centimeters at STP, from a thorium nitrate solution which was irradiated in facility C-44 of the LITR for 93 min at 3000 kw is listed below (Th concentration = 300 g/liter; D = 1.50; flux = 2.8×10^{13} neutrons/sq cm·sec; Co monitor):

H_2	0.726
O_2	0.397
N_2	0.014_7
CO_2	0.002_7
N_2O	0.005_5
NO_2	0.015_6

Hydrogen Yield

The number of molecules of hydrogen for each 100 ev of energy absorbed, G_{H_2}, has been calculated for a 2.15 *M* thorium nitrate solution irradiated in hole 12 of the ORNL Graphite Reactor. The energy was calculated by multiplying the calorimetric value for pure water[5] by the ratio between the fluxes for the sample and that for the calorimetric measurement. It was estimated[5] that the energy absorbed by the thorium nitrate solution was 82% of that for pure water under the same flux. The value for G_{H_2} was found to be 0.04, which is an order of magnitude lower than would be expected on the basis of a uranyl nitrate solution of comparable concentration.

Nitrogen Yield

The value for G_{N_2} in the LITR has been calculated in two different ways, the two methods differing by a factor of 2.7. The discrepancy arises from the estimation of energy absorbed by the solution. The first method, which gives the lower

[3] S. Glasstone, *Textbook of Physical Chemistry*, 2d ed., p 824, Van Nostrand, New York, 1946.

[4] E. Barnes, *J. Chem. Soc.* 1931, 2605.

[5] D. M. Richardson, *Calorimetric Measurement of Radiation Energy Dissipated by Various Materials Placed in the Oak Ridge Pile*, ORNL-129 (Oct. 1, 1948).

G_{N_2} value (higher estimation of energy) of 0.002 for 2.15 M $Th(NO_3)_4$, was based on the assumption that the yield for hydrogen per 100 ev is the same in the LITR and in the ORNL Graphite Reactor. This assumption probably leads to too low an energy estimation in the LITR as the ratio of y/n is much greater in the LITR than in the ORNL Graphite Reactor, and the gas yield for gammas is probably lower than for neutrons.

The second method, which gives the higher G_{N_2} value (lower estimation of energy) of 0.005, is based on a calorimetric measurement[6] in facility HB-2 which was 0.19 w/g at 1.5 Mw reactor power. The assumption is made that the energy in facility C-44 is the same as that in facility HB-2. The proper value for G_{N_2} probably lies between the two values quoted.

The nitrogen yields were calculated for two concentrations, 2.15 and 1.29 M $Th(NO_3)_4$, for which it was assumed that there was the same energy input per gram of solution, and were found to be directly proportional to the concentration. The assumption that the energy absorbed per gram was the same for the two concentrations is probably true within a few per cent. It was found[6] that in facility HB-2 the material made little difference in the amount of energy absorbed per gram.

The reduction of carbon dioxide by hydrogen on a hot (barely visible) platinum wire is of interest in gas analysis. This reaction proceeds at a measurable rate, but improper interpretations of results can be made if it is assumed that carbon dioxide is inert. Depending on the temperature, an equilibrium is reached if the water vapor is not condensed out as it forms.

THE UO_3-SO_3-H_2O SYSTEM ABOVE 300°C

G. M. Hebert D. W. Sherwood

Attempts to build a suitable large pressure vessel equipped with long (4 in.) viewing windows have continued. The previously reported model (ORNL-1658) proved unsatisfactory on heating, apparently due to a flexing of the metallic parts which cracked the viewing window. Variations of this model were subsequently made which involved several methods of forcing the glass window against the gold sealing gasket (unsupported-area principle of Bridgeman). However, in each case the pressure was either insufficient to form the initial seal or the glass cracked because of the bending of the supporting metal. Finally, a new type 347 stainless steel supporting flange was made from 2-in.-thick sheet stock, but even this extreme thickness was found to bend sufficiently to break the heavier (0.700-in.-thick) glass when the metallic parts were bolted together. Examination of the assembled apparatus with polarized light indicated that there were severe pressure-induced strain patterns in the window and that significant strains were introduced when the bolts were tightened or the assembly lightly clamped. It appears that this method of mounting large windows is impractical without the use of gasketing materials which are much softer than any known to date and which are as able to withstand the proposed working temperatures. (Our experience here agrees with that of personnel at the Mound Laboratory who found that they were not able to use gold gaskets against glass in a vessel designed for lower working temperatures.)

The American Instrument Co., Inc., has indicated that they are willing to attempt to fabricate the desired vessel but will not guarantee the results. In view of these difficulties, this approach for obtaining pressure-volume-temperature data for uranyl sulfate systems in the two-phase region has been abandoned, at least for the present, and other approaches have been tried.

After consideration of indirect methods for determining liquid levels in the two-phase region of uranyl sulfate solutions, experiments were undertaken to measure the electrical properties of the phases in high-frequency fields. A quartz tube filled with solution was mounted in a viewing furnace with a suitable mechanism to enable controlled vertical movement of the tube. Leads from a 100-Mc oscillator were brought into the furnace through a coaxial "cable," which consisted of a copper tube containing tubular ceramic insulators and a concentric wire. At the end of the copper tube a small coil (three to four turns) was connected in such a way that the quartz tube, which acted as the core of the coil, was allowed to move vertically. Measurement of the inductance of the core was achieved by coupling a coil of three turns to the tank circuit of the oscillator. The coil is supplied with leads to a galvanometer whose deflection was an indication of the power being

[6] J. B. Trice, F. W. Smith, and F. J. Muckenthaler, *Solid State Semiann. Prog. Rep. Aug. 1, 1953*, ORNL-1606, p 25.

furnished by the oscillator. Definite differences in the inductance of the coil in the furnace were found when light and heavy phases of the uranyl sulfate solution were moved into the core region; however, the changes were not so large nor was the phase interface so sharply defined as were desired.

Two horizontal-and-parallel silver wires were then substituted for the coil in the furnace in such a way that they formed condenser plates with the quartz tube which moved vertically between them. With the circuits properly tuned (by approximation only with this apparatus), quite large differences in dielectric properties were found when the three phases were successively presented to the condenser. Inasmuch as large differences in the dielectric properties of two normal aqueous solutions of electrolytes were expected, this may be an indication of the condition of the heavy phase. In other words, it would not seem to be a solution of a dissociated electrolyte – a condition which is perhaps worthy of further investigation. However, while the "break" between the liquid phases could be made quite sharp, as indicated by the galvanometer, it did not coincide with the actual movement of the phase interface between the condenser wires. This lack of coincidence has been attributed to a probable bending of the electric field through the phase of higher dissociation which may have actually passed the horizontal plane of the condenser. It was concluded that the method showed promise but would require extensive development for application as a detector for this work.

During this period the high-pressure testing unit used by the group has been refurbished, the gages have been calibrated, and an automatic cut-off device has been installed which will limit, at a predetermined value, the pressure developed. Suitable valves and tubing have been installed which will allow small increments of pressure change in an attached vessel that will serve as a pressure-balancing unit in subsequent high-temperature vapor-pressure determinations.

At present, work is in progress to determine the volumes of the three phases of a tube of uranyl sulfate solution as a function of the fractional filling of the tube. It is hoped to couple these values with vapor-pressure measurements, in correspondingly fractionally filled vessels. Such a procedure would allow exact calculations of volumes and concentrations of the phases in equilibrium at several temperatures in the region in question to be made. This is admittedly a somewhat tedious method for ascertaining the desired answers but appears to be the most practical of those considered and attempted.

AN ALTERNATE METHOD FOR THE DETERMINATION OF THE COMPOSITION, VOLUME, AND DENSITY OF THE THREE PHASES IN THE UO_3-SO_3-H_2O SYSTEM ABOVE 300°C

D. M. Richardson

Consider three identical closed vessels, each of which contains the same fractional filling with the same solution of uranyl sulfate. Alternatively, vessels of different volume could be used, provided they contained the same fractional filling.

When at equilibrium at a given temperature, in the two-liquid-phase region, each vessel is sampled by separation into two disconnected, sealed volumes. In the first vessel a portion of the heavy phase is separated, in the second vessel the entire heavy phase and part of the light phase are separated from the remainder, and in the third vessel the entire heavy phase and a larger part of the light phase are separated from the remainder.

After cooling to room temperature, the concentration in weight per cent and the volume, corrected to the sampling temperature, are determined for each of the samples.

From the first sample the concentrations of the three components in the heavy phase are now known to be (C_A^b), (C_B^b), and (C_C^b).

From the second and third samples the concentrations of the three components in the light phase are obtained by difference as follows:

$$V_3(C_A)_3 - V_2(C_A)_2 = [V_3 - V_2](C_A^1) ,$$

$$(C_A^1) = \frac{V_3(C_A)_3 - V_2(C_A)_2}{V_3 - V_2} ,$$

for component A, and similarly for the other components.

The volume of the heavy phase can now be calculated by difference as follows:

$$V_3(C_A)_3 - V^b(C_A^b) = [V_3 - V^b](C_A^1) ,$$

$$V^b = \frac{V_3(C_A^1) - V_3(C_A)_3}{(C_A^1) - (C_A^b)} .$$

When one component is nonvolatile, as component A (or UO_3), the volume of the light phase can be calculated in the following manner:

Let W_A equal the total weight of the nonvolatile component A in a given vessel. Then

$$V^b(C_A^b) + V^1(C_A^1) = W_A \ ,$$

$$V^1 = \frac{W_A - V^b(C_A^b)}{(C_A^1)} \ .$$

The volume of the gas phase is now obtained by difference as follows:

$$V^g = V - V^b - V^1 \ .$$

The volatile-component concentrations can now be calculated in the following manner:

Let W_B equal the total weight of the volatile component B in a given vessel. Then

$$V^g(C_B^g) + V^1(C_B^1) + V^b(C_B^b) = W_B \ ,$$

$$(C_B^g) = \frac{W_B - V^1(C_B^1) - V^b(C_B^b)}{V^g} \ ,$$

for component B, and similarly for the other components.

It is assumed that the volume changes which occur in the act of sampling do not result in immediate changes of liquid-phase compositions. The initial effect of a volume decrease is assumed to be condensation in the gas phase and is followed by slower diffusion through the liquid phases.

This method places stringent demands on experimental accuracy since it involves the taking of differences. In addition, the high pressure and the corrosive nature of these liquids require special materials and techniques. Several experimental approaches are being investigated.

The method can also be applied to a three-component solubility study where the three phases are solid, liquid, and gas.

THE ACIDITY OF UO_3-SO_3-H_2O MIXTURES AT 25°C AND ITS APPLICATION TO THE DETERMINATION OF THE SOLUBILITY OF UO_3 IN DILUTE SULFURIC ACID

W. L. Marshall

The acidity of uranium trioxide–sulfuric acid–water mixtures has been determined to an accuracy of ±0.005 pH units from 0.024 to 10^{-4} *m* sulfuric acid and at UO_3/SO_3 mole ratios from 0.70 to 1.20. Deductions from these data concerning the hydrolysis of uranyl sulfate will be discussed in a forthcoming ORNL report.

The solubility of UO_3 in dilute sulfuric acid at elevated temperatures (150 to 300°C) has been determined by isolating a UO_3-saturated sample, cooling to 25°C, determining the pH, and comparing the results with the pH data mentioned above. By this method several isotherms in the concentration range from 0.02 to 10^{-4} *m* have been obtained. Details of the method and the data will be presented in an ORNL report.

PHASE EQUILIBRIA OF URANIUM TRIOXIDE AND AQUEOUS HYDROFLUORIC ACID IN STOICHIOMETRIC CONCENTRATIONS

W. L. Marshall C. H. Secoy

Experimental data have been reported on the phase equilibria for uranyl fluoride in water from the ice eutectic to the critical temperature of the system.[7] These data indicated the ice-eutectic temperature, the presence of three solid hydrate phases of uranyl fluoride and a two-liquid-phase region, and the critical temperature for various initial concentrations. Data were also presented to show the formation of a compound, uranyl orthosilicate trihydrate,[7,8] by reaction of the solutions with the silica-tube containers at the elevated temperature. At the time this work was carried out, the experimental technique was such that, by necessity, the solutions were in contact with silica containers for several hours at temperatures between 100 and 400°C. That period of time was sufficient to allow considerable reaction with the tube to take place and to produce the silicate compound. It had been assumed that the solid phase observed in the dilute region at the elevated temperature was due entirely to this reaction and that no solid phase would appear in a system in which an inert container was used to hold the solution.

Since then, several new techniques have been developed which do not involve the long periods of time necessary to reach the higher temperatures.

[7] W. L. Marshall, J. S. Gill, and C. H. Secoy, *Chem. Quar. Prog. Rep. June 30, 1950*, ORNL-795, p 22.

[8] W. L. Marshall and J. S. Gill, *Chem. Quar. Prog. Rep. Sept. 30, 1950*, ORNL-870, p 23; *Chem. Quar. Prog. Rep. Dec. 31, 1950*, ORNL-1036, p 15.

By the use of the semimicro phase-study apparatus,[9] it has been possible to obtain data reproducible to ±1°C on the two-liquid-phase portion of the system. With this apparatus, only short times of exposure were required for each determination, thereby eliminating essentially all the interference due to the reaction with the container vessel. By use of filtration techniques within titanium bombs[10] and also by use of a direct-sampling technique, it has been possible to obtain solid-phase samples which correspond to compounds other than the silicate previously reported and which are an *integral* part of the phase equilibria of the system UO_3-HF-H_2O. The revised data are listed in Table 42 and are shown graphically in Fig. 110. These data are more accurate than those reported previously and definitely indicate a solid phase, represented along line *AB*, which cannot, in any way, be attributed to reaction with silica. The appearance and disappearance of the solid phase along this line are reversible in less than 30 min; this was not the case with uranyl orthosilicate, which was obtained only after holding the solution in silica containers for several hours between 200 and 350°C.

[9]W. L. Marshall, H. W. Wright, and C. H. Secoy, *J. Chem. Educ.* 31, 34 (1954).

[10]J. S. Gill, E. V. Jones, and W. L. Marshall, *HRP Quar. Prog. Rep. March 31, 1953*, ORNL-1554, p 99.

Solid Phase in Dilute Region

Samples of the solid phase in the dilute region have been obtained by removing the solution at the equilibrium temperature by means of a stainless steel capillary sampling tube. The bomb was then cooled to room temperature, and the crystals of solid phase were removed and analyzed for uranium and fluoride. Reduction of the uranyl ion in solution is prevented by adding 2 cc of 30% hydrogen peroxide to 50 cc of uranyl fluoride solution in the 100-cc bomb. The peroxide decomposes above 100°C to produce oxygen. Analytical data are given in Table 43. A picture of the solid phase is shown in Fig. 111. H. L. Yakel of the Metallurgy Division has done much work on the lattice dimensions and, at M. A. Bredig's suggestion, has postulated a solid solution. The analytical data given in Table 43 and shown in Fig. 112 verify this solid-solution concept and indicate that

TABLE 42. REVISED PHASE-EQUILIBRIA DATA FOR AQUEOUS SOLUTIONS CONTAINING TWO MOLES OF HF PER MOLE OF UO_3

UO_2F_2 (wt %)	Temperature (°C)	Phases Appearing or Disappearing	Solidification Temperature, Invariant Point (°C)	Critical Point (°C)
68.95	331	Aqueous	334	
66.3	327	Aqueous	333	376
58.42	321	Aqueous	333	376
52.75	320	Aqueous	334	377
48.17	319	Liquid salt	334	376
43.40	318	Liquid salt	334	376
38.45	317	Liquid salt	333	376
33.66	316	Liquid salt	333	376
29.06	316	Liquid salt	333	376
24.53	316	Liquid salt (solid solution forms shortly after)	333	374
19.49	319	Liquid salt (solid solution forms immediately after)		
19.49	297	Solid solution		
13.94	272	Solid solution		
9.51	256	Solid solution		
4.99	232	Solid solution		
Below 4.99	Below 232	UO_3 hydrate?		

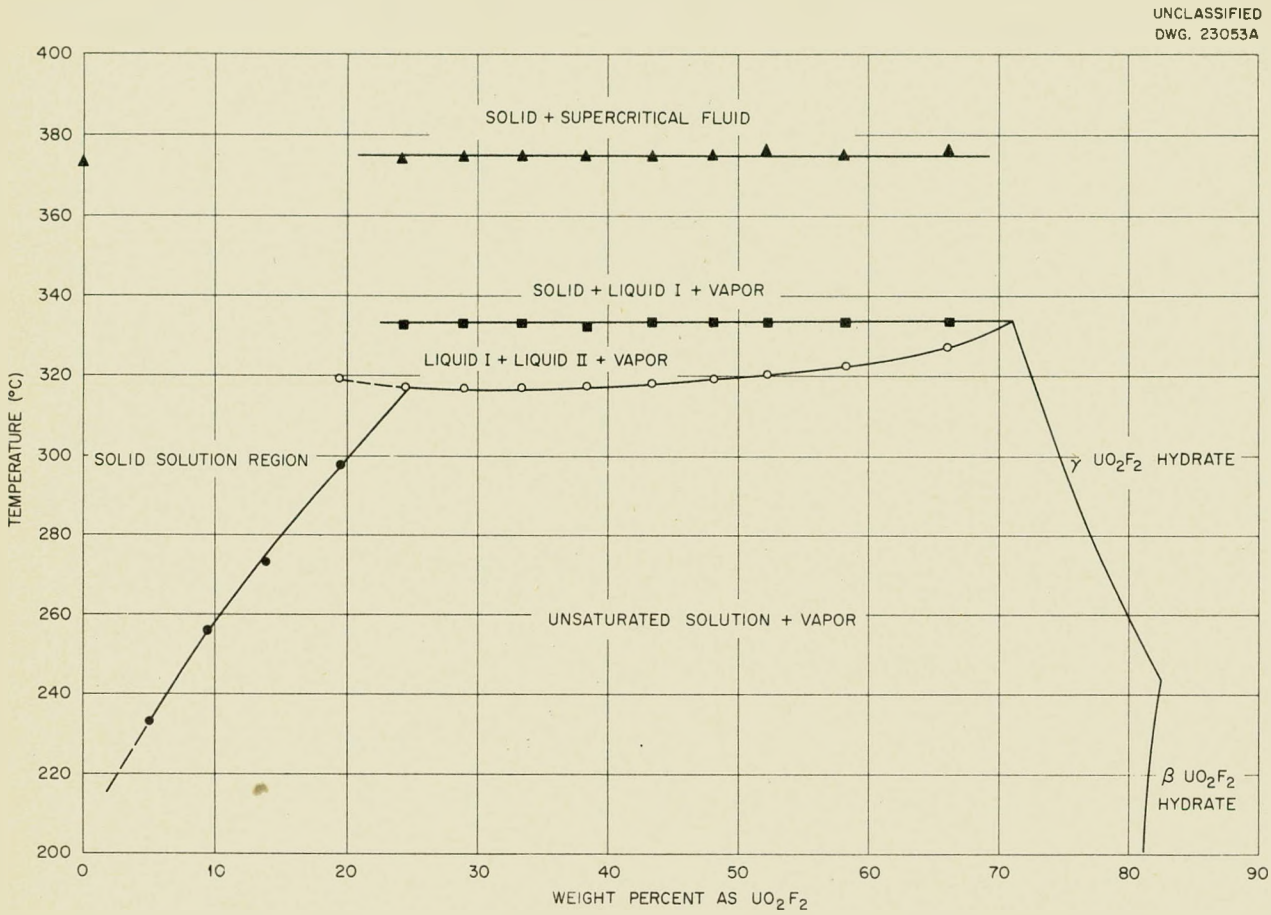

Fig. 110. Revised Phase-Equilibria Data for Aqueous Solutions Containing 2 moles of HF per mole of UO_3.

TABLE 43. SOLID-SOLUTION ANALYTICAL DATA – SYSTEM UO_3-HF-H_2O

Uranium (wt %)	Fluoride (wt %)
78.29	0*
77.33	1.61
76.99	2.10
76.26	2.62
77.18	3.57
77.36	3.35
76.02	4.39
75.04	6.31
75.56	6.03**
73.01	11.65***

*Theoretical $UO_2(OH)_2$.
**Theoretical $UO_2(OH)F \cdot \frac{1}{2}H_2O$.
***Theoretical $UO_2F_2 \cdot H_2O$.

one exists between $UO_3 \cdot H_2O$ and either $UO_2(OH)F \cdot \frac{1}{2}H_2O$ or $UO_2F_2 \cdot H_2O$.

Conclusions

Previous findings on the system UO_2F_2-H_2O, that dilute concentrations of UO_2F_2 in H_2O are phase-stable up to the two-liquid-phase temperatures, are in error. Instead, solutions more dilute than 25% yield a solid phase at temperatures indicated by line *AB* of Fig. 110 well below the two-liquid-phase region. The analytical data shown in Fig. 112, as well as conclusions drawn from x-ray diffraction data, indicate that a solid solution occurs in this region.

UNCLASSIFIED
T-1753

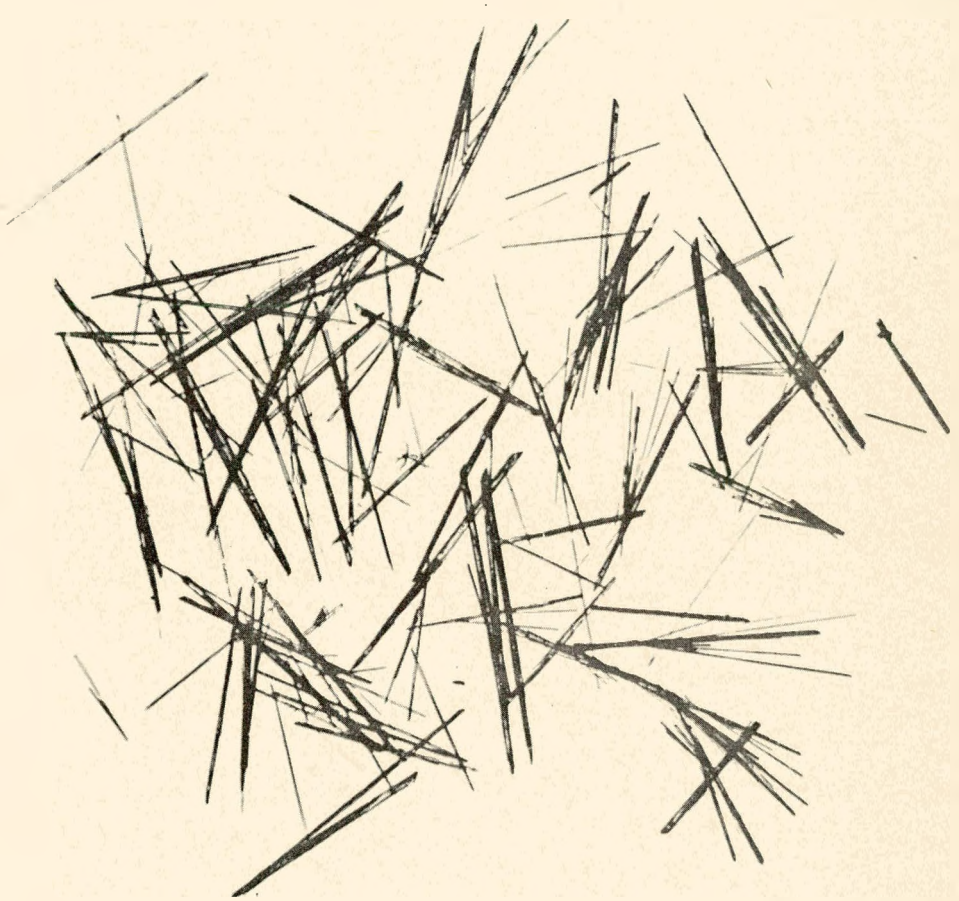

Fig. 111. Photomicrograph of Solid-Solution Crystals.

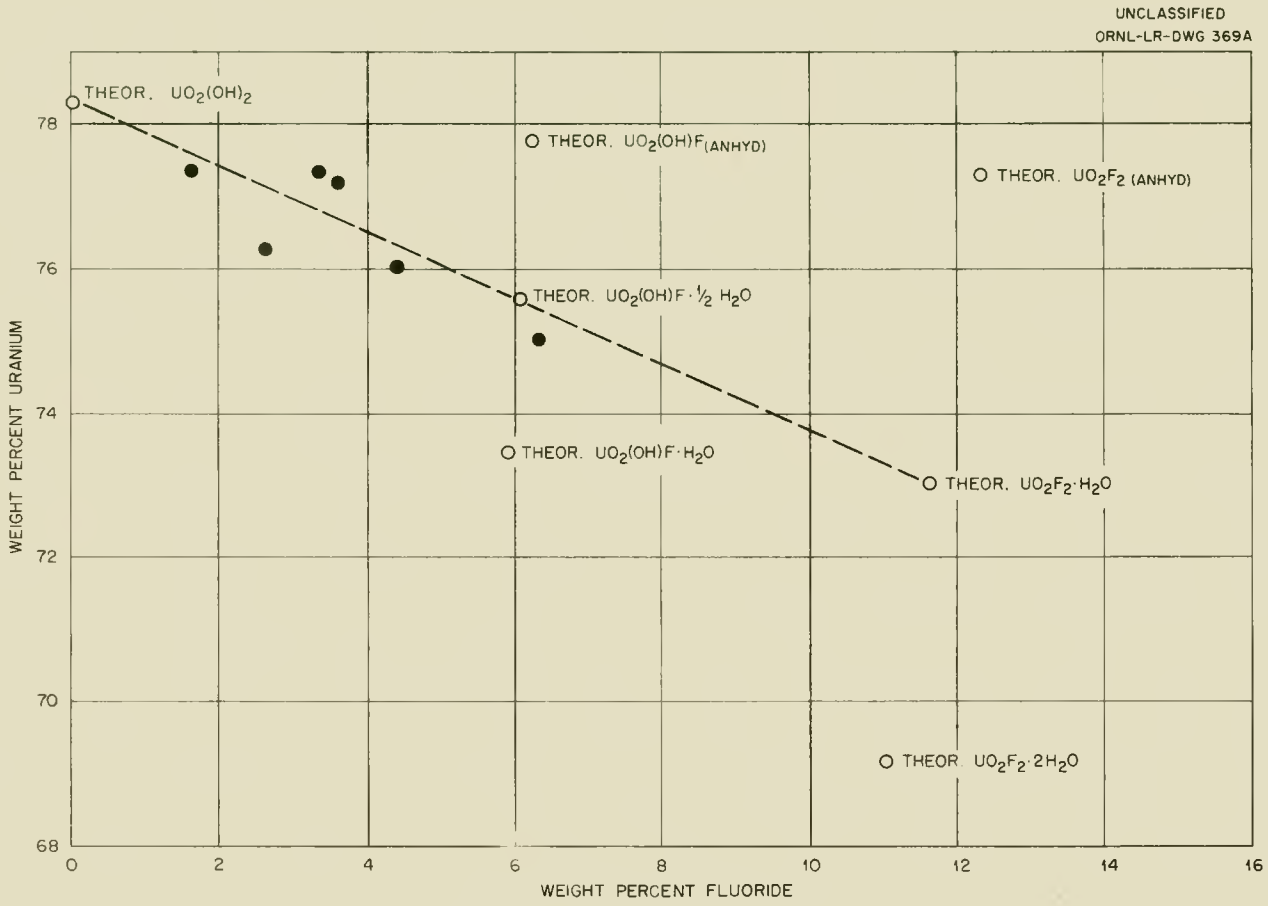

Fig. 112. Solid-Solution Analytical Data for the System UO_3-HF-H_2O.

THORIUM OXIDE BLANKET DEVELOPMENT

R. N. Lyon, Section Chief
A. S. Kitzes, Group Leader
S. R. Buxton[1] C. A. Gifford
P. R. Crowley W. Q. Hullings
R. B. Gallaher S. A. Reed
Reactor Experimental Engineering Division

D. E. Ferguson, Assistant Section Chief
R. G. Mansfield L. E. Morse
J. P. McBride W. L. Pattison
Chemical Technology Division

LOOP TESTS

Two loops described in a previous report[2] have been in operation with thorium oxide screened through 100 mesh; the actual size of the particles was 100 to 200 Å. The ThO_2 slurries were circulated without difficulty, and the concentrations have been essentially constant except for those runs in which a titanium impeller was used and plating-out of the solids on the walls of the pipe was observed. However, this phenomenon has been an exception rather than a rule, and the cause for the plating-out of solids is still unknown. Examination of the cake removed from the pipe walls revealed nothing to explain the plating out; the solids consisted of thorium oxide and the corrosion products of stainless steel. In all runs, the Graphitar or Stellite 98M2 bearings were continually lubricated with water that was supplied by condensing steam from the pressurizer; both the front and back bearings showed no wear after 500 hr of operation and are still in use. The life of the bearings has been prolonged by careful dynamic balancing of the pump impeller and rotor and by replacing the stainless steel wear rings with titanium.

Table 44 is a summary of the results of the runs in which thorium oxide, prepared by various methods, was circulated at 250°C. In each run, the test was arbitrarily stopped after 140 hr of operation because these runs were made to compare oxides prepared by the different methods.

[1]On loan from Chemistry Division.

[2]R. N. Lyon *et al.*, *HRP Quar. Prog. Rep. Oct. 31, 1953*, ORNL-1658, Fig. 82, p 128.

[3]R. N. Lyon *et al.*, *HRP Quar. Prog. Rep. Jan. 31, 1954*, ORNL-1678, p 96.

Results of Circulation Tests in Which Slurries Prepared from Different Oxides Are Compared

Run S-44. A slurry containing 400 g of thorium per liter, as oxide prepared from thorium formate, was circulated[1] in Loop S at 250°C for 143 hr with a flow of water through the back of the pump to lubricate the Graphitar bearings. A $\frac{3}{8}$-in. titanium rod was suspended by means of spiders through the throat of a venturi tube, installed downstream from the pump, so that effects of velocity could also be studied.

After 143 hr of operation it was found that all the pump parts, including the new stainless steel impeller, were unaffected. The upstream face of the stainless steel orifice plate was slightly attacked around the opening, and the titanium rod was covered with a dark oxide film except in the high-velocity region of the venturi tube where it had a dull, lustrous finish. The orifice plate lost 245 mg in weight, whereas the titanium rod showed a net gain of 60 mg. No dimensional change in the diameter of the rod was observed. The velocity of the slurry through the throat of the venturi tube was estimated to have been between 48 and 50 fps.

Chemical and spectrographic analyses of the dull, lustrous surface of the titanium rod did not substantiate the previous speculation[3] of chromium deposition but revealed that the surface was either bare titanium metal or an extremely thin oxide coating.

Run S-45. Run S-45 was similar to S-44 except that the titanium rod through the venturi tube was replaced with a type 347 stainless steel rod. A slurry containing approximately 400 g of thorium per liter, as oxide prepared from the formate, was circulated at 250°C through the combined system.

TABLE 44. CIRCULATION OF ThO_2 SLURRIES AT 250°C WITH WESTINGHOUSE 100A PUMP WITH A COMPARISON OF OXIDE PREPARED FROM THORIUM FORMATE WITH THAT PREPARED FROM AMES THORIUM OXALATE

Sample No.**	Circulation Time (hr)	Solids*					Filtrate			Gas Analysis			
		Th (g/liter)	Fe (ppm)	Ni (ppm)	Cr (ppm)	Fe (mg) / Th (g)	pH	Fe (ppm)	Ni (ppm)	Volume of Gas (cc)	H_2 (%)	O_2 (%)	CO_2 (%)
S-44-0	2	360	36	<5	<5	0.1	6.7	<1	<1	68.5	0	18	0
S-44-1	21	405	207	22	34	0.68	6.9	<1	<1	***	***	***	***
S-44-2	27									18	7.5	5	0
S-44-3	94	410	600	11	146	1.46	5.1	<1.	<1	26	1.2	2.8	2.4
S-44-4	117	405	717	14	186	1.77	5.6	<1	<1	16	31	3.5	0
S-44-5	143	401	800	15	230	2.00	5.4	<1	<1				
S-45-0	1	327	43	<1	9	0.13	6.2	<1	<1	6	25	0	0
S-45-1	22	416	157	24	43	0.38	6.4	<1	<1	19	28	0	0
S-45-2	93	420	740	14	150	1.76	6.8	<1	<1	30	59	1	0
S-45-3	116	420	930	1	207	2.20	6.4	<1	<1	44	49	1	0
S-45-4	140	405	1050	13	275	2.58	5.7	<1	<1	77	31	6.5	0
S-46-0	3	364	123	20	30	0.34	7.7	<1	<1	68	23	16	0
S-46-1	71	419	960	10	217	2.3	6.8	<1	<1	2	86	0	0
S-46-2	94	419	1250	11	330	3.0	6.6	<1	<1	39	78	0	0
S-46-3	118	390	1420	10	388	3.66	6.7	<1	<1	44	66	0	0

*Based on total slurry.

**Run S-44: oxide prepared from the formate.
Run S-45: oxide prepared from the formate.
Run S-46: oxide prepared from the oxalate (Ames).

***Gas sample lost during analysis.

The attack by the slurry was similar to that discussed for Run S-44. The flow restrictor lost 183 mg in weight, the pump impeller lost 6.5 g and appeared to be pitted along its periphery, and the rod lost 2.2 g. The surface of the rod in the high-velocity region of the venturi tube was shiny and showed evidence of pitting. In the velocity range between 20 and 30 fps, an adherent black oxide film was deposited on the rod; thus velocities up to 30 fps might not cause excessive attack on stainless steel.

Run S-46. In order to compare the abrasive properties of oxide prepared from the thermal decomposition of thorium formate with that prepared by the calcination of thorium oxalate (Ames process), a slurry containing 400 g of thorium per liter, as Ames oxide screened through 100 mesh, was circulated for 118 hr at 250°C. The titanium rod from Run S-44 was suspended through the venturi meter. A comparison of the data is shown in Table 44. The attack, as measured by the ratio of the milligrams of iron to the grams of thorium, in each case shows that the oxide prepared from the formate is apparently less detrimental than that prepared by calcining the oxalate.

The titanium rod was not attacked; however, the stainless steel impeller and flow restrictor were damaged and both lost weight.

Run S-47. The Ames Laboratory no longer produces thorium oxide. A new batch of material was received from the Lindsay Light & Chemical Co., West Chicago, Illinois, and a loop test was made in which the new product was used. After 42 hr of circulation at 250°C, the run was stopped because of the excessive build-up of corrosion products as measured by the iron concentration of the solids. The pH of the slurry was approximately 9; thus the presence of alkali metals was suggested. A subsequent analysis in which flame-spectrophotometer techniques were used substantiated this conclusion.

Severe pitting of the impeller and the pump-annulus weld pads was observed, and this probably accounts for the high iron contamination of the solids.

By recalcining the Lindsay oxide at 1450°C, a product was obtained which did not change the pH of distilled water when slurried. A run in which this material is used will be made in order to determine the effect of recalcination.

ALTERNATE MATERIALS OF CONSTRUCTION

In order to determine the mechanism of the metal removal that takes place when thorium oxide slurries are circulated at 250°C, a two-phase program is under way which is directed toward developing easily prepared, less chemically reactive, and/or softer oxides and more resistant materials of construction. Stainless steel in straight pipes and elbows has shown little, if any, attack by the slurry at flow rates below 20 fps. In regions of high velocity (~90 fps) both the 300- and 400-series stainless steels are attacked drastically, whereas titanium, zirconium, gold, platinum, and Zircaloy-2 are only slightly attacked.

The previously described[4] Loop T, converted into a system similar to Loop S, was used to compare the resistance of various metals to slurry attack.

In order to determine whether the particles actually remove the base metal, mechanically, or whether they merely remove the protective oxide film and expose the base metal to corrosive attack by the water, 400-series stainless steel, zirconium, gold, platinum, titanium, and Zircaloy-2 were tested. In addition, wear-resistant and extremely hard materials such as Carboloy (tungsten-carbide-base alloy), Stellite 98M2 (cobalt-base alloy), and the Chromalloys (a facing rich in chromium carbides) will be tested.

The materials to be tested were inserted in the loop as orifice plates (flow restrictors). Quartered sections of the various metals, joined by a tongue and groove, formed the orifices. The velocity through the orifice was approximately 90 fps. For each run except Run T-29, a slurry containing 300 g of thorium per liter, as Ames oxide screened through 100 mesh, was circulated at 250°C for approximately 140 hr.

The runs were arbitrarily stopped after 140 hr so that the orifices could be inspected; the results are shown in Table 45 and in Figs. 113 through 118. Visual inspection of the 400-series stainless steel showed attack under the stainless steel retaining ring, where there was essentially no flow. Corrosion also took place in the tongue-and-groove sections of the mating metals which were dissimilar to the 400-series stainless steels. Thus the drastic attack on the 300- and the 400-series stainless

[4] R. N. Lyon *et al.*, *HRP Quar. Prog. Rep. Oct. 31, 1953*, ORNL-1658, Fig. 81, p 127.

TABLE 45. RESISTANCE OF CONSTRUCTION MATERIALS TO ATTACK BY ThO_2 SLURRIES CIRCULATED AT 250°C WITH A WESTINGHOUSE 100A PUMP

Run Number	Circulation Time (hr)	Thorium Concentration (g/liter)	Quartered Orifice Combination	Superficial Rockwell Hardness	Weight Change (mg)	Remarks
1-29	142	150	Inconel X, heat treated	C-38	−17.0	Mated with type 347 stainless steel (4) and titanium (3)[a]
			Armco type 17-4PH stainless steel	C-37	−66.0	Mated with type 347 stainless steel (4) and titanium (3)
			Titanium	B-80	+3.0	Mated with Inconel X (1) and Armco type 17-4PH stainless steel (2)
			Type 347 stainless steel	B-80	−69.0	Mated with Armco type 17-4PH stainless steel (2) and Inconel X (1)
T-30	141	300	Zirconium, crystal bar	B-88	−12.0	Mated with types 416 and 430 stainless steel; shiny film around opening
			Zircaloy-2	B-95	−34	Mated with types 416 and 430 stainless steel; shiny film around opening
			Type 416 stainless steel, untreated	B-83	−1700.0	Badly attacked
			Type 430 stainless steel	B-67.5	−1200.0	Badly attacked
T-31	137	300	Gold	*b*	−269.0	Mated with type 430 stainless steel and zirconium; attacked near the stainless steel
			Zirconium, crystal bar	B-90	−17.0	Mated with platinum and gold; shiny film around opening
			Type 430 stainless steel	B-77.5	−697.0	Badly corroded
			Platinum	B-76.6	−17.0	Slightly abraded
T-32	89[c]	300	Platinum (upstream face)[d]	B-76.6	−36.0	Slightly abraded
			Platinum	B-76.6	+3.0	Black film deposit accounts for weight gain
			Platinum	B-76.6	+14.0	Black film deposit accounts for weight gain
			Platinum (downstream face)	B-76.6	+20	Black film deposit accounts for weight gain

[a]Numbers in parentheses refer to specimens in Figs. 113 and 114.

[b]Too soft for a reading to be obtained.

[c]Run short because of stator-winding failure — no fault of slurry.

[d]Complete orifice fabricated from four 0.032-in. platinum sheets.

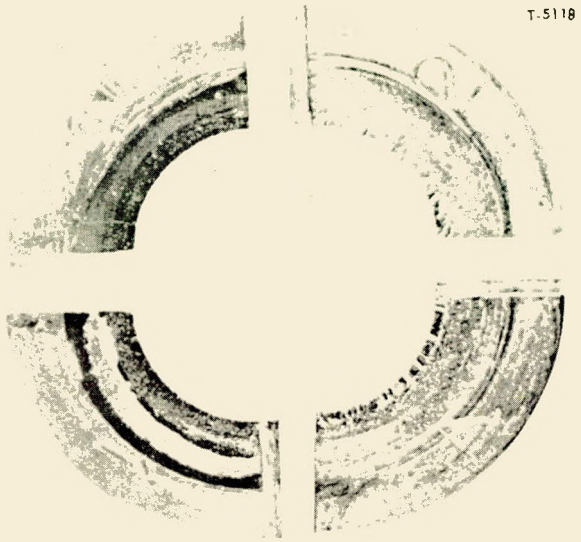

Fig. 113. Upstream Face of Flow Restrictor Indicating the Method of Assembly; Pits in Inconel X (1) and Type 347 Stainless Steel (4) Indicate Corrosion Attack; Dark Area Around Opening on Titanium (3) Is Black Oxide Film; Sample 2 Is Armco 17-4PH Steel. 2X. Reduced 24%.

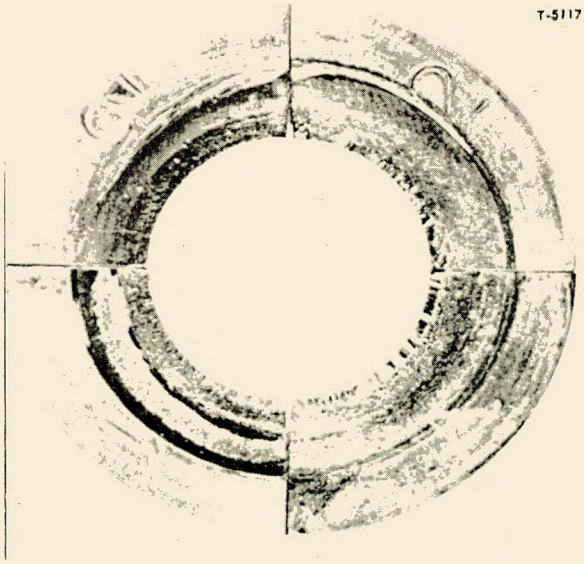

Fig. 114. Quartered Orifice Plate Used in Run T-29; Front Face Shown After 142 hr of Service at 250°C with Circulating ThO_2 Slurries; Sample 1, Inconel X, Hardened; Sample 2, Armco 17-4PH Steel, Hardened; Sample 3, Titanium; Sample 4, Type 347 Stainless Steel. 2.5 X. Reduced 32%.

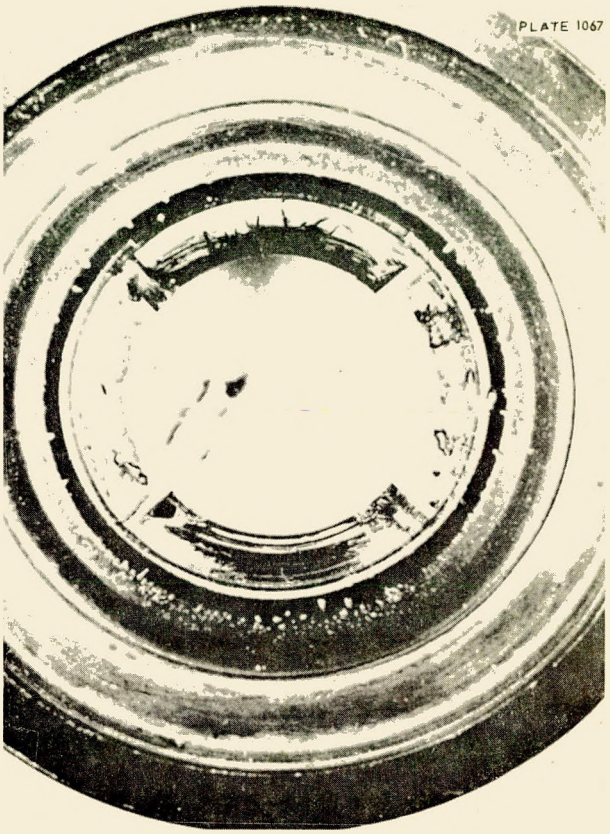

Fig. 115. Upstream Faces of Quartered Orifice Combination for Run T-30; Samples in Clockwise Order, Zirconium, Type 416 Stainless Steel, Zircaloy-2, Type 430 Stainless Steel, After 141 hr of Service in Circulating ThO_2 Slurry at 250°C; Badly Corroded Specimens Are Types 416 and 430 Stainless Steel.

steels may be due to galvanic action between dissimilar metals. To eliminate this phenomenon, a test will be made in which Teflon will be used to insulate the various metals from each other and from the holder.

It is concluded from the present data that attack by thorium oxide slurries is severe; corrosion rather than abrasion controls the rate of attack. The attack consists in the removal of the protective oxide layer by chemical attack or by abrasion; this is followed by rapid reaction of the metal, with the corrosion products being continuously removed from the surface by the slurry. Evolution of hydrogen and depletion of oxygen are the results of the attack of the base metal by water. The

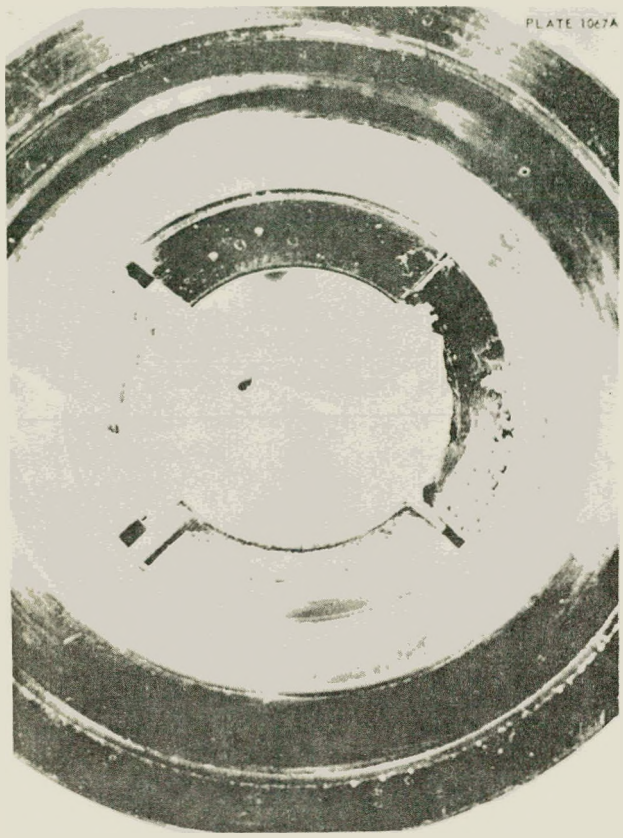

Fig. 116. Downstream Face of Combination Orifice; Samples in Clockwise Order, Zirconium, Type 430 Stainless Steel, Zircaloy-2, and Type 416 Stainless Steel Showing Corrosion Attack on the Stainless Steels.

Fig. 117. Upstream Face of Combination Orifice Used in Run T-31; Samples in Clockwise Order, Zirconium, Gold, Type 430 Stainless Steel, and Platinum.

oxide film on the titanium, zirconium, and Zircaloy is hard, adherent, and unreactive; so the base metal is well protected from reaction with water. Gold and platinum, on the other hand, are chemically inert and do not react appreciably when the base metal is exposed under these conditions. In order to further substantiate the evidence for the proposed mechanism of attack, metals which have a superficial hardness equivalent to that of thorium oxide (Rockwell C-50 to C-60) will be tested. Carboloy, Stellite 98M2, and the Chromalloys fall in this category. Metallographic examination of the specimens after testing should indicate the nature of the attack if any occurs. Intergranular attack would indicate corrosion, whereas no attack would probably indicate abrasion resistance, since these materials are known for their wear resistance because of their hard surfaces.

WESTINGHOUSE 100A PUMPS

One of the major difficulties encountered when thorium oxide slurries are circulated with a Westinghouse 100A pump is the maintenance of axial thrust balance in the pump. In this pump, the balance of thrust forces is maintained by the relative flow between the front and back weld pads. The flow is controlled, in turn, by the clearance between the wear rings and the impeller hubs. If the front wear rings are damaged, by slurry attack for example, the impeller-rotor assembly rides forward against the back edge of the front Graphitar bearing, and, under these conditions, the bearing often cracks and allows the rotor to rub against and to damage the walls of the stator can. In order to avoid such damage, two approaches have been investigated.

1. Stellite 98M2 bearings were substituted so

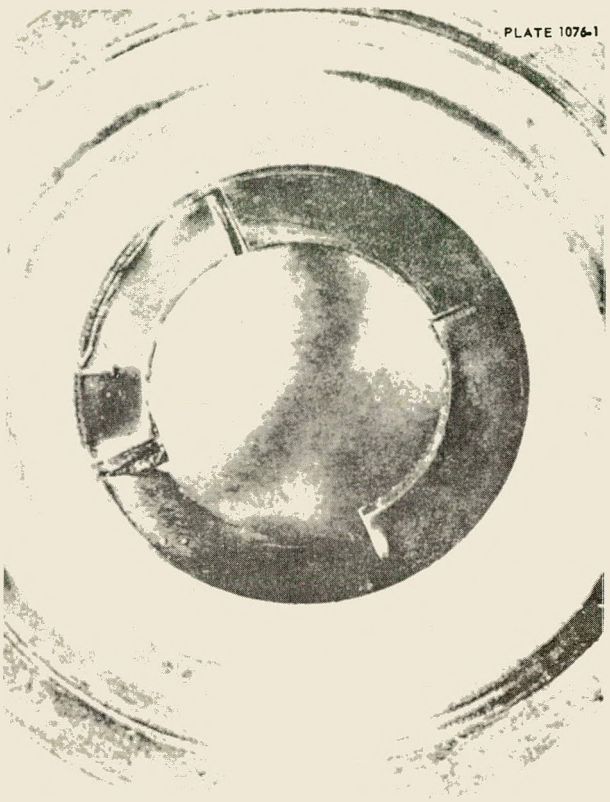

Fig. 118. Downstream Face of Combination Orifice Used in Run T-31; Samples in Clockwise Order, Zirconium, Platinum, Type 430 Stainless Steel, and Gold.

that the bearing-journal assembly consisted of Stellite against Stellite instead of the usual combination of Graphitar against Stellite. This bearing-journal assembly was run satisfactorily with water at 250°C for 85 hr with a flow of water through the back of the pump for lubrication. At the end of the run, a black oxide coating covered both bearings and journals, but there was no dimensional change in either, as measured with a micrometer to ±0.001 in. In addition, there was no evidence of galling, seizing, or wear.

2. Careful dynamic balancing of the pump impeller and rotor by grinding metal from the shrouds rather than by drilling deep holes in the hubs, as was done in the past, and the replacement of the stainless steel wear rings with titanium have prolonged the life of the Graphitar bearings. Previously, dense cakes of ThO_2 (density 10) formed in the deep holes and caused an imbalance. After about 130 hr of circulation with the slurry at 250°C, the front bearing failed, apparently as a result of radial imbalance of the impeller. The front bearing and journal were badly worn, but the back set showed no evidence of wear.

It is safe to conclude from the data that metal-to-metal bearing-journal assemblies are operable, provided that the system is in dynamic balance and that the wearing surfaces are lubricated at all times.

After 500 hr of operation with the slurry, there was no evidence of wear in either the front or the back Graphitar bearing.

5-gpm LOOPS

Fifteen kilograms of ThO_2 is required for an experiment in which a slurry containing 1000 g of thorium per liter is circulated in a Westinghouse 100A pump loop. So that laboratory-prepared oxides can be tested, a small loop has been designed which will require only 1 kg of solids for a concentration of 1000 g/liter. A layout of the loop is shown in Fig. 119. A 5-gpm ORNL pump[5] will be used to circulate the slurry at 250 to 300°C. The slurry velocity in the straight runs of pipe will be about 10 fps; the velocity through the venturi tube will be about 50 to 60 fps. The system can be pressurized with either steam or gas.

The loop is now being installed, and the shakedown run with water should begin about May 15, 1954.

HOMOGENEITY OF CIRCULATING SLURRIES

In order to minimize sampling errors, two methods of determining concentration changes without sampling the loop are being investigated.

1. The difference between the pressure drop in a vertical pipe and that in a horizontal pipe of the same length indicates the pressure which would be exerted by the slurry in a static vertical column of the same length. From this pressure differential, the density of the slurry is easily computed. Results obtained by circulating zinc bromide solutions and thorium oxide slurries at room temperature are shown in Table 46. Pressure drops were measured by means of Foxboro differential-pressure cells. The reliability of the method is within ±0.03 g/cc, or ±30 g of thorium per liter.

[5]R. J. Kedl, T. H. Mauney, C. B. Graham, and W. L. Ross, *HRP Quar. Prog. Rep. Jan. 1, 1953*, ORNL-1478, p 58.

UNCLASSIFIED
ORNL-LR-DWG 2076

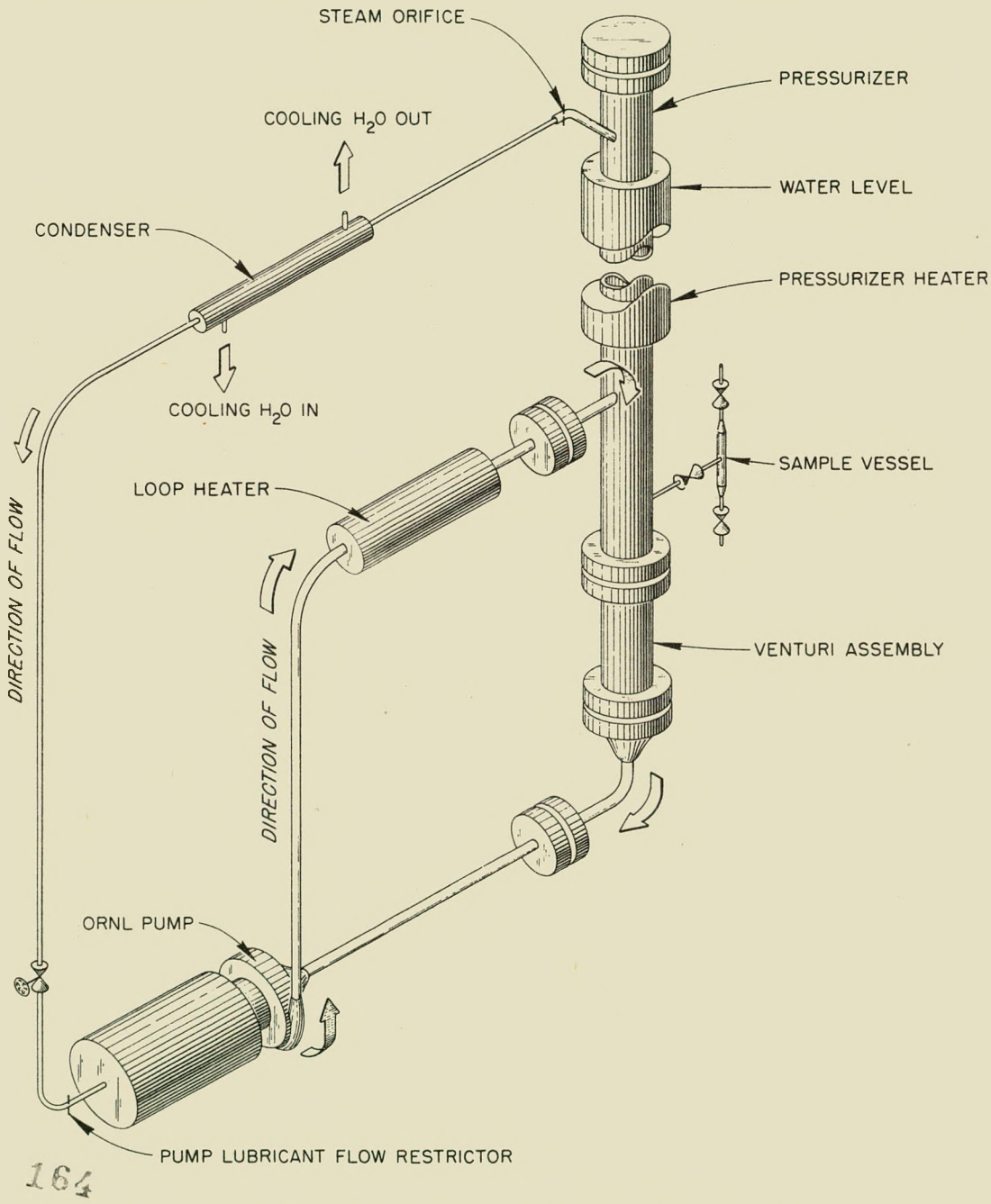

Fig. 119. Schematic Layout for 5-gpm Slurry Loop.

TABLE 46. DENSITY DETERMINATIONS FROM PRESSURE-DROP MEASUREMENTS

Liquid	Actual Density (g/cc)	Density from Pressure-Drop Measurements (g/cc)
$ZnBr_2$	1.977*	1.991
$ZnBr_2$	1.685*	1.684
$ZnBr_2$	1.502*	1.509
ThO_2 slurry (115 g of thorium per liter)	1.112**	1.103
ThO_2 slurry (233 g of thorium per liter)	1.230**	1.251

*Density determined by means of a pycnometer.
**Density determined by weighing oxide and water.

A loop is being fabricated to test this principle at elevated temperatures and pressures (Fig. 120). A 5-gpm ORNL pump will be used to circulate the slurry in a loop similar to the Westinghouse 100A pump loops. Foxboro differential-pressure cells and other measuring devices will be investigated.

2. A faulty probe precluded the testing of the Ultra-Viscoson as a concentration-measuring device. A new probe has been ordered and will be tested in a high-velocity circulating system. The Ultra-Viscoson, marketed by the Bendix Aviation Corp., measures the product of the density and viscosity of the fluid.

ABRASION TESTS

The fabrication of the high-temperature abrasion tester has been completed. The system (Fig. 121) consists of a close-fitting disk which is moved as a reciprocating piston in a closed system containing the slurry. The high-pressure seals are two stainless steel, three-ply bellows arranged in series and are manufactured by the Fulton Sylphon Division. Two taps are provided – one for a pressure gage and the other for gas pressurization, if desired. Heat is supplied by means of a Calrod heater wrapped around the bottom of the bomb.

The bulk of the displaced slurry passes through small holes in the disk, and a small amount passes through the 0.005-in. clearance between the disk and the cylinder walls. The velocity of the slurry through the openings can be varied by changing the size of the holes or by varying the rate of displacement.

The system has been operated successfully with water at 250°C for 40 hr; the disk was moved 60,000 cycles at the rate of 15 cpm by means of a Foxboro air operator. At the completion of the test, inspection of the component parts indicated water corrosion of the disk, the internal bellows, and the cylinder walls. The system is now in operation with a slurry containing 1000 g of thorium per liter as Ames oxide screened through 100 mesh. No data are as yet available.

The future program for the abrasion tester includes the testing at 300 to 350°C of disk and cylinder walls constructed of various materials and slurries of oxides prepared by different methods. The device, if proved satisfactory by out-of-pile tests, will be modified for in-pile studies.

LABORATORY PREPARATION OF THORIUM COMPOUNDS

Chemical investigations relative to the slurry-blanket program have been directed toward a study of methods for preparing experimental batches of thorium compounds which are of interest as slurry media. Foremost among the studies has been the development of a method for preparing a nonabrasive form of thorium oxide. Use of a nonabrasive solid in the slurry would reduce the number of places where special metals such as titanium would be required in the system. Thorium formate, $Th(OOCH)_4$, has been studied as an intermediate for the preparation of a nonabrasive thorium oxide. Results from preliminary tests indicate that $Th(OOCH)_4$ can be prepared either in a batchwise manner or as a continuous process by adding a 2 M solution of thorium nitrate to hot

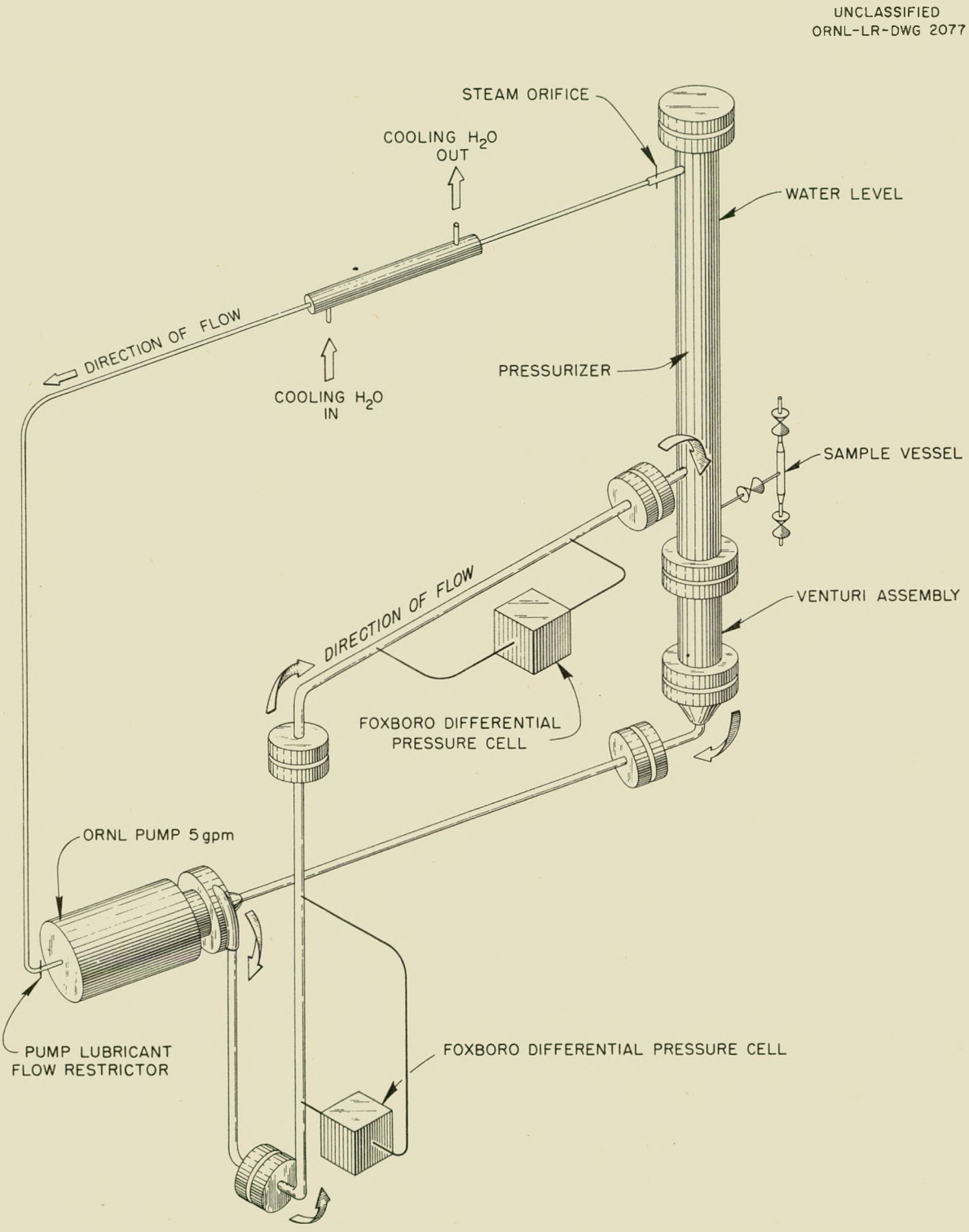

Fig. 120. Schematic Layout for Making Measurements of Slurry Concentration.

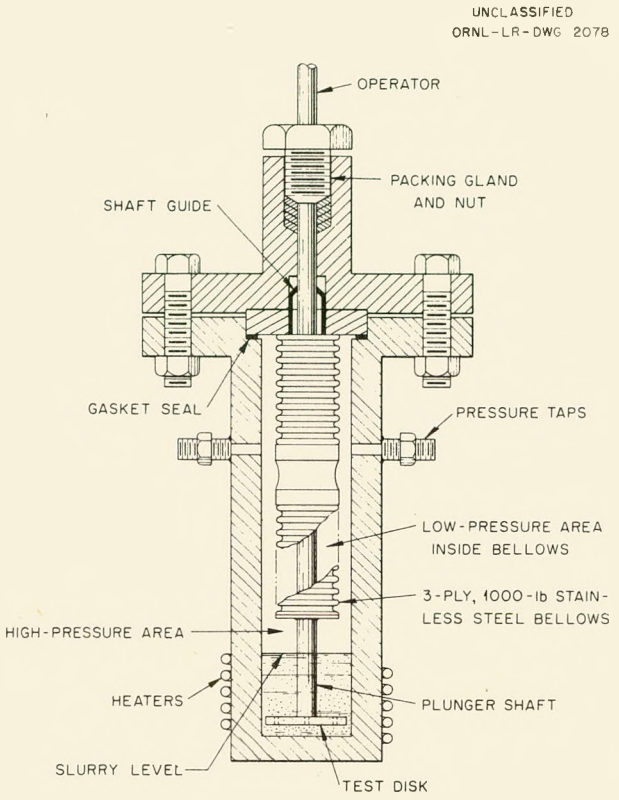

Fig. 121. High-Temperature Abrasion Tester.

(95–98°C) concentrated formic acid.[6] The reaction may be written as follows:

$$Th(NO_3)_4 + 12HCOOH \longrightarrow Th(OOCH)_4 + 2N_2O + 8CO_2 + 10H_2O$$

The product is essentially free of anions such as nitrate, sulfate, and chloride, and it may be readily decomposed to thorium oxide at 650°C.

It appears, from initial work, that thorium formate may also be suitable for preparing high-purity thorium hydroxide. Formic acid is decomposed to carbon dioxide and hydrogen when in contact with metallic palladium. The catalytic reaction occurs at room temperature and appears to progress more rapidly at higher temperatures. A study of this reaction is currently being made by using a saturated solution of $Th(OOCH)_4$ in contact with a bed of thorium oxide beads which are coated with a layer of metallic palladium.

[6]D. E. Ferguson *et al.*, *HRP Quar. Prog. Rep. Jan. 31, 1954*, ORNL-1678, p 88-9.

Tests are in progress to study the feasibility of incorporating small amounts of base metals or their oxides into the crystal lattice of thorium oxide. Techniques for the addition of copper, palladium, and lead, which may be suitable catalysts for the recombination of hydrogen and oxygen gases, are being investigated.

Other compounds of interest are thorium-uranium mixtures and thorium phosphate. Thorium phosphate, because of hydrolysis at elevated temperatures, may release sufficient phosphate ions to act as a corrosion inhibitor. Incorporation of uranium with thorium oxide may produce a softer material. X-ray diffraction studies appear to show that the presence of uranium reduces the crystallinity of thorium oxide.

PREPARATION OF THORIUM OXIDE SLURRIES FROM THORIUM HYDROXIDE

The least abrasive thorium oxide slurry which has been obtained at a thorium concentration of 800 to 1000 g/liter was prepared from thorium hydroxide. The hydroxide was precipitated from thorium formate solution with ammonium hydroxide and dehydrated at 500°C; the resulting oxide was autoclaved in water at 250°C before being tested for relative abrasivity by the jet-impingement method.

The thorium hydroxide was prepared by adding, dropwise with stirring, 2 M ammonium hydroxide solution to 0.13 M thorium formate solution until pH 9 was attained. After the precipitate had settled, the supernatant was decanted, and the solids were washed to pH 7 by decantation with 4 volumes of 0.5 M ammonium hydroxide followed by 3 volumes of water. The solid was then recovered by filtration, and the cake was washed with water and reslurried. The final pH of the slurry was 5 to 6, as measured with indicator paper.

The hydroxide precipitated from formate solution was less gelatinous and more easily handled than that precipitated from thorium nitrate solution. Autoclaving a portion of the hydroxide in water at 250°C yielded a bulky slurry with a maximum thorium concentration of 300 g/liter, which was very much less abrasive than a slurry of Ames oxide. A second portion of the hydroxide was dehydrated by heating successively at 100, 300, and 500°C. A sample of the product obtained at each temperature was autoclaved in water at 250°C. The resulting slurries were all very much

less abrasive than Ames oxide. The slurry obtained from the material dried at 500°C and subsequently autoclaved was the least abrasive thorium slurry which has yet been prepared.

The weight losses observed at 300 and 500°C were 10.5 and 1.25%, respectively, which indicates that the product of the drying period at 100°C was essentially $Th(OH)_4$.

Further experimentation revealed that the product obtained by autoclaving the undried hydroxide in water at 250°C and drying at 500°C is extremely difficult to slurry in water and is much more gritty than the solid obtained by first drying the hydroxide at 500°C, autoclaving in water at 250°C, and redrying at 500°C. The gritty effect may have been caused during autoclaving by recrystallization, occasioned by the presence of ionic impurities in the undried hydroxide, which were removed from the latter solid by the initial heating at 500°C. The result is significant in that it presents a problem as to whether the hydroxide obtained by the steam stripping of thorium formate at elevated temperature will yield as desirable an oxide product on dehydration at 500°C as that yielded by the hydroxide obtained by a simple precipitation from thorium formate solution.

MIXED-OXIDE STUDIES

A study of the effect of a second oxide on crystal formation and crystal growth in thorium oxide during calcination has been initiated. The approach was patterned after the studies of Weiser, Milligan, and Mills,[7] who found that the addition of as little as 10 to 30 mole % of BeO, ZrO_2, Bi_2O_3, or SnO_2 to Al_2O_3 by coprecipitation of the hydroxides retarded the crystallization of Al_2O_3 when the mixed hydroxides were calcined to the oxides at 565°C. In the zones of protection observed by these investigators, the mixed oxides were amorphous to x rays or consisted of finely divided crystals.

During the past quarter, x-ray diffraction studies of thorium oxide containing 10 to 40 mole % ZrO_2, 10 to 40 mole % Bi_2O_3, or 20 to 30 mole % Al_2O_3, made by coprecipitation of the hydroxides and subsequent calcination of the mixtures to the oxide at 545°C, showed that the added oxide had no effect on the crystal formation of ThO_2. The addition of 10 mole % Al_2O_3 to ThO_2 in a similar experiment partially inhibited the crystal-growth process, as evidenced by the broadening of the x-ray diffraction bands of the ThO_2.

PREPARATION OF THORIUM OXALATE

In the preceding quarterly report, results were presented of a study of the various methods of preparation of thorium oxalate for use as a starting material in the preparation of thorium oxide. Additional physical and chemical information has been obtained on the thorium oxalate products. From these data and the previous information, it is now concluded that thorium oxalate for use in the preparation of slurry thoria is best prepared by the addition of 10% excess solid oxalic acid to a 1 *M* thorium nitrate solution at 40°C.

Four methods[8] of preparing the oxalate had been investigated and are described in Table 47.

The cold preparation of thorium oxalate yielded precipitates of much smaller particle size than those yielded by the hot preparations; they were much less than 0.5 μ in average size, as compared with 5 to 7 μ. The cold precipitates also contained 1 to 1.4% nitrate contaminant, as compared with the 0.5% nitrate impurity in the hot-precipitated material. However, as reported previously, the nitrate impurity was more easily removed from the cold-precipitated oxalate during the thermal-decomposition process. Hence, on the basis of the higher thorium concentration used, the smaller particle size obtained, and the purity of the oxide product, method 1 appears to be the most desirable precipitation method.

THORIUM FORMATE STUDIES

Investigation of the properties of thorium formate as a starting material in the preparation of thorium oxide slurries has continued. The formate for these studies was precipitated from boiling concentrated formic acid by the addition of 2 *M* $Th(NO_3)_4$ solution.

Aqueous Solubility

The solubility of thorium formate in water was determined at room temperature and at 74, 76, 96, and 97°C. The solubility exhibited a negative temperature coefficient. The thorium concentration of an apparently saturated solution decreased from a value of 57 to 62 g/liter at 22°C to 24 g/liter at 97°C (see Table 48).

[7] H. B. Weiser, W. O. Milligan, and G. A. Mills, *J. Phys. Chem.* 52, 942 (1948).

[8] D. E. Ferguson *et al.*, *HRP Quar. Prog. Rep. Jan. 31, 1954*, ORNL-1678, p 86.

TABLE 47. METHODS OF PRECIPITATION OF THORIUM OXALATE

Method	Reagent Concentrations	Precipitation Conditions	Washing Procedures
1	1.0 M $Th(NO_3)_4$; 10% excess oxalic acid (solid)	Add solid to solution at 40°C	Wash with water at room temperature
2	0.8 M $Th(NO_3)_4$; 3.2 M HNO_3; 10% excess oxalic acid (solid)	Add solid to solution at room temperature	Wash with water at room temperature
3	0.5 M $Th(NO_3)_4$; 1.0 M HNO_3; 10% excess oxalic acid (solid)	Add solid to solution at 70°C	Digest in water at 70°C
4	0.5 M $Th(NO_3)_4$; 1.0 M HNO_3; 10% excess oxalic acid (solution)	Heat both solutions to 70°C and add oxalic acid solution to thorium solution	Digest in water at 70°C

TABLE 48. AQUEOUS SOLUBILITY OF THORIUM FORMATE*

Experiment No.	Temperature of Solubility Determination (°C)	Equilibration Time (hr)	Thorium Concentration of Saturated Solution (g/liter)
1	22	16	62.4
2	74	1	28.3
3	96	2.5	24.6
4	97	2.5	23.6
5	76	2	22.0
6	76	16	23.8
7**	22	16	57.1

*Thorium formate dried 16 hr at 115°C.

**Thorium formate used in this determination was dried an additional 16 hr at 130°C.

The determinations above room temperature were made by using a glass apparatus which was kept completely immersed in a thermoregulated water bath during the experiments. Aliquots of the supernatant were withdrawn through a sintered-glass filter tube to a sampling vessel suspended in the water bath.

The data obtained at 74 to 76°C are somewhat inconclusive, but it is certainly established that thorium formate is much less soluble at the higher temperatures than at room temperature.

Dehydration and Thermal-Decomposition Studies

The data obtained from a heating experiment in which thorium formate was used are presented in Table 49. A portion of the thorium formate that had been precipitated from formic acid was washed, air-dried, and subjected to heating at successively higher temperatures. Weight losses were determined at the various temperatures, and small samples were withdrawn for chemical analysis.

The air-dried thorium formate was apparently the dihydrate. At 100°C the solid was the monohydrate, which became anhydrous at 125 to 200°C. At 250°C, decomposition to the oxide became pronounced and was essentially complete at 300°C; however, even after heating at 500°C, traces of carbon were present which may have resulted partly from the adsorption of CO_2.

Abrasion tests on thorium oxide prepared by the calcination of the formate at 550°C showed

TABLE 49. THERMAL STABILITY OF A THORIUM FORMATE SAMPLE HEATED AT SUCCESSIVELY HIGHER TEMPERATURES

Drying Temperature (°C)	Drying Time (hr)	Weight Loss (%)	Chemical Composition (%)			OOCH/Th
			Th	OOCH	C	
22			51.2	38.5		3.9
100	20	6.3	54.8	39.8		3.7
125	20	4.2	57.3	41.8		3.8
150	20	0.11	56.9	40.0		3.6
175	68	0.25	57.8	40.5		3.6
200	20	0.27	57.7	40.2		3.6
225	21	0.85	59.1	38.8		3.4
250	24	27.4	79.2		0.51	
275	63	6.1	83.8		0.11	
300	27	0.86	84.6		0.18	
325	23	0.84	85.5		0.11	
400	46	1.50				
450–500	48	0.12	86.9		0.16	

it to have essentially the same abrasive properties as oxide prepared by the thermal decomposition of thorium oxalate carried out at the same temperature.

LABORATORY ABRASION TESTS

Abrasion Tests on Titanium Metal

Titanium metal exhibited approximately the same abrasive resistance as type 304 stainless steel when tested with slurries of SiC and high-burned ThO_2 in laboratory jet-impingement abrasion tests.[9] The data are presented in Table 50.

The results of the slurry-pumping studies showed that titanium has more resistance to erosion than does stainless steel; therefore the results of the laboratory abrasion tests at first appear anomalous. The data obtained in the slurry-loop experiments could have resulted from the formation of a much stronger oxide film on titanium in water at 250°C than on stainless steel. On the other hand, the film on titanium might have been more rapidly replaced when abraded. If either of these is the case, it may indicate that an investigation of the abrasive resistance of oxide films found on steel and titanium in aqueous solutions at 250°C could yield information of value to the development of abrasion-resistant slurry systems.

Experiments for Evaluation of the Laboratory Abrasion Test

The laboratory, jet-impingement, slurry-abrasion tester described previously[9] has proved to be extremely useful in determining the relative abrasive hardness of various slurry preparations. In tests reported so far, a single set of conditions has been used. In order to make the results of the test more definitive, it is necessary that the effects of changes in slurry concentration, particle size, velocity, etc. be more fully evaluated. In addition, a systematic correlation of the laboratory test with the loop tests would be valuable. The standardization of the abrasion test is also important because changes in abrasive hardness are likely to occur when the oxide slurries are subjected to reactor irradiation.

Experimental abrasion studies in which SiC and Al_2O_3 as well as high-burned ThO_2 were used have been completed during the quarter (see Table 51).

[9] J. P. McBride and W. L. Pattison, *HRP Quar. Prog. Rep. July 31, 1953*, ORNL-1605, p 139.

TABLE 50. COMPARISON OF ABRASIVE RESISTANCES OF TITANIUM AND TYPE 304 STAINLESS STEEL

Conditions: slurry volume, 20 ml
nitrogen pressure, 40 psi
stirring-speed setting, 90

Test-Plate Metal	Test-Plate Thickness (mils)	Abrasive	Concentration of Abrasive (g/liter)	Penetration Time (min)
Stainless steel	5	900°C ThO_2*	250 (Th)	2.17
Titanium, Ti-75A	10	900°C ThO_2*	250 (Th)	3.85**
Stainless steel	5	900°C ThO_2***	250 (Th)	3.33
Titanium, Ti-75A	10	900°C ThO_2***	250 (Th)	6.66**
Stainless steel	5	600-mesh SiC	250 (Si)	1.25
Titanium, Ti-75A	10	600-mesh SiC	250 (Si)	2.33**

*Aged.

**Note that the titanium test plate was twice as thick as the stainless steel test plate.

***Freshly prepared (4-hr heating).

TABLE 51. EXPERIMENTS FOR EVALUATION OF THE LABORATORY ABRASION TEST

Conditions: slurry volume, 20 ml
nitrogen pressure, 40 psi

Experiment No.*	Abrasive	Concentration (g/liter)	Stirring-Speed Setting	Test-Plate Thickness (mils)	Penetration Time (min)	Specific Penetration Rate (mils/min)
1_a	800-mesh SiC	250 (Si)	70	5	2.0	2.5
1_b	800-mesh SiC	250 (Si)	90	5	2.0	2.5
1_c	800-mesh SiC	250 (Si)	90	25	10.5	2.4
2_a	800-mesh SiC	125 (Si)	70	5	2.0	2.5
2_b	800-mesh SiC	125 (Si)	100	5	2.6	1.92
2_c	800-mesh SiC	125 (Si)	80	5	2.3	2.17
2_d	800-mesh SiC	125 (Si)	80	25	12.3	2.04
3_a	600-mesh Al_2O_3	250 (Al)	90	5	2.4	2.08
3_b	600-mesh Al_2O_3	250 (Al)	70	5	2.0	2.5
3_c	600-mesh Al_2O_3	250 (Al)	90	25	14.3	1.75
4_a	600-mesh Al_2O_3	125 (Al)	90	5	3.0	1.66
4_b	600-mesh Al_2O_3	125 (Al)	90	5	2.9	1.72
4_c	600-mesh Al_2O_3	125 (Al)	90	25	17.6	1.43

*Subscripts a, b, c, d indicate that the abrasion tests were run consecutively using the same sample of slurry but a new test piece.

Although the data are preliminary in nature and not, as yet, complete enough for an evaluation of the laboratory test, the following conclusions can be drawn:

1. The penetration times show a deviation of less than 10% for a given thickness of metal when tested under the same conditions.
2. Halving the slurry concentration (250 g of Si or Al per liter to 150 g/liter) decreases the penetration rate by less than 20%.
3. Slurry homogeneity, as expected, markedly affects reproducibility of results and demonstrates the necessity of investigating the effect of stirring speed on homogeneity for each slurry system studied.

In the studies with Al_2O_3, it was noted that the specific penetration rate was greatly decreased when a 25-mil rather than a 5-mil test plate was used. This was probably the result of a breakdown of the slurry particles. The harder SiC did not show such a pronounced change with the thicker test piece.

STUDIES ON THE IRRADIATION OF THORIUM OXIDE SLURRIES

Facilities for the irradiation of thorium oxide slurries in vertical hole 11 of the ORNL Graphite Reactor have been designed and are under construction. In the initial studies it is planned to obtain data on the effect of reactor irradiation on the properties of the bulk slurry, the gas production rate, and the abrasive hardness of the slurry solids. Portions of the irradiated slurries will be used in dissolution experiments and chemical processing studies. Particular attention will be given to the distribution of fission products, Pa^{233}, and U^{233} in the irradiated slurries.

CHEMICAL PROCESSING

W. K. Eister, Section Chief – Unit Operations

D. E. Ferguson, Assistant Section Chief – Chemical Development

W. E. Unger, Assistant Section Chief – Process Design

W. L. Carter, J. M. Delozier, W. B. Howerton, R. E. Leuze, R. G. Mansfield, D. R. Hendrix[1], F. C. McCullough, R. A. McNees, E. O. Nurmi, R. H. Rainey, A. M. Rom, H. F. Soard, O. K. Tallent, W. E. Tomlin, M. E. Whatley, D. O. Campbell[1], D. C. Overholt[1]

PLUTONIUM PROCESSING

The primary objective in processing a homogeneous reactor blanket is to remove the plutonium as rapidly as possible in order to minimize Pu^{240} buildup. The secondary objectives are to remove fission-product poisons and enough uranium so that natural uranium can be added to the blanket in order to replenish the supply of U^{235}. Two unknown factors that may greatly affect Pu^{240} production, and hence the process volumes and allowable concentrations, are the time required for plutonium to precipitate after it is formed and the amount of Pu^{240} produced by neutron capture by Np^{239}.

Preliminary Chemical Flow Sheet

A preliminary chemical flow sheet (Fig. 122) has been developed for the method now being considered for processing a homogeneous reactor blanket. The process consists in solid-liquid separation, D_2O recovery by evaporation, and plutonium and uranium isolation by the Purex process. The solid-liquid separation is possible because the solubility of plutonium under reactor conditions is only about 0.003 g/liter. The plutonium precipitates as PuO_2 which is to be concentrated into a small portion of blanket solution and then removed for further processing. The clarified uranium solution is recycled directly to the reactor. The procedure for storing the slurry for radioactive decay and then for recovering the D_2O by evaporating and drying the UO_2SO_4 cake is only one of several possible methods. Economic considerations may make it desirable to recover only part of the D_2O before the plutonium is decontaminated. It would then be necessary to operate the modified Purex process with a system of mixed light and heavy water. Decontamination of the water and re-enrichment of the D_2O would be necessary.

Neptunium Chemistry

There was no precipitation or change in the valence state of neptunium when uranyl sulfate

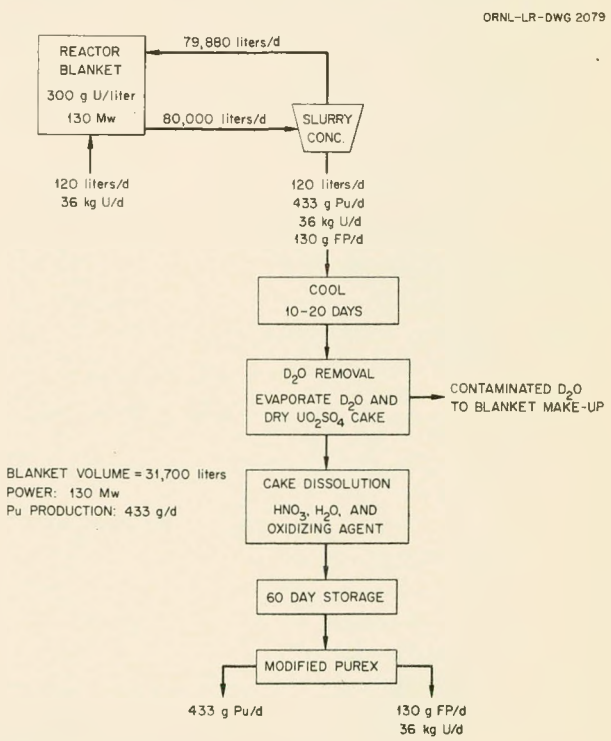

Fig. 122. Schematic Chemical Process for K-49 Reactor Blanket.

[1]Part time.

solutions (238 and 300 g of uranium per liter) containing 0.07 mg of Np(V) and Np(VI) per milliliter and 0.004 mg of Np(IV) per milliliter were heated in quartz tubes at 300°C for 24 hr under air and at 275°C for 24 hr under 120 psi of oxygen and 240 psi of hydrogen. This indicates that neptunium probably will remain in solution in the reactor blanket. If the neptunium remains in solution and if the neutron-capture cross section of Np^{239} is of the same order of magnitude as that of Pu^{239}, it will be necessary to devise some method of removing neptunium from the blanket solution in order to control the Pu^{240} content of the product.

Design and Engineering Development

Calculations have been made for the preliminary design and material balances for processing both the HRT and K-49 reactors for plutonium and heavy-water recovery. Although process-equipment design is incomplete, a plant layout based on currently available information has been started in order to estimate space requirements for chemical processing in the new HRT building.

A titanium column has been installed, and it will be used mainly in dynamic studies of the precipitation of rare earths from homogeneous reactor fuel at elevated temperatures. A 50-gal, type 347 stainless steel tank, heavily shielded and equipped with remote instrumentation, has been installed to store, for future processing, radioactive fuel from the homogeneous reactor in-pile corrosion-loop studies. Preliminary designs that include shielding and venting have been prepared for possible methods of storing of the HRE fuel. Because of the intense radioactivity of the fuel, considerable difficulty would be experienced if the fuel were to be handled at the present time; however, a six- to eight-month period of storage in the 7500 area will minimize the difficulty.

A study of solid-liquid separation has been started in order to develop a method of continuously removing the precipitated PuO_2 from the blanket and the insoluble fission products from the fuel solution of the K-49 reactor. Four of the requirements of the method are that it be (1) capable of separating 0.5-μ particles of plutonium and fission products from the bulk of the fuel and blanket solution and concentrating them by factors of 100 and 1000, respectively; (2) capable of handling a high flow rate at a low holdup; (3) operable at a temperature of 300°C at 2000-psi pressure in an intense radiation field; and (4) capable of continuous trouble-free operation. A review of the relative advantages of available devices for effecting solid-liquid separation has shown liquid cyclones to be most promising, with centrifuges, filters, and settling vessels less desirable, in that order.

A facility for testing commercial liquid cyclones has been completed. It consists of a Johnson pump capable of a wide range of flows and pressures, a 70-gal surge tank, a heat exchanger to either heat or cool the liquid, and pressure gages and flowmeters on each stream. The facility is intended for general physical-performance studies at moderate temperatures and pressures. Preliminary work has been done on the design of a high-pressure facility for performing out-of-pile experiments on solid-liquid separations. It will operate at pressures up to 2000 psi and temperatures up to 300°C in order to simulate the operating conditions of the HRT and K-49 reactors.

The conditions in the proposed reactor system are beyond the range of the performance data available for separation devices. Liquid cyclones have been used commercially for the desliming of coal; a 3-in.-dia cyclone is used to effect a separation of 50-μ particles. Recently, a 10-mm-dia cyclone that is capable of separating 2-μ particles of clay from water was developed. Because the blanket system is characterized by a low viscosity and a high solid-liquid density difference, there is an excellent probability that a small-diameter cyclone will be effective.

A significant factor in applying liquid cyclones to the separation of PuO_2 is the assumed abrasiveness of the material. Wear is reportedly most pronounced at the conical tip (underflow nozzle) of conventional cyclones of small dimensions. The effect of tip erosion may be minimized by eliminating the cone of the cyclone and reverting to a cylindrical design. Equipment Engineers, Inc., describe a cyclone of cylindrical design which is reported to have reduced erosion and high separation efficiencies at pressure requirements somewhat lower than those of conventional designs.

Determination of Reactor Neutron-Capture Cross Section of Np^{239}

A process for isolating milligram amounts of plutonium from LITR-irradiated uranium metal slugs has been developed for use in connection with the

measurement of the neutron-capture cross section of Np^{239}. The measurements are being carried out in cooperation with the Chemistry and Analytical Chemistry Divisions. The procedure will be to irradiate uranium metal slugs in the LITR for periods of from 1 to 16 days, chemically isolate the plutonium formed after suitable neptunium decay, and measure the abundance of Pu^{240}.

The chemical separation procedure consists of a modified Purex-process cycle for the separation of plutonium from the fission products and uranium, the concentration of the plutonium from the Purex product solution by carrier precipitation on ferrous hydroxide, and a final separation of plutonium from iron and traces of uranium by a fluoride precipitation. In a full-scale test, more than 90% of the initial plutonium was recovered with an acceptable product purity.

FUEL-SOLUTION PROCESSING

Solubility data collected at the Laboratory show that it is feasible to control the amount of neutron poison that results from rare-earth fission products in the fuel solution of a two-region homogeneous reactor by removing insoluble rare-earth sulfates as they precipitate. Figure 123 is a schematic chemical flow sheet of the method. The various volumes and weights given in the flow sheet are based on the poison due to rare-earth fission products being limited to 2% and the total fission- and corrosion-product poisons being limited to 5%. It is believed that this process is the best method yet advanced for achieving a good neutron economy with a low processing cost.

Solubility of Rare-Earth Sulfates in 0.02 M UO_2SO_4–0.005 M H_2SO_4

The solubility of two mixtures of rare-earth sulfates and of several individual rare-earth sulfates in simulated fuel solution for a two-region homogeneous reactor was determined as a function of temperature up to 300°C. Examination of these data (Figs. 124 and 125) and of those reported by the Vitro Corp. shows that the solubility above 250°C of a mixture of rare-earth sulfates approximating the composition expected in the reactor fuel will certainly be much less than the 0.24 g/liter which represents 2% neutron poisoning from rare-earth fission products. At 275°C the concentration of rare-earth sulfates in solution will be about 0.05 g/liter. The rare-earth elements with high

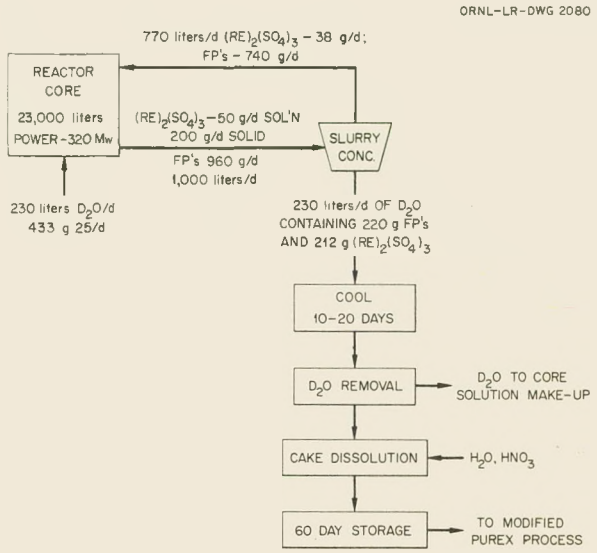

Fig. 123. Schematic Chemical Process for K-49 Reactor Core.

atomic numbers are more soluble than those with lower numbers which will lead to some fractionation during operation and will tend to favor enrichment of neodymium in solution. This enrichment is undesirable since neodymium has a high neutron cross section, as compared with lighter rare earths. Neodymium is now being studied in dynamic experiments to determine the degree of enrichment. At ORNL the most reliable results were those obtained by sealing simulated fuel solutions containing known amounts of rare-earth sulfates in quartz tubes and observing visually the appearance and disappearance of a solid phase as the temperature of the solution was changed. The first set of determinations, on mixed rare-earth sulfates, was made in pyrex tubing, but uranium oxide precipitated when the tube was heated above 260°C or when a sample was heated a second time. No uranium precipitation was observed in quartz tubes when the tube was repeatedly heated to 300°C.

Mixed Rare-Earth Sulfates. The rare-earth sulfate mixture used to approximate fission-product rare earths was Lindsay Code 302 salt, with the following composition: Ce, 48%; La, 24%; Pr, 6%;

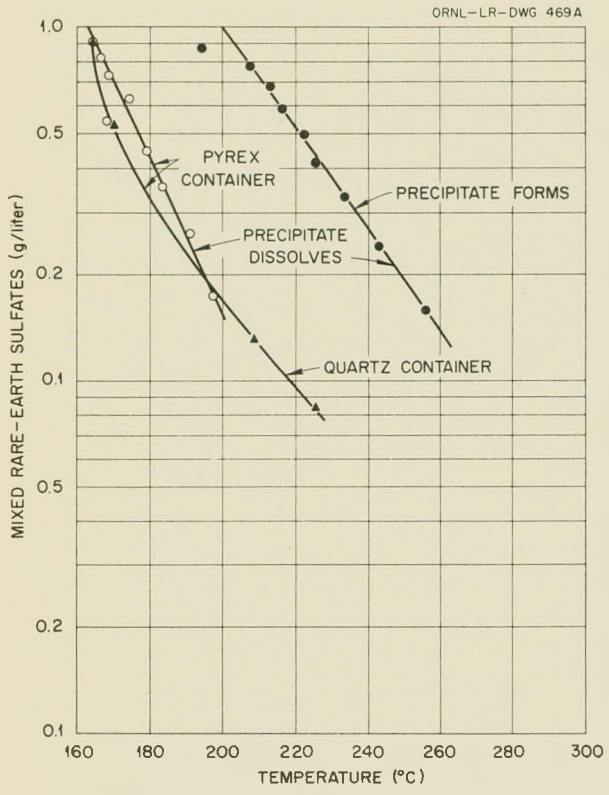

Fig. 124. Solubility of Mixed Rare-Earth (48% Cerium, 24% Lanthanum, 19% Neodymium, 6% Praseodymium, 2% Samarium, 1% Others) Sulfates in 0.02 *m* Uranyl Sulfate Solution Containing 0.005 *m* H_2SO_4.

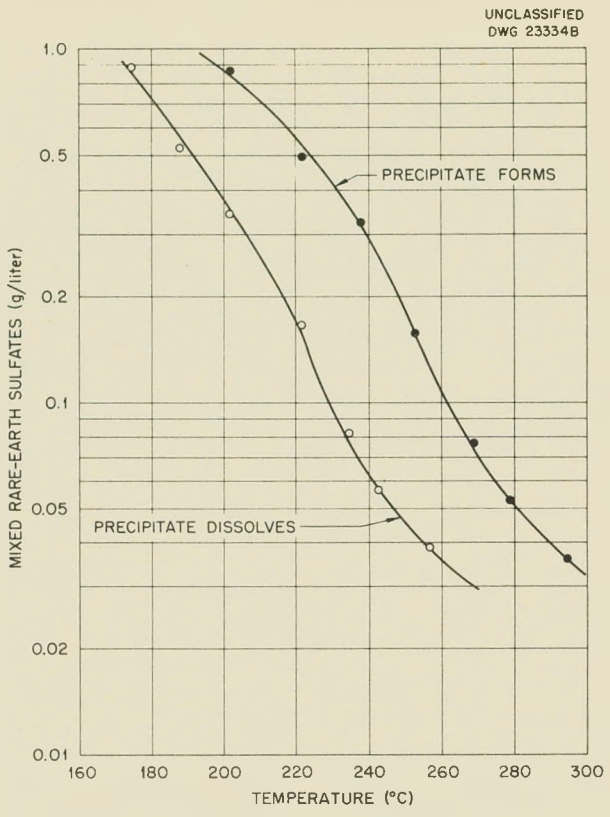

Fig. 125. Solubility of Mixed Rare-Earth Sulfates (41% $La_2(SO_4)_3$, 32% $Pr_2(SO_4)_3$, 27% $Nd_2(SO_4)_3$) in 0.02 *m* Uranyl Sulfate Solution Containing 0.005 *m* H_2SO_4.

Nd, 19%; Sm, 2%; others, 1% . The solubility data obtained with this material are shown in Fig. 124.

Cerium-Free Mixed Rare-Earth Sulfates. The above work was repeated on a mixture of rare earths free of cerium. The cerium-free mixture had the following composition: La, 41.3%; Pr, 31.8%; Nd, 26.9%. The solubility of this mixture (Fig. 125) was significantly higher than that of the Code 302 mixture at temperatures below 220°C, but the difference largely disappeared by the time a temperature of 250°C was reached.

Ce(III) Sulfate. Since cerium constitutes roughly one-half of the fission-product rare earths, the solubility of Ce(III) in the fuel solution is important. This was determined by the visual observation method. In this series, unambiguous observation of phase changes (Fig. 126) could be made up to 300°C and at a $Ce_2(SO_4)_3$ concentration of less than 0.04 mg/ml. The $Ce_2(SO_4)_3$ preparation that was used contained some free acid; so the amount of acid in the test solutions ranged from 0.005 M for the most dilute solution to 0.008 M for the most concentrated solution.

Lanthanum Sulfate. Good solubility data (Fig. 127) were obtained for $La_2(SO_4)_3$ down to a concentration of 0.023 mg/ml which is a saturated solution at 250°C.

Neodymium Sulfate. Much higher salt concentrations than those in the other studies had to be used in order to obtain a reliable solubility curve for $Nd_2(SO_4)_3$. Visual observations yielded erratic results when the concentration of neodymium sulfate was below 0.3 mg/ml (solid line, Fig. 128). From these dilute solutions the precipitate formed so slowly and in such extremely fine particles that

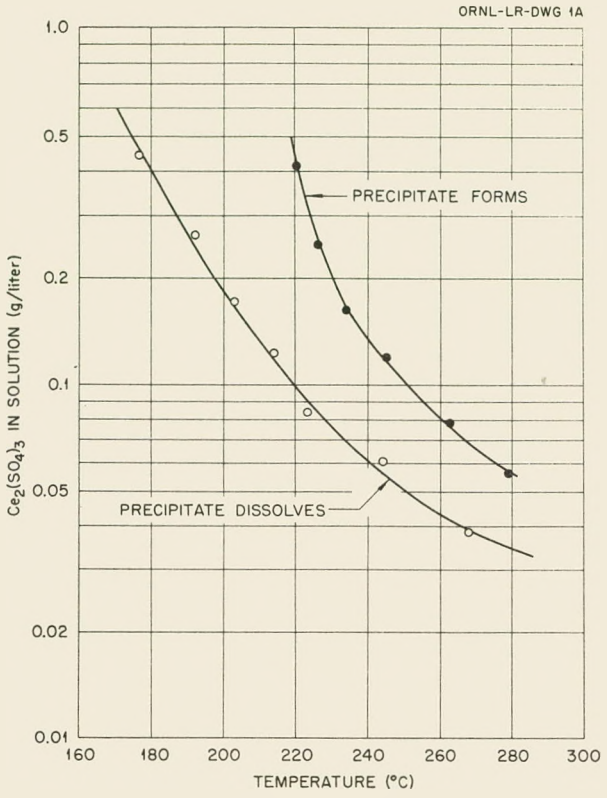

Fig. 126. Solubility of $Ce_2(SO_4)_3$ in 0.02 *m* Uranyl Sulfate Solution Containing 0.005 *m* H_2SO_4.

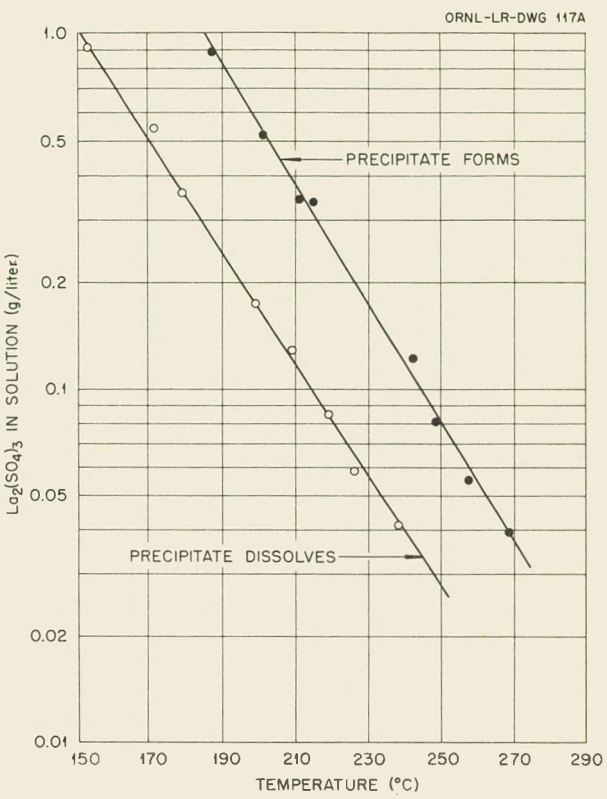

Fig. 127. Solubility of $La_2(SO_4)_3$ in 0.02 *m* Uranyl Sulfate Solution Containing 0.005 *m* H_2SO_4.

the temperature at which the solid phase disappeared could not be determined accurately.

Since neodymium is a major neutron poison, very precise knowledge of its behavior under reactor conditions is desired. Data on the solubility of neodymium sulfate were extended to 295°C by using tracer techniques and filtration (broken line, Fig. 128). The solubility values were obtained with three different initial neodymium sulfate concentrations for each temperature but with a constant specific activity of Nd^{147} as tracer. Best agreement between various determinations at 250°C was obtained when the solutions were heated to 270 to 280°C, cooled to 250°C, and held there until filtered 1 hr later. It is believed that in this process the extremely fine particles were dissolved and better filtration was obtained. This explanation agrees with the observation, made during the visual-observation runs, that precipitates from dilute solutions were much finer than the same precipitates from more concentrated solutions.

Biological-Hazards Control

In order to minimize the biological hazard associated with some of the longer-lived fission products in the event of a fuel leak from the reactor, it would be desirable to keep the concentration of certain fission products in the reactor to as low a value as possible. Calculations by the Long-Range Planning Group of the Chemical Technology Division indicate that, if the rare gases are excluded, iodine is the most dangerous element. Next in order of importance are the alkali and alkaline-earth elements. Work is now under way to determine the concentration of strontium that may be expected in the core solution at operating temperature. Preliminary data indicate that this value is about 0.04 mg/ml at 275°C. This concentration is equivalent to 30 days' production of strontium in the K-23 or K-49 reactor fuel solution at full power.

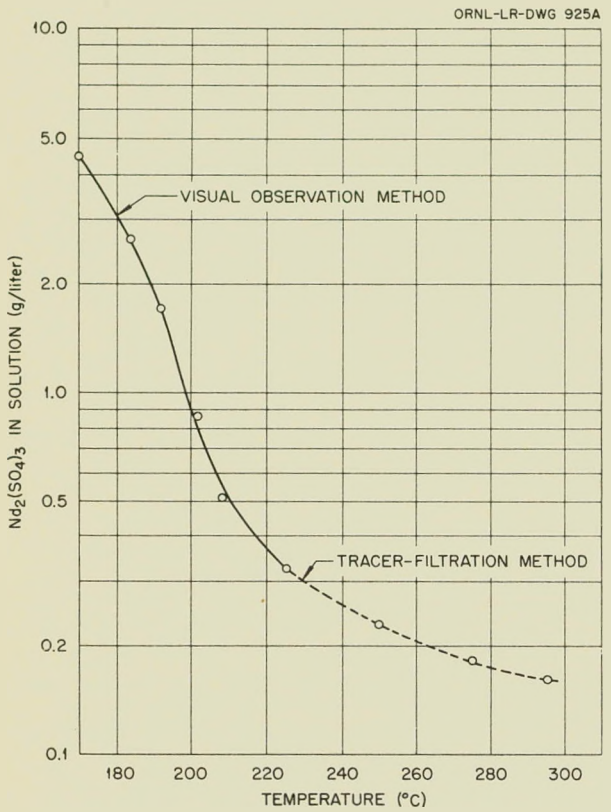

Fig. 128. Solubility of $Nd_2(SO_4)_3$ in 0.02 *m* Uranyl Sulfate Solution Containing 0.005 *m* H_2SO_4.

SUMMARY OF WORK AT THE VITRO LABORATORIES[2]

Calcium Fluoride Process

Pilot-plant tests of the calcium fluoride method for the removal of rare-earth fission products from the fuel solution of a homogeneous reactor have been essentially completed at the Vitro laboratory. Tentative cost estimates (Table 52) based on the results of these pilot-scale tests indicate that, with complete fluoride removal after the CaF_2 treatment, the process will cost at least 0.5 mill per kilowatt-hour of electricity produced. With only partial fluoride removal (about 60 ppm of fluoride in the treated fuel solution) the process cost is estimated to be 0.3 mill/kwh; however, this amount of fluoride would probably cause excessive corrosion of the zirconium core tank of the reactor.

The CaF_2 process with complete fluoride removal by evaporation is now considered to be a feasible method for removing rare-earth fission products from the fuel of a two-region homogeneous reactor. However, removal of these materials as insoluble rare-earth sulfates by a solid-liquid separation at reactor temperature appears to be simpler. The pilot-plant equipment at the Vitro laboratory is also being used to evaluate precipitation methods for removing fission products from reactor fuel

[2]KLX number to be supplied later.

TABLE 52. COST OF CaF_2 PROCESS COUPLED WITH VARIOUS FLUORIDE-REMOVAL TREATMENTS

Basis: plant to process 11 lb of uranium per day for 330 days per year

Fluoride-Removal Treatment	Fluorine Content of Product (ppm)	Capital Investment	Annual Direct Costs (dollars/yr)	Annual Fixed Charges* (dollars/yr)	Processing Costs**	
					Cents Per Gram of U Processed	Mills Per Kilowatt-Hour of Electricity
None	>300	$ 731,200	161,300	108,600	16	0.3
$Th(SO_4)_2$ addition to precipitate ThF_4	60	868,000	188,100	124,600	19	0.3
Evaporation to solid followed by calcination at 300°C for 1 hr	<1	1,363,000	244,100	201,800	27	0.5

*Amortization period is 10 years; includes variable but not general overhead expenses.

**Assuming no uranium loss during processing and 1% D_2O loss.

solution. This work is in support of engineering development on solid-liquid separation devices at ORNL.

Rare-Earth Sulfate Solubility

Preliminary data (Table 53) on the solubility of various rare-earth sulfates, as determined by the Vitro Corp. with the use of a filter-bomb technique, confirm the results of visual-observation tests made at ORNL. A stainless steel high-pressure vessel containing a filter in its cavity was equipped with an exit tube and valve so that the solution in the bomb was filtered, at the temperature and pressure of the vessel, as it was withdrawn. The filter was a tube filled with finely crushed quartz. Samples were analyzed either by tracer technique or by spectroscopic methods. In general, the tracer results appear to be more reliable since a large and varying blank correction is needed in the spectroscopic method.

TABLE 53. SOLUBILITY OF ANHYDROUS RARE-EARTH SULFATES IN 0.02 *m* UO_2SO_4 WHICH CONTAINS 0.005 *m* H_2SO_4

Element	Solubility[a] (g/liter of rare-earth sulfate)			
	250°C	280°C	310°C	325°C
Cerium	0.23 (9)[b]	0.07 (7)	0.04 (7)	
Praseodymium[c]	0.17	0.14	0.17	0.14
Neodymium[d]	0.34	0.11	0.06	0.05
Samarium[c]	0.41	0.42	0.17 (3)	0.10
Yttrium[e]	0.24 (8)	0.24 (7)	0.09 (8)	0.08
	0.11		0.08	
Mixed rare earths[f]	0.19	0.09	0.09	0.10

[a]Data not corrected for volume changes as temperature increased.

[b]Numbers in parentheses indicate final uranium concentration, in grams per liter, where changes in uranium concentration occurred during the experiment.

[c]Solubility determined by chemical analyses; not corrected for blank which varied between 0.0 and 0.08 g of rare earths per liter.

[d]Traced with Nd^{147}.

[e]Traced with Y^{91}.

[f]Traced with Eu^{155}.